The Price of Electrogenicity : Studies on the Carrier and Channel like Properties of a Type II NaPi Cotransporter System

Dissertation

zur

Erlangung der naturwissenschaftlichen Doktorwürde

(Dr. sc. nat.)

vorgelegt der

Mathematisch-naturwissenschaftlichen Fakultät

der

Universität Zürich

von

Andrea Bacconi

aus Italien

Promotionskomitee

Prof. Dr. Heini Murer

Prof. Dr Jürg Biber

Dr. Ian C. Forster

Zürich 2006

Dedicata ad Elisa ed Ashlee le due donne della mia vita

TABLE OF CONTENTS

1. SUMMARY/ZUSAMMENFASSUNG

Summary

The first part of this work was concerned with the theme of *electrogenicity* in membrane transport. Two type II Na^+/P_i cotransporter isoforms were studied: NaPi-IIa and NaPi-IIc, both previously cloned from mouse kidney (Paper 1). These proteins share high sequence homology and a predicted secondary topology with eight transmembrane domains, but a strikingly different kinetic phenotype: type IIa (NaPi-IIa) is electrogenic, whereas type IIc (NaPi-IIc) is electroneutral. The high similarity between these isoforms suggested that relatively small changes in the amino acid sequence might be responsible for conferring their respective electrogenicity and electroneutrality. To investigate this hypothesis we constructed a group of chimeras between the two isoforms. By means of $^{32}P_i$ tracer flux and two-electrode voltage clamp assays, we showed that the first 6 predicted transmembrane domains (TMDs) and the interconnecting loops were critical for the electrogenicity of NaPi-IIa. A sequence comparison between members of type IIa, IIb and IIc Na^+/P_i transporters highlighted the existence of three clusters of amino acids, that differed between electrogenic and electroneutral isoforms, including the extracellular loop 3 (ECL-3) and intracellular loop 1 (ICL-1), which previous studies had suggested play a role in the determination of the transport pathway. The exchange of three amino acids (AAD motif), found in the electrogenic NaPi-IIa conferred electrogenicity to NaPi-IIc. Dual uptake and two-electrode voltage clamp assays of AAD-IIc gave data that suggested the three substitutions created, directly or indirectly, a Na^+ interaction site, the occupancy of which led to the stoichiometric translocation of an additional Na^+ ion per transport cycle. Moreover, the presence of presteady-state charge movements in the absence of external Na^+ supported the idea that voltage sensing elements were introduced into AAD-IIc. However, a detailed kinetic analysis of AAD-IIc showed significant functional deviations from the electrogenic NaPi-IIa phenotype: a weaker steady-state voltage dependency, a lower apparent affinity for P_i and a transient charge imbalance. These findings underlined the complexity of the interactions among the structural elements involved in the transporter activity and the necessity of additional elements in the second half of NaPi-IIc, as suggested by the chimera study, to fully restore an electrogenic phenotype like the wild type. An attempt to characterize the function of the reciprocal of the mouse AAD-IIc mutant (SSG-IIa) was unsuccessful either due to its function being below the detectable limit or membrane mistargeting.

The electrogenicity theme was also part of two parallel studies that applied the substituted cysteine scanning method (SCAM) to the predicted 1st and 4th extracellular loops (ECL-1, ECL-4) (Papers 2 and 3) and TMD-3 (Paper 4) of the NaPi-IIa isoform. SCAM combined with a detailed

kinetic analysis on ECL-1 and ECL-4 suggested their involvement in determining the voltage dependent kinetic of type IIa transporters. This identified a cys-mutant in each linker that displayed reciprocal electrogenic behaviour depending on the state of cys-modification. These findings led to a proposal of a novel structure-function relation for electrogenic Na^+/P_i cotransporters, whereby the TMDs at the N- and C-terminal ends of the protein are relatively static and the respective linkers ECL-1 and ECL-4 allow flexibility for movement of the remaining TMDs during the transport cycle. In the second study (Paper 4), SCAM applied to TMD-3 identified residues involved in substrate binding and in defining the electrogenic behavior. In the context of cotransporter electrogenicity, the most important finding was that removal of the negative charge at the corresponding site in TMD-3 of the human NaPi-IIa isoform gave a mutant (D224G) that displayed a detectable $^{32}P_i$ uptake, but was electrically silent. This further supported the notion that the Asp in the AAD motif may participate in forming a binding site for one of the three Na^+ ions.

The second part of this work (Paper 5) concerned the theme of the *channel nature of carrier proteins* in the context of the uncoupled leak current of type II Na^+/P_i cotransporters. The study was based on the idea that the activation energy for movement of an ion through a channel is much less than that associated with the transport of solute by a carrier. Using a two-electrode voltage clamp assay at different temperatures, we determined the activation energy (E_a) for the steady-state currents at different voltages for the P_i induced current and the uncoupled leak current. We found that as expected the E_a for the P_i -dependent current was above 18 kcal/mol for $-140mV < V < -20$, whereas the leak current showed a $E_a \sim 12$ kcal/mol for $-120 < V < -60$ mV. These results could suggest the existence of two different mechanisms: carrier-like behaviour for the cotransport mode and uniporter-like behaviour for the leak mode. In addition to the steady-state data, we also recorded presteady-state currents at different temperatures. These data indicated that lowering the temperature shifted the equilibrium potential of the presteady-state charge distribution as temperature was lowered, together with an increase in the main relaxation time constant. This might reflect temperature-dependent changes in the kinetics of Na^+ binding, the reorientation of the empty carrier, or a combination of both.

Zusammenfassung

Der erste Teil dieser Arbeit befasst sich mit dem Thema der *Elektrogenizität* im Membrantransport.Es wurden zwei vom Typ II Na+/P_i Cotransporter-Isoformen untersucht: zum Einen NaPi-IIa und zum anderen NaPi-IIc, beide wurden zuvor aus der Niere der Maus geklont (Paper 1). Diese Proteine teilen eine hohe Sequenzhomologie und eine gemeinsame vorhergesagte Sekundärstruktur mit acht Transmembrandomänen, allerdings besitzen sie eine voellig unterschiedliche Kinetik: Typ IIa (NaPi-IIa) ist elektrogen, wogegen Typ IIc (NaPi-IIc) elektroneutral ist. Die starke Ähnlichkeit zwischen diesen Isoformen weist darauf hin, dass relativ kleine Änderungen in der Aminosäurensequenz für die jeweilige Elektrogenizität und Elektroneutraliät verantwortlich sein könnten. Um diese Hypothese zu untersuchen haben wir zwischen diesen Isoformen eine Gruppe von Schimären konstruiert. Anhand des ^{32}Pi Indikatorflusses und der ‚two-electrode voltage clamp' Methode haben wir gezeigt, dass die ersten 6 vorhergesagten Transmembrandomänen (TMDs) und die verbindenden Schleifen ausschlaggebend für die Elektrogenizität von NaPi-IIa sind. Ein Sequenzvergleich mit Mitgliedern der Typ IIa, IIb und IIc Na^+/Pi Transporter machte deutlich, dass es drei Cluster an Aminosäuren gibt, die sich in ihren elektrogenen und elektroneutralen Isoformen unterschieden, einschließlich der extrazellulären Schleife 3 (ECL-3) und der verbindenden Schleife 1 (ICL-1), auf welche in vorangegangenen Studien darauf hingewiesen wurde, dass sie eine Rolle bei der Bestimmung des Transportweges spielten. Der Austausch von drei Aminosäuren (AAD-Motiv) aus dem elektrogenen NaPi-IIa verlieh dem NaPi-IIc Elektrogenizität. Die Daten der Doppel-Aufnahm- und ‚two-electrode voltage clamp'-Methode von AAD-IIc wiesen darauf hin, dass die drei Substitutionen, direkt oder indirekt, eine Na^+ Interaktionsstelle erschufen, die bei Belegung zu einer stoichiometrischen Translokation eines weiteren Na^+-Ions per Transportzyklus führte. Die Anwesenheit von ‚presteady-state' Ladungsbewegungen und die gleichzeitige Abwesenheit von externem Na^+ förderte darueber hinaus die Vorstellung, dass spannungssensorische Elemente in den AAD-IIc eingeführt worden sind. Allerdings zeigte eine detaillierte Kinetikanalyse von AAD-IIc, dass es signifikante Funktionsabweichungen vom elektrogenen NaPi-IIa Phänotyp gab: eine schwächere ‚steady-state' Spannungsabhängigkeit, eine niedrigere scheinbare Affinität für Pi und ein transientes Ladungsungleichgewicht. Diese Befunde unterstrichen zum Einen die Komplexität der Interaktionen zwischen den strukturellen Elementen, die in der Transportaktivität beteiligt sind, ‚und die Notwendigkeit zusätzlicher Elemente im zweiten Teil von NaPi-IIc, wie sie in der Schimärenstudie vorgeschlagen werden, einzufügen um so den elektrogenen Phänotyp voll wiederherzustellen wie den Wildtyp. Einen Versuch die Funktion der umgekehrten AAD-IIc

Mutante (SSG-IIa) zu charakterisieren, war nicht erfolgreich, zum Einen weil ihre Funktion unter der Detektionsgrenze lag oder zum anderen wegen eines fehlerhaften Membrantargetings.
Das Elektrogenizitäts-Thema war auch Teil zweier Parallelstudien, die die Cystein-Austausch-Scanning–Methode (SCAM) auf die erste und vierte vorhergesagte extrazelluläre Schleife (ECL-1, ECL-4) (Paper 2 und 3) und die TMD-3 (Paper 4) der NaPi-IIa Isoform anwendeten. SCAM kombiniert mit einer detaillierten Kinetikanalyse von ECL-1 und ECL-4 deuteten auf eine Beteiligung in der Ermittlung der spannungsabhängigen Kinetik der Typ IIa Transporters hin. Dies identifizierte eine Cys-Mutante in dem jeweiligen Linker, welche je nach Lage der Cys-Modifikation ein ungekehrtes elektrogenes Verhalten zeigte. Diese Ergebnisse führten zu einem Vorschlag eines neuartigen Struktur-Funktionsverhältnisses für elektrogene Na^+/Pi Cotransporter, wonach die TMDs am N- und C-terminalen Ende des Proteins relativ statisch sind und die zugehörigen Linker ECL-1 und ECL-4 die Flexibilität für die Bewegung der restlichen TMDs während des Transportzyklus erlauben. In der zweiten Studie (Paper 4) wurde SCAM auf die TMD-3 angewendet und identifizierte Reste, die bei der Substratbindung beteiligt sind und das elektrogene Verhalten bestimmte. Im Zusammenhang der Cotransporter-Elektrogenizität ist das wichtigste Ergebnis, dass die Beseitigung der positiven Ladung an der entsprechenden Stelle in der TMD-3 der humanen NaPi-IIa Isoform eine Mutante (D224G) erbrachte, die eine detektierbare $^{32}P_i$-Aufnahme zeigte, aber elektrisch stumm war. Des Weiteren unterstützt dies die Vorstellung, dass Asp im AAD-Motiv bei der Schaffung einer Bindungsstelle für eine der drei Na^+-Ionen verantwortlich sein könnte.

Der zweite Teil dieser Arbeit (Papier 5) befasst sich mit dem Thema der *Kanal-ähnlichen Natur von Carrier-Proteinen* zusammen mit dem ungekoppelten Leckstrom vom Typ II Na^+/Pi Cotransportern. Diese Studie basierte auf der Idee, dass die Aktivierungsenergie für die Bewegung einen Ions durch einen Kanal sehr viel geringer ist, als die Energie, die mit dem Transport von gelösten Substanzen durch einen Carrier verknüpft ist. Unter Zuhilfenahme der ‚two-electrode voltage clamp'-Methode bei verschiedenen Temperaturen, bestimmten wir bei verschiedenen Spannungen die Werte für die Aktivierungsenergie (E_a) in die ‚steady-state' Ströme zum Einen für den Pi induzierten und zum Anderen für den ungekoppelten Leckstrom. Wie erwartet, beobachteten wir, dass die E_a für den Pi-abhängigen Strom bei über 18 kcal/mol für $-140mV < V < -20mV$ lag, wogegen der Lecktrom für die E_a einen Wert von ~ 12 kcal/mol für $-120 < V < -60$ mV aufzeigte. Diese Ergebnisse wiesen auf eine eventuelle Existenz von zwei verschiedenen Mechanismen: einerseits auf ein carrier-ähnliches Verhalten im Cotransporter-Modus und andererseits auf ein ‚uniporter'-ähnliches Verhalten im Leckstrom-Modus. Zusätzlich zu den ‚steady-state' Daten haben

wir auch ‚presteady-state' Ströme bei verschiedenen Temperaturen aufgezeichnet. Diese Daten indizierten, dass bei einer Erniedrigung der Temperatur sich das Gleichgewichtspotential der ‚presteady-state' Ladungsverteilungen gleichermaßen erniedrigten wie die Temperatur selbst, einhergehend mit einer Zunahme der Hauptrelaxationszeitkonstanten. Dies könnte eine Temperatur-abhängige Verschiebung in der Na^+-Bindungskinetik, die Reorientierung des leeren Carriers oder eine Kombination beider widerspiegeln.

2. INTRODUCTION

2.1 Membrane transport proteins

All living cells are surrounded by an approximately 40 Å thick phospholipid bilayer that, due to its hydrophobic nature, acts as a barrier between the intra- and extracellular compartments. As a result, the intercompartmental movement of most polar molecules, and the major ions Na^+, K^+, Ca^{2+} and Cl^-, is impeded. The barrier function of the cell membrane is crucially important because it allows the cell to maintain solute concentrations in the cytosol different from those in the extracellular compartment. On the other hand, the selective and regulated transfer of solutes across the cell membrane is essential to accomplish different tasks such as solute distribution, cell signalling, cell regulation and activation of cell-specific metabolic pathways. The movement of ions and small water-soluble organic molecules across the lipid bilayer is achieved through the action of membrane transport proteins. These can be classified according to their structure-function complexity, which is reflected in the translocation mechanics and according to the energetics of the transport process, as summarized in Figure 1.

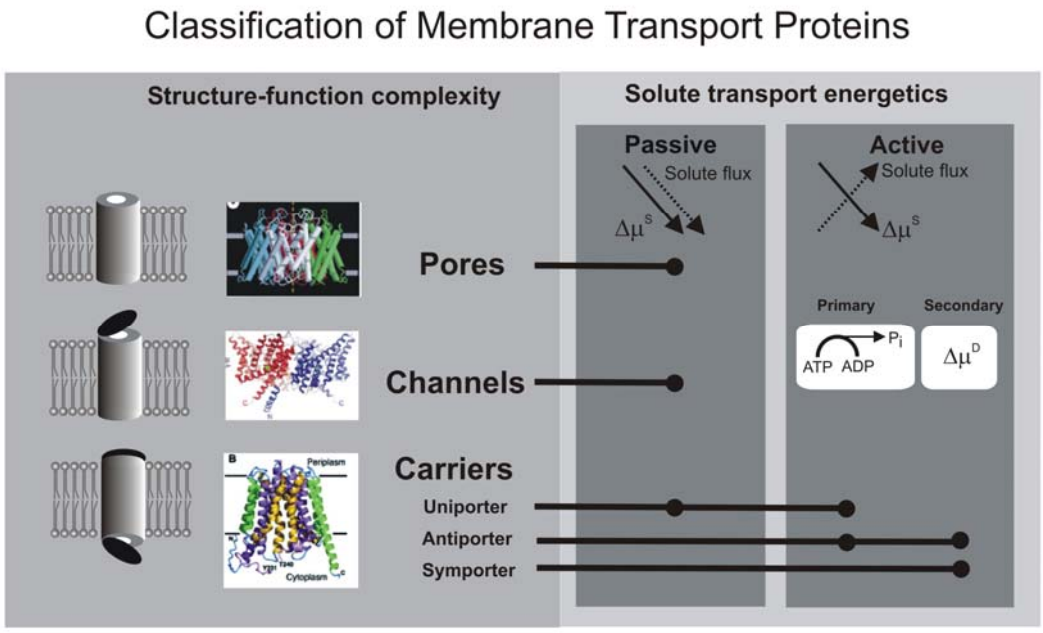

Figure 1: Classification of membrane transport proteins according to their structure-function complexity (left) and the solute transport energetics (right). An example of recently crystallized transport proteins from the pore (AQP1, (Murata et al., 2000)); channel (ClC, (Dutzler et al., 2002; Dutzler et al., 2003)) and carrier (Gly-3P, (Huang et al., 2003; Lemieux et al., 2005)) is shown alongside a simple cartoon representation. In passive transport, the solute flux and its

electrochemical gradient ($\Delta\mu^S$) are in the same direction; in active systems they are opposite. Two examples of sources of energy for active transport systems are indicated: ATP-ADP hydrolysis that drives some primary active systems and $\Delta\mu^D$ denotes the electrochemical potential of the driving species in secondary active transport systems.

From the viewpoint of translocation mechanics, we can consider membrane transport proteins as *pores*, *channels* or *carriers*, depending on how the hydrophilic transmembrane pathway is accessed from the intra- and extracellular compartments (Boron and Boulpaep, 2003).

Pores provide an aqueous transmembrane conduit that is always open. Typical examples include porins found in the outer membrane of gram-negative bacteria and mitochondria; perforins, the pore-forming proteins used by cytotoxic T lymphocytes to kill their target cells and aquaporins that allow the permeation of molecules like water and glycerol. Pores can allow the passage of up to approximately 10^9 particles s^{-1}.

Ion channels or "gated" pores are next in order of functional complexity.. They comprise one or more polypeptide subunits with α-helical membrane-spanning segments. All channels comprise a *gate* that determines the state of the channel pore (open or closed), a *selectivity filter* that determines the type (cations or anions) and size/valency (e.g. Na^+, K^+, Ca^{2+}) of the ions that have access to the channel pore and a *sensor* that regulates the transitions between the open and closed state by responding to changes in transmembrane potential, second messengers (e.g. Ca^{2+}) and other ligands or mechanical force. Channels are extremely selective for specific ions, and allow the passage of up to 10^8 ions s^{-1}.

Carriers represent a further step in functional complexity by having a permeation pathway that has an extremely low probability of being open simultaneously to both intracellular and extracellular solutions. For example, this might be achieved by having two gates on each side of the membrane that allow access to the pore. Carriers bind the specific solute to be transported on one side and undergo a series of conformational changes to transfer the solute across the membrane, releasing it on the opposite side (Figure 2). Unlike the unidirectional electrodiffusive flux through an open ion channel, solute transport takes place by means of a so-called transport cycle, during which a fixed number of solute molecules are translocated, most likely with ordered binding steps. This means that carriers exhibit saturation with respect to substrate concentration, because of a defined number of binding sites are available and mediate much slower rates of solute translocation, typically in the range 10-50,000 s^{-1}.

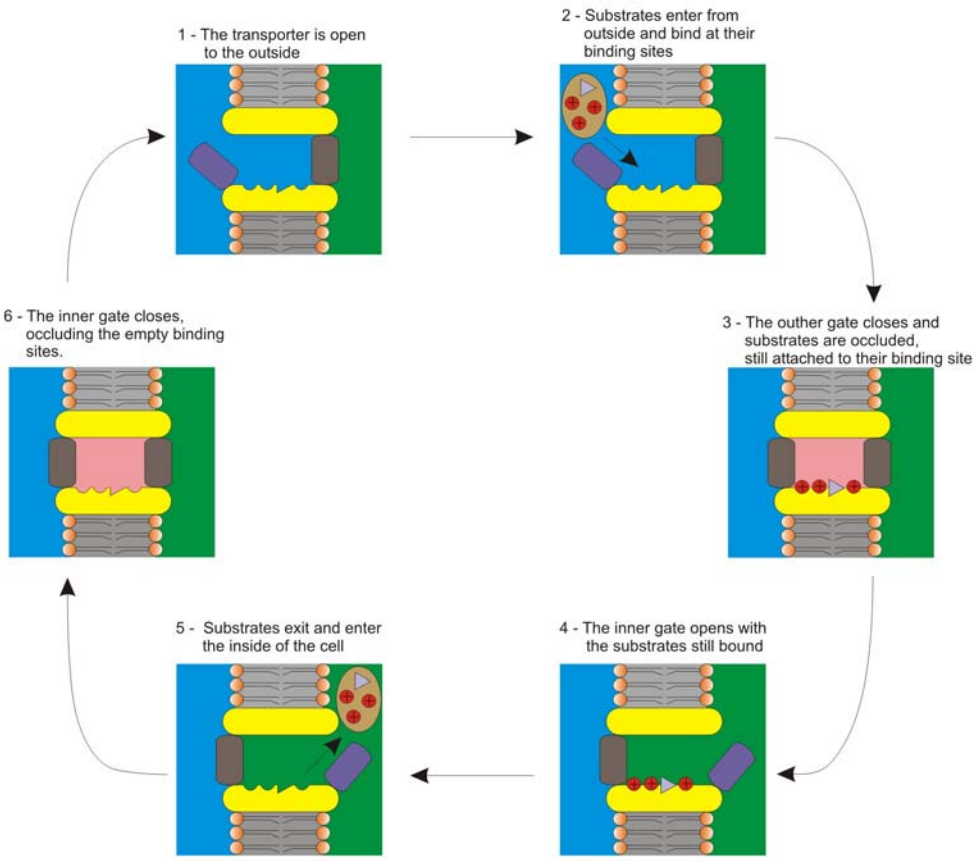

Figure 2: Schematic representation of substrate translocation in a carrier protein (adapted from (Boron and Boulpaep, 2003)). Red balls represent the ions required for the transport event; gray triangle represents the translocated substrate. The cartoon depicts how the type II Na^+/P_i cotransporters could translocate 3 Na^+ ions and one P_i as a cyclic sequence of transitions between unique conformational states of the protein. The direction of the cycle is determined by the driving force of the substrates.

We can subdivide carrier-mediated transport systems further into three subtypes according to whether one or more different solutes are involved in the transport and their relative direction of movement, as follows:

i) *uniporters*: move a solute only in one direction;

ii) *symporters* (or *cotransporters*): translocate two or more substrates across the membrane in the same direction;

iii) *antiporters* (or *exchangers*): translocate two substrates in opposite directions.

Cotransporters and antiporters translocate solutes conditional on the presence of both substrates involved in the transport cycle, whereas uniporters require the presence of only one substrate to perform their transport function.

In terms of the solute transport energetics, we can also classify membrane transport proteins as active or passive systems (Figure 1).

In *passive* transport the solute can only move "downhill", i.e. the driving force for substrate movement is given by the chemical potential ($\Delta\mu$) resulting from the different solute concentrations across the membrane and thus solutes move diffusively. For charged solutes, the transporter activity also depends on the free energy contained in the transmembrane electrical field, which results from the asymmetrical distribution of charged species across the membrane. Examples of passive transporters are pores, channels and uniporter carriers.

In *active* transport the solute can be moved "uphill" against its electrochemical gradient and therefore a source of energy is required. *Primary* active transporters use the energy available from the direct hydrolysis of the high energetic pyrophosphate bonds (ATP, GTP), such as the Na^+,K^+-ATPase, an example of an active exchanger or the vacuolar H^+-ATPase, an active uniporter. *Secondary* active transporters, on the other hand, dissipate the energy stored in the electrochemical gradient of ions such as Na^+ and H^+ to translocate another solute across cell membranes. The two main carrier types so far identified as secondary active transporters are symporters (or cotransporters) and antiporters (Boron and Boulpaep, 2003).

2.2 Structure determination of membrane transport proteins

It would be advantageous to know the 3-D protein structure of membrane transport proteins because we can use this information to locate previously identified functionally important sites within a 3-D structure and gain insight into the protein dynamic of conformational changes. From the clinical/pharmaceutical viewpoint, 3-D structural information is important for designing specific compounds (e.g. inhibitors) directed against particular epitopes. Protein purification and subsequent diffraction by X-ray spectrometry of the crystals can give 3-D structures with resolution down to ~2 Å or to ~10 Å in the case of 2-D crystallization methods, using high-resolution electron microscopy. An intrinsic property of all membrane proteins is that they have both hydrophobic and hydrophilic surfaces, which means that they are insoluble in aqueous buffers, whereas they can be denatured in organic solvents. The consequence of this property is that it is more difficult to obtain the amount of purified protein necessary to grow diffracting crystals, compared with soluble proteins. An additional obstacle to crystallization is the intrinsic protein metastability, i.e. the ability to be stable enough to generate a crystal. Many efforts have been made to overcome these limitations, such as the co-crystallization with antibody fragments that led to the successful crystallization of the voltage gated K^+-channel KvAP of *Aeropyrum pernix* (Jiang et al., 2003a). The difficulty of crystallizing membrane proteins is also reflected in the number of structures in the database: thousands of soluble proteins can be found, yet only few of them are membrane proteins

(roughly 50) (RCSB, protein databank, www.rcsb.org/pdb). In addition to the technical limits, a major criticism of the crystallographic approach is the lack of knowledge for protein dynamics. The coordinates obtained from the crystallized structure represent just one possible state of the protein, determined in a particular environment that is often very different from physiological conditions (see below). This observation underscores the importance of addressing the structure-function problem from different directions without focusing only on the structure. The ideal solution for dynamic studies would be to crystallize membrane proteins in different states of their functional cycle.

A second problem in protein structure determination arises from the crystallization conditions, which are often non-physiological: e.g. high pH, low temperature or having complexes with antibodies to stabilize the protein before crystallization can occur. This situation could lead to significant structural artefacts, which are difficult to analyze and interpret if functional data or other structural assays, such as 2D-crystals, are unavailable. An example of a crystal structure that contains artefacts is the multidrug resistance efflux transporter EmrE of *E. coli* (Ma and Chang, 2004), where the contacts within the crystal cell generated a distortion in the helix packing and the published structure did not resemble the one obtained with the 2-D crystal (Tate et al., 2003).

Channels and pores have been among the first membrane transport proteins to yield crystal structures, the most important being:

-the K^+-channel KcsA-1 of *Streptomyces lividans* (Doyle et al., 1998),

-the voltage gated K^+-channel KvAP of *Aeropyrum pernix* (Jiang et al., 2004; Jiang et al., 2003a; Jiang et al., 2003b),

-the mammalian voltage-dependent shaker family K-channel (Long et al., 2005), -the chloride channel ClC of *E. coli* (Dutzler et al., 2002),

-the water channel aquaporin AQP1 of human (Sui et al., 2001) and

-the ammonia channel Amtb of *E. coli* (Khademi et al., 2004).

Importantly, a number of carrier type membrane transport proteins have also been crystallized to yield their structures:

-the Na^+/H^+-antiporter (NhaA) from *E. coli* (Hunte et al., 2005),

-the glycerol-3-phosphate transporter GlpT (Huang et al., 2003; Lemieux et al., 2005),

-the lactose permease LacY of *E. coli* (Abramson et al., 2003),

-the glutamate transporter homolog of *P. horikoshii* (Yernool et al., 2004),

-the ABC transporter BtuCD of *E. coli* (Locher, 2004; Locher and Borths, 2004; Locher et al., 2002) and, most recently

-the bacterial homolog of the Na/Cl neurotransmitter transporter (Yamashita et al., 2005).

Many of the resolved crystal structures show a two-fold symmetry - the division of protein structure into two structurally similar halves that may have evolved from a gene-duplication (Dutzler et al., 2002) and the proteins are mainly of bacterial origin. The latter observation underlines the difficulty of dealing with mammalian membrane proteins and the lack of structural knowledge for these isoforms. So far, the 3-D structures that have been obtained represent only one of the possible protein conformational states. Although the optimal situation would be to crystallize the proteins in different states, the most recently resolved structures of LacY and GlpT, which showed the transporter in an outward "facing" conformation, gave the researchers the possibility to merge the functional data with the structures to propose a model for protein transport cycle (Abramson et al., 2003; Huang et al., 2003; Lemieux et al., 2005). Moreover, the recent resolution of KvAP a voltage-gated potassium channel raised the controversy about the nature of the molecular movement of its voltage sensor. To address these issues properly, crystal structure studies must be "integrated" with structure-function studies based on having membrane proteins functioning in the "normal" membrane context, to give real-time data. For example, a recent paper described the use of a fluorescence resonance energy transfer (FRET) based assay, has provided compelling evidence that the gating charge displacement in voltage-gated ion channels involves only limited transmembrane movement (Chanda et al., 2005). This contrasts with the predictions from the "paddle" gating model originally proposed from the crystal structure of KvAP (Jiang et al., 2004; Jiang et al., 2003a; Jiang et al., 2003b).

2.3 Non-crystallographic methods link structure and function

Given the difficulties and time requirements to obtain membrane protein crystal structures, a number of techniques have evolved that attempt to: (1) identify functionally important sites and/or motifs and (2) generate structural information and (3) link (1) and (2). In general, these techniques involve testing engineered mutant proteins, the kinetic properties of which are analyzed and compared with the wild type protein. They have an important advantage that the experiments can usually be performed under physiological conditions. These assays open the way to identifying functionally critical sites and provide a potential link between structure and function.

2.3.1 Cysteine scanning or SCAM (Substituted Cysteine Accessibility Method)

The idea behind this technique is the mutation of amino acid residues into novel cysteines that can serve as a reactive site when the protein is exposed to bulky thiol reagents, such as methanethiosulfonate (MTS) compounds. Assays are then used to determine accessibility of the cysteine i.e. the formation of a disulfide bond between the novel cysteine and the thiol reagent (Javitch, 1998; Karlin and Akabas, 1998) (Figure 3). In some cases, the cys-modification results in a clear alteration in transport function that can be detected using standard electrophysiological or tracer-flux techniques. In other cases, biochemical/immunohistochemical methods are used (e.g. MTS-biotin compounds allow the detection of accessible cysteines indirectly by streptavidin precipitation). MTS based reagents can be selected by size, membrane permeability and superficial charge. SCAM therefore has the potential to report if a site is accessible, the extent of accessibility, depending on the conformational state of the protein and the potential functional importance of the native residue for the transport cycle. Using these data an "accessibility" map can be drawn and compared with predictions from conventional hydrophobicity and secondary structure prediction algorithms. For example, the periodicity of accessible cysteines is a strong indication to infer the presence of secondary elements, such as α-helices, β-sheets and the orientation of linker regions with respect to the membrane.

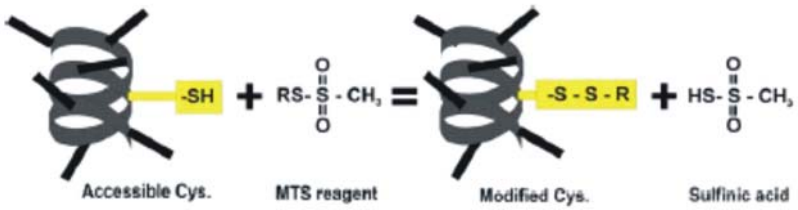

Figure 3: Reaction of thiol reactive substances with cysteines. Example of the reaction for a MTS-reagent with the SH-group of a cysteine

The validity of this approach relies on two important assumptions. First, it is assumed that the site of perturbation coincides with the site of functional importance, nevertheless allosteric and structural artefacts due to the mutation itself and/or thiol binding cannot be easily excluded. A solution to avoid allosteric effects could be the removal of all native cysteines, although such a cys-less construct may be either not expressed or non-functional. Under these circumstances, the wild type protein can be used under the tacit assumption that only the novel cysteine can be modified. Second, it is assumed that free native cysteines do not become accessible as a result of the

mutagenesis and give rise to false positive indications of cys-modification (e.g. (Kamdar et al., 2001).

2.3.2 Thiol cross-linking

The rational behind these studies is to investigate *in situ* the helix packing of a transporter by expressing it as two contiguous non-overlapping fragments, each hosting a single Cys residue. Fragments are then exposed to disulfide or thiol specific chemical cross-linkers and if the new cysteines are close enough, accordingly to the used cross-linker, a disulfide bridge will form**.** This is detected by chromatographic techniques as a complex with higher molecular weight than the two fragments. Knowing the dimension of the cross-linker and the bond length it is possible to predict the distance between the cysteine residues. The principal limits of this assay are related to the chemistry of the cross-linkers used. The solubility and stability of linkers in the environment where the experiment is performed can strongly affect the efficiency of the reaction; in addition, the time any two proteins are at the specific distance for the cross-linker to react may interfere with the efficiency of the linkage. Finally, these compounds are not specific enough to distinguish between actual interacting proteins and molecules that are simply close to each other; this can lead to artefacts that can be reduced if the cross-linking reaction is followed by immunoprecipitation of the protein of interest.

2.3.3 A success story: LacY

Despite the limitations of the these approaches using a combination of SCAM and crosslinking studies, together with a number of other non-crystallographic techniques (excimer fluorescence, engineered metal binding sites, chemical cleavage, electron paramagnetic resonance), the Kaback group succeeded in proposing a structural model for LacY (Kaback et al., 2001). This model showed a striking similarity with the recently resolved crystal structure (Abramson et al., 2003).

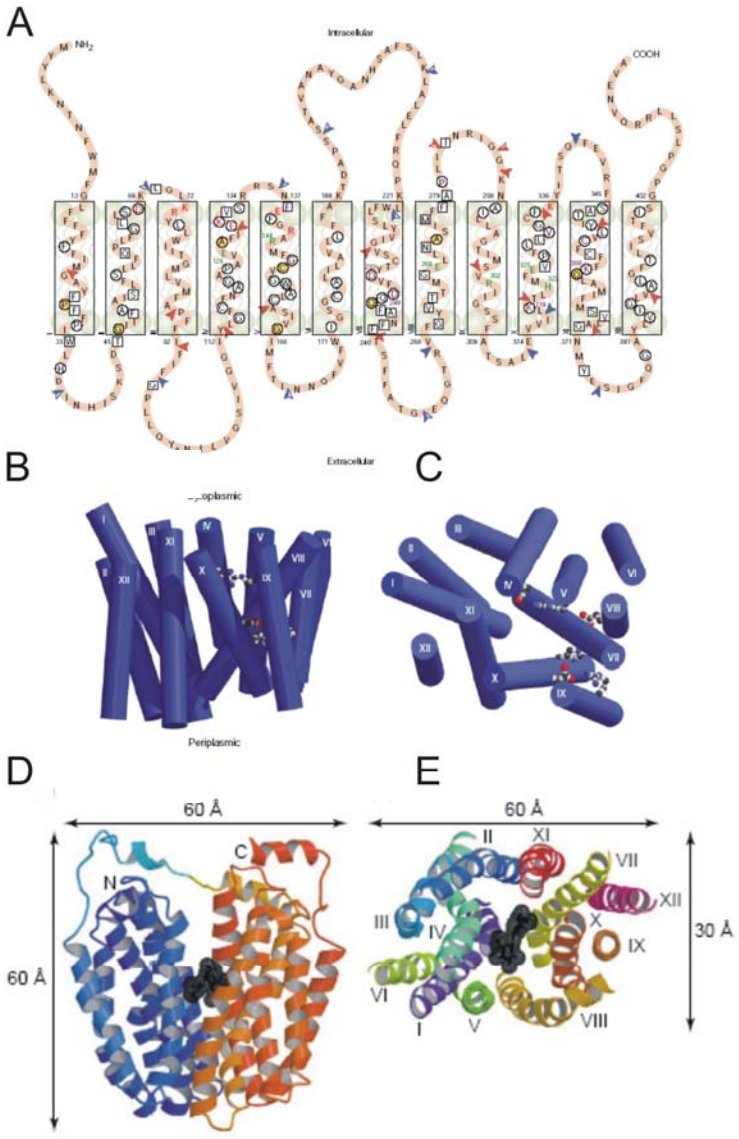

Figure 4: Comparison of a helix packing model with the crystal structure of LacY transporter. (A) Secondary topology scheme for the 12 predicted transmembrane domains of LacY transporter (from (Kaback et al., 2001)); (B) Helix packing model derived using over 100 distance constraints. View parallel to the membrane and from the cytoplasmic side (from (Kaback et al., 2001)); (C) The crystal structure of Lac Y transporter based on C154G mutant with a bound substrate homolog TDG (black). View parallel to the membrane and from the cytoplasmic side (from (Abramson et al., 2003). Loops have been omitted for clarity. Romans numerals indicate the transmembrane helices.

The predicted LacY tertiary structure predicted the helix packing with good agreement with the helix packing of crystallized lactose permease, and thus gave strong support to the continued application of non-crystallographic methods. Moreover, direct binding assays suggested a model for the substrate binding site, correctly guessing the helices and amino acids involved in its formation that were later found in the crystal structure (Kaback et al., 2001).

2.3.4 Protein structure prediction

The determination of protein structures is a central problem in structure-function studies. Often crystal structures are not available for the studied proteins, due to the difficulties already discussed, so the development of protein structure prediction (PSP) methods become necessary. PSP methods represent one of the most important techniques available in computational structural biology. The aim is to determine the 3-dimensional structure of proteins from their amino acid sequences. This involves the prediction of protein tertiary structure from primary structure. The use of PSP methods implies massive computational power; usually computer clusters are necessary for the most complex tasks. The main advantage of this method is the ability to deal with all the protein sequence data, derived from modern large-scale DNA sequencing efforts, on a short time scale, compared with other methods as X-ray crystallography or NMR spectroscopy that are both more time-consuming and expensive.

PSP methods must deal with three main problems:

i) The number of possible structures that proteins may possess is extremely large, as highlighted by the Levinthal paradox, which addresses the observation that proteins fold into their specific three-dimensional conformations within a time span that is much shorter (on the order of milliseconds) than would be possible if the molecule actually searched the entire conformation space for the lowest energy state (Levinthal, 1968)

ii) The physical basis of protein structural stability is not fully understood.

iii) The primary sequence may not fully specify the tertiary structure. For example, proteins known as chaperones have the ability to induce proteins to fold in specific ways avoiding a discontinuity in the folding sequence.

Despite above-mentioned caveats, significant progress has been made and prediction of structures for small proteins is now a perfectly realistic goal (Clementi et al., 2001; Rao et al., 2005; Settanni et al., 2005). The main approaches for such predictions could be divided into two main classes; *de novo* modelling and comparative modelling.

2.3.4.1 *De novo* protein modelling

De novo- or *ab initio*- protein modelling methods seek to build three-dimensional protein models "from scratch". There are many possible procedures that either attempt to mimic protein folding or apply some stochastic method to search for possible solutions (i.e. global optimization of

a suitable energy function). These procedures tend to require huge computational resources, and have thus only been carried out for small proteins (20-residue peptides) (Rao et al., 2005; Settanni et al., 2005)

2.3.4.2 Comparative protein modelling

Comparative protein modelling uses previously solved structures as the starting point or template. The efficiency of this approach depends on evidence that although the number of actual proteins is vast, there is a limited set of tertiary structural motifs to which most proteins belong. These methods can be further subdivided into homology modelling and protein threading.

2.3.4.2.1 Homology modelling

Homology modelling is based on the assumption that two homologous proteins will share very similar structures. Given the amino acid sequence of an unknown structure and the solved structure of a homologous protein, each amino acid in the solved structure is computationally mutated, into the corresponding amino acid of the unknown structure. The distance and dihedral angle restraints for the model are calculated from its alignment with template 3D structure. The spatial restraints and Charmm force field are combined into an objective function (MacKerell et al., 1998). Finally, the model is obtained by optimizing the objective function in Cartesian space. The optimization is carried out by the use of the variable target function method employing methods of conjugate gradients and molecular dynamics with simulated annealing (Braun and Go, 1985). Homology modelling together with functional data could be a powerful tool to build a structural model. The structure of the yeast mitochondrial citrate transporter (CTP) (Walters and Kaplan, 2004) and the human facilitative glucose transporter (glut1) (Salas-Burgos et al., 2004) have been modelled on the basis of bovine mitochondrial ADP/ATP carrier and the glycerol-3-phosphate transporter, respectively. In each case, the model was in agreement with critical amino acids identified by functional studies.

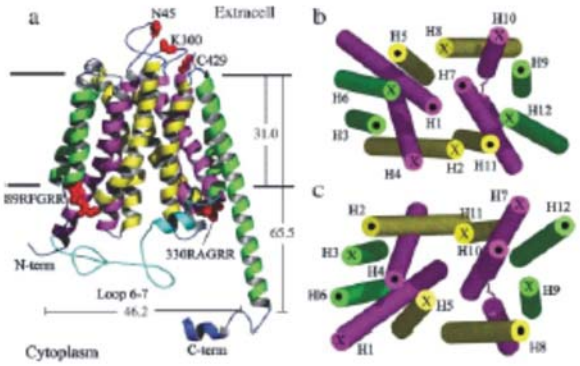

Figure 5: Representations of Glut1 generated by homology modelling using glycerol-3-phosphate as template. (a) Side view showing relative positions of the helices. Residues in red represent topology constraints derived from experimental results involving N45, K300, and C429 for the extracellular side, and motifs 89RFGRR93 and 330RAGRR for the cytoplasmic side. Glut1 measures ~ 35.6 Å x 26.3 Å viewed from the top, and ~ 46.2 Å x 27.2 Å from the bottom and its height is ~ 61 Å . (b) View from the extracellular side showing the tilt of the 12 transmembrane helices. X marks loops entering, whereas dots mark loops exiting. (c) Cytoplasmic view; color scheme as above. The helix colors are in accordance with the symmetry template found by Hirai et al. (2002). Figure drawn using PYMOL (http://pymol.sourceforge.net/).

2.3.4.2.2 Protein threading

Protein threading scans the amino acid sequence of an unknown structure against a database of solved structures. A scoring function is used to assess the compatibility of the sequence to the structure, thus yielding possible 3-D models.

2.4 The ion channel-cotransporter controversy

The classical biophysical studies undertaken by Hodgkin and Huxley to explain sodium and potassium permeability in neurons, postulated that ions were carried across the membrane rather than moving through a pore (Hille, 2001). At the outset, therefore, there was not a real theoretical distinction between channels and carriers. The Hodgkin and Huxley model treated channels like carriers with simulations able to fit the their experimental data (Hille, 2001). Only in 1952 Widdas introduced for the first time the concept of cotransporter, whereby one species drives the transport of another, establishing for the first time a different nomenclature for carriers and channels (Widdas, 1952). The further adoption of enzymatic theory and carrier kinetics for cotransporters was responsible for the theoretical division in explaining the different behaviour of channels and carriers, electro-diffusion and enzyme theory respectively. Finally, the different methodologies

applied to characterize channels (electrical measurements) and carriers (radiolabelled tracer flux), were the final steps to define a division that is still present today (Defelice, 2004).

Classically, the main difference between channels and carriers is the flux rate for the solute moving across the membrane, up to 10^8 ions s^{-1} in the former case, whereas carriers exhibit a solute translocation rate in the range of 10-50,000 particles s^{-1}. The main reason for this difference is thought to be the conformational change underlying the substrate translocation across the membrane in transporters and which is absent in channels. The dogma began to blur in the last decade with the introduction of high-resolution electrophysiology (patch clamp) techniques that demonstrated the existence of channel-like currents in cotransporters. Almost every cotransporter studied exhibits ion channel properties: glutamate and dopamine cotransporters harbor chloride selective channels (Carvelli et al., 2004); GABA; serotonin and norephinephrin cotransporters contain sodium and lithium channels, respectively (Galli et al., 1998; Galli et al., 1997; Lester et al., 1996; Petersen and DeFelice, 1999). Recently it was reported that the bacterial ClC homologue is not simply an ion channel as originally imagined (Maduke et al., 1999), but rather acts as a H^+-Cl^- exchange transporter with a likely stoichiometric ratio of 2 Cl^-/H^+ (Accardi and Miller, 2004). Significantly a simple mutation returned it to pure chloride selectivity with a channel-like properties (Dutzler et al., 2003). Finally, Bezanilla and colleagues recently proposed that the operation of the voltage sensor of the voltage-gated Shaker K^+ channel could be analogous to a transporter with "tethered" substrates (the mobile charge associated with arginine residues), such that the accessibility to a "binding site" alternates between the inside and outside with each transport cycle (Chanda et al., 2005).

These findings have blurred the distinction between channels and carriers, necessitating a revision of the classical view. At least two possibilities arise: cotransporters might obey enzyme theory when they are active, but occasionally slip into a passive channel mode; alternatively, they may obey channel theory and rely on flux coupling for their secondary activity (Defelice, 2004). The controversy will only be solved by combined studies that involve crystallography, structure-function and kinetic models. The importance of the latter will now be discussed.

2.5 Kinetic models for secondary active carriers

A useful approach to understanding membrane transport mechanisms is by means of a model that describes the essential features of the transport cycle derived experimentally. The model should not only provide a qualitative description of the transport process, but also offer a quantitative tool that can be used for simulating the transport mechanism and even predicting

kinetic behaviour that may not have been observed experimentally. In essence, such models are the result of a reductionist approach that simplifies a highly complex multivariant system -the transport protein- down to an analytically manageable number of kinetic states that the protein is assumed to occupy. Physically these states might represent unique, kinetically stable molecular conformations that the protein occupies and which can be defined in terms of external parameters, e.g. substrate concentration, membrane potential, temperature etc. The transitions between these states can be described analytically, for example, by transition rate theory of Eyring (e.g.(Hille, 2001)), whereby a change of state occurs when a certain activation energy level is exceeded and the system proceeds through a transition state.

To date, two main kinetic schemes have been proposed to describe the net flux of solute across the membrane by means of a carrier protein. The alternating access model (Figure 3) considers the transport protein similar to a channel, where the 'pore' contains all the sites that bind, or simply accept, all the permeable substrates. Its two "gates" are alternatively close or open, thereby preventing direct transmembrane solute movement. When the external "gate" is open the first substrate can access its site, the consequence of this step is a conformational change in the protein structure, which would expose other binding sites for the substrates necessary to create the fully loaded complex. In this state, the external "gate" would close, with the consequent occlusion of substrates and binding sites. The instability connected with this event would lead to the opening of the internal "gate" allowing the solutes inside the transport protein to access the cytoplasm. After the substrates are released into the cytoplasm, the transporter returns to its initial state. The alternating access scheme can also account for ordered or random binding in the case of multiple substrates, by defining alternative "routes" by which the system moves between any two states.

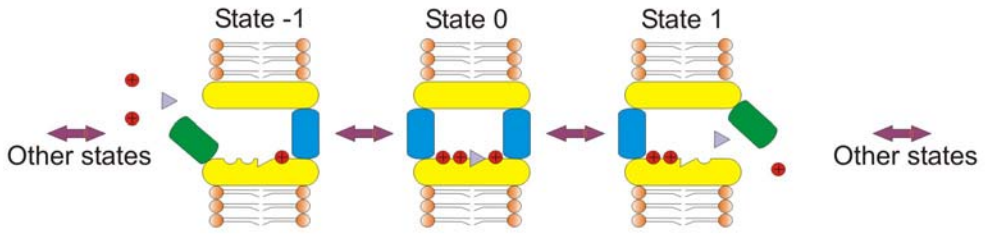

Figure 6: Schematic representation of the alternating access model. The cartoon depicts the individual states from the transport cycle involving the conformational changes responsible for gates opening/closing. (adapted from (Lester et al., 1996))

The alternating access model can explain only some of the properties related to substrate permeation through the transporter, such as transport coupled currents with a strict coupling stoichiometry and transient currents, due to the movement of charges within the membrane electric

field, in the case of electrogenic carriers. However, this model cannot give a satisfactory explanation for other kinetic transport features as leakage currents in the absence of substrate or variable stoichiometry.

To resolve these issues, the multi-substrate single file model has been proposed. This considers the transporter to behave like a channel with all the binding sites linearly distributed through a "pore" structure, similar to the earlier Hodgkin and Keynes model for single file ion movement in a K^+ channel (e.g.(DeFelice et al., 2001)). After the substrate enters the transporter, it can move from one site to the next only if the latter is empty otherwise the substrate must "wait" until one of the surrounding sites is free. This "single file" substrate movement continues up to its exit from the transporter. The multisubstrate single file model does not require large conformational changes as have been previously proposed to take place in the alternating access model. Instead it proposes that the transporter forms a pore that is always open and ready to translocate substrate in a defined direction depending on substrate availability. It also explains the nature of interactions between substrates within the transporter. Finally, this model does not define a sequence of transitions for the transport, but postulates the existence of many possible states accessible to the carrier (Su et al., 1996).

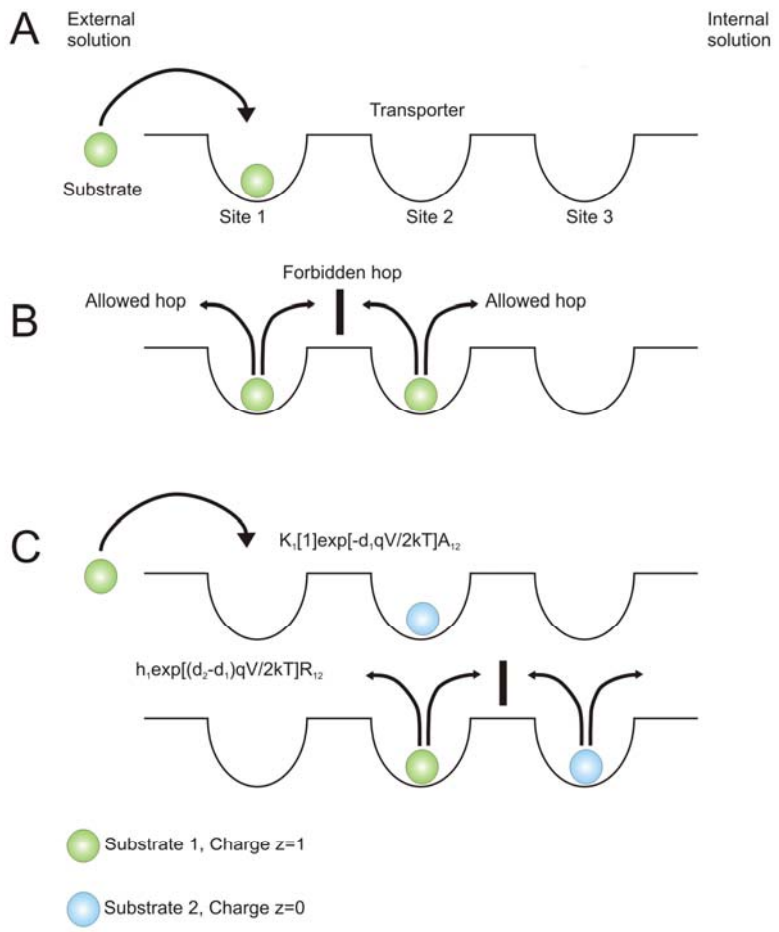

Figure 7: Schematic representation of the multi-substrate single file model. (A) Structure of the transporter, including three binding sites. (B) Allowed hopping events. (C) Rules for obtaining the hopping frequencies, including the effects of voltage and attraction/repulsion (from (Su et al., 1996)).

Both models take into account the effect of membrane potential, which strongly influences the transport rate. An energy barrier separates binding sites and substrates must pass this to proceed in their movement. The free energy associated with these barriers can be modulated by the interaction among the charged substrates and by the external transmembrane electric field.

Recently, a concerted attempt was made to resolve the differences between these two schemes by comparing the behavior of a transport system under a wide range of kinetic conditions (Hilgemann and Lu, 1999; Lu and Hilgemann, 1999a; Lu and Hilgemann, 1999b) applied to the GABA transporter (GAT1) with model predictions**.** This study favored the alternating access model**.** Although these models can be useful for understanding the transport mechanism from a theoretical viewpoint, they inherently lack a link to the real structure and dynamics of the molecule during the transport process.

2.6 The type II Na^+/P_i cotransporters

2.6.1 Phosphorus in living organisms

In eukaryotes and prokaryotes, phosphorus is an essential compound involved in cellular energetics, metabolism, signalling pathways and structures. At the level of higher organisms, such as mammals, the regulation of inorganic plasma phosphate (P_i) levels is an essential requirement for the whole body homeostasis, the chronic disturbance of which can lead to serious pathological conditions. The P_i present in the food intake is absorbed in the small intestine and then transferred to the blood for transport throughout the organism. Subsequently, it is filtered from the blood by the glomeruli and finally 70-80% is reabsorbed from the glomerular filtrate along the proximal tubule and returned to the circulation. The reabsorption of P_i in the proximal tubule is dependent on the luminal Na^+ concentration and on the function of the basolateral Na-K-ATPase that maintains a low intracellular Na^+ (Baumann et al., 1975). This dependency suggests the existence of a secondary active transport mechanism that uses the chemical free energy of Na^+ gradient defined across the apical membrane, to drive the uptake of P_i against its electrochemical gradient (Murer and Biber, 1996; Murer et al., 1998).

In renal P_i *reabsorption* and intestinal P_i *absorption*, the transport task is undertaken by a family of Na^+ dependent secondary active P_i cotransporters located in the luminal (apical) membranes of the respective bush border membranes. The mechanism and specific membrane proteins responsible for the exit of P_i at the basolateral side of these epithelia into the plasma remain to be identified, possible candidates being Na^+/P_i cotransporters, anion exchange or non-specific leak pathways (Murer and Biber, 1998; Murer et al., 2000).

2.6.2 Epithelial Na^+/P_i cotransporters

The proteins responsible for the epithelial P_i transport belong to the family of Na^+-dependent secondary active P_i cotransporters, of which three different types have been identified at the molecular level, the type I, II, and III Na^+/P_i cotransporters (Hilfiker et al., 1998; Murer and Biber, 1996; Murer and Biber, 1997; Murer and Biber, 1998; Murer et al., 2000). All three types showed a high Na^+ dependent P_i uptake when expressed in heterologous expression systems, but they do not show a high homology at the level of their primary amino acid sequence (Murer and Biber, 1997; Murer and Biber, 1998; Murer et al., 2000).

Solute carriers are classified according to the HUGO (the Human Genome Organization) Gene Nomenclature Committee. The new nomenclature was introduced to have uniform and systematic protein naming of those belonging to the Solute Carrier (SLC) series (see: http://www.bioparadigms.org). There are 43 SLC families with overall more than 320 transporter genes (Wright M. W. et al., 2003), of which 3 are Na^+-driven P_i carrier families The type II Na^+P_i cotransporters are grouped in the SLC34 family, which comprises three members designated NaPi-IIa, NaPi-IIb and NaPi-IIc (Murer et al., 2004). Table 1 summarizes the characteristics of the three gene families.

Table 1. Molecular and kinetic properties of the three families of Na^+/P_i cotransporters

Family name	Type I (SLC17)	Type II (SLC34)			Type III (SLC20)
		IIa	IIb	IIc	
Molecule name	NaPi-I rabbit,mouse, human	NaPi-IIa Mouse,rat, Human, rabbit, opossum	NaPi-IIb Mouse, human, Flounder, Xenopus	NaPi-IIc Mouse, human, dog	Glvr-1 (PiT-1) Ram-1 (PiT-2) human, mouse, rat
Amino acids	465	640	690	600	679,656
Function (in Xenopus oocytes)	Na^+/P_i cotransport, Cl^- channel activity, interaction with organic anions	Na^+/P_i cotransport, electrogenic, pH dependent	Na^+/P_i cotransport, electrogenic, pH dependent	Na^+/P_i cotransport, pH dependent electroneutral	Na^+/P_i cotransport, electrogenic
Affinity for Na^+	50-60 mM	50-70 mM	33 mM	48 mM	40-50 mM
P_i	1.0 mM	0.1-0.2 mM	0.05 mM	0.07 mM	0.025 mM
Tissue expression	Kidney cortex/ proximal tubule, liver, brain	Kidney cortex/ proximal tubule	Small intestine, lung and other tissues	Kidney cortex/ proximal tubule	Kidney cortex, bone, liver, heart, brain and other tissues

2.6.2.1 Type I Na^+/P_i cotransporters

The screening of a rabbit kidney library for expression of P_i transport activity in *Xenopus* oocytes led to the identification of the Type I Na^+/P_i cotransporter (SLC17A1) (Werner et al., 1991), which is localized at the brush border membrane of the proximal tubular cells (Biber et al., 1993; Custer et al., 1993). The hydropathy plot analysis of the protein amino acid sequence suggests a monomeric secondary structure comprising six or eight transmembrane domains, with three N-glycosylation sites. Functional assays performed on *Xenopus* oocytes expressing NaPi-I gave a Na^+-dependent P_i uptake (Broer et al., 1998; Busch et al., 1996a; Busch et al., 1996b). Electrophysiological measurements performed on *Xenopus* oocytes expressing NaPi-I suggest a multifunctional activity for this transporter, as a time and dose-dependent chloride conductance was also documented (Broer et al., 1998). A possible interpretation of this observation was that an intrinsic Na^+/P_i cotransport system of the oocyte itself, was modulated by the Type I transporter; in this context SLC17A1 would not be a Na^+/P_i cotransporter, but rather a protein with Cl^- channel-like activity, expressed in the renal brush border membrane. Moreover, this transporter does not show the typical kinetic characteristics (such as the pH dependency) of Na^+-dependent P_i uptake measured from brush border membranes, so that the Type I cotransporter is not the major protein responsible for mediating the P_i transport across the apical membrane of proximal tubular cells (Murer et al., 2000).

2.6.2.2 Type II Na^+/P_i cotransporter family

As for the type I cotransporter, the screening of a rat and human cDNA kidney library, by expression cloning in *Xenopus* oocytes, led to the discovery of type II Na^+/P_i cotransporters (NaPi-II) (Magagnin et al., 1993) and subsequently to the identification of homologous proteins in other organisms based on their sequence similarity. Type II transporters have been further subdivided into NaPi-IIa (SLC34A1), NaPi-IIb (SLC34A2), NaPi-IIc (SLC34A3) according to their molecular and functional characteristics (Murer et al., 2004).

NaPi-IIa is expressed preferentially at the apical membrane of kidney proximal tubular cells and it is the main mediator of renal P_i reabsorption in mammals. The transport kinetics (apparent substrate affinity, substrate dependency of maximum transport rate, pH dependency) of NaPi-IIa expressed in heterologous systems are in close agreement with the original data obtained from brush border membranes (Murer et al., 2004).

In mammals, NaPi-IIb is found ubiquitously in several organs, including lung, small intestine and testis, but not in kidney (Hilfiker et al., 1998; Traebert et al., 1999). However, in the winter flounder, NaPi-IIb is expressed in both kidney and intestine (Kohl et al., 1996).

NaPi-IIc is a third subtype recently cloned from a human and mouse kidney (Segawa et al., 2002). This transporter could play a role during development as it is not as strongly expressed in adult tissue as in young animals.

Hydrophobicity analysis, performed on the primary sequence of the three members of the subgroup, predicts a similar secondary structure. Moreover, the degree of homology for the three subtypes is quite high, especially in the predicted transmembrane domains, which suggests that they preserved regions, whereas the amino- and carboxy- termini have the highest variability. From an evolutionary viewpoint, the type II Na^+/P_i cotransporter appeared quite early in the phylogenetic tree of Na^+/P_i cotransporters, because related genes have been found in *Vibrio cholerae* and *Caenorabditis elegans* (Werner and Kinne, 2001).

2.6.2.3 Type III Na^+/P_i cotransporters

In 1994 the study of the receptors for gibbon ape leukaemia and for the mouse amphotropic retrovirus demonstrated that they were able to mediate Na^+/P_i cotransport when expressed in *Xenopus* oocytes (Kavanaugh and Kabat, 1996; Kavanaugh et al., 1994; Olah et al., 1994). They were named Pit-1 (SLC20A1) and Pit-2 (SLC20A2), and classified as type III Na^+/P_i cotransporters. These transporters are expressed ubiquitously, with related mRNAs found in all segments of the kidney (Olah et al., 1994; Tatsumi et al., 1998; Tenenhouse et al., 1998a; Tenenhouse et al., 1998b). In contrast to type I and type II, type III transporters are expressed in the basolateral membrane of the proximal tubular cells, two orders of magnitude less than the type IIa cotransporters (based on mRNA levels). Therefore, they do not seem to be involved in transcellular P_i, but rather in the uptake of P_i if the entry of luminal P_i is insufficient for cell metabolism (Tenenhouse et al., 1998b).

2.7 Structure-function relationships of type IIa Na^+/P_i cotransporters

2.7.1 Secondary structure and functional unit

The rat isoform of the type IIa Na^+/P_i cotransporter protein has 637 amino acids with a glycosylated apparent molecular weight of 80-90 kDa in native brush border membranes and when expressed in *Xenopus* oocytes (Custer et al., 1994; Hayes et al., 1994). Although previous

radiation-inactivation studies on native membranes suggested that the Na^+-dependent P_i function unit was oligomeric (for review, see (Forster et al., 2002)**,** a function-based study established that the rat isoform of NaPi-IIa was a functional monomer when expressed in *Xenopus* oocytes (Kohler et al., 2000).

The analysis of protein hydropathy plot, based on the Kyte and Doolittle scale, suggests a secondary structure comprising eight transmembrane domains (TMD). In addition, there is a large extracellular loop containing two N-glycosylation sites, a cysteine bridge identified between Cys-306 and Cys-334 and intracellularly located amino- and carboxy- termini (Lambert et al., 2000). An additional cysteine bridge between Cys-225 and Cys-520 is also predicted (Kohler et al., 2003; Lambert et al., 2000). An intrasequence comparison of NaPi-IIa reveals the existence of two regions within the transporter that show high similarity; they are located on the linkers between TMD 2 and 3 (first intracellular loop, ICL-1) and TMD 5 and 6 (third extracellular loop, ECL-3) (Lambert et al., 2000) and an analysis, using the BLAST tool (http://www.ncbi.nlm.nih.gov/BLAST/), for the Na^+/P_i cotransporters reveals that these sequences are highly preserved.

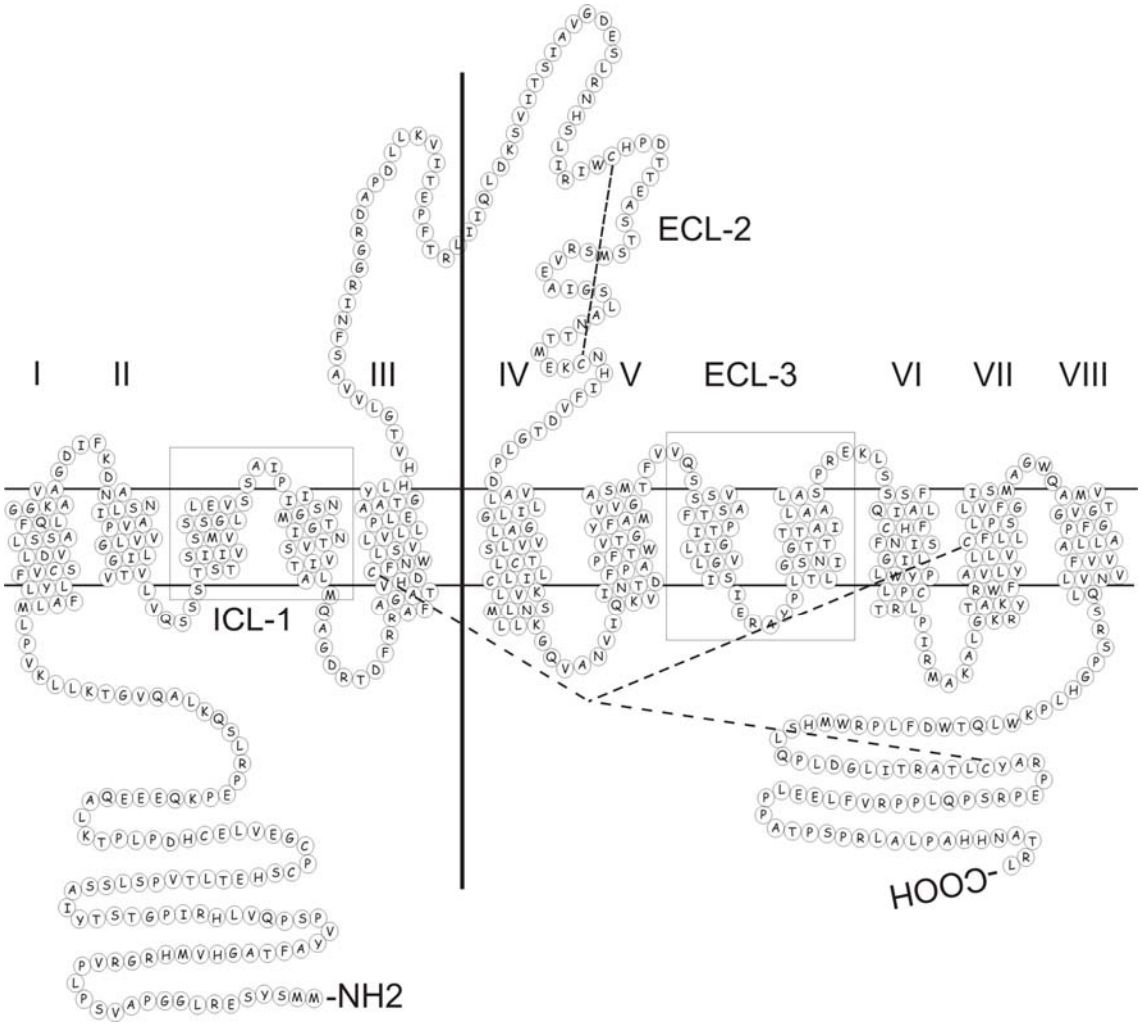

Figure 8: Secondary topology prediction for mouse type II Na^+/P_i cotransporter isoform generated by the HMMTOP program (http://www.enzim.hu/hmmtop/).The two boxed regions contribute to the proposed common transport pathway

formed when the N- and C- terminal halves of the protein are folded together. Stability of the 3-D structure is afforded by two disulfide bridges between Cys-306 and Cys-334 in ECL-2 and between Cys-225 and either Cys-520 or Cys-597.

2.7.2 Steady-state kinetics and stoichiometry

The initial characterization of the type IIa Na^+/P_i cotransporter kinetics was performed using native renal brush border membranes before identification of the protein itself. The basic findings were confirmed in subsequent studies using heterologous systems (mainly *Xenopus* oocytes). Brush border membrane vesicle kinetic studies had suggested a Na^+: P_i stoichiometry of 2:1, based on the sigmoidicity of the Na^+-activation kinetics (Hoffmann et al., 1976). For predominantly divalent P_i (the ratio divalent:monovalent P_i is 4:1 at pH 7.4), this result implied that the brush border transport mechanism was possibly electroneutral. Nevertheless, a study by Samarzija et al. (1983) indicated that in kidney proximal tubules, P_i induced a membrane depolarisation in the presence of Na^+ and, furthermore, Burkhardt et al (1981) showed that P_i induced a change in membrane potential in brush border membrane vesicles when loaded with a potential sensitive dye (Burckhardt et al., 1981; Samarzija et al., 1983). Moreover, it was not clear from these studies whether the transport system had a preference for mono- or divalent P_i. The issues of electrogenicity and substrate preference of type II Na/Pi cotransporters was ultimately resolved with expression cloning of NaPi-IIa and functional studies in *Xenopus* oocytes, where the transport kinetics could be studied under voltage clamp (Busch et al., 1994a; Busch et al., 1995; Forster et al., 1998). If an oocyte expressing NaPi-IIa, is voltage clamped to hyperpolarizing potential, external application of P_i in the presence of 100 mM Na^+, induces an inward current. The magnitude of this current depends on the transmembrane potential as well as the substrate concentration. That this current is a direct measure of the cotransport activity was definitively established by simultaneously measuring P_i uptake and charge translocation on the same oocyte (Forster et al., 1999). This study showed that for the rat NaPi-IIa and flounder NaPi-IIb isoforms, there is a fixed Na^+:P_i stoichiometry of 3:1, and moreover, that the stoichiometry was independent of external pH, so that divalent P_i is the preferred species cotransported.

The typical current voltage relationship for the P_i induced current shows a linear dependence of the current in the physiological range of potentials (-70 to -20 mV). However, outside this range a flattening is observed, which indicates that voltage-independent rate-limiting steps dominate the transport cycle. It is important to note that even at 0 mV (i.e. in the absence of electrical driving force) there is still electrogenic activity. For NaP_i-IIa, the P_i activation curve shows saturation above about 0.3 mM P_i (at pH 7.4, 100 mM Na^+) and follows the Michaelis-Menten kinetics with a K_m of 0.06-0.1 mM P_i, whereas the Na^+ activation shows shows a sigmoidal behaviour with a K_m of 60-80

mM (at 1 mM P_i) (Forster et al., 1998), and a Hill coefficient in the range 2-3, consistent with the 3:1 Na^+:P_i stoichiometry.

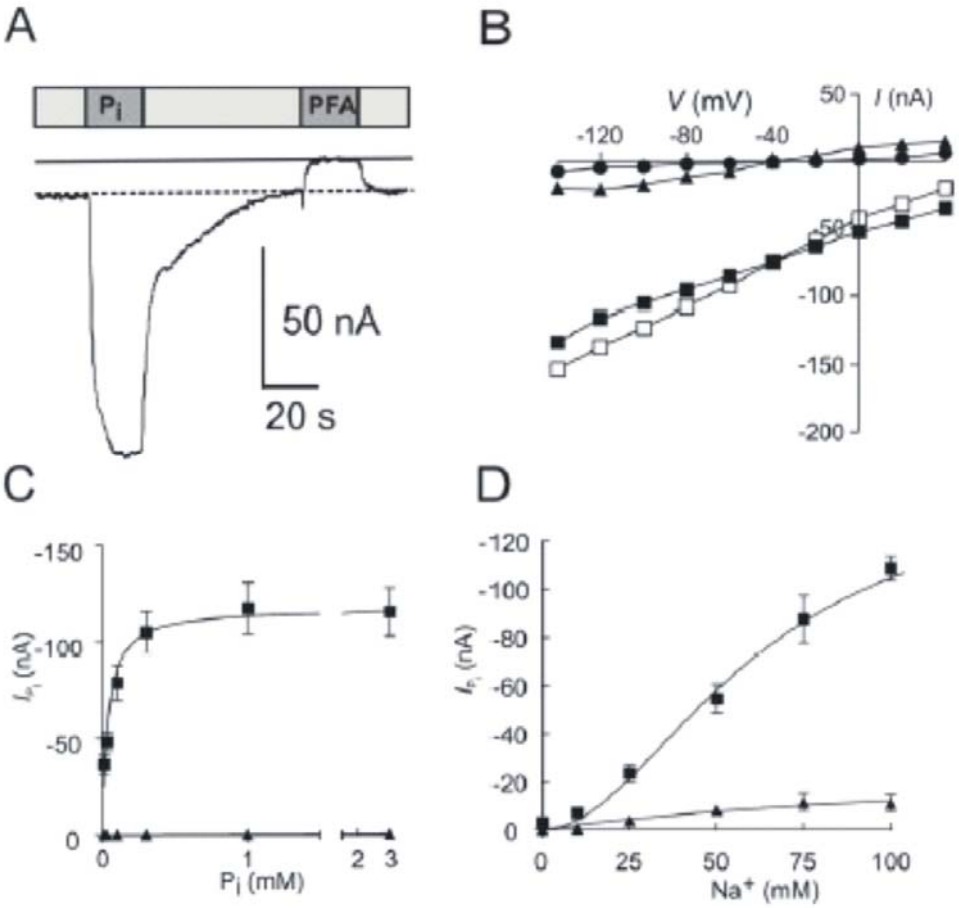

Figure 9: Electrogenic properties of NaPi-IIa under steady-state conditions. (A) P_i activation current recorded from a *Xenopus* oocyte expressing NaPi-IIa, voltage clamped to –50 mV, in the presence of 100 mM Na^+. Application of 1 mM P_i induced an inward current and application of 3 mM PFA induced an upward deflection of the holding current due to blockage of the constitutive Na^+ leak. Continuous line indicates zero transport baseline, dashed line indicates reference current level in the absence of substrate. (B) Current-voltage (I-V) curves. The P_i induced current (I_{P_i}) in the absence (filled circles) and presence (filled squares) of external Na^+ (100 mM), is shown as the change in holding current with and without Pi at each test potential. The constitutive Na^+ leak is quantitated as the difference between the holding current in the absence of substrate and the PFA induced current (filled triangles) in 100 mM Na^+. Addition of the leak current to I_{P_i} gives the true cotransport mode current (open square) according to the current kinetic scheme. (C) P_i activation curve (at –50 mV, in 100 mM Na^+). The curve can be fit with a modified Hill equation, resulting in an apparent $K_m^{P_i}$ of 0.04 mM. Non-injected oocytes gave no significant response to P_i (filled triangles). (D) Na^+ activation curve (at –50 mV, in 1 mM P_i). Each data point is the difference between the P_i induced current and the holding current at the given Na^+ concentration. The data points were fit with a Hill equation, resulting in an apparent K_m^{Na} of 62 mM. In 0 mM P_i, the Na^+ dependency of the constitutive leak (filled triangles) corrected for endogenous effects was best fit with a Michaelis-Menten function giving K_m^{Na} = 150 mM. (Taken from (Forster et al., 2002)).

A competitive inhibitor for brush border membrane Na^+/ P_i cotransport is the antiviral agent foscarnet (phosphonoformic acid, PFA) (al-Mahrouq and Kempson, 1991; Szczepanska-Konkel et al., 1987; Szczepanska-Konkel et al., 1986). In electrophysiological studies this compound inhibits the P_i inward induced current, but does not elicit PFA induced inward currents (Busch et al., 1995) implying that it is not a transported substrate but it can interfere with the P_i binding. For voltage clamped *Xenopus* oocytes expressing NaP_i-IIa, PFA induces a small upward deflection of the holding current. This has been interpreted as evidence of the block by PFA of constitutive leak current through the transporter. In individual oocytes this current is proportional to the P_i induced current, which indicates that it is directly related to the amount of functional NaPi-IIa expressed and it accounts for 10% of the P_i induced component (Forster et al., 1998).

2.7.3 Voltage dependent transitions and pre-steady state relaxations

The voltage dependency of the steady-state cotransport activity implies the existence of voltage dependent transitions within the transport cycle. Voltage dependent kinetics implies that mobile charges, located in the transmembrane electric field are able to sense it and can transduce changes in its energy landscape, thereby driving the protein into a different conformational state. For a fixed number of mobile charges (i.e. fixed number of membrane-localized transporter proteins), we would predict rate limiting, voltage-independent behaviour of the transport kinetics at extreme potentials, as is indeed the case (see above). The exposure of NaP_i-IIa expressing oocytes to voltage step protocols gives rise to transient decaying currents, called presteady-state relaxations that reflect a time-dependent redistribution of charges, consistent with the mobile charge hypothesis. The time integration of the transient current relaxations gives the charge distribution that shows an expected sigmoidal relation with membrane potential. These data can be fit with a single Boltzmann function to estimate the total charge movement and apparent valency, from which an estimate of the transporter turnover can be made (Forster et al., 2002).

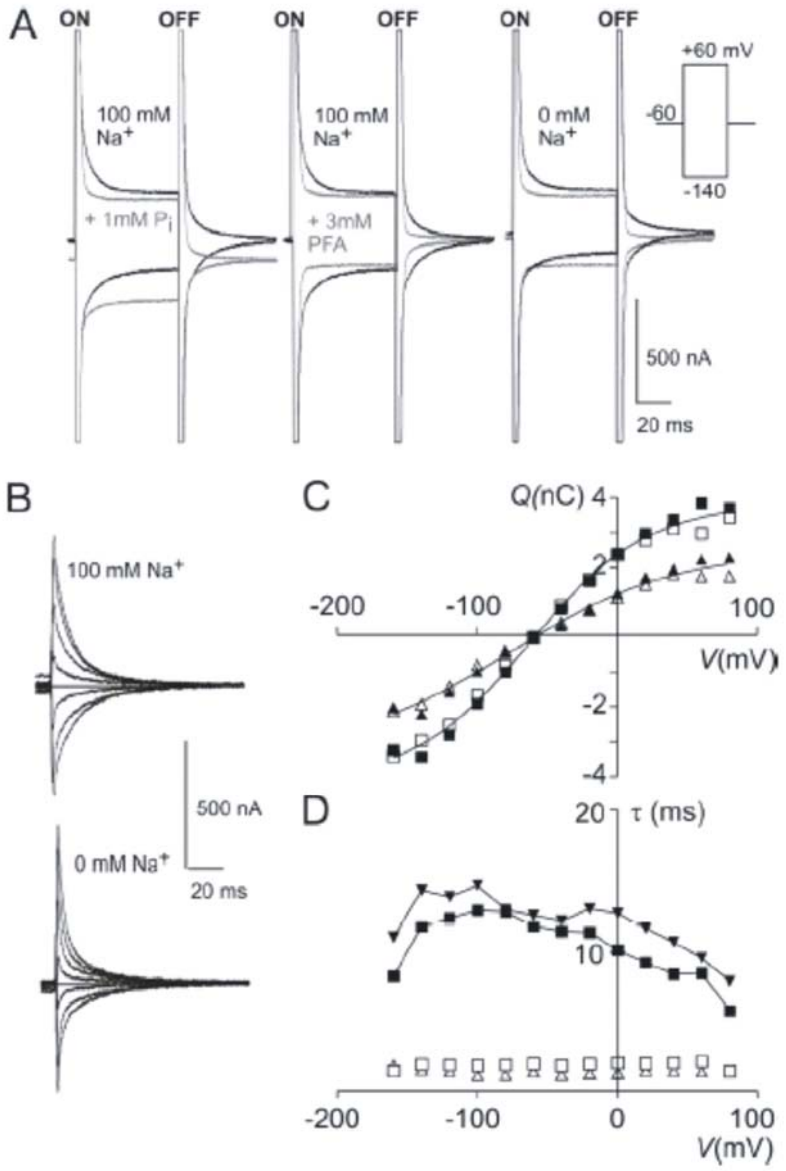

Figure 10: Electrogenic properties of NaPi-IIa under presteady-state conditions. (A) Typical transient current recorded from a *Xenopus* oocyte expressing NaPi-IIa under different superfusion conditions in response to a voltage step from -60 mV to voltages in the range of –140 mV to +60 mV. Presteady-state relaxations are superimposed on the oocyte endogenous charging current that lasts approximately 1 ms. Superfusion in 100 mM Na^+ with 1 mM P_i (left panel) and 3 mM PFA (center panel) suppresses relaxations (grey traces). In 0 mM external Na^+, relaxations reflect charge movements associated with the empty carrier (right panel). PFA data have been superimposed (grey traces) for comparison. (B) Elimination of endogenous components in the record of (A) by subtracting the PFA records and adjusting baselines, shown for ON steps of two superfusion conditions for voltage steps from a holding potential of –60 mV to voltages in the range of –160 to +80 mV. (C) Integration of the relaxations in (B) gives the charge (Q) as a function of V (Q-V curve) for superfusion in 100 mM Na^+ (squares) and 0 mM Na^+ (triangles). The data were fit with a single Boltzmann function

$Q = Q_{hyp} + Q_{\max} /(1 + \exp(-ze(V - V_{0.5})/kT)$, where *z* is the apparent valency for an equivalent charged entity that moves across the whole membrane field, $V_{0.5}$ is the voltage at which 50% of the charge hase been translocated, *Q*max is the total charge available to move and Q_{hyp} is the charge moved at the hyperpolarizing limit from a given holding

potential. Charge conservation is confirmed by the good agreement between ON (filled symbols) and OFF (open symbols) charge movements. The fit parameters (values for 0 mM in parentheses) are: Q_{max} = 8.0 (5.8) nC; $V_{0.5}$ = -63(-76) mV and z = 0.60(0.43). (D) The relaxations in (B) were best described by fitting them with a double exponential function to give the time constants for the ON step (τ) as a function of V for superfusion in 100 mM Na^+ (squares) and 0 mM Na^+ (triangles). The slow components (filled symbols) for both superfusion conditions show voltage dependence, whereas the fast components (open symbols) are very weakly voltage dependent and represent the limit of detection using the two-electrode voltage clamp. (Taken from (Forster et al., 2002)).

2.7.4 pH dependency of NaPi-II kinetics

NaPi-IIa transport activity is strongly dependent on pH, as it is suppressed in acidic environments (Busch et al., 1994a; Forster et al., 2000; Hartmann et al., 1995; Virkki et al., 2005). A pH change from 7.4 to 6.2 results in a 60-80% loss of cotransport activity. The effect of protons on the NaPi-IIa kinetics is complicated by the titration of divalent to monovalent P_i under acidic pH conditions. Steady-state measurements suggest a competitive interaction of H^+ with the last Na^+ binding transition (Forster et al., 2000) and an interaction with the first Na^+ binding transition that precedes P_i interaction (Virkki et al., 2005). A third effect, connected with protons, is their direct interaction with the empty carrier with the subsequent alteration of its reorientation kinetics. A study using chimeric constructs between the more pH sensitive NaPi-IIa and less pH sensitive NaPi-IIb (both cloned from mouse) and single point mutagenesis (de la Horra et al., 2000), identified residues responsible for the pH sensitivity. This was also confirmed by subsequent cysteine scanning in the same region (Lambert et al., 2001). Recent studies also indicate that protons can modulate the apparent P_i and Na^+ affinities of the human NaPi-IIa isoform, strengthening the idea of an interaction between protons and the binding sites for P_i and Na^+ (Virkki et al., 2005).

2.7.5 An eight-state model for NaPi-IIa

The kinetic data obtained from the two-electrode voltage clamp studies led to the generation of an eight state alternating access model for NaP_i-IIa (Figure 11). Four states are considered "outward" facing (1, 2, 3, 4) that correspond to four conformations in which the protein exposes binding sites to the extracellular milieu. The remaining 4 states correspond to "inward" facing conformations. In this scheme, the charge associated with the empty carrier (transitions 1-8) is

assumed to have a valency of -1 and can interact with one Na^+ ion at the extracellular surface. The displacement of this intrinsic negative charge at hyperpolarizing potentials increases the probability of occupying state 1. At least two voltage dependent partial reactions have been identified from studies of the presteady-state kinetics: the interaction between the first Na^+ ion and the transporter (transition 1-2) and the reorientation of the empty carrier (transition 8-1). After binding of the first Na^+ ion to the transporter, the carrier translocates this ion (transitions 2-7) in an electroneutral step (transitions 2-7) and this was proposed to constitute the uncoupled Na^+-leak that is blockable by PFA. This first Na^+ interaction is fundamental for the cotransport to occur as it allows the subsequent interaction with HPO_4^{2-} (or the inhibitor PFA) with the protein (transitions 2-3). This is also consistent with the finding from steady-state kinetics that the apparent affinity for P_i is dependent on Na^+ concentration, i.e. ordered substrate binding. The last transition in the outward facing orientation is the formation of the fully loaded complex with two more Na^+ ions (transitions 3-4). From state 4 the carrier can proceed to state 5 through an electroneutral transition.

Experimentally, it has been shown that NaP_i-IIa exhibits two transport modes that involve two cycles sharing the empty carrier and first Na^+ ion interactions: a leak mode (cycle: 1-2-7-8) and the cotransport mode (cycle: 1-2-3-4-5-6-7-8) that appear to be mutually exclusive. The Na^+ leak is blocked by PFA and from studies on NaPi-IIa proteins that contain cysteine substitutions at functionally important sites (Kohler et al., 2002a; Lambert et al., 1999), it was proposed that saturating P_i also blocks the leak mode, consistent with the current kinetic scheme (Figure 11**)**. In the presence of P_i, the transport cycle proceeds to states 3 and 4 in its cotransport mode. The net result of one complete cycle is the inward movement of a single positive charge, due to the reorientation of the charged (-1) empty carrier (Forster et al., 1999; Forster et al., 2002). The net charge movement has been established experimentally using simultaneous uptake and charge movement on individual oocytes (Forster et al., 1999) (Figure 10).

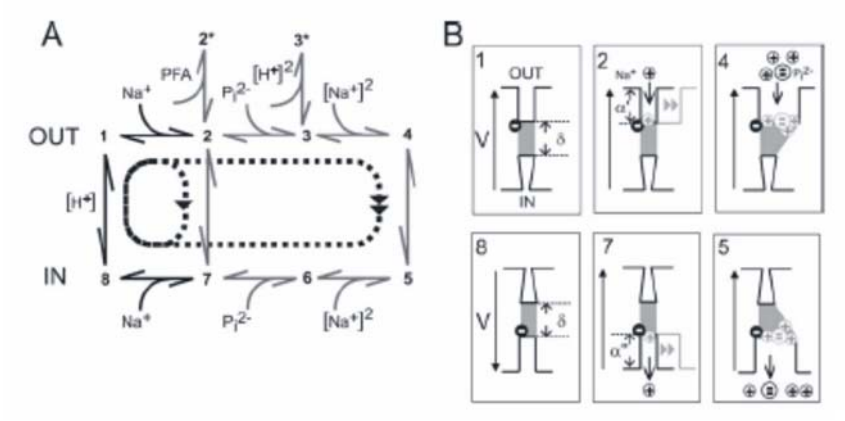

Figure 11: A kinetic scheme for NaPi-IIa. (A) The model shows eight main conformational states and the two transport cycles for the Na^+ leak and the cotransport mode (see text for details). Two additional states (2* and 3*) account for the effect of PFA and protons, respectively. (B) Cartoon of the proposed translocation steps for NaPi-IIa consistent with the scheme in (A). The first Na^+ ion is assumed to bind at a site within the transmembrane electric field, an electrical distance α'or α''from the external and internal surfaces, respectively. The mobile intrinsic charges of the empty carrier are represented as a single negative charge that moves an electrical distance δ through the transmembrane field. This leads to exposure/occlusion of the access to the translocation pore. (From (Forster et al., 2002)).

2.8 Structure-function studies on NaPi-IIa using SCAM

The application of SCAM (Section 2.3.1) has led to the confirmation of topological features of NaPi-IIa as well as the identification of functionally important sites associated with the transport pathway. The finding of a site (Ser-460) in the 3rd predicted extracellular loop (Figure 8), which when mutated to a cysteine, could be modified by external MTS reagents (Lambert et al., 1999), paved the way for further SCAM studies in ECL-3 (Kohler et al., 2002a; Kohler et al., 2002b; Lambert et al., 2001) and the 1st intracellular linker (ICL-1) (Kohler et al., 2002a). In the former case, a periodic MTS accessibility of neighboring residues was compatible with the existence of short α-helical segment. From these studies, a putative transport pathway architecture was proposed that involves these two re-entrant loops, analogous to the "hourglass" structure proposed for aquaporin (e.g.(Murata et al., 2000)). That these loops contain a repeat sequence (Ehnes et al., 2002), preserved among all NaPi-II isoforms, as well as the prokaryotic homolog from *vibrio cholerae*, further underlies their potential importance as representing key functional elements in the protein. The SCAM studies also highlighted areas of the protein that determine other kinetic characteristics such as voltage and pH dependence. Of particular importance was the property of one site (Ser-460), which when mutated to a cysteine, could be modified by MTS reagents and resulted in loss of cotransport function, but preservation of the leak mode (Lambert et al., 1999).

2.9 Unresolved aspects of the NaPi-II transport kinetics

The kinetic and structure-function studies referred to in Section 1.7 began to reveal important structure-function relation of type II Na^+/P_i transporters. These studies established that the functional unit for Na^+/P_i transporters is the monomer and also revealed voltage and pH dependent transitions in the transport cycle. Taken together, these studies were used to test and reinterpret the original eight state kinetic model proposed by Forster (e.g. (Kohler et al., 2002b; Virkki et al., 2005). Although the generation of a functional model is a fundamental step towards the understanding of the different features for type II Na^+/P_i transporters, many aspects are still unknown and/or unclear. Identification of the elements involved in defining the substrate binding sites, the kinetics of the internal transitions (order of debinding, apparent substrate affinities), elements that define the voltage dependent behaviour and and transport stoichiometry, and the nature of the leak pathway are just a few of the aspects that remain to be addressed.

2.10 Aims of the study

The work presented in this PhD thesis comprises two parts based on the following aims:

1) Identification of the molecular determinants of electrogenicity/electroneutrality of type IIa and c Na^+/P_i cotransporters, respectively;

2) Understand the nature of the uncoupled leak current observed in electrogenic type II Na^+/P_i cotransporters

Type IIa and type IIc transporters show high sequence identity (46.5% identity; 61.7% similarity; 13.8% gap) but a strikingly different kinetic phenotype: type IIa is electrogenic whereas type IIc is electroneutral. I took advantage of this clear kinetic difference to address aim 1. My first approach was to engineer the proteins by constructing a group of chimeras between the two isoforms. The main conclusion of this analysis was that the first six TMDs and the interconnecting loops were important for the electrogenicity of NaPi-IIa. Secondly, a bioinformatics analysis involving a sequence comparison between members of type IIa, IIb and IIc Na^+/P_i transporters identified three main clusters of highly preserved amino acids (>90% preservation); these residues were different in the NaPi-IIc sub-group. Finally, I made point mutations in the cluster in which there was a transition from a charged (in NaPi-IIa) to a non-charged amino acid (NaPi-IIc). Two

additional point mutations were required at neighboring sites in the 3rd TMD to confer electrogenicity to NaPi- IIc.

In the second study, the temperature-dependent kinetics of the cotransport and leak modes of an electrogenic type II Na^+/P_i cotransporter were determined. This study used the high-expressing flounder NaPi-IIb isoform using conventional two-electrode voltage clamp for acquiring both steady-state and presteady-state current data. The main conclusion of this study is that the kinetics of the leak and transport modes show different temperature dependencies, which suggested that different molecular events could be responsible for the two transport modes of electrogenic type II Na^+/P_i cotransporters.

3. METHODS AND RESULTS

Publication that contributed to this work:

Paper 1:

Renouncing electroneutrality is not free of charge: Switching on electrogenicity in a Na^+-coupled phosphate cotransporter.

Methods used:

i) Single point mutagenesis
ii) Two electrode voltage clamp
iii) Bioinformatic analysis
iv) Radiotracer uptake

Paper 2:

Structure-function relations of the first and fourth predicted extracellular linkers of the type IIa Na^+/Pi cotransporter:

I:Cysteine scanning mutagenesis

Methods used:

i) Single point mutagenesis
ii) Two electrode voltage clamp
iii) Biotinylation assay
iv) SCAM
v) Radiotracer uptake

Paper 3:

Structure-function relations of the first and fourth extracellular linkers of the type IIa Na+/Pi cotransporter:

II. Substrate interaction and voltage dependency of two functionally important sites

Methods used:

i) Single point mutagenesis
ii) Two electrode voltage clamp
iii) SCAM
iv) Radiotracer uptake

Paper 4:

Functionally important residues in the predicted 3rd transmembrane domain of the type IIa sodium-phosphate cotransporter (NaPi-IIa)

Methods used:

i) Single point mutagenesis

ii) Two electrode voltage clamp

iii) SCAM

iv) Western blot

v) Radiotracer uptake

Paper 5:

Temperature-dependent kinetics of the cotransport and leak modes for the flounder type IIb Na^+/P_i cotransporter.

Methods used:

i) Two electrode voltage clamp

3.1 Summary of publication:

Renouncing electroneutrality is not free of charge: Switching on electrogenicity in a Na^+-coupled phosphate cotransporter

Der Verzicht auf Elektroneutralität ist nicht gratis: Der Umschaltung der Elektrogenizität in einem Na^+-gekoppelten Phosphatcotransporter

Renale Typ IIa Na^+-gekoppelte anorganische Phosphat(Pi)-Cotransporter (NaPi-IIa) vermitteln einen divalenten elektrogenen Pi-Transport. Obwohl die renale Typ IIc-Isoform (NaPi-IIc) eine hohe Sequenz-Identität zu NaPi-IIa aufweist ist ihr Transport elektroneutral. Kombinierte Aufnahmemessungen ($^{32}Pi/^{22}Na$) bestätigen, dass NaPi-IIc einen Na^+-gekoppelten Pi-Transport mit einer 2:1 (Na^+:Pi) Stöchiometrie statt einer 3:1 Stöchiometrie, wie sie bei NaPi-IIa vorliegt, aufweist. Diese Ergebnisse deuten darauf hin, dass die Elektrogenizität von NaPi-IIa, verglichen zu NaPi-IIc, von der Interaktion mit einem zusätzlichen Na-Ion herrührt. Um die molekularen Elemente die für den funktionellen Unterschied verantwortlich sind zu identifizieren, benutzten wir Chimeren- und Aminosäurenaustauschmethoden. Die Transportaktivität der Chimeren, die aus NaPi-IIa und NaPi-IIc konstruiert wurden zeigte, dass die Aminosäurereste der ersten sechs Transmembrandomänen essentiell für die Elektrogenizitaet von NaPi-IIa sind. Sequenzvergleiche zwischen den elektrogenen und elektroneutralen Isoformen offenbarten Unterschiede in Ladung und Polaritaet der Aminosäuren, die in drei Zonen dicht gebündelt sind von denen eine die vorhergesagte dritte Transmembrandomäne enthält. Hier führte die Substitution von drei Aminosäuren im NaPi-IIa durch ihre Äquivalente des NaPi-IIc zu einem Transporter, der ein 1:1 Verhältnis zwischen Ladung und Pi hat, eine 3:1 Na:Pi –Stöchiometrie und transiente Ströme aufweist, welche „Pre-steady-state Relaxationen“ ähneln. Die im Vergleich zum NaPi-IIa schwächere Spannungsabhängigkeit und 10fach niedrigere Pi-Affinitaet der Mutanten, deutet darauf hin, dass es andere Aminosäurereste gibt, die wichtig für die NaPi-IIa-Kinetik sind. Unsere Ergebnisse demonstrieren, dass wir durch eine minimale Anzahl von Seitenkettensubstitutionen ein Umschalten von elektroneutraler zu elektrogener Cotransporterfunktion bewirken können, welcher mit dem Auftreten einer Kosubstratinteraktionsstelle zusammenhaengt.

Renouncing electroneutrality is not free of charge: Switching on electrogenicity in a Na^+-coupled phosphate cotransporter

Andrea Bacconi, Leila V. Virkki, Jürg Biber, Heini Murer, and Ian C. Forster*

Institute of Physiology and Center for Integrative Human Physiology, University of Zürich, Winterthurerstrasse 190, CH-8057 Zürich, Switzerland

Communicated by Gerhard Giebisch, Yale University School of Medicine, New Haven, CT, July 14, 2005 (received for review April 28, 2005)

Renal type IIa Na^+-coupled inorganic phosphate (P_i) cotransporters (NaPi-IIa) mediate divalent P_i transport in an electrogenic manner, whereas the renal type IIc isoform (NaPi-IIc) is electroneutral, yet it shows high sequence identity with NaPi-IIa. Dual uptake ($^{32}P_i/^{22}Na$) assays confirmed that NaPi-IIc displayed Na^+-coupled P_i cotransport with a 2:1 (Na^+:P_i) stoichiometry compared with 3:1 established for NaPi-IIa. This finding suggested that the electrogenicity of NaPi-IIa arises from the interaction of an additional Na^+ ion compared with NaPi-IIc. To identify the molecular elements responsible for the functional difference between isoforms, we used chimera and amino acid replacement approaches. Transport activity of chimeras constructed with NaPi-IIa and NaPi-IIc indicated that residues within the first six transmembrane domains were essential for the electrogenicity of NaPi-IIa. Sequence comparison between electrogenic and electroneutral isoforms revealed differences in the charge and polarity of residues clustered in three areas, one of which included part of the predicted third transmembrane domain. Here, substitution of three residues with their NaPi-IIa equivalents in NaPi-IIc (S189A, S191A, and G195D) resulted in a transporter that displayed a 1:1 charge/P_i coupling, a 3:1 Na^+:P_i stoichiometry, and transient currents that resembled pre-steady-state relaxations. The mutant's weaker voltage dependency and 10-fold lower apparent P_i affinity compared with NaPi-IIa indicated that other residues important for the NaPi-IIa kinetic fingerprint exist. Our findings demonstrate that, through a minimal number of side chain substitutions, we can effect a switch from electroneutral to electrogenic cotransporter function, concomitant with the appearance of a cosubstrate interaction site.

Secondary-active transporter proteins mediate uphill transport of a solute by tapping into the free energy provided by the concentration gradient of a coupled ion that is specific to the transporter protein (e.g., H^+, K^+, or Na^+). The coupling between driving and driven species confers a strict stoichiometric ratio on cotransport function. When stoichiometrically coupled movement of net charge accompanies cotransport, an additional driving force is available, derived from the free energy established by the transmembrane electric field. For such electrogenic cotransporters, it follows that membrane voltage also becomes a kinetic determinant of the transport mechanism; moreover, under physiological conditions, it can serve to enhance the concentrating ability of the transport protein.

One of the many physiologically important transport processes that rely on a secondary active mechanism is reabsorption of inorganic phosphate (P_i) in the renal proximal tubule. Two isoforms of type II Na^+-coupled P_i cotransporters (NaPi-II), both localized at the proximal tubule apical brush border membrane, have been identified. Both cotransporters mediate inward transport of P_i by using the inwardly directed Na^+ gradient (1, 2). Type IIa cotransporters (SLC34A1 or NaPi-IIa) couple three Na^+ ions to the cotransport of one divalent P_i ion, and each transport cycle is accompanied by the inward translocation of one net positive charge (3, 4). The NaPi-IIa cotransport rate is strongly dependent on transmembrane potential. This dependency is hypothesized to result from voltage-dependent transitions between favored conformational states of the protein that include the interaction of one Na^+ ion with intrinsic mobile charges of the NaPi-IIa protein (4–9).

In contrast, renal type IIc cotransporters (SLC34A3 or NaPi-IIc) (2, 10) mediate electroneutral Na^+-coupled P_i cotransport yet, with respect to other steady-state transport parameters (e.g., apparent substrate affinities and pH dependency), resemble NaPi-IIa. Consistent with electroneutral cotransport of divalent P_i, it has been proposed that NaPi-IIc cotransports with a 2:1 Na^+/HPO_4^{2-} stoichiometry (2, 10). It follows that NaPi-IIc may lack one of the three Na^+ binding sites postulated for NaPi-IIa. So far, neither the absence of a Na^+ binding site nor the stoichiometry have been experimentally established. Topological prediction algorithms indicate no significant differences between NaPi-IIa and NaPi-IIc (4), which suggests that their respective transmembrane topologies are most likely identical. Moreover, a sequence comparison of NaPi-IIa and NaPi-IIc indicates a high degree of similarity (10), particularly in the predicted transmembrane domain (TMD) regions. These findings imply that only small changes in the amino acid sequence may be required to perform a functional switch between the electrogenic and electroneutral behavior, together with a concomitant change in the stoichiometry.

To identify the molecular elements responsible and gain insight into the underlying mechanism that confers electrogenicity to NaPi-IIa, we took advantage of the functional difference between the NaPi-IIa and NaPi-IIc isoforms by engineering complementary chimeras between each isoform and expressing these in *Xenopus* oocytes. We then refined the localization procedure by using a bioinformatic approach. This approach led to the identification of three residues in the predicted third TMD (TMD-3) that are conserved in all electrogenic NaPi-II transporters so far identified. By substituting the equivalent NaPi-IIa amino acids at these sites in the NaPi-IIc sequence, functional expression of this transport protein in *Xenopus* oocytes displayed Na^+-dependent P_i-induced steady-state currents and voltage step-induced transient currents, neither of which were observed in oocytes that expressed the WT NaPi-IIc. Our findings document that TMD-3 mutations transformed the electroneutral NaPi-IIc into an electrogenic cotransporter, and we propose that the electrogenicity results from an increase in the number of Na^+ ion binding sites from two to three.

Materials and Methods

Molecular Biology. Chimeras were based on mouse NaPi-IIa (in pSport) and mouse NaPi-IIc (in pT7T3D-Pac, a kind gift from K.-I. Miyamoto, Tokushima University, Tokushima, Japan). To obtain the NaPi-IIa and NaPi-IIc fragments, we introduced new restriction sites at the junctions. The necessary amino acid substitutions were located in predicted TMD linkers, where substitutions are usually well tolerated (11). Mutagenesis and cRNA preparation were

Abbreviations: P_i, inorganic phosphate; NaPi-II, type II Na^+-coupled P_i cotransporter; TMD, transmembrane domain; PFA, phosphonoformic acid; NI, noninjected; *I–V*, current–voltage.

*To whom correspondence should be addressed. E-mail: iforster@access.unizh.ch.

performed as described in ref. 9. Oocytes were injected with 50 nl of water or with 50 nl of water containing 10 ng of cRNA.

Reagents and Solutions. The solution compositions were as follows. Control superfusate (ND100): 100 mM NaCl/2 mM KCl/1.8 mM $CaCl_2$/1 mM $MgCl_2$/10 mM Hepes-Tris, pH 7.4, unless otherwise stated. For pH <6.2, Mes was substituted for Hepes. Na^+-free superfusate (ND0): as for ND100 with isosmotic substitution of choline Cl for NaCl. Solutions with intermediate Na^+ concentrations were prepared by mixing ND0 and ND100 in appropriate proportions. Substrate test solutions: P_i was added from 1 M K_2HPO_4 and KH_2PO_4 stocks premixed to give the required pH. Phosphonoformic acid (PFA) was added from 100 mM stock.

Functional Assays and Data Analysis. Uptake assays (^{32}Pi and ^{22}Na) are described in refs. 3 and 9 and typically involved 5–9 oocytes per group. For the dual $^{32}P_i/^{22}Na$ uptake, the Na^+ concentration was lowered to 40 mM to achieve a high enough specific activity for ^{22}Na with 2 mM total P_i. Electrophysiology was performed with a two-electrode voltage clamp (5). Simultaneous uptake and electrophysiology were performed on single oocytes with a chamber designed by D. D. F. Loo (University of California, Los Angeles), which was perfused at 50 μl/min with a peristaltic pump (3). Steady-state current–voltage (I–V) relations were determined by using a voltage staircase from −120 mV to +40 mV with 100-ms steps (5) and by subtracting the control response in the absence of substrate from the test response.

The P_i and Na^+ activation kinetics were determined as described in ref. 8. Proton dependency was determined in ND100 with pH ranging from 5.0 to 8.0 and total P_i adjusted to give 1 mM divalent P_i. Transient currents were acquired by using voltage steps from a holding potential (V_h) = −60 mV to test potentials in the range −160 mV to +80 mV as described (9). Charge (Q) was quantified by fitting a single exponential commencing ≈6 ms after the step onset, extrapolating this to the step onset, and performing numerical integration.

Data points are shown as mean ± SEM. Curve fitting to data points was performed by using nonlinear regression analysis (PRISM, GraphPad, San Diego).

Results and Discussion

Dual Uptake Assays Establish That NaPi-IIa and NaPi-IIc Have Different Stoichiometries. In two previous studies, the cotransport stoichiometry of rat NaPi-IIa, flounder NaPi-IIb (3), and human NaPi-IIa (9) isoforms were determined under voltage clamp conditions and yielded a Na/P_i/charge ratio of 3:1:1. This ratio is consistent with the inward translocation of one net charge per transport cycle, given that divalent P_i is the preferred species transported. To determine the stoichiometry of the electroneutral NaPi-IIc, we performed a dual uptake ($^{32}P_i$ and ^{22}Na) assay at pH 7.4 and plotted ^{22}Na uptake against $^{32}P_i$ uptake for each oocyte (Fig. 1). The fitted slope of a linear regression line was 2.0 ± 0.2 for n = 19 oocytes from three donor frogs, which was consistent with electroneutral cotransport of two Na^+ ions for each HPO_4^{2-} ion.

To investigate whether membrane potential influenced the rate of $^{32}P_i$ uptake by NaPi-IIc, we performed a $^{32}P_i$ assay on individual oocytes that were voltage-clamped at −20 or −80 mV. NaPi-IIc expressing oocytes clamped to −20 mV gave an uptake rate (expressed as pmol per oocyte per minute) of 42 ± 8 (n = 9) compared with 44 ± 8 (n = 9) at −80 mV. Control oocytes from the same donor frog gave uptakes of 6 ± 3 (n = 4) and 3 ± 1 (n = 4) at −20 mV and −80 mV, respectively. These data confirmed that in this voltage range, the NaPi-IIc cotransport cycle did not include rate-determining voltage-dependent transitions (12).

Chimeras Localize NaPi-IIa Electrogenicity to Sites in the First Six TMDs. To identify the molecular elements that distinguish the electrogenic and stoichiometric properties of NaPi-IIa from those

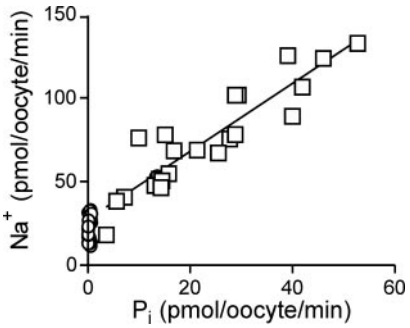

Fig. 1. NaPi-IIc has a 2:1 cotransport stoichiometry. Dual $^{22}Na/^{32}P_i$ uptake assay data for oocytes expressing NaPi-IIc (□) and control oocytes (○) from the same donor frog. Slope of linear regression line: 2.0 ± 0.2.

of NaPi-IIc, our first strategy was to engineer chimeras between each cotransporter. The chimeras were based on a consensus topological model for NaPi-II proteins comprising eight TMDs and intracellular N and C termini predicted by a hydropathy analysis (4) (Fig. 2*A*). We split the primary sequences at convenient sites in the predicted linker regions to preserve the structural integrity of the TMDs to make six chimeric constructs that comprised complementary sections of the C-terminal and N-terminal parts of each full-length protein (Fig. 2*B*). We also constructed two triple chimeras in which a central portion of NaPi-IIa or NaPi-IIc that comprised five TMDs was inserted between the complementary N terminus plus the first TMD and the C terminus plus the last two TMDs, respectively. For all chimeras, we left intact the native amino acid sequence that included the first intracellular and third extracellular linkers (ICL-1 and ECL-3, respectively) and the two

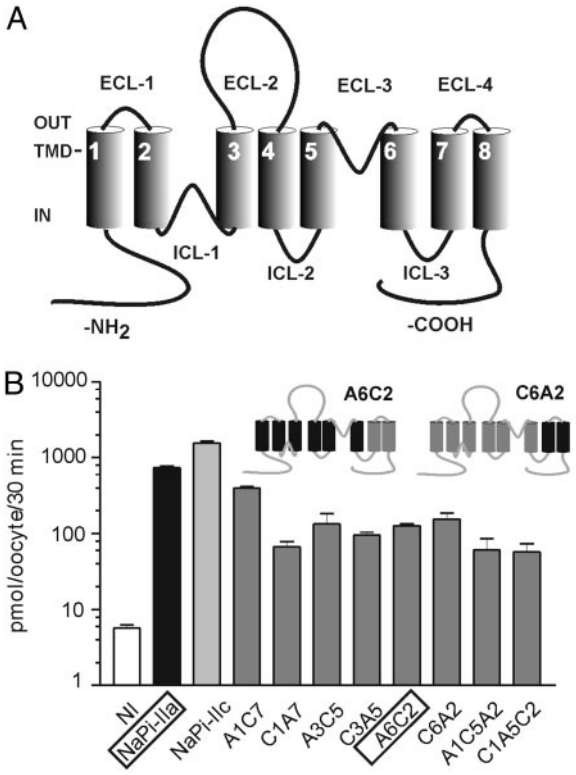

Fig. 2. Chimeras of NaPi-IIc and NaPi-IIa localize elements critical for the NaPi-IIa electrogenic phenotype to TMDs 1–6. (*A*) Topology of NaPi-II protein based on hydrophobicity analysis. (*B*) $^{32}P_i$ uptake of chimeras compared with WT NaPi-IIc and NaPi-IIa. (*Inset*) Example of chimera composition for A6C2 and C2A6.

PHYSIOLOGY

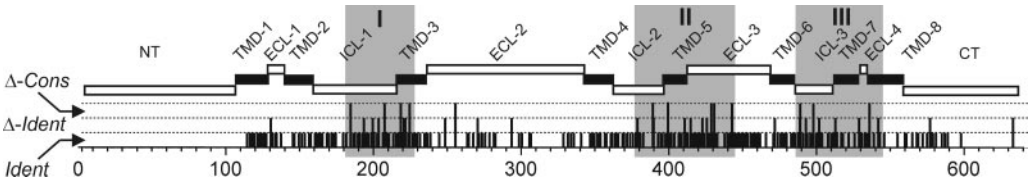

Fig. 3. Sequence comparison of NaPi-IIa/c. Multiple sequence alignment indicates position of residues that are 100% identical in all 21 candidate sequences (*Ident*), changed between putative electrogenic and electroneutral sequences with 100% identity at the respective site (Δ-*Ident*) or changed with conservative substitutions in either or both groups (Δ-*Cons*). Shaded areas (I, II, and III) indicate clusters of changed residues. Residue numbering is according to mouse NaPi-IIa sequence. Topological designation shows position and relative lengths of TMDs and linker stretches as predicted by hydrophobicity analysis. NT, N-terminal; CT, C-terminal.

neighboring TMDs. These linkers are present in all NaPi-II isoforms and are thought to contain structural motifs that define the cotransport pathway (13–15).

The $^{32}P_i$ uptake from oocytes expressing each chimera was noticeably smaller than the uptake obtained from oocytes that expressed either WT transporter (Fig. 2*B*). However, the activity was at least 10-fold higher than noninjected (NI) oocytes from the same donor frog, which indicated that functional chimeras were targeted to the oocyte plasma membrane. Despite this low activity, we expected that P_i-induced electrogenic responses would be detectable over and above any endogenous oocyte activity (3).

Whether chimeras were electrically active or silent allowed us to draw conclusions about the localization of determinants of electrogenicity. First, replacement of the last two TMDs of NaPi-IIa with the corresponding stretch from NaPi-IIc (chimera A6C2) gave a construct that was still electrogenic. Application of 1 mM P_i induced an inward current under voltage clamp [-42 ± 4 nA ($n = 5$) at -60 mV] that was clearly larger than the magnitude of the endogenous response, observed for NI oocytes (typically <5 nA under the same conditions) (data not shown). A6C2 showed a weaker steady-state voltage dependency than the NaPi-IIa WT. For NaPi-IIa, a change in membrane voltage from 0 to -100 mV resulted in an ≈60% increase in P_i-induced current (for an example, see Fig. 4*D*), whereas A6C2 showed only an ≈20% increase (data not shown). Moreover, at -50 mV the estimated apparent affinity for P_i ($K_m^{P_i}$) was 0.82 ± 0.08 mM, which was significantly larger than for WT NaPi-IIa determined from cells from the same donor frog (0.14 ± 0.01 mM). Although the small magnitude of the P_i-induced currents for A6C2 precluded further detailed kinetic characterization, these findings indicated that kinetic determinants of the NaPi-IIa fingerprint, including voltage dependency, were also located within the stretch that included the last two TMDs of NaPi-IIa. As expected, the reciprocal chimera (C6A2) was electrically silent but exhibited $^{32}P_i$ uptake comparable with A6C2. Second, starting from A6C2, we replaced its TMD-1 with that from NaPi-IIc in an attempt to narrow down the critical region. This triple chimera (C1A5C2) showed $^{32}P_i$ uptake comparable with A6C2, but it was electrically silent, which suggested that TMD-1 was also critical for conferring electrogenic behavior to NaPi-IIa. We confirmed this idea by replacement of TMD-1 from NaPi-IIc alone, which gave a functional but electrically silent chimera (C1A7). Moreover, we concluded that TMD-1 from NaPi-IIa was, by itself, insufficient to confer electrogenicity to NaPi-IIc by documenting that the dual (A1C7) and triple (A1C5A2) chimeras were electrically silent. Finally, we retained TMDs 1–3 of NaPi-IIa and replaced TMDs 4–8 of the NaPi-IIa sequence with the corresponding elements from NaPi-IIc. This chimera (A3C5) was functional but electrically silent, which suggested that, in addition to TMD-1, elements critical for the electrogenicity of NaPi-IIa must also reside in the stretch involving TMDs 4–6.

The chimera study indicated that although elements were distributed throughout the protein that contribute to the NaPi-IIa electrogenicity, essential residues were most likely located in the region encompassing TMDs 1–6.

Sequence Alignment Reveals Altered Polarity and Charge of Residues in NaPi-IIc. Our second strategy involved making a multiple sequence alignment of four currently available mammalian NaPi-IIc sequences and 17 sequences of NaPi-IIa as well as NaPi-IIb isoforms, several of which mediate P_i-dependent electrogenic activity when expressed in oocytes (3, 16–19). The alignment showed that, among the 21 sequences (excluding the N and C termini and ECL-2, where large variations are observed between isoforms), ≈75% of residues were 100% identical or in a few cases involved conservative substitutions (Fig. 3, *Ident*). The alignment revealed 22 sites that differed between each group but were 100% identical within the respective group (Fig. 3, Δ-*Ident*). In addition, we identified a further 13 sites that differed between electrogenic and electroneutral transporters and involved conservative substitutions among members of each group (Fig. 3, Δ-*Cons*). Interestingly, the majority of changed sites clustered into three areas (Fig. 3, shaded boxes): cluster I comprised nine residues distributed in the second half of ICL-1 and the first half of TMD-3; cluster II comprised 10 residues in TMD-5 and its neighboring linkers, ICL-2 and ECL-3; and cluster III comprised eight residues distributed within the

Table 1. Changes in residues belonging to clusters from multiple sequence alignment

Cluster	Site	Polarity	Charge
I	A184S/C	+/−	
	I193V	+	
	N199S	−	
	A203S	+	
	A/V207S	+	
	A218S/G	+	
	A220S	+	
	T221A	−	
	D224G/S		−(−)
II	Q378R		+(+)
	T/Q389A	−	
	T/A489G/S	+	
	M410L	+	
	V414L	−	
	S422A	−	
	T425V	−	
	I/V428M	−	
	I/L430V	+	
	T/S442L/F	−	
III	P488L/V	−	
	T492L	−	
	R/H497P		−(+)
	L502F	−	
	F512V	+	
	V528A	+	
	W536G/S	+	
	G541A	−	

Each entry refers to a residue in consensus electrogenic transporters that has been changed in the NaPi-IIc sequence. Numbering refers to mouse NaPi-IIa sequence. +/− indicates increase/decrease in polarity or charge, respectively, according to a hydrophobicity scale (25).

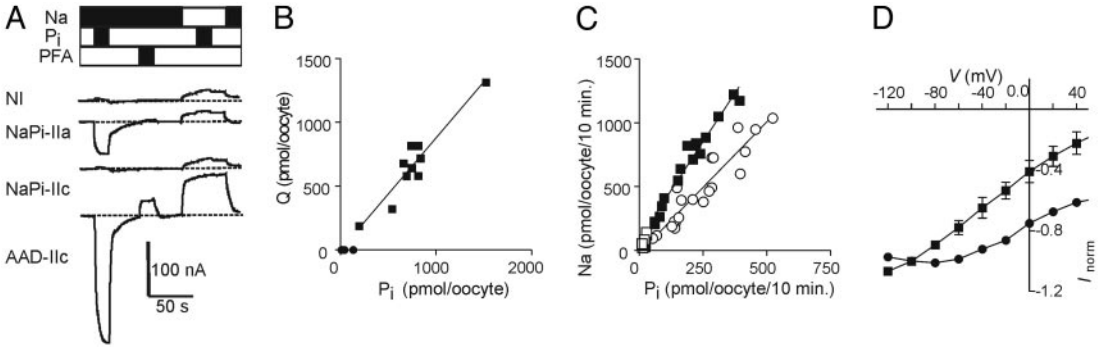

Fig. 4. Steady-state properties of the triple mutant AAD-IIc. (*A*) Representative current tracings of oocytes from the same batch, comparing NI, NaPi-IIc, NaPi-IIa, and AAD-IIc under the superfusion conditions indicated. Na, ND100; P_i, ND100 plus 1 mM P_i; PFA, ND100 plus 1 mM PFA. Oocytes were voltage-clamped at −50 mV. (*B*) Net charge translocated plotted as a function of P_i uptake for individual oocytes expressing AAD-IIc (■) and control oocytes from the same donor frog (●). Slope of linear regression line: 0.9 ± 0.1. (*C*) Dual uptake for AAD-IIc (■) and control oocytes (□) from the same donor frog. Slope of linear regression line: 3.0 ± 0.2. For comparison purposes, the data of Fig. 1 for the WT NaPi-IIc have been replotted with the respective mean of control oocytes subtracted (○). (*D*) Normalized I–V plots that compare NaPi-IIa (■, $n = 5$) and AAD-IIc (●, $n = 6$). Each data point is the difference between the currents recorded in ND100 plus 1 mM P_i and ND100, respectively, at a given *V*. Data for each cell were normalized to the P_i-induced current at −100 mV.

region, including ICL3 and the last two TMDs. The distribution of changed residues between electrogenic and electroneutral transporters was consistent with the findings of the chimera study. Surprisingly, TMD-1 contained no nonconserved substitutions; yet, from the chimera study, we concluded that its presence was essential for conferring electrogenic behavior to NaPi-IIa. This requirement might be a consequence of our choice of restriction site for constructing the C1A7 chimera, whereby the part of ECL-1 that contains a Gly–Ser substitution in all NaPi-IIc isoforms was included with TMD-1. In contrast, Cys substitution at this site does not alter the electrogenic properties of NaPi-IIa, which indicated that the residue at this site was not a critical determinant of electrogenicity but may play a modulatory role (8).

Next, we focused on the amino acid changes in the three clusters (Table 1). We categorized the changes in terms of polarity and charge, because these properties would potentially affect the electrogenicity and substrate coordination. Cluster I showed the most significant changes with the majority of substitutions involving an increase in side-chain polarity (most commonly Ala→Ser) and removal of negative charge at site 224 (Asp→Gly/Ser). Significantly, this charge is conserved in all putative electrogenic transporters, particularly in view of the finding that substituting Asp-224 in human NaPi-IIa with Gly resulted in electroneutral Na-dependent P_i transport (L.V.V., I.C.F., A.B., J.B., and H.M., unpublished data). In contrast, clusters II and III showed mixed changes in polarity, together with a gain and loss of positive charge at sites 380 and 499, respectively. Furthermore, cluster III included TMDs 7 and 8 and ECL-4, which we showed were not essential for preserving electrogenicity in NaPi-IIa (Fig. 2*B*) but could nevertheless play a modulatory role, as evidenced by the weak voltage dependency of chimera A6C2 and Cys mutagenesis studies in ECL-4 (7, 8).

Substitution of NaPi-IIa Residues in TMD-3 Confers Electrogenicity to the NaPi-IIc Backbone. Next we investigated the impact of the residue changes in TMD-3 by using NaPi-IIc as a backbone into which we substituted the equivalent NaPi-IIa residues. When we substituted Gly-195 with the NaPi-IIa equivalent Asp-224 (mutant D-IIc) or Ser-189 and Ser-191 with the NaPi-IIa equivalents Ala-218, Ala-224 (mutant AA-IIc), we obtained functionally expressed mutants as evidenced by Na^+-dependent $^{32}P_i$ uptakes that were significantly greater than NI cells (data not shown). However, in neither case

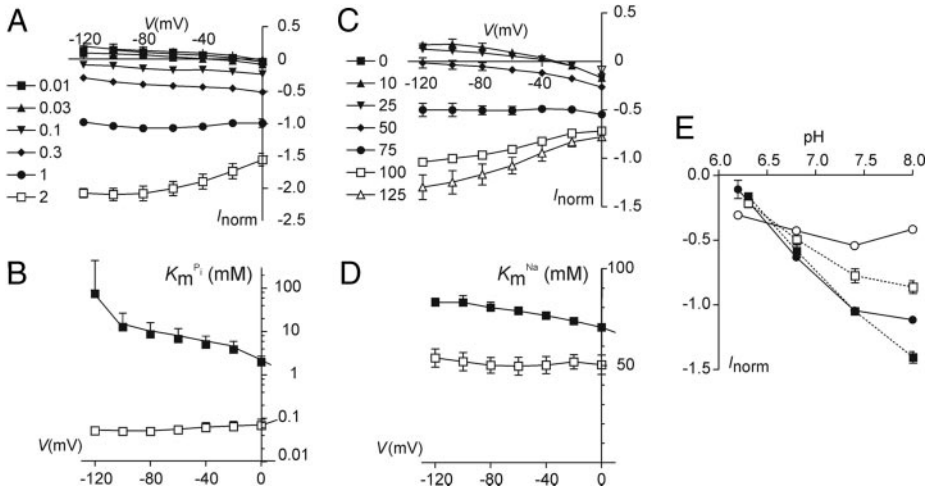

Fig. 5. Substrate dependency of AAD-IIc. (*A*) I–V plots for P_i activation. Data for individual oocytes were determined for the P_i concentrations indicated (in mM) and data for each cell were normalized to the P_i-dependent current at 1 mM P_i and −100 mV ($n = 4$). (*B*) Apparent affinity for P_i-activation ($K_m^{P_i}$) for NaPi-IIa (□, $n = 3$) and AAD-IIc (■, $n = 4$) as found by fitting a form of the Michaelis–Menten equation, $I_{P_i} = I_{P_i}^{max}([P_i]/([P_i] + K_m^{P_i}) + K$, to the data of *A* at each membrane potential, where $[P_i]$ is the P_i concentration, $K_m^{P_i}$ is the apparent affinity for P_i, $I_{P_i}^{max}$ is the maximum cotransport rate, and *K* is a variable offset (7). Note the logarithmic ordinate scale. (*C*) I–V plots for Na^+ activation. Data for individual oocytes were determined for the Na^+ concentrations indicated (in mM) with 1 mM P_i , and data for each cell were normalized to the P_i-dependent current at 1 mM P_i and −100 mV ($n = 4$). (*D*) Apparent affinities for Na^+ activation (K_m^{Na}) for NaPi-IIa (□, $n = 4$) and AAD-IIc (■, $n = 4$) as reported from fitting a form of the modified Hill equation: $I_{P_i} = I_{P_i}^{max}\{[Na]_H^n/[[Na]_H^n + (K_m^{Na})_H^n]\} + K$, to the data of panel C at each membrane potential, where [Na] is the concentration of Na^+, n_H is the Hill coefficient, K_m^{Na} is the apparent affinity for Na^+. (*E*) Proton dependency for NaPi-IIa (circles, continuous lines) and AAD-IIc (squares, dotted lines) at 0 mV (open symbols) and −120 mV (filled symbols). Data for NaPi-IIa ($n = 5$) and AAD-IIc ($n = 5$) were normalized to the response to 1 mM HPO_4^{2-} at −100 mV, pH 7.4. Current reversal at low substrate concentrations in *A* and *C* results from the subtraction of the uncoupled leak current (7, 9).

could we detect P_i-induced currents. For mutant D-IIc, where the $^{32}P_i$ uptake was only ≈4-fold greater than the NI uptake, we were nevertheless confident that electrogenic activity should have been detectable, because this uptake rate would correspond to currents with a magnitude >10 nA. Remarkably, after we substituted all three NaPi-IIa residues at the corresponding sites in NaPi-IIc, the triple NaPi-IIc mutant (AAD-IIc) displayed Na^+-dependent $^{32}P_i$ uptake and a P_i-induced electrogenic response (Fig. 4). When challenged with 1 mM P_i in ND100, AAD-IIc gave robust, inward currents (typically in the range 50–250 nA)) at −50 mV; in zero external Na^+ (ND0), no significant current was detected under the same conditions (Fig. 4*A*). Furthermore, we did not detect a response to P_i when Li^+ was substituted for Na^+ (data not shown), which indicated that AAD-IIc had retained the NaPi-II specificity for Na^+ as its cosubstrate. Like WT NaPi-IIa, AAD-IIc also responded to the Na^+ P_i cotransporter inhibitor, PFA, which was evidence of block for a Na^+-dependent leak current associated with the expressed cotransporter protein (5). Neither control (NI) nor NaPi-IIc-expressing oocytes from the same donor frog showed significant responses to P_i or PFA under the same superfusion conditions (Fig. 4*A*). The holding current decrease observed after removal of external Na^+ was in part due to endogenous Na^+-dependent channels and a transporter-related leak.

To determine whether the P_i-induced currents were stoichiometrically coupled to P_i cotransport, we assayed the charge and $^{32}P_i$ uptake on individual voltage-clamped oocytes ($V_h = -50$ mV). This assay yielded a slope of 0.9 ± 0.1, which established that AAD-IIc transported one net charge per cotransported P_i molecule (Fig. 4*B*). Moreover, by dual $^{22}Na/^{32}P_i$ uptake, we documented a slope of 3.0 ± 0.2, which indicated a 3:1 Na/P_i stoichiometry (Fig. 4*C*). Taken together, these findings demonstrate conclusively that the three TMD-3 mutations alone were sufficient to establish Na^+-coupled electrogenic P_i cotransport in the electroneutral NaPi-IIc backbone, namely a Na/P_i/charge stoichiometry of 3:1:1. Moreover, the increased Na/P_i stoichiometry suggests that the mutagenesis had revealed a new Na^+ interaction site.

The steady-state voltage dependency of AAD-IIc was, however, clearly weaker than NaPi-IIa when the normalized I–V data were compared (Fig. 4*D*). This finding indicated that residue changes at other sites in the NaPi-IIc backbone would be necessary to establish the type IIa electrogenic profile.

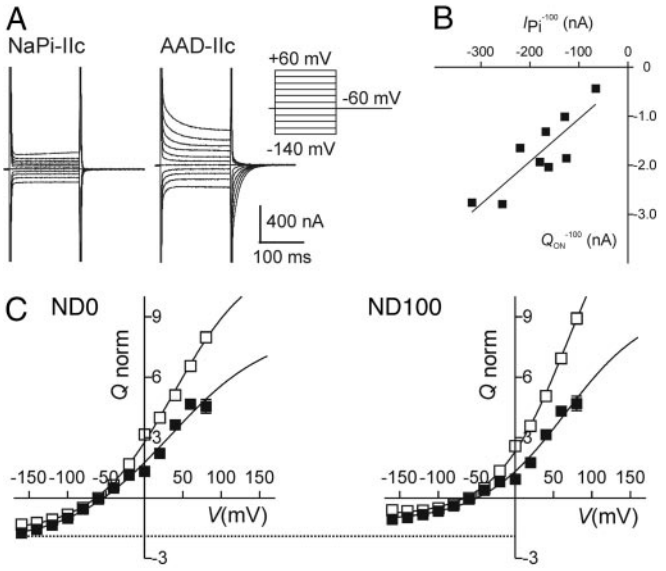

Fig. 6. Voltage steps induce transient currents. (*A*) Currents recorded in response to a series of voltage steps in the range −140 mV to +60 mV from a −60-mV holding potential for a representative WT NaPi-IIc- and AAD-IIc-expressing oocyte from the same donor frog (superfusion in ND100). (*B*) Correlation of charge movement for AAD-IIc induced by a voltage step from −60 mV to −100 mV for superfusion in ND0, with the steady-state current induced by 1 mM P_i at −100 mV (superfusion in ND100). Line is a linear regression, with $r^2 = 0.74$, $n = 9$. (*C*) Normalized charge–voltage (*Q–V*) data for superfusion in ND0 and ND100 for the same batch of AAD-IIc-expressing oocytes ($n = 8$). The charge induced by a voltage step from −60 mV to −100 mV (in ND0) was used to normalize data for each cell before pooling. Error bars smaller than symbols are not shown. □ indicates ON charge movement from −60 mV to target potential. ■ indicates OFF charge movement from target potential to −60 mV. Continuous lines are fits to data using a Boltzmann equation of the form: $Q = Q_{hyp} + Q_{max}/[1 + \exp(-ze(V - V_{0.5})/kT)]$, where Q_{max} is the maximum charge translocated, Q_{hyp}, is the steady-state charge at the hyperpolarizing limit and depends on V_h, $V_{0.5}$ is the voltage at which the charge is distributed equally between two hypothetical states, z is the apparent valency per cotransporter, e is the elementary charge, k is Boltzmann's constant, and T is the absolute temperature. The dashed line indicates the hyperpolarizing limit for ON charge movement with ND0 superfusion.

AAD-IIc Shows Altered Substrate Activation Characteristics. The P_i cotransport kinetics for NaPi-IIc (10) are similar to those previously reported for NaPi-IIa isoforms from several mammalian species (5, 9, 20), i.e., similar apparent affinities for P_i and Na^+ and a strong proton dependency. This finding suggested that both isoforms share the same molecular elements for substrate recognition and interaction and, importantly, that these processes are not directly dependent on the electrogenic properties of the transporter. To investigate whether engineering in TMD-3 had altered these parameters, we assayed the P_i, Na^+, and H^+ dependency of AAD-IIc under voltage clamp.

P_i-dependent currents in 100 mM Na^+ (pH 7.4) showed a weak voltage dependency even up to 2 mM total P_i, with no evidence of saturation for potentials in the range $-120 \text{ mV} \le V \le 0$ mV (Fig. 5*A*). At higher substrate concentrations, P_i complexed with divalent cations in ND100 solution, thereby rendering the estimate of free P_i uncertain. Because oocytes were electrically unstable in divalent-free conditions, we were unable to achieve saturating activation, which resulted in a large uncertainty in the estimate of $K_m^{P_i}$ (Fig. 5*B*). Nevertheless, this parameter was ≈10-fold larger than the values documented in this study for NaPi-IIa or for NaPi-IIc determined from $^{32}P_i$ uptake (10) (70 μM). Whereas $K_m^{P_i}$ for NaPi-IIa showed a weak increase with depolarization, as previously reported for the rat isoform (5), the estimates of $K_m^{P_i}$ for AAD-IIc reported by the fit suggested an inverse relationship with membrane potential. However, the fit uncertainties precluded drawing a definite conclusion.

In contrast to P_i activation, Na^+ activation at constant P_i (1 mM) showed a saturating electrogenic response (Fig. 5*C*). The activation characteristic for a given $V < 0$ mV was sigmoidal with an inflection at low Na^+ (data not shown), indicative of a system in which more than one Na^+ ion interacted with the protein per transport cycle. Compared with NaPi-IIa, the apparent affinity for Na^+ (K_m^{Na}) of AAD-IIc was ≈50% greater and slightly increased with depolarization (Fig. 5*D*).

Finally, we examined the effect of external acidification on AAD-IIc because protons are known to modulate the kinetics of electrogenic type II Na^+/P_i cotransporters (5, 6, 9, 16). To eliminate errors from the titration of P_i, we maintained the divalent P_i at 1 mM so that any change in activity would reflect the effect of protons on the cotransport rate. At $V = 0$ mV, a pH change from 7.4 to 6.2 gave a 43% loss of electrogenic activity for NaPi-IIa compared with 80% for AAD-IIc under the same conditions (Fig. 5*E*). The latter result is consistent with the reported NaPi-IIc pH dependency data (10, 21) when account is taken of the reduced availability of divalent P_i and suggested that AAD-IIc has preserved the proton sensitivity of NaPi-IIc. In contrast, at $V = -120$ mV, both AAD-IIc and NaPi-IIa showed similar dependency for $5.0 \le \text{pH} \le 7.4$. These findings suggest that mutagenesis in the NaPi-IIc backbone has established the same proton interaction mechanism in AAD-IIc as for NaPi-IIa (6, 9).

AAD-IIc Displays Transient Currents Related to Transport Function. A common kinetic feature of electrogenic cotransporters is that voltage steps induce transient currents referred to as pre-steady-state relaxations (5, 22). We documented robust transient currents in AAD-IIc-expressing oocytes (Fig. 6*A*). These currents were easily distinguishable from the oocyte linear capacitive charging and were undetectable in oocytes that expressed NaPi-IIc, which we confirmed to mediate substantial $^{32}P_i$ uptake, and NI oocytes from the same donor frog (data not shown). We also detected transient currents in the absence of external Na^+, which suggested that the TMD-3 mutations introduced mobile charges to the NaPi-IIc backbone. We note that our inability to detect transient relaxations in NaPi-IIc does not necessarily exclude the possibility that it has charges that respond to the transmembrane field, but they are immobilized over the range of potentials used.

The magnitude of the charge in ND0 for a 40-mV step to −100 mV correlated with the P_i-induced steady-state currents at −100 mV (Fig. 6*B*) for oocytes with different steady-state cotransport activities. These data indicate that the transient currents were directly associated with the amount of functionally expressed AAD-IIc in the membrane. We determined the voltage dependency of the charge movements in the range −160 mV to +80 mV for superfusion in ND0 and ND100 (Fig. 6*C*). Because pre-steady-state relaxations reflect the reversible movement of a fixed number of charges, we expected charge balance and saturation of charge movement at extreme potentials. These criteria were only satisfied for hyperpolarizing voltage steps, where we documented clear evidence of saturation and <20% error in charge balance. The rate-limiting behavior of charge movement for steps to hyperpolarizing potentials also agreed with the steady-state I–V data for AAD-IIc (Fig. 4*D*), which exhibited similar behavior for $V < 0$. This finding strongly suggested that the transient currents were directly associated with the AAD-IIc transport cycle. Moreover, the charge at the hyperpolarizing limit in ND100 was suppressed by ≈50% compared with ND0 (Fig. 6*C*). This finding suggests that the interaction of external Na^+ ions with the protein had immobilized part of the intrinsic charge movement. Importantly, this interaction occurred in the absence of P_i, in support of an ordered kinetic scheme for Na^+-coupled electrogenic transport in which the binding of one Na^+ ion precedes P_i binding (5).

For depolarizing steps, the corresponding ON charge was significantly smaller than the OFF charge that accompanied a return to −60 mV from depolarizing voltages. It is possible that some charge was missed by the fitting procedure if, for example, a very fast component were masked by the oocyte charging transient. In contrast, the monotonic increase in charge and initial amplitude with starting potential in the OFF transient suggested the involvement of another mechanism. For example, part of the transient current could be resistive and reflect voltage-dependent closure of a channel-like pore, as suggested for the 5HT transporter (23, 24). A fit of the ON charge movements with a Boltzmann function reported midpoint potentials ($V_{0.5}$) of +22 ± 12 mV ($n = 7$) in ND0 and +61 ± 14 mV ($n = 7$) in ND100 and a paired t test indicated that the shift in $V_{0.5}$ was statistically significant ($P = 0.05$). The apparent valencies (z) were 0.42 ± 0.03 ($n = 7$) in ND0 and 0.47 ± 0.04 ($n = 7$) in ND100. These were similar to values reported for NaPi-IIa (5, 8, 9) and NaPi-IIb isoforms (6, 16).

In terms of an alternating access model for cotransport, whereby the empty carrier can assume either an outward or inward facing conformation, depending on the transmembrane electric field, the positive $V_{0.5}$ suggested that for $V \leq 0$, AAD-IIc already favors an outward conformation that would allow Na^+ ions easy access to their binding site. When Na^+ ions interact with AAD-IIc, the intrinsic charge movements are constrained so that stronger depolarization is required to mobilize charge, consistent with the more positive $V_{0.5}$ in ND100. This result is in agreement with the rate-limiting behavior and weak voltage dependency of the steady-state P_i-activation (Fig. 4*D*). AAD-IIc differs from NaPi-IIa isoforms, which typically show a $V_{0.5}$ in the range −20 to −60 mV (5, 6, 9) and which we previously interpreted as evidence of the empty carrier occupying an inwardly facing conformation at $V = 0$ that changes to outward facing with increasing membrane hyperpolarization (7).

Conclusions

AAD-IIc displays three characteristics unique to Na^+-dependent electrogenic P_i cotransport: 3:1 Na^+/P_i stoichiometry, 1:1 P_i/charge coupling, and transient charge movements that correlate with steady-state activity. These findings suggest that (*i*) mutagenesis of the NaPi-IIc backbone has created, directly or indirectly, a Na^+ interaction site, the occupancy of which leads to the stoichiometric translocation of an additional Na^+ ion per transport cycle; (*ii*) P_i-induced steady-state currents result from a net movement of +1 charge per cycle; and (*iii*) the voltage dependency of the transient charge movements is a direct determinant of the steady-state voltage dependency

Detailed kinetic analysis of AAD-IIc and comparison with the typical fingerprint of electrogenic type NaPi-IIa/b cotransporter isoforms also revealed significant functional differences: a weak steady-state voltage dependency, which, according to the alternating access model, suggested that the empty carrier favors an outward-facing conformation for $V < 0$, a low apparent affinity for P_i, and a transient charge imbalance that may indicate that the mutagenesis has created a channel-like leakage pathway. These differences underscore the complexity of structure–function relationships and indicate that mutagenesis at other sites is required to establish the typical electrogenic behavior in the NaPi-IIc backbone.

We thank Dr. Anne-Kristine Meinild for helpful discussions. This work was supported by grants from the Swiss National Science Foundation, the Hartmann Müller-Stiftung, the Olga Mayenfisch-Stiftung, the Union Bank of Switzerland, and the Gebert Rüf Stiftung (to H.M.).

1. Murer, H., Hernando, N., Forster, I. C. & Biber, J. (2000) *Physiol. Rev.* **80,** 1373–1409.
2. Miyamoto, K., Segawa, H., Ito, M. & Kuwahata, M. (2004) *Jpn. J. Physiol.* **54,** 93–102.
3. Forster, I. C., Loo, D. D. & Eskandari, S. (1999) *Am. J. Physiol.* **276,** F644–F649.
4. Forster, I. C., Kohler, K., Biber, J. & Murer, H. (2002) *Prog. Biophys. Mol. Biol.* **80,** 69–108.
5. Forster, I. C., Hernando, N., Biber, J. & Murer, H. (1998) *J. Gen. Physiol.* **112,** 1–18.
6. Forster, I. C., Biber, J. & Murer, H. (2000) *Biophys. J.* **79,** 215–230.
7. Ehnes, C., Forster, I. C., Bacconi, A., Kohler, K., Biber, J. & Murer, H. (2004) *J. Gen. Physiol.* **124,** 489–503.
8. Ehnes, C., Forster, I. C., Kohler, K., Bacconi, A., Stange, G., Biber, J. & Murer, H. (2004) *J. Gen. Physiol.* **124,** 475–488.
9. Virkki, L. V., Forster, I. C., Biber, J. & Murer, H. (2005) *Am. J. Physiol.* **288,** F969–F981.
10. Segawa, H., Kaneko, I., Takahashi, A., Kuwahata, M., Ito, M., Ohkido, I., Tatsumi, S. & Miyamoto, K. (2002) *J. Biol. Chem.* **277,** 19665–19672.
11. de La Horra, C., Hernando, N., Forster, I. C., Biber, J. & Murer, H. (2001) *J. Physiol.* **531,** 383–391.
12. Lester, H. A., Mager, S., Quick, M. W. & Corey, J. L. (1994) *Annu. Rev. Pharmacol. Toxicol.* **34,** 219–249.
13. Lambert, G., Forster, I. C., Stange, G., Kohler, K., Biber, J. & Murer, H. (2001) *J. Gen. Physiol.* **117,** 533–546.
14. Kohler, K., Forster, I. C., Stange, G., Biber, J. & Murer, H. (2002) *Am. J. Physiol.* **282,** F687–F696.
15. Kohler, K., Forster, I. C., Stange, G., Biber, J. & Murer, H. (2002) *J. Gen. Physiol.* **120,** 693–705.
16. Forster, I. C., Wagner, C. A., Busch, A. E., Lang, F., Biber, J., Hernando, N., Murer, H. & Werner, A. (1997) *J. Mem. Biol.* **160,** 9–25.
17. Hilfiker, H., Hattenhauer, O., Traebert, M., Forster, I. C., Murer, H. & Biber, J. (1998) *Proc. Natl. Acad. Sci. USA* **95,** 14564–14569.
18. Nalbant, P., Boehmer, C., Dehmelt, L., Wehner, F. & Werner, A. (1999) *J. Physiol.* **520,** 79–89.
19. Graham, C., Nalbant, P., Scholermann, B., Hentschel, H., Kinne, R. K. & Werner, A. (2003) *Am. J. Physiol.* **284,** F727–F736.
20. Hartmann, C. M., Wagner, C. A., Busch, A. E., Markovich, D., Biber, J., Lang, F. & Murer, H. (1995) *Pflügers Arch.* **430,** 830–836.
21. Ohkido, I., Segawa, H., Yanagida, R., Nakamura, M. & Miyamoto, K. (2003) *Pflügers Arch. Eur. J. Physiol.* **446,** 106–115.
22. Loo, D. D., Hazama, A., Supplisson, S., Turk, E. & Wright, E. M. (1993) *Proc. Natl. Acad. Sci. USA* **90,** 5767–5771.
23. Li, M., Farley, R. A. & Lester, H. A. (2002) *FEBS Lett.* **513,** 247–252.
24. Mager, S., Min, C., Henry, D. J., Chavkin, C., Hoffman, B. J., Davidson, N. & Lester, H. A. (1994) *Neuron* **12,** 845–859.
25. Engelman, D. M., Steitz, T. A. & Goldman, A. (1986) *Annu. Rev. Biophys. Biophys. Chem.* **15,** 321–353.

3.2 Summary of publication:

Structure-function relations of the first and fourth predicted extracellular linkers of the type IIa Na^+/Pi cotransporter:
I:Cysteine scanning mutagenesis

Zusammenhänge zwischen Funktion und Struktur des ersten und vierten extrazellulären Verbindungsstückes des Typ IIa Na^+/P_i Kotransporters
I: Cysteinmutagenese

Es ist bekannt, dass das erste intrazelluläre (ECL-1) und das vierte extrazelluläre (ECL-4) Verbindungsstück eine wichtige Rolle bei der Definition der Transporteigenschaften des Na^+ gekoppelten Typ IIa Phosphat Kotransporters (NaPi-IIa) spielt. Um zu untersuchen ob andere Verbindungsstücke zwischen vorhergesagten Transmembrandomänen ebenfalls beteiligt sind, wurde SCAM („Substituted Cysteine Accessibility Method“) an Positionen aus dem ersten und vierten extrazellulären Verbindungsstück (ECL-1 und -4) angewendet. Mutationen des Wildtyps mit neu eingefügten Cysteinen wurden in *Xenopus* Eiern exprimiert und ihre Funktion durch Aufnahme von radioaktiv markiertem Phosphat und Elektrophysiologie untersucht. Es konnten in beiden Verbindungsstücken funktionell wichtige Positionen identifiziert werden, indem die Eizellen membrangängigen und nicht membrangängigen Methanethiosulfonat (MTS) Reagenzien ausgesetzt wurden. Die Reaktionsraten dieser Cysteinmodifikationen waren für das ECL-1 schneller wie die für das ECL-4, was darauf schliessen lässt, dass letztere vom extrazellulären Medium aus weniger gut zugänglich sind. Generell blieb am Ende der Modifikationsreaktion eine geringfügige Kotransportaktivität bestehen. Die Aktivitätsänderung konnte auf eine Veränderung der spannungsabhängigen Kinetik des P_i induzierten Stromes zurückgeführt werden. Der Austausch von Gly-134 aus dem ECL-1 mit einem Cystein resultierte zum Beispiel in einer limitierenden, spannungsunabhängigen Kotransportaktivität für $V \leq$ -80 mV, wogegen der WT eine lineare Spannungsabhängigkeit aufwies. Nach der Modifikation dieses Cysteins wies diese Mutante ebenfalls eine lineare Spannungsabhängigkeit über dieselbe Spannungsbandbreite auf. Ein entgegengesetztes Verhalten wurde für einen Cysteinaustausch an der Position Met-533 im ECL-4 dokumentiert. Cysteinmodifikationen an zwei weiteren Positionen des ECL-1 (Ile-136, Phe-137) resultierte ebenfalls in einer linearen Spannungsabhängigkeit bei hyperpolarisierenden Potentialen. Zusammenfassend deuten unsere Ergebnisse darauf hin, dass die ECL-1 und ECL-4 wahrscheinlich nicht direkt an der Formation des Kotransportweges beteiligt sind, jedoch spezifische Positionen in

diesen Verbindungsstücken direkt oder indirekt mit den Anteilen von NaPi-IIa interagieren können, welche spannungsabhängigen Konformationsänderungen unterworfen sind.

Structure–Function Relations of the First and Fourth Predicted Extracellular Linkers of the Type IIa Na^+/P_i Cotransporter: I. Cysteine Scanning Mutagenesis

Colin Ehnes, Ian C. Forster, Katja Kohler, Andrea Bacconi, Gerti Stange, Jürg Biber, and Heini Murer

Institute of Physiology, University of Zurich, CH-8057 Zurich, Switzerland

ABSTRACT The putative first intracellular and third extracellular linkers are known to play important roles in defining the transport properties of the type IIa Na^+-coupled phosphate cotransporter (Kohler, K., I.C. Forster, G. Stange, J. Biber, and H. Murer. 2002b. *J. Gen. Physiol.* 120:693–705). To investigate whether other stretches that link predicted transmembrane domains are also involved, the substituted cysteine accessibility method (SCAM) was applied to sites in the predicted first and fourth extracellular linkers (ECL-1 and ECL-4). Mutants based on the wild-type (WT) backbone, with substituted novel cysteines, were expressed in *Xenopus* oocytes, and their function was assayed by isotope uptake and electrophysiology. Functionally important sites were identified in both linkers by exposing cells to membrane permeant and impermeant methanethiosulfonate (MTS) reagents. The cysteine modification reaction rates for sites in ECL-1 were faster than those in ECL-4, which suggested that the latter were less accessible from the extracellular medium. Generally, a finite cotransport activity remained at the end of the modification reaction. The change in activity was due to altered voltage-dependent kinetics of the P_i-dependent current. For example, cys substitution at Gly-134 in ECL-1 resulted in rate-limiting, voltage-independent cotransport activity for $V \leq -80$ mV, whereas the WT exhibited a linear voltage dependency. After cys modification, this mutant displayed a supralinear voltage dependency in the same voltage range. The opposite behavior was documented for cys substitution at Met-533 in ECL-4. Modification of cysteines at two other sites in ECL-1 (Ile-136 and Phe-137) also resulted in supralinear voltage dependencies for hyperpolarizing potentials. Taken together, these findings suggest that ECL-1 and ECL-4 may not directly form part of the transport pathway, but specific sites in these linkers can interact directly or indirectly with parts of NaPi-IIa that undergo voltage-dependent conformational changes and thereby influence the voltage dependency of cotransport.

KEY WORDS: mutagenesis site directed • electrophysiology • phosphate transport proteins • electrogenic • *Xenopus laevis*

INTRODUCTION

The task of reabsorbing inorganic phosphate (P_i) at the brush border membrane of the renal proximal tubule is largely fulfilled by the type IIa Na^+/P_i cotransporter (NaPi-IIa) (SLC34A1) and consequently this protein plays a central role in mammalian phosphate homeostasis (for review see Murer et al., 2000, 2003). NaPi-IIa isoforms from several species have been cloned and their transport kinetics characterized by expression in *Xenopus laevis* oocytes using isotope tracer and electrophysiological assays (for review see Forster et al., 2002). The key functional features are as follows: Na^+-dependent P_i cotransport (3:1 Na^+:P_i stoichiometry), ordered substrate binding (Na^+–P_i^{2-}–$2Na^+$), substrate specificity (divalent P_i is the preferred species), and voltage-dependent transport (one net charge transfer per transport cycle); uniport or uncoupled Na^+-dependent leak in the absence of P_i; and intrinsic pH dependency (suppressed P_i transport with external acidification) (Forster et al., 2002). Elucidation of the structure–function relationships between molecular entities and kinetic properties of NaPi-IIa is an ongoing challenge that we are currently addressing using the substituted cysteine accessibility method (SCAM) (e.g., Karlin and Akabas, 1998).

The predicted topology of NaPi-IIa, derived from studies on the rat isoform, suggests a protein with eight transmembrane domains, a large extracellular loop

C. Ehnes and I.C. Forster contributed equally to this paper.

Address correspondence to Ian C. Forster, Physiologisches Institut, Universität Zürich-Irchel, Winterthurerstrasse 190, CH-8057 Zürich, Switzerland. Fax: 41-1-635 5715; email: IForster@access.unizh.ch

K. Kohler's present address is Laboratory of Morphogenesis and Cell Signaling, UMR144, Institut Curie, Paris, France.

Abbreviations used in this paper: DTT, dithiothreitol; MTS, methanethiosulfonate; MTSEA, 2-aminoethyl MTS hydrobromide; MTSES, sodium (2-sulfonatoethyl) MTS; MTSET, 2-(trimethylammonium)ethyl MTS bromide; NaPi-IIa, type IIa Na^+/Pi cotransporter; PFA, phosphonoformic acid; SCAM, substituted cysteine accessibility method; WT, wild type.

with two N-glycosylation sites and intracellular NH_2 and COOH termini (Magagnin et al., 1993; Murer et al., 2000) (Fig. 1 A). Antibody accessibility studies (Lambert et al., 1999b) and cysteine scanning approaches (Lambert et al., 1999a, 2000; Kohler et al., 2002a,b) also support this model. Using SCAM we have identified sites in the putative third extracellular linker (ECL-3) (Lambert et al., 1999a, 2001) and the putative first intracellular linker (ICL-1) (Kohler et al., 2002a,b) that when modified by methanethiosulfonate (MTS) reagents result in block of cotransport mode activity. Given that NaPi-IIa is a functional monomer (Kohler et al., 2000), and taking into account our previous SCAM findings, we currently postulate that these two topologically opposed linker regions associate with one another to constitute the transport pathway (Kohler et al., 2002a,b). To examine if other external linker regions may also define NaPi-IIa transport properties, we performed SCAM on sites in the first and fourth predicted linker regions, designated ECL-1 and ECL-4, respectively (Fig. 1 A). As shown in Fig. 1 B, these regions are very well conserved among several isoforms of the SLC34A family and therefore we might expect them to play common functional roles.

Cysteine substitution at nine sites in ECL-1 and four sites in ECL-4 was well tolerated, and these mutants displayed no significant deviations from wild-type (WT) behavior, based on a two-point screening assay for substrate and cosubstrate activation. In both linker regions, altered kinetic phenotypes were documented for membrane-impermeant MTS reagents, which established that these sites were accessible from the extracellular milieu, in agreement with the current NaPi-IIa secondary topology. Estimated rates of modification suggested that ECL-1 was more accessible than ECL-4. Some mutations in each linker showed significantly modified voltage dependency before and after exposure to MTS reagents. Of particular significance were the complementary changes that resulted from in situ molecular manipulations of certain residues in ECL-1 and ECL-4. Our results suggest that these linkers are most likely not directly part of the transport pathway, but they contain specific sites that may interact directly or indirectly with voltage-sensitive elements of the NaPi-IIa protein.

MATERIALS AND METHODS

Mutagenesis

Mutations were introduced following the Stratagene Quickchange Site-Directed Mutagenesis Kit manual. 10 ng of the plasmid (pSPORT; GIBCO BRL) containing the WT rat NaPi-IIa cDNA was amplified with 2.5 U of Pfu Turbo DNA polymerase (Stratagene), in the presence of primers (200 nM). PCR amplification was performed with 20 cycles, with each cycle consisting of one 95°C (30 s), one 55°C (1 min), and one 68°C (15 min) step. Afterwards, 10 U of Dpn I was added directly to the amplification reaction, and the sample was incubated for 1 h at 37°C to digest the parental DNA. XL1-blue supercompetent cells were transformed with 1 μl of the reaction mixture and plated onto LB-ampicillin plates. The sequence was verified by sequencing (Microsynth) and the plasmid linearized by digestion with NotI. In vitro synthesis of capped cRNA was done following the Ambion MEGAscript T7 kit manual (Ambion). In brief, 1 μg linearized DNA encoding the rat NaPi-IIa constructs was incubated in the presence of 40 U of T7 RNA polymerase and Cap Analogue (New England Biolabs, Inc.) at 37°C for 4 h. Oocytes were injected with either 50 nl water or 50 nl of water containing 10 ng cRNA.

Reagents and Solutions

All standard reagents were obtained from either Sigma-Aldrich or Fluka. Methanethiosulfonate (MTS) reagents were obtained from Toronto Research Chemicals (Downsview). The solution compositions (in mM) were as follows. (a) Oocyte incubation (modified Barth's solution): NaCl (88), KCl (1), $CaCl_2$ (0.41), $MgSO_4$ (0.82), $NaHCO_3$ (2.5), $Ca(NO_3)_2$, HEPES (7.5), adjusted to pH 7.6 with TRIS and supplemented with antibiotics (10 mg/l gentamycin, streptomycin). (b) Control superfusate (ND100): NaCl (100); KCl (2); $CaCl_2$ (1.8); $MgCl_2$ (1); HEPES-TRIS (10) at pH 7.4. Solutions with intermediate Na^+ concentrations were prepared by mixing ND0 and ND100 in the appropriate proportions. (c) Substrate test solutions: inorganic phosphate (P_i) was added to the control superfusate from 1 M K_2HPO_4 and KH_2PO_4 stocks that were mixed to give the required pH (7.4 or 6.2). Phosphonoformic acid (PFA) was added to ND100 from frozen 100 mM stock (in H_2O) to yield a final concentration of 1 mM. (d) MTS reagents, 2-aminoethyl MTS hydrobromide (MTSEA), 2-(trimethylammonium)ethyl MTS bromide (MTSET), and sodium (2-sulfonatoethyl) MTS (MTSES) were prepared from dry stock in DMSO to give 1 M stock solutions. These were stored at −20°C until required and added to ice-cold ND100 solution. The final concentration of DMSO did not exceed 0.1%, and DMSO alone at this concentration was confirmed not to alter the kinetic characteristics of the expressed constructs.

Immunoblotting of Oocyte Homogenates: Western Blotting

Yolk-free homogenates were prepared 3 d after injection of cRNA. Pools of eight oocytes were lysed together with 160 μl homogenization buffer (1% eluent [Calbiochem] in 100 mM NaCl, 20 mM Tris/HCl, pH 7.6) by pipetting the oocytes up and down (Turk et al., 1996). To pellet the yolk proteins, samples were centrifuged at 16,000 *g* for 3 min at 22°C. 10 μl supernatant was mixed with 10 μl 2× loading buffer (4% SDS, 2 mM EDTA, 20% glycerol, 0.19 M Tris/HCl, pH 6.8, 2 mg/ml bromphenol blue, 200 mM dithiothreitol [DTT]), denatured for 2 min at 95°C and separated on a 10% SDS-PAGE gel. Separated proteins were transferred onto a nitrocellulose membrane (Schleicher & Schuell). The membrane was then processed according to standard procedures (Sambrook et al., 1989) using a rabbit polyclonal antibody raised against a synthetic peptide from the NH_2 termini of the rat NaPi-IIa cotransporter (dilution 1:2,000). The specificity of the antibody has been demonstrated previously (Custer et al., 1994). Immunoreactive proteins were detected with a swine anti-rabbit Ig horseradish peroxidase–linked $F(ab')_2$ secondary antibody (dilution 1:5,000) (Amersham Biosciences) and visualized with a chemiluminescence system (Pierce Chemical Co.).

Streptavidin Precipitation of MTSEA-biotinylated Protein

Groups of eight oocytes per NaPi-IIa mutant were incubated for 10 min in 1 mM MTSEA-Biotin, prepared as above. Oocytes ex-

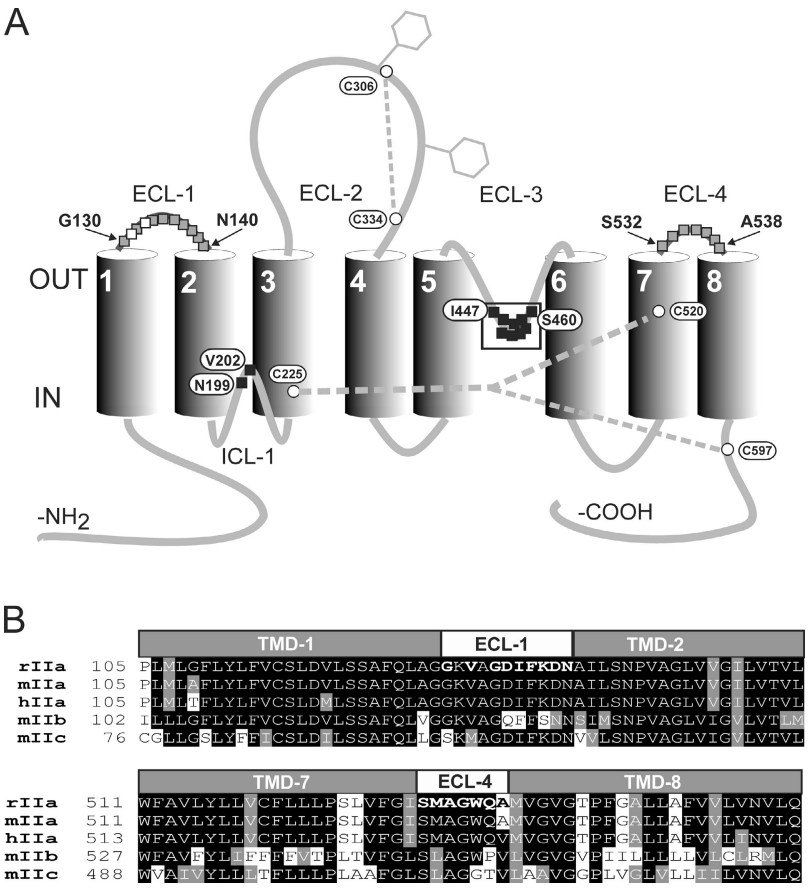

FIGURE 1. (A) Topological representation of the rat type IIa Na^+/P_i cotransporter comprises a backbone of eight putative membrane-spanning domains (TMD-1 to -8) and corresponding linker regions. A functionally essential cysteine bridge is formed between Cys-306 and Cys-334 in the large second extracellular linker (ECL-2) and an additional bridge between Cys-225 and either Cys-520 or Cys-597 has also been recently proposed (Kohler et al., 2003). The cluster of functionally important (MTS-accessible) sites previously identified by SCAM in the third extracellular linker (ECL-3) (Lambert et al., 2001) and two sites in the first intracellular linker (ICL-1) (Kohler et al., 2002a) are indicated (filled squares). Sites 130–140 in the putative first extracellular linker (ECL-1) and 532–538 in the predicted fourth extracellular linker (ECL-4) were mutated to cysteines in this study (gray-filled squares) (B) Comparison of the amino acid sequences for the predicted transmembrane domains flanking ECL-1 (TMD-1 and -2) and ECL-4 (TMD-7 and -8) show a high degree of homology between different isoforms of the type II Na^+/P_i cotransporter family (SLC34). Bold lettered amino acids in ECL-1 and ECL-4 for the rat isoform were mutated to cysteines for the present study. Amino acids are named using the single letter code.

pressing the S460C or the WT protein were taken as positive and negative control, respectively. Biotin-streptavidin precipitation was performed as previously described (Lambert et al., 1999a). In brief, after homogenization in 160 μl of homogenization buffer and centrifugation (see immunoblot of oocyte homogenates), a sample for Western blotting was taken. The rest of the supernatant (~120 μl) was incubated for 2 h with 60 μl ImmunoPure immobilized streptavidin beads (Pierce Chemical Co.) on a rotator. After five washing steps with homogenization buffer, precipitated proteins were eluted with 2× loading buffer (including DTT) at 95°C for 5 min. Samples were loaded on a 10% SDS gel and immunoblotted after protein separation.

Functional Assays and Data Analysis

Radiolabeled P_i Uptake. This procedure has been described in detail elsewhere (Werner et al., 1990). $^{32}P_i$ uptake was measured 3 d after injection in water-injected (control) and cRNA-injected oocytes ($n \geq 10$).

Electrophysiology. The standard two-electrode voltage clamp technique was used as previously described (Forster et al., 1998). The voltage clamp was a laboratory-built system with membrane current measured using a virtual ground bath electrode and with active series resistance compensation to reduce clamp errors. Oocytes were mounted in a small recording chamber (100 μl volume) and continuously superfused (5 ml/min) with test solutions precooled to ~20°C. Data were acquired online using Digidata 1200 hardware and compatible pClamp8 software (Axon Instruments, Inc.). Recorded currents were prefiltered at a bandwidth less than twice the sampling rate (typically 20 Hz for fixed voltage recording and 200 Hz for *I–V* determination).

Steady-state Current-Voltage (I–V) Relations. These were determined by using a voltage staircase from −120 mV to +40 mV with 100-ms-long steps, as previously described (Forster et al., 1998), and subtracting the response in the absence of substrate (P_i or PFA) from that in the presence of substrate. Only single sweeps were used.

Incubation with MTS Reagents and Determination of Rate of Modification. Freshly prepared MTSEA/ET/ES (see above) was delivered to the oocyte chamber using a stainless steel cannula (inner diameter 0.3 mm) positioned near the cell and fed by gravity. Reagents were always applied in the presence of ND100 at a holding potential $V_h = -50$ mV. Incubation was followed by a 1-min washout period before applying P_i (1 mM) as the test assay. A further 1-min washout period was allowed before reincubation at the next concentration of MTS reagent to ensure complete removal of substrate and return of response to a steady-state holding current.

Cys Modification Reaction Rate. The effective second order reaction rates were determined by fitting a single decaying exponential to the peak P_i-dependent current after a cumulative exposure time t, ($I_{P_i}{}^t$) determined following each successive MTS exposure:

$$I_{P_i}{}^t = (I_{P_i}{}^0 - I_{P_i}{}^\infty)\exp(-ctk^*) + I_{P_i}{}^\infty, \quad (1)$$

where $I_{P_i}{}^0$ is the P_i response at $t = 0$; $I_{P_i}{}^\infty$ is the response at $t = \infty$; c is the concentration of MTS reagent (assumed to be in excess), and k^* is the effective second order rate constant (Zhang and Karlin, 1997; Karlin and Akabas, 1998).

All curve fitting was performed using GraphPad Prism version 3.02/4.02 for Windows (GraphPad Software).

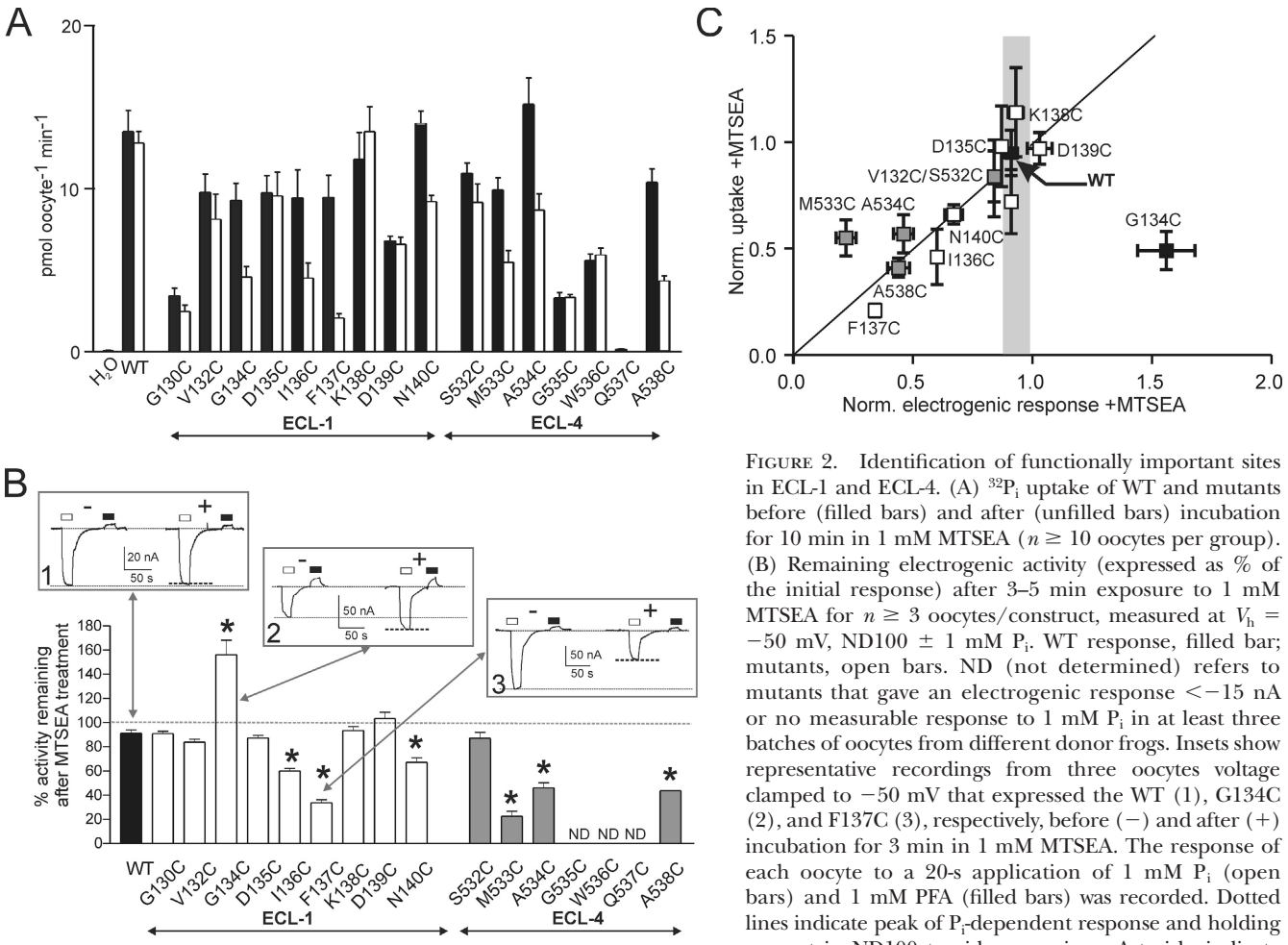

FIGURE 2. Identification of functionally important sites in ECL-1 and ECL-4. (A) $^{32}P_i$ uptake of WT and mutants before (filled bars) and after (unfilled bars) incubation for 10 min in 1 mM MTSEA ($n \geq 10$ oocytes per group). (B) Remaining electrogenic activity (expressed as % of the initial response) after 3–5 min exposure to 1 mM MTSEA for $n \geq 3$ oocytes/construct, measured at V_h = −50 mV, ND100 ± 1 mM P_i. WT response, filled bar; mutants, open bars. ND (not determined) refers to mutants that gave an electrogenic response <−15 nA or no measurable response to 1 mM P_i in at least three batches of oocytes from different donor frogs. Insets show representative recordings from three oocytes voltage clamped to −50 mV that expressed the WT (1), G134C (2), and F137C (3), respectively, before (−) and after (+) incubation for 3 min in 1 mM MTSEA. The response of each oocyte to a 20-s application of 1 mM P_i (open bars) and 1 mM PFA (filled bars) was recorded. Dotted lines indicate peak of P_i-dependent response and holding current in ND100 to aid comparison. Asterisks indicate mutants that showed statistically significant deviations from the WT, as reported by an unpaired *t* test ($P < 0.05$), applied to the normalized data. (C) Comparison of activity after MTSEA exposure for mutants for which reliable electrophysiological data was available (ECL-1, empty squares; ECL-4, gray-filled squares; WT, filled square) normalized to control (−MTSEA) condition. Vertical error bars indicate SEM for normalized uptake data, horizontal error bars indicate SEM from data in B. Gray bar represents mean ± SEM to indicate change of electrogenic activity observed for WT-expressing oocytes after MTSEA exposure.

RESULTS

Expression of Mutants and Identification of MTS-accessible Sites

Fig. 1 A shows the currently proposed secondary structure of the rat NaPi-IIa protein to indicate the location of the residues in the predicted first and fourth extracellular loops (ECL-1/-4) that were mutated individually to cysteines (indicated in bold in Fig. 1 B). We injected *Xenopus laevis* oocytes with cRNA coding for each mutant and screened them for functional transport by using $^{32}P_i$ uptake (Fig. 2 A) and a basic electrophysiological assay (ND100 ± 1 mM P_i, holding potential [V_h] = −50 mV) (Fig. 2 B). For all mutants that gave functional expression, we detected a main band in the Western blots, the position of which corresponded to the expected molecular weight of the WT (80–100 kD) (Fig. 3). We assumed that mutant Q537C in ECL-4 was not expressed based on the Western blot data, as well as the lack of both detectable $^{32}P_i$ uptake (Fig. 2 A) and electrogenic response (not depicted). Taken together, these findings indicated that for the functional mutants, Cys mutagenesis did not affect the basic transport function and these constructs were indistinguishable from the WT in terms of the size of the expressed protein.

We assayed the functional activity of oocytes that expressed each mutant before and after exposure to 1 mM of the Cys-modifying reagent MTSEA for 10 min by $^{32}P_i$ uptake (Fig. 2 A) and electrophysiology (ND100 ± 1 mM P_i at V_h = −50 mV) (Fig. 2 B), to determine if the Cys substitutions were made at sites that might directly or indirectly alter basic transport function. The electrogenic response to P_i superfusion varied among mutants and typically fell within the range −30 to −100 nA at −50 mV. Comparison of these datasets indicated that the trends revealed by the two assays were similar;

i.e., those mutants for which MTSEA treatment led to a reduced $^{32}P_i$ activity also showed reduced P_i-dependent currents (I_{P_i}), as indicated in Fig. 2 C, in which both datasets have been normalized to the respective activities before exposure to MTSEA. A notable exception to this general behavior was mutant G134C, which showed the opposite behavior in the two assays; i.e., after MTS exposure, we observed a decreased $^{32}P_i$ uptake, but an increased I_{P_i}. Depending on the oocyte batch, the uptake assays often showed a large spread in response that we attributed to variability in expression level. Therefore we focused on the electrophysiological assays to study the mutants on an individual cell basis. We also confirmed that the change in electrogenic activity after MTS incubation could be reversed by incubation in the reducing agent DTT (10 mM, 5 min) for selected mutants, whereas no change in WT activity was documented (unpublished data). This finding confirmed that the change in activity most likely resulted from the introduction of a reducible covalent bond between the novel cysteine and MTS reagent. Moreover, the rapidity of the reversal in activity indicated that the number of active transporters in the membrane had not changed as a result of the MTS treatment.

As shown in Fig. 2 B, mutants displayed three types of behavior, depending on their response to 1 mM P_i before and after MTSEA exposure: (1) WT-like (see Fig. 2 B, inset 1) in which little change in activity occurred, found for five mutants in ECL-1 (G130C, V132C, D135C, K138C, and D139C) and one in ECL-4 (S532C); (2) one mutant in ECL-1 (G134C) that showed increased activity (Fig. 2 B, inset 2); and (3) those in which a loss of activity occurred, like F137C (Fig. 2 B, inset 3) and others in ECL-1 (I136C and N140C) and ECL-4 (M533C, A534C, and A538C). In addition to cotransport mode (I_{P_i}), the leak mode was assayed electrophysiologically by measuring the response to the blocker PFA (1 mM) (Forster et al., 1998) under the same experimental conditions. At $V_h = -50$ mV, all the functional mutants showed a reduced holding current during PFA application (I_{PFA}), which indicated that the leak mode was still viable. Two mutants in ECL-4 (G535C and W536C) gave $^{32}P_i$ uptake significantly greater than H_2O-injected cells (Fig. 2 A); however, the magnitude of the P_i-dependent currents was typically ≤15 nA using oocytes from three donor frogs. This low electrogenic activity and the absence of any detectable effect of MTSEA on $^{32}P_i$ uptake led to the exclusion of these mutants from further investigation.

The invariance of I_{P_i} before and after MTSEA exposure (G130C, V132C, D135C, K138C, and D139C in ECL1; S532C in ECL-4), could indicate that (a) the mutated sites were functionally unimportant, (b) other characteristics were modified that were not identified under the assay conditions, or (c) the sites were not accessible from the external medium by MTSEA. To test the latter possibility, we incubated mutant-expressing oocytes in MTSEA-Biotin and performed a streptavidin precipitation with immunodetection using an antibody raised against the NH_2 terminus of the NaPi-IIa protein. We used the mutant S460C in ECL-3 (Fig. 1 A), which we have previously shown to be accessible by MTSEA (Lambert et al., 1999a), and WT-expressing oocytes as positive and negative controls, respectively. As shown in Fig. 3, except for D135C (ECL-1) and W536C and Q537C (ECL-4), MTSEA-biotin was able to bind to all mutants, which confirmed the accessibility of these linkers from the external medium.

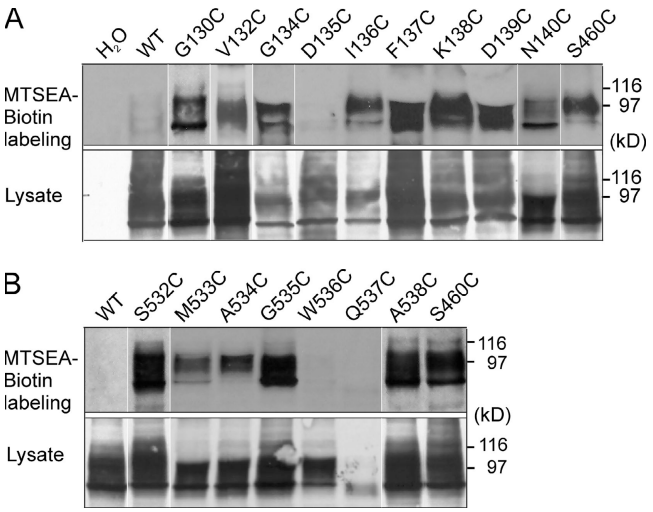

FIGURE 3. Accessibility of cysteine mutants in ECL-1 (A) and ECL-4 (B) by MTSEA-Biotin. Western blots show streptavidin precipitates of MTSEA-biotinylated oocytes (top) and the corresponding whole cell lysates (bottom) from oocytes that expressed the indicated mutants probed with an antibody raised against the NH_2 terminus of NaPi-IIa. Biotinylation data have been combined from several assays made from different batches of oocytes. In each assay, WT and water (H_2O) injected oocytes were used as negative controls, and oocytes injected with cRNA coding for the mutant S460C (Lambert et al., 1999a) were used as a positive control. The band in the range 80–100 kD confirms that the labeled protein is NaPi-IIa. White lines indicate that intervening lanes have been spliced out.

Rate of MTS Modification Reveals Differences in Apparent Accessibility

We estimated the rate of the Cys modification reaction for mutants that showed a significant change of cotransport function after MTS exposure under standard assay conditions, by measuring I_{P_i} after successive exposures to a fixed concentration of MTS reagent. The MTS reagent concentration was chosen initially by trial and error so that a 2-min exposure resulted in an intermediate change of activity, typically in the range 30–60% of the initial response. The test concentration was found to vary over two orders of magnitude, de-

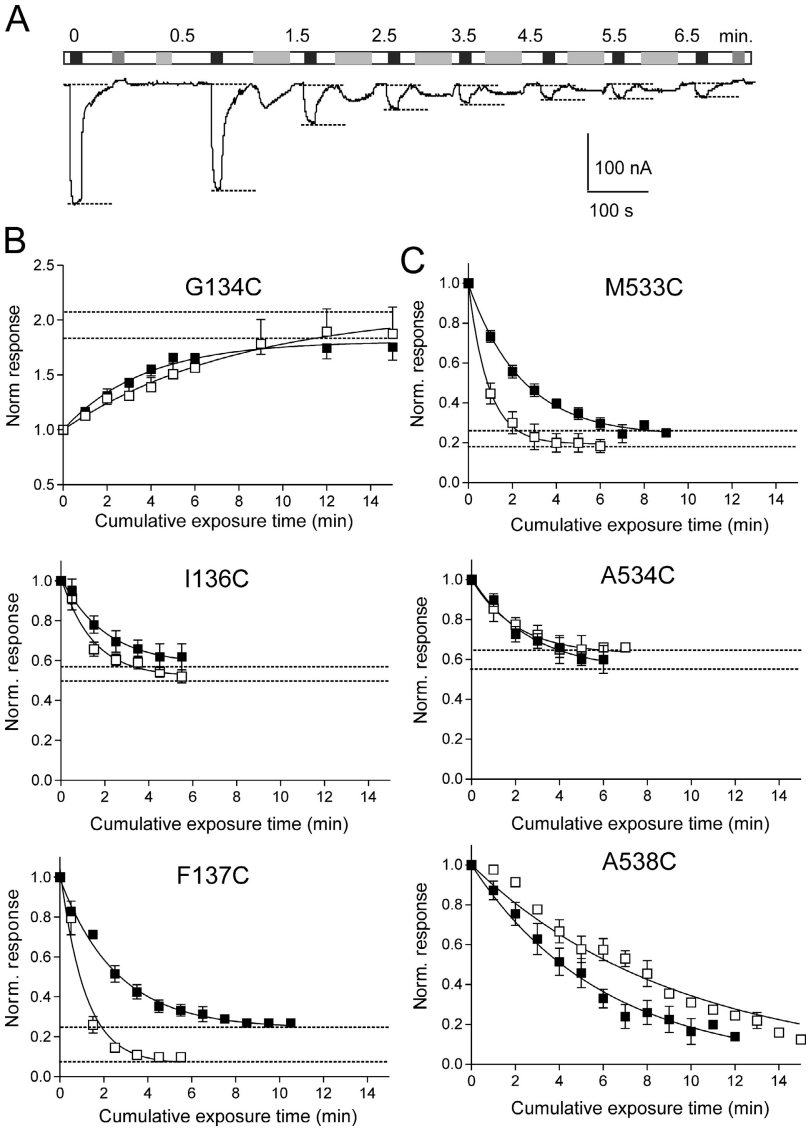

FIGURE 4. Determination of MTS-Cys reaction rates for mutants that showed a change of activity after MTS exposure. (A) Representative recording of current from an oocyte that expressed mutant F137C after successive applications of MTSET (10 μM) (light gray bars). The cumulative exposure time (min) is indicated above each test response. Test substrates P_i (1 mM, black bars) and PFA (1 mM, dark gray bars) were applied for ~20 s. (B and C) P_i-dependent currents at V_h = −50 mV, normalized to the initial value plotted as a function of cumulative MTS reagent exposure time for selected mutants in ECL-1 (B) and ECL-4 (C). Cells were exposed to either MTSEA (filled squares) or MTSET (open squares) for the cumulative time indicated and at the concentrations given in Table I. Continuous line is a fitted single exponential function with plateau (Eq. 1) from which the reaction rate and plateau were estimated. Each data point is pooled from ≥3 cells. Broken lines indicate plateau levels ($I_{P_i}^{\infty}$) estimated from the fit of Eq. 1 (Table I).

pending on the mutation site (Table I). Fig. 4 A shows a representative record from an oocyte that expressed mutant F137C (ECL-1) during repeated exposure to 10 μM MTSET. After each exposure and washout, the response to P_i was tested and the holding current was allowed to recover to the initial baseline before the next exposure. After normalization, these data were fit with a single exponential function (Eq. 1). Under the assumption that the MTS reagent was always in excess, we could estimate the effective second order reaction rate (k^*) (Table I). Impermeant (MTSET) and semi-permeant (MTSEA) reagents were used to confirm the sidedness of the reaction, i.e., to confirm that modification occurred from the external medium in the present study. Fig. 4 (B and C) illustrates the behavior of selected mutants from ECL-1 and ECL-4, respectively.

Three features were readily apparent. First, there was a finite response to P_i after the reaction was complete, indicated by the nonzero plateau ($I_{P_i}^{\infty}$). $I_{P_i}^{\infty}$ varied depending on the site of mutation and the type of MTS reagent used. For mutant A538C (ECL-4), the time window used for the assay (15 min) did not allow the reaction to reach completion using 1 mM of reagent. Incubation at longer times indicated that the plateau was <10% of the initial amplitude (unpublished data). Second, with the exceptions of G134C, N140C (ICL-1), and A538C (ECL-4), MTSET incubation resulted in significantly faster reaction rates compared with MTSEA applied at the same concentration (Table I). Third, the reaction rates for mutants with cys substitutions in ECL-1 were faster than those in ECL-4.

We previously reported that oocytes that expressed the flanking mutations in ECL-4 (S532C and A538C) did not show a significant loss of transport function when exposed to MTSEA at 100 μM (Lambert et al., 1999a). However, in the present study, at 10-fold

TABLE I

Reactivity of Mutated Sites

Linker	Site	c (mM)	$I_{P_i}^{\infty}$		k^* ($M^{-1}s^{-1}$)	
			MTSEA	MTSET	MTSEA	MTSET
ECL-1	G-134	0.01	1.81 ± 0.03	2.10 ± 0.08	455 ± 42	206 ± 27
	I-136	0.01	0.58 ± 0.03	0.52 ± 0.03	835 ± 134	1170 ± 250
	F-137	0.01	0.24 ± 0.02	0.07 ± 0.05	651 ± 67	1470 ± 300
	N-140	0.1	0.60 ± 0.02	0.60 ± 0.13	122 ± 23	109 ± 21
ECL-4	M-533	0.5	0.24 ± 0.01	0.19 ± 0.01	13.7 ± 0.9	37.1 ± 1.8
	A-534	0.1	0.54 ± 0.03	0.63 ± 0.06	60.1 ± 10.8	75.2 ± 24.4
	A-538	1.0	0	0	2.67 ± 0.11	1.97 ± 0.08

Each entry is the mean ± SEM obtained from the fit of Eq. 1 to data as illustrated in Fig. 4 (B and C). For A538C, the best fit was obtained by assuming $I_{P_i}^{\infty} = 0$.

greater MTSEA concentration, significant loss of function was observed for A538C, but still not for S532C (Fig. 2 B). Additional electrophysiological assays (unpublished data) on mutant S532C showed ~20% loss of response to 1 mM P_i ($V_h = -50$ mV) when exposed to 1 mM MTSEA for 10 min and ~40% after 25 min (unpublished data; $n = 3$). Because of its low reactivity compared with the other mutants in ECL-4, this site was considered only marginally accessible. At 1 mM concentration, it is possible that MTSEA was also present intracellularly, due to its reported membrane permeability (e.g., Holmgren et al., 1996), and therefore the loss of cotransport function may have been due to cytosolic action on other, internally accessible cysteines. However, exposure to 1 mM of MTSET also led to a comparable loss of activity for A538C, albeit with slower reaction rates (Fig. 4 C; Table I). This confirmed that the novel cysteines were accessible from the extracellular medium, in agreement with their predicted topology and the surface biotinylation assay.

Substrate Activation Unaffected by Cys Substitution and Cys Modification

The finite activity that remained at the completion of the MTS modification reactions suggested that kinetic properties of the mutated cotransporter were sensitive to cys modification. The most likely explanation would be a reduction (or increase, in the case of G134C) of the apparent substrate affinities at −50 mV. We therefore screened all the functional mutants to compare their substrate activation properties before and after a 5-min application of 1 mM MTSEA. To detect large deviations from the WT behavior of the apparent affinities for P_i ($K_m^{P_i}$) and Na^+ (K_m^{Na}), we applied a two-point assay, because in the case of poorly expressing mutants, a complete dose response could be difficult to obtain due to contamination from endogenous currents at low substrate concentrations. We have previously applied these assays to identify a mutant in the first intracellular linker region that showed significantly decreased apparent substrate affinities compared with the WT (Kohler et al., 2002a).

P_i activation was assayed by comparing the ratio of the responses to 0.1 mM P_i and 1 mM P_i for superfusion in ND100, termed the P_i activation index. Similarly, a Na^+ activation index, given by the ratio of the responses to 1 mM P_i for superfusion in ND50 and ND100, was used to quantitate the Na^+ activation. We confirmed the sensitivity of using this assay with simulations in which we assumed the P_i and Na^+ activation characteristics could be described by the modified Hill equation. For P_i activation (Fig. 5 A, left), the typical range of the index for the WT, based on assays performed in this study as well others (Lambert et al., 2000; Kohler et al., 2002a), should allow detection of changes in $K_m^{P_i}$ outside the range $0.05 < K_m^{P_i} < 0.12$ mM. For the Na^+ activation (Fig. 5 A, right), we would conservatively expect to detect changes in K_m^{Na} outside the range $40 < K_m^{Na} < 60$ mM. For example, if in the case of mutant G137C, the 60% decrease in the electrogenic response to 1 mM P_i after MTSEA exposure were due only to an increase in the apparent $K_m^{P_i}$ from the typical WT value of 0.06 mM to 1.65 mM, the P_i activation index would decrease from ~0.66 to 0.15, based on a simple Michaelian model for P_i activation and the same maximum transport rate ± MTSEA.

As shown in Fig. 5 B, for all functional mutants, both activation indices lay within or close to the WT range. Moreover, the indices before and after MTS exposure were similar for individual mutants. This suggested that at −50 mV, assuming an invariant Na^+:P_i 3:1 stoichiometry and that the degree of cooperativity of Na^+ binding does not deviate significantly from the WT, neither the cys substitution nor MTS modification had a significant effect on the apparent substrate affinities ($K_m^{P_i}$ and K_m^{Na}), and was most likely not the underlying reason for the altered transport activity.

Cys Substitution and Cys Modification Alter Voltage Dependency

Further insight into the mechanism underlying the changes in transport activity after cys modification was

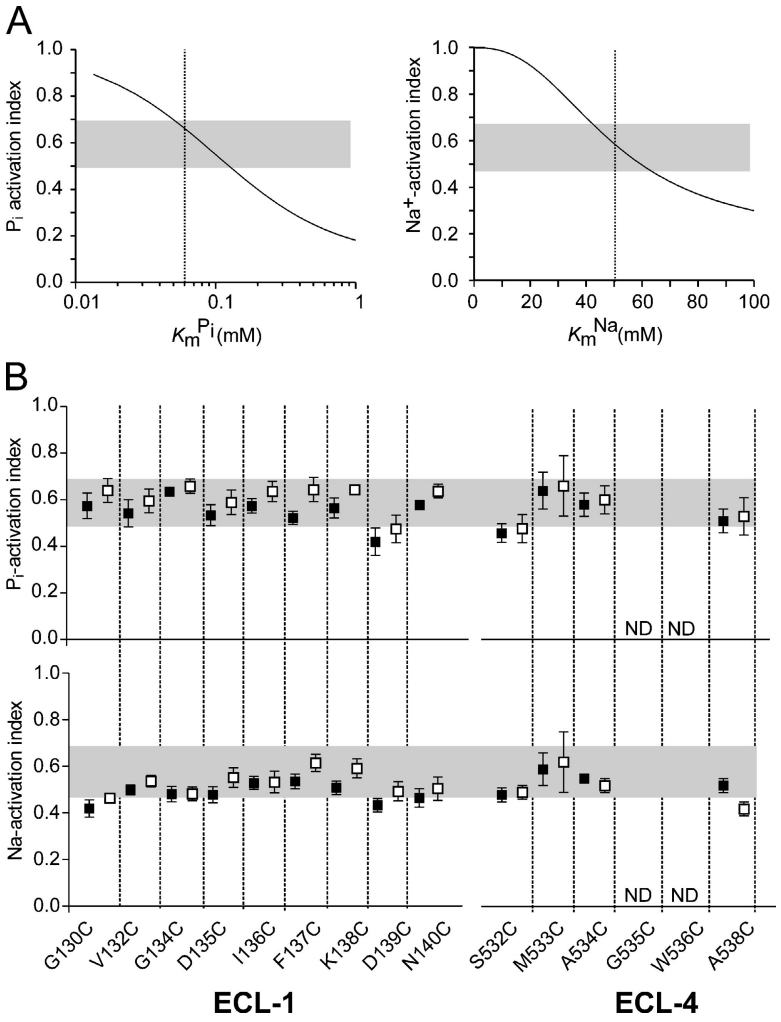

FIGURE 5. Screening for deviations from WT behavior of substrate activation kinetics at −50 mV using a two-point assay. (A) Two-point assay sensitivity for P_i activation (left) and Na^+ activation (right). Continuous lines are the P_i activation index (ratio of response in 100 mM Na^+ to 0.1 mM P_i and 1 mM P_i) as a function of apparent affinity for P_i ($K_m^{P_i}$) and Na^+ activation index (ratio of response to 1 mM P_i in 50 mM Na^+ and 100 mM Na^+) as a function of apparent affinity for Na^+ (K_m^{Na}), respectively. Indices were determined as a function of $K_m^{P_i}$ or K_m^{Na} using the modified Hill equation to describe the electrogenic response to P_i, $I_{P_i} = I_{P_i}^{max} (S^{n_H})/(S^{n_H} + K_m^{Sn_H})$, where S is the concentration of the variable substrate, K_m^S is the apparent affinity constant, n_H is the Hill coefficient (n_H = 1.0 for P_i activation, n_H = 2.5 for Na^+-activation; Forster et al., 1998, 1999), and $I_{P_i}^{max}$ is the P_i-dependent change in holding current at the saturating limit. In general, K_m^S and $I_{P_i}^{max}$ can also depend on the concentration of the invariant substrate and holding potential (V_h). Lower test concentration was chosen close to previously reported estimates for the WT apparent affinity, and upper test concentration was chosen close to the saturation concentration for P_i or maximum usable Na^+ concentration, for the P_i and Na^+ activation screens, respectively. For each case, the gray bar represents range of index values observed for WT-expressing oocytes (n = 9, three donor frogs). Vertical lines indicate typical $K_m^{P_i}$ for WT (0.06 mM) and K_m^{Na} for WT (50 mM) at −50 mV, previously reported (e.g., Forster et al., 1998), respectively. (B) P_i activation index (top) and Na^+ activation index (bottom), where each point is mean ± SEM for ≥4 oocytes. Gray bars indicate typical range observed for WT-expressing oocytes measured under the same experimental conditions. ND, not determined; −MTS, filled squares; +MTS, empty squares.

obtained from the current–voltage (*I–V*) relationships for P_i-dependent current. These were determined for superfusion with ND100 in response to the application of 1 mM P_i over voltage window $-120 \leq V \leq +20$ mV, in which contamination by endogenous currents was negligible. *I–V* data for four mutants that showed significantly changed activity after MTSEA treatment (1 mM, 3–5 min), G134C, I136C, F137C (ECL-1), and M533C (ECL-4), are shown in Fig. 6 A. Similar *I–V* data was also obtained using the positively charged MTSET and the negatively charged MTSES (unpublished data). To account for differences in expression levels between oocytes that expressed the same mutant, *I–V* data were normalized to the magnitude of I_{P_i} at −100 mV (1 mM P_i) before MTSEA exposure for WT, I136C, F137C and M533C. In the case of G134C, data were normalized to the magnitude of I_{P_i} after MTSEA exposure to aid comparison with the WT data. For the WT, MTSEA, MTSET, MTSES treatment at concentrations up to 10 mM resulted in insignificant changes to I_{P_i} over the voltage window shown (unpublished data).

The *I–V* curves of three mutants that showed a significant decrease in both $^{32}P_i$ uptake (Fig. 2 A) and electrogenic activity at −50 mV after MTS exposure (Fig. 2 B), I136C (Fig. 6 A, 1), F137C (Fig. 6 A, 2), and M533C (Fig. 6 A, 3), each showed only a small deviation from the normalized WT *I–V* relation before MTS exposure. This indicated that the cys substitution was reasonably well tolerated at these sites. At 0 mV after MTS incubation, there was a loss of transport activity, compared with WT, with the relative residual activity of F137C being significantly lower than the other mutants. Interestingly, the *I–V* data for M533C + MTS showed a negative slope over the voltage window used for these assays, whereas I136C + MTS and F137C + MTS showed curvilinear *I–V* relationships. Mutant G134C (Fig. 6 A, 4), which gave a reduced $^{32}P_i$ uptake (Fig. 2 A), but increased electrogenic activity at −50 mV (Fig. 2 B) also exhibited an *I–V* relationship with a negative slope before MTS exposure like M533C + MTS. After MTS exposure, the normalized *I–V* data for G134C showed a curvilinear *I–V* relationship compared with the WT.

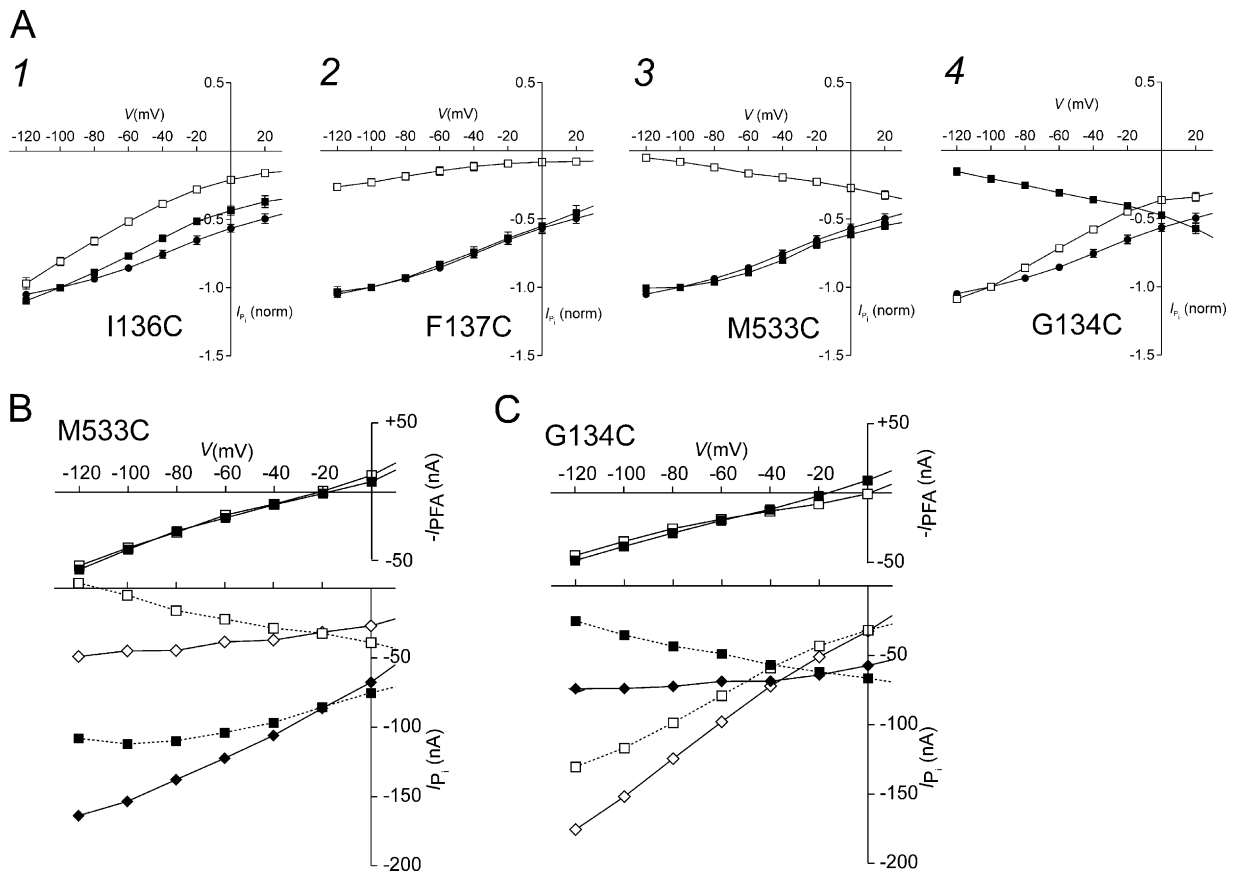

FIGURE 6. Current–voltage (*I–V*) curves for selected mutants. (A) Mutants that showed significantly decreased electrogenic activity at −50 mV after MTSEA exposure: I136C (1), F137C (2) in ECL-1, and M533C (3) in ECL-4, before MTSEA exposure (filled squares) and after 3–5 min exposure to 1 mM MTSEA (empty squares) ($n \geq 4$). G134C (4) in ECL-1 showed increased electrogenic activity at −50 mV after MTSEA exposure. Each data point is the change in holding current induced by 1 mM P_i (pH 7.4, in ND100), normalized to the magnitude of I_{P_i} at −100 mV, 1 mM P_i, before MTSEA exposure. For G134C, the data were normalized to the magnitude of I_{P_i} at −100 mV after MTSEA exposure. WT steady-state *I–V* data for I_{P_i} (filled circles) for WT-expressing oocytes, normalized to the magnitude of I_{P_i} at −100 mV ($n = 4$), are superimposed. SEMs smaller than symbol size are not shown. (B) *I–V* data showing the respective leak current (top) and P_i-dependent current (1 mM P_i) (bottom) for a representative oocyte that expressed M533C before (filled squares) and after (empty squares) MTSEA exposure; data points joined by dotted lines. The leak was estimated from the response to superfusion in 1 mM PFA ($-I_{PFA}$). The P_i-dependent currents were leak corrected by adding the respective leak values at each test potential before MTSEA exposure (filled diamonds) and after MTSEA exposure (empty diamonds); data points joined by continuous lines. (C) *I–V* data showing the respective leak current (top) and P_i-dependent current (1 mM P_i) (bottom) for a representative oocyte that expressed G134C before (filled squares) and after MTSEA exposure (empty squares); data points joined by dotted lines. The P_i-dependent currents were leak corrected by adding the respective leak values at each test potential before MTSEA exposure (filled diamonds) and after MTSEA exposure (empty diamonds); data points joined by continuous lines.

The negative slopes for G134C − MTS and M533C + MTS were inconsistent with the expected behavior of an electrogenic secondary-active transport system in which one net positive charge is transported per cycle (Forster et al., 1998). However, we could reconcile this apparent anomaly when we took account of an error introduced by the subtraction procedure used to obtain I_{P_i}. In these assays, we eliminated oocyte endogenous currents by subtracting the holding current in ND100 from the current in ND100 + P_i. However, if the leak and cotransport modes are assumed to be mutually exclusive (Kohler et al., 2002b), this procedure would underestimate the true cotransport mode current by an amount equal to the leak, if we assume that it is fully suppressed in the presence of 1 mM P_i. The leak mode activity was estimated by recording the change in holding current when superfusing in 1 mM PFA ($-I_{PFA}$). Fig. 6 B shows the P_i-dependent and leak currents for a representative oocyte that expressed M533C (B) and G134C (C) before and after incubation in 1 mM MTSEA for 3 min. The effect of MTS exposure on the leak current was minimal over the voltage range $-120 < V < 0$. For $V > 0$ mV, we found that endogenous Cl^- currents could also be induced by PFA in noninjected oocytes, and these data were therefore considered unreliable. When I_{P_i} was corrected for the leak error by

adding $-I_{PFA}$ at each potential, the leak-corrected I_{P_i} data now showed a positive slope with voltage-independent rate-limiting behavior at hyperpolarizing potentials for M533C + MTS and G134C − MTS.

The unique behavior of the G134C steady-state *I–V* data before and after MTS exposure can also account for the apparent anomaly between the $^{32}P_i$ uptake assay and the electrophysiological assay at $V_h = -50$ mV for this mutant. As shown in Fig. 6 C there is a crossover of the leak-corrected G134C *I–V* data before and after MTS exposure at approximately −40 mV for this oocyte. Under voltage clamp conditions for $V_h < -50$ mV, we would therefore predict an increased cotransport activity after MTS exposure. However, for the $^{32}P_i$ assay conditions used in this study, the membrane potential (V_m) was undefined. Therefore, externally applied P_i would induce a net inward positive charge movement (3 Na^+ + 1 HPO_4^{2-} per cycle) that would depolarize the oocyte membrane. If the shift in V_m were more positive than the crossover potential, a reduced uptake would be expected, since $^{32}P_i$ uptake and net translocated charge are tightly coupled for electrogenic type II Na^+/P_i cotransporters (Forster et al., 1999).

To test this hypothesis, we measured the change in membrane potential (V_m) with the voltage clamp loop open before and after MTS exposure. For the representative G134C-expressing oocyte in Fig. 6 C, application of 1 mM P_i induced a change in V_m from −28 mV to +5 mV, whereas after MTS exposure, V_m changed from −35 to −10 mV. For a given cell impedance, the P_i-dependent change in V_m is proportional to the net charge translocated, which is a function of the number of transporters in the membrane (assumed constant) and the transporter turnover rate. It follows from these data that we would expect a reduced $^{32}P_i$ uptake after MTS exposure, as we observed. We found that this result was also consistent with the corresponding currents at the V_m reached during P_i application (−MTS, −56 nA; +MTS, −42 nA), which we found by interpolation of the leak-corrected *I–V* data of Fig. 6 C. The reduced depolarizing shift in V_m after MTS exposure was confirmed for a batch ($n = 9$) of G134C-expressing oocytes, under the same conditions as for the tracer flux assay. The change in V_m due to P_i superfusion was +31 ± 1 mV for −MTS, and this decreased to +19 ± 1 mV for +MTS. These findings serve to underscore the importance of defining the membrane potential in transport assays involving electrogenic membrane proteins.

From the *I–V* data of Fig. 6 A, it was obvious that the effect of cys substitution at Gly-134 and modification of Cys-136, Cys-137C, and Cys-533 was to reduce the transport activity induced by 1 mM P_i over a wide voltage range. By normalizing the leak-corrected *I–V* data to $V = 0$, the relative effect of hyperpolarizing membrane potentials on the cotransport activity before and after

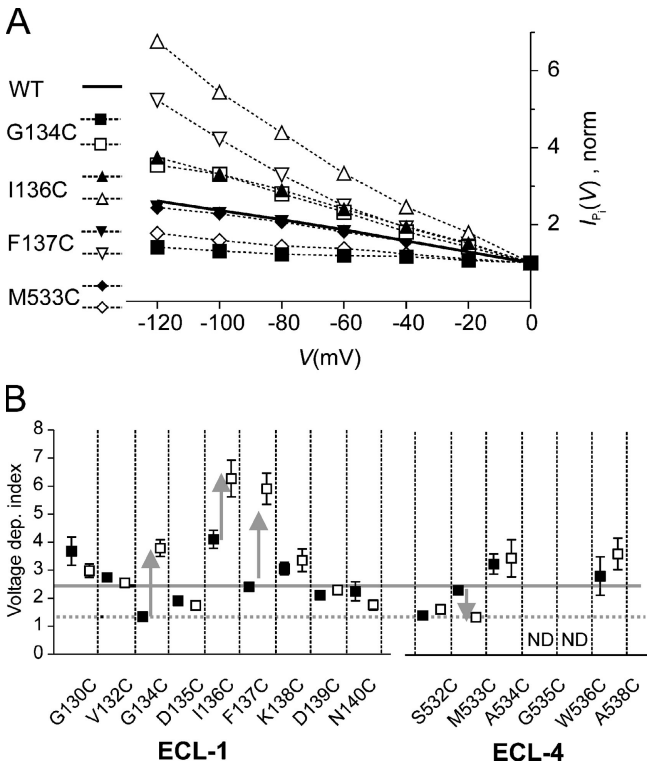

FIGURE 7. Cysteine engineering at sites in ECL-1 and ECL-4 induces deviations from WT voltage dependency. (A) Voltage dependency of G134C (squares), I136C (triangles), F137C (inverted triangles), and M533C (diamonds), before (filled symbols) and after (open symbols) incubation in MTSEA (1 mM, 3 min). P_i-dependent currents, corrected for leak, were normalized to the response at 0 mV. The ordinate scale represents the relative change in I_{P_i} as a function of membrane potential. Data pooled from $n > 4$ cells. WT data is represented by continuous line. (*B*) Voltage dependency index for all functional mutants given by ratio of response to 1 mM P_i at −100 mV to that at 0 mV (100 mM Na^+) before (filled squares) and after (open squares) MTS treatment (1 mM MTSEA, 3 min). Continuous reference line indicates WT index. Dotted reference line indicates that G134C-MTS, S532C ± MTS, and M533C + MTS have the same index. Arrows indicate direction of voltage dependency change for selected mutants after MTS incubation.

MTS exposure was determined (Fig. 7 A). These data showed that cys substitution at Ile-136 and Met-533 resulted in constructs with a voltage dependency that was indistinguishable from the WT. Cys modification at these sites increased (I136C + MTS) and decreased (M533 + MTS), respectively, the response to changes in membrane potential in the hyperpolarizing direction relative to the WT. Cys substitution at Phe-137 gave an increased voltage dependency compared with the WT that was further augmented after MTS exposure, like I136C + MTS. Finally, cys substitution at Gly-134 gave a reduced voltage dependency compared with the WT that was comparable to M533C + MTS. After MTS exposure, the voltage dependency of G134C was similar to that of I136C + MTS.

To quantify changes in voltage dependency after MTS exposure of other functional mutants that had shown little or no change in electrogenic activity at −50 mV (Fig. 2 B), we assigned a voltage dependency index to each mutant. This was given by the ratio of leak-corrected I_{P_i} at −100 mV to I_{P_i} at 0 mV, before and after MTS exposure (Fig. 7 B). This index represents the change in cotransport activity for a voltage change from 0 to −100 mV. Cys substitution produced changes in this index relative to the WT for nearly all mutants. Mutants that showed no change in activity after MTS exposure also showed no significant change in their respective voltage dependency indices (G130C, V132C, D135C, K138C, D139C in ECL-1 and A534C, S532C in ECL-4); however, the cys substitution itself resulted in altered voltage dependencies compared with the WT. The general trend was for the voltage dependency index to increase after cys modification in both ECL-1 and ECL-4, with the notable exception of M533C in ECL-4.

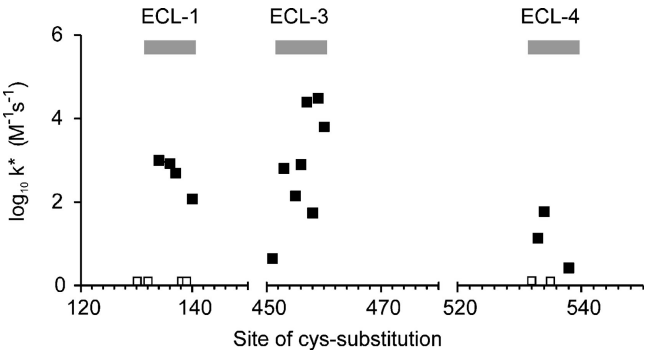

FIGURE 8. Graphical representation of accessibility of three putative extracellular linkers based on effective second order reaction rate k^* plotted on a logarithmic scale (filled squares). A larger k^* indicates that the site has a greater accessibility from the external aqueous medium. Sites that were labeled with MTSEA-Biotin, for which the respective mutants showed no detectable change in activity, are indicated (empty squares). Data for ECL-1 and ECL-4 were obtained from this study (Table I); data for ECL-3 were replotted from a previous study (Lambert et al., 2001).

DISCUSSION

In this study of the structure–function relationships of sites in putative external linkers ECL-1 and ECL-4 of the rat NaPi-IIa isoform, SCAM yielded both structural and functional information. First, it established the location of substituted sites in hydrophilic regions accessible from the external medium, in agreement with current topological predictions. Second, based on an analysis of the steady-state *I–V* relationships before and after cys modification, we show that cysteine engineering at sites in each linker determines the sensitivity of cotransport activity to changes in membrane potential.

To interpret our data, which is based on the introduction of novel Cys residues in the WT backbone, we made a tacit assumption that the target Cys residue was the novel Cys itself and not one or more of the 12 native Cys residues. Ideally, SCAM should be performed on a cys-less backbone to avoid ambiguities that could arise if the introduction of a novel Cys exposes a previously inaccessible and functionally important native Cys (Kaback et al., 2001; Kamdar et al., 2001). Unfortunately, a cys-reduced construct of NaPi-IIa shows significantly lower transport activity compared with the WT (Kohler et al., 2003) and this would exacerbate detailed kinetic analyses. Nevertheless, three pieces of evidence support the validity of the above assumption: (1) when removed singly, no native Cys appears to be critical for viable cotransport function (Lambert et al., 2000); (2) up to eight Cys can be removed, while retaining transport function (Kohler et al., 2003), the remaining four being involved in two disulfide bridges (Lambert et al., 2000; Kohler et al., 2003); and (3) introduction of a Cys at site 460, previously found to be functionally important for the WT backbone (Lambert et al., 1999b), shows the same behavior in the cys-reduced NaPi-IIa (Kohler et al., 2003).

Accessibility and Membrane Topology

Although we used MTSEA as the standard probe reagent, exposure to impermeant MTSET gave qualitatively similar results. This confirmed that the sites were accessible from the external medium only. Small differences in reactivity between MTSEA and MTSET were observed in the rates of modification (i.e., the rate of change of the electrogenic activity) at different sites in ECL-1 and ECL- 4 (Table I). The faster reaction rates of MTSET for most mutants most likely reflect the higher reactivity of this reagent with small thiols compared with MTSEA (Karlin and Akabas, 1998). For G134C and A538C, MTSEA was more reactive than MTSET, perhaps because the greater bulk of MTSET restricts its access to these sites. As summarized in Fig. 8, the effective second order reaction rate constants lay within the range of values that we have previously reported for Cys mutants in ECL-3 (Lambert et al., 2001) and establish conclusively that these three regions are accessible from the external aqueous environment. Rates of modification for extracellularly accessible sites in other transport proteins such as the excitatory amino acid transporter (EAAT1) (e.g., Leighton et al., 2002), the mitochondrial citrate transporter (Ma et al., 2004), and the serotonin transporter (SERT) (Chen et al., 1997) have been reported to lie in the same range as we found for NaPi-IIa. In the present study, the modification rates for mutants in ECL-1 were consistently faster than those in ECL-4. This would suggest that ECL-4 was less accessible from the extracellular medium. At one site in ECL-1 (Asp-135) and one site in ECL-4 (Trp-536) we were un-

able to detect the novel cysteines using the biotinylation assay, which indicated that these cysteines were inaccessible, either because of the bulk of MTSEA-Biotin or the specific folding of the linkers at these sites.

The functional consequences of exposure to MTS reagents varied considerably among neighbors. For example, Cys-135 could not be labeled with MTSEA-Biotin, and, consistent with this result, mutant D135C showed no change in its kinetics after MTS exposure. In contrast, we could detect its immediate neighbors (Cys-134 and Cys-136) with MTSEA-Biotin; however, G134C and I136C showed significantly altered voltage dependencies after MTS exposure. In other cases, cys substitution did not result in MTS-sensitive mutants, although we could successfully detect the novel cysteines with the biotinylation assay (e.g., Cys-130, Cys-132, Cys-138, and Cys-139). This suggested that these sites were not functionally critical. Finally, the striking behavior of mutant G134C indicated that the native Gly at this site is crucial for normal electrogenic behavior. Gly-134 is conserved among a number of NaPi-II isoforms, and its small size might confer a unique flexibility to this linker and the associated transmembrane domains that is restricted when replaced with a bulkier Cys.

Modulation of Steady-state Voltage-dependent Kinetics

In a previous SCAM study, a cluster of mutants was found in ECL-3, most of which showed full suppression of cotransport mode activity after MTS exposure (Lambert et al., 2001). These constructs yielded characteristically similar P_i and PFA responses at the end of the modification reaction, from which we concluded that P_i could interact with NaPi-IIa and thereby inhibit the leak mode, but the cotransport mode was suppressed. This led us to postulate that these sites are associated with the transport pathway itself (Lambert et al., 1999a, 2001; Kohler et al., 2002a,b). In the present study, all the MTS-sensitive mutants, except A538C, showed a P_i-dependent electrogenic response at −50 mV that asymptoted to a nonzero level, at the end of the modification reaction. This behavior suggested that they may not be directly associated with the transport pathway or the substrate recognition site as, in the latter case, kinetic analysis of these mutants under voltage clamp conditions revealed that apparent substrate affinities appeared unchanged, either from cys substitution or cys modification. On the other hand, cysteine engineering at sites in ECL-1 and ECL-4 resulted in significantly altered voltage-dependent activity compared with the WT, depending on the site of cys substitution or cys modification.

Mutants could be broadly classified according to whether there was increased, decreased, or unchanged activity compared with the WT for hyperpolarizing membrane potentials (0 to −100 mV) (Fig. 7 B). The finding that most mutants deviated from WT behavior suggested that the amino acid residues in ECL-1 and ECL-4 were critical determinants of the NaPi-IIa voltage-dependent kinetics. Several "hot spots" emerged from these assays, for which the voltage-dependent activity of the corresponding mutants deviated significantly from the WT, either due to cys substitution alone, cys modification, or both. For example, cys substitution at Ile-136 increased the voltage-dependent activity, whereas at the neighboring Phe-137, cys substitution was well tolerated. However, cys modification at both sites led to a significantly increased voltage-dependent activity. Interestingly, cys substitution at Gly-130 and Ile-136 led to the same increase in activity. This was mimicked by cys modification of Cys-134, intermediate in the amino acid sequence in ECL-1, and by cys substitution at Ala-534 and Ala-538 in ECL-4. Such similar behavior indicated that engineering at sites in each linker had induced the same voltage-sensitive conformational changes in the protein. Complementary behavior was also documented, in which the opposite effects on voltage dependency were found for cys substitution at Gly-134 in ECL-1 and Met-533 in ECL-4. G134C-MTS and M533C + MTS both exhibited a weakly voltage-dependent activity, whereas that of G134C + MTS exceeded the WT, and the voltage dependency of M533C − MTS was indistinguishable from the WT. Interestingly, cys substitution at the Ser-532 resulted in the same weak voltage-dependent activity as shown by M533C + MTS with little change in activity after MTS exposure. This suggested that the conformational change induced by modification of Cys-533 in ECL-4 was the same as that made by introducing a cysteine at the preceding site (Ser-532), or at Gly-134 in ECL-1. The novel complementary behavior of G134C and M533C is the subject of a more detailed kinetic analysis in the accompanying study (Ehnes et al., 2004).

In addition to relative changes in voltage-dependent activity, the *I–V* behavior revealed that for G134C − MTS and M533C + MTS, the maximum transport rate at the hyperpolarizing limit was also affected. In each case, the leak-corrected *I–V* curves showed rate-limiting behavior in the same voltage range where the WT, G134C + MTS, and M533C − MTS voltage-dependent activity was still approximately linear. The overall behavior of these mutants suggested that the cys substitution and cys modification at these sites had (a) slowed one or more voltage-independent rate constants in the transport cycle and (b) induced a depolarizing shift in voltage-dependent transitions associated with either the empty carrier, first Na^+ binding transition, or both, in accordance with the current alternating access model for NaPi-IIa (Forster et al., 2002).

Are sites in ECL-1 and ECL-4 part of the voltage-sensing mechanism of NaPi-IIa? Three pieces of evidence

suggest this is not the case. First, one might expect mobile charged or polar residues to constitute the voltage sensor and their removal would have a dramatic effect on the electrogenic behavior of the protein. Although ECL-4 has no charged residues, three sites in ECL-1 (D-135, K-138, and D-139) could be potential candidates, but when replaced by cysteines, the resulting mutants were still electrogenic (Fig. 7 B), albeit with only small deviations in voltage dependency from the WT. Similarly, substitution of the polar Ser-532 (ECL-4) with a nonpolar Cys weakened the voltage dependency (Fig. 7 B). These findings suggest that the particular charged or polar residues may certainly interact with the putative voltage-dependent elements to modulate the voltage dependency of transport, but the intrinsic voltage sensitivity of the protein remains intact. In another electrogenic cotransporter, the Na^+-coupled glucose transporter (SGLT-1), polar residues have been shown to modulate charge movements and alter empty carrier kinetics without affecting the overall apparent valency of the cotransporter (Panayotova-Heiermann et al., 1994). Second, one member of the SLC34 family, the renal type IIc isoform, is electroneutral (Segawa et al., 2002; unpublished data). NaPi-IIc has a high homology with the electrogenic type IIa Na^+/P_i cotransporter, with both charged residues in ECL-1 being conserved (Fig. 1 B). Third, the same MTS-induced changes to the voltage dependency occurred using either positively or negatively charged MTS reagents. This suggests that the charge introduced by these reagents either lies outside the transmembrane field or does not interact with the intrinsic voltage-sensing elements.

In summary, the outermost external linkers of the NH_2- and COOH-terminal halves of NaPi-IIa contain sites that when occupied by Cys residues, are localized in an externally accessible, hydrophilic environment, which is consistent with hydropathy predictions. The native residues in these linkers are not absolutely essential for Na^+-coupled P_i cotransport function; however, cys substitution or covalent modification of the novel cysteines by externally applied MTS reagents affected the voltage-dependent kinetics of the mutant transporters. As changes in membrane potential are expected to induce major conformational changes in the native protein during the transport cycle (e.g., Loo et al., 1998), the findings reported here suggest that linkers ECL-1 and ECL-4 contain specific sites that may interact directly or indirectly with mobile, voltage-sensitive elements of the NaPi-IIa protein.

We thank Dr. Leila Virkki (University of Zurich) for helpful comments on the manuscript.

This work was supported by grants to H. Murer from the Swiss National Science Foundation (31-46523), the Hartmann Müller-Stiftung (Zurich), the Olga Mayenfisch-Stiftung (Zurich), and the Union Bank of Switzerland (Zurich) (Bu 704/7-1).

Lawrence G. Palmer served as editor.

Submitted: 12 March 2004
Accepted: 14 September 2004

REFERENCES

Chen, J.G., S. Liu-Chen, and G. Rudnick. 1997. External cysteine residues in the serotonin transporter. *Biochemistry.* 36:1479–1486.

Custer, M., M. Lotscher, J. Biber, H. Murer, and B. Kaissling. 1994. Expression of Na-P(i) cotransport in rat kidney: localization by RT-PCR and immunohistochemistry. *Am. J. Physiol.* 266:F767–F774.

Ehnes, C., I.C. Forster, K. Kohler, A. Bacconi, J. Biber, and H. Murer. 2004. Structure–function relations of the first and fourth extracellular linkers of the type IIa Na^+/P_i cotransporter. II. Substrate interaction and voltage dependency of two functionally important sites. *J. Gen. Physiol.* 124:489–503.

Forster, I., N. Hernando, J. Biber, and H. Murer. 1998. The voltage dependence of a cloned mammalian renal type II Na^+/P_i cotransporter (NaPi-2). *J. Gen. Physiol.* 112:1–18.

Forster, I., D.D. Loo, and S. Eskandari. 1999. Stoichiometry and Na^+ binding cooperativity of rat and flounder renal type II Na^+-P_i cotransporters. *Am. J. Physiol.* 276:F644–F649.

Forster, I.C., K. Kohler, J. Biber, and H. Murer. 2002. Forging the link between structure and function of electrogenic transporters: the renal type IIa Na^+/P_i cotransporter as a case study. *Prog. Biophys. Mol. Biol.* 80:69–108.

Holmgren, M., Y. Liu, Y. Xu, and G. Yellen. 1996. On the use of thiol-modifying agents to determine channel topology. *Neuropharmacology.* 35:797–804.

Kaback, H.R., M. Sahin-Toth, and A.B. Weinglass. 2001. The kamikaze approach to membrane transport. *Nat. Rev. Mol. Cell Biol.* 2:610–620.

Kamdar, G., K.M. Penado, G. Rudnick, and M.M. Stephan. 2001. Functional role of critical stripe residues in transmembrane span 7 of the serotonin transporter. Effects of Na^+, Li^+, and methanethiosulfonate reagents. *J. Biol. Chem.* 276:4038–4045.

Karlin, A., and M.H. Akabas. 1998. Substituted-cysteine accessibility method. *Methods Enzymol.* 293:123–145.

Kohler, K., I.C. Forster, G. Lambert, J. Biber, and H. Murer. 2000. The functional unit of the renal type IIa Na^+/P_i cotransporter is a monomer. *J. Biol. Chem.* 275:26113–26120.

Kohler, K., I.C. Forster, G. Stange, J. Biber, and H. Murer. 2002a. Identification of functionally important sites in the first intracellular loop of the NaPi-IIa cotransporter. *Am. J. Physiol. Renal Physiol.* 282:F687–F696.

Kohler, K., I.C. Forster, G. Stange, J. Biber, and H. Murer. 2002b. Transport function of the renal type IIa Na^+/P_i cotransporter is codetermined by residues in two opposing linker regions. *J. Gen. Physiol.* 120:693–705.

Kohler, K., I.C. Forster, G. Stange, J. Biber, and H. Murer. 2003. Essential cysteine residues of the type IIa Na^+/P_i cotransporter. *Pflugers Arch.* 446:203–210.

Lambert, G., I.C. Forster, G. Stange, J. Biber, and H. Murer. 1999a. Properties of the mutant Ser-460-Cys implicate this site in a functionally important region of the type IIa Na^+/P_i cotransporter protein. *J. Gen. Physiol.* 114:637–652.

Lambert, G., M. Traebert, N. Hernando, J. Biber, and H. Murer. 1999b. Studies on the topology of the renal type II NaPi-cotransporter. *Pflugers Arch.* 437:972–978.

Lambert, G., I.C. Forster, J. Biber, and H. Murer. 2000. Cysteine residues and the structure of the rat renal proximal tubular type II sodium phosphate cotransporter (rat NaPi IIa). *J. Membr. Biol.* 176:133–141.

Lambert, G., I.C. Forster, G. Stange, K. Kohler, J. Biber, and H.

Murer. 2001. Cysteine mutagenesis reveals novel structure-function features within the predicted third extracellular loop of the type IIa Na^+/P_i cotransporter. *J. Gen. Physiol.* 117:533–546.

Leighton, B.H., R.P. Seal, K. Shimamoto, and S.G. Amara. 2002. A hydrophobic domain in glutamate transporters forms an extracellular helix associated with the permeation pathway for substrates. *J. Biol. Chem.* 277:29847–29855.

Loo, D.D., B.A. Hirayama, E.M. Gallardo, J.T. Lam, E. Turk, and E.M. Wright. 1998. Conformational changes couple Na^+ and glucose transport. *Proc. Natl. Acad. Sci. USA.* 95:7789–7794.

Ma, C., R. Kotaria, J.A. Mayor, L.R. Eriks, A.M. Dean, D.E. Walters, and R.S. Kaplan. 2004. The mitochondrial citrate transport protein: probing the secondary structure of transmembrane domain III, identification of residues that likely comprise a portion of the citrate transport pathway, and development of a model for the putative TMDIII-TMDIII interface. *J. Biol. Chem.* 279:1533–1540.

Magagnin, S., A. Werner, D. Markovich, V. Sorribas, G. Stange, J. Biber, and H. Murer. 1993. Expression cloning of human and rat renal cortex Na/Pi cotransport. *Proc. Natl. Acad. Sci. USA.* 90: 5979–5983.

Murer, H., N. Hernando, I. Forster, and J. Biber. 2000. Proximal tubular phosphate reabsorption: molecular mechanisms. *Physiol. Rev.* 80:1373–1409.

Murer, H., N. Hernando, I. Forster, and J. Biber. 2003. Regulation of Na/Pi transporter in the proximal tubule. *Annu. Rev. Physiol.* 65:531–542.

Panayotova-Heiermann, M., D.D. Loo, M.P. Lostao, and E.M. Wright. 1994. Sodium/D-glucose cotransporter charge movements involve polar residues. *J. Biol. Chem.* 269:21016–21020.

Sambrook, J., E.F. Fritsch, and A.M. Maniatis. 1989. Molecular Cloning: A Laboratory Manual. Cold Spring Harbor Laboratory, Cold Spring Harbor, NY. 18.66–18.75.

Segawa, H., I. Kaneko, A. Takahashi, M. Kuwahata, M. Ito, I. Ohkido, S. Tatsumi, and K. Miyamoto. 2002. Growth-related renal type II Na/Pi cotransporter. *J. Biol. Chem.* 277:19665–19672.

Turk, E., C.J. Kerner, M.P. Lostao, and E.M. Wright. 1996. Membrane topology of the human Na^+/glucose cotransporter SGLT1. *J. Biol. Chem.* 271:1925–1934.

Werner, A., J. Biber, J. Forgo, M. Palacin, and H. Murer. 1990. Expression of renal transport systems for inorganic phosphate and sulfate in *Xenopus laevis* oocytes. *J. Biol. Chem.* 265:12331–12336.

Zhang, H., and A. Karlin. 1997. Identification of acetylcholine receptor channel-lining residues in the M1 segment of the beta-subunit. *Biochemistry.* 36:15856–15864.

3.3 Summary of publication:

Structure-function relations of the first and fourth extracellular linkers of the type IIa Na^+/Pi cotransporter:
II. Substrate interaction and voltage dependency of two functionally important sites

Zusammenhänge zwischen Funktion und Struktur des ersten und vierten extrazellulären Verbindungsstückes des Typ IIa Na^+/P_i Kotransporters
II: Substratinteraktion und Spannungsabhängigkeit von zwei kritischen Positionen

Durch Anwendung von SCAM wurden funktionell wichtige Positionen im ersten und vierten extrazellulären Verbindungsstück des Typ IIa Na^+/P_i Kotransporters (NaPi-IIa) identifiziert (Ehnes et al., 2004). Das Einfügen von Cysteinen oder ihre Modifikation durch permeable und nicht-permeable Methanethiosulfonat (MTS) Reagenzien resultierte in signifikanten Veränderungen der Spannungsabängigkeit des Proteins im transportierenden Zustand (1 mM P_i, 100 mM Na^+, pH 7.4). An den Positionen Gly-134 des ECL-1 und Met-533 des ECL-4, wurde ein komplementäres Verhalten der Spannungsabhängigkeit durch das Einfügen und Modifizieren von Cysteinen dokumentiert. Die Mutante G134C wies eine schwache Spannungsabhängigkeit auf, die nach MTS Inkubation zu einer stark spannungsabhängigen, mit dem WT vergleichbaren Funktion zurückkehrte. Die Mutante M533C zeigte eine mit dem WT vergleichbare Reaktion gegenüber Spannung, die sich nach MTS Inkubation signifikant abschwächte. Um den zugrundeliegenden Mechanismus aufzudecken, wurden die Kinetiken dieser Mutanten im transportierenden und die der Ladungsverteilungen über die Membran im Detail untersucht. Die Spannungsabhängigkeit der gemessenen Affinitätskonstanten für Na^+ und P_i waren über den gesamten gemessenen Spannungsbereich vergleichbar mit denen des WT. Die Abhängigkeit gegenüber externen Protonen veränderte sich jedoch in reziproker Art und Weise. Dies lässt darauf schliessen, dass die Cysteinmutationen und -modifikationen Konformationsänderungen bewirkten, welche den Einfluss von Protonen auf die Regulierung der Transportkinetiken veränderte.

Das Verhalten im transportierenden Zustand und das der Ladungsverteilungen über die Membran wurde durch ein kinetisches Modell dargestellt, in dem der Kotransportmechanismus durch 8 Konformationen beschrieben wird. In diesem Modell waren die Übergangskonstanten des leeren und des voll beladenen Transportproteins bestimmende Faktoren für die Transportkinetiken. Die Simulation sagt für die Cysteinsubstitution des Gly-134 oder die Cysteinmodifikation des Cys-533

eine bedeutende Umorientierung der bevorzugten Konformation des leeren Proteins voraus: die nach innen orientierte Konformation geht bei hyperpolarisierenden Potentialen in die nach aussen orientierte über. Dies impliziert eine modulierende Rolle der ECL-1 und -4 innerhalb des NaPi-IIa Transportmechanismus.

Structure–Function Relations of the First and Fourth Extracellular Linkers of the Type IIa Na^+/P_i Cotransporter: II. Substrate Interaction and Voltage Dependency of Two Functionally Important Sites

Colin Ehnes, Ian C. Forster, Andrea Bacconi, Katja Kohler, Jürg Biber, and Heini Murer

Institute of Physiology, University of Zurich, CH-8057 Zurich, Switzerland

ABSTRACT Functionally important sites in the predicted first and fourth extracellular linkers of the type IIa Na^+/P_i cotransporter (NaPi-IIa) were identified by cysteine scanning mutagenesis (Ehnes et al., 2004). Cysteine substitution or modification with impermeant and permeant methanethiosulfonate (MTS) reagents at certain sites resulted in changes to the steady-state voltage dependency of the cotransport mode (1 mM P_i, 100 mM Na^+ at pH 7.4) of the mutants. At Gly-134 (ECL-1) and Met-533 (ECL-4), complementary behavior of the voltage dependency was documented with respect to the effect of cys-substitution and modification. G134C had a weak voltage dependency that became even stronger than that of the wild type (WT) after MTS incubation. M533C showed a WT-like voltage dependency that became markedly weaker after MTS incubation. To elucidate the underlying mechanism, the steady-state and presteady-state kinetics of these mutants were studied in detail. The apparent affinity constants for P_i and Na^+ did not show large changes after MTS exposure. However, the dependency on external protons was changed in a complementary manner for each mutant. This suggested that cys substitution at Gly-134 or modification of Cys-533 had induced similar conformational changes to alter the proton modulation of transport kinetics. The changes in steady-state voltage dependency correlated with changes in the kinetics of presteady-state charge movements determined in the absence of P_i, which suggested that voltage-dependent transitions in the transport cycle were altered. The steady-state and presteady-state behavior was simulated using an eight-state kinetic model in which the transition rate constants of the empty carrier and translocation of the fully loaded carrier were found to be critical determinants of the transport kinetics. The simulations predict that cys substitution at Gly-134 or cys modification of Cys-533 alters the preferred orientation of the empty carrier from an inward to outward-facing conformation for hyperpolarizing voltages.

KEY WORDS: phosphate transport proteins • mutagenesis site directed • cysteine • electrophysiology • transport model

INTRODUCTION

Structure–function studies on membrane transport proteins are used to identify functionally important sites and confirm or establish secondary topological features. The application of the substituted cysteine accessibility method (SCAM) to the renal type IIa Na^+/P_i cotransporter (NaPi-IIa) has enabled us to identify functionally important sites that may constitute part of the transport pathway through the protein (Lambert et al., 2001; Kohler et al., 2002a,b). This involves the first intracellular loop (ICL-1) in the NH_2-terminal half of the protein and the third extracellular loop located in the COOH-terminal half of the protein. The modification of cysteines substituted at these sites in almost all cases led to complete block of the cotransport mode, and in some cases increased the leak mode activity (Kohler et al., 2002b). To continue our study of the functional contribution of predicted transmembrane domain linker regions of NaPi-IIa, we have applied SCAM to the two putative extracellular loops ECL-1 and ECL-4 (Ehnes et al., 2004). Cys substitution at each of nine sites in ECL-1 and six sites in ECL-4 was well tolerated, and $^{32}P_i$ uptake and electrogenic behavior were documented for these mutants (Ehnes et al., 2004). In contrast to our previous studies (Lambert et al., 1999, 2001; Kohler et al., 2002a,b), at the completion of the methanethiosulfonate (MTS) modification reaction, these mutants still exhibited a finite cotransport activity that we attributed to altered steady-state voltage-dependent kinetics (Ehnes et al., 2004). Two mutants were selected for more detailed investigation in this study because their voltage dependency changed in a reciprocal manner depending on whether the novel cysteine was modified or not.

C. Ehnes and I.C. Forster contributed equally to this work.

Address correspondence to Ian C. Forster, Physiologisches Institut, University of Zurich, Winterthurerstrasse 190, CH-8057 Zurich, Switzerland. Fax: 41-1-635 5715; email: IForster@access.unizh.ch

K. Kohler's present address is Laboratory of Morphogenesis and Cell Signaling, UMR144, Institut Curie, Paris, France.

Abbreviations used in this paper: MTS, methanethiosulfonate; MTSEA, 2-aminoethyl MTS hydrobromide; NaPi-IIa, type IIa Na^+/P_i cotransporter; WT, wild type.

J. Gen. Physiol. © The Rockefeller University Press • 0022-1295/2004/11/489/15 $8.00
Volume 124 November 2004 489–503
http://www.jgp.org/cgi/doi/10.1085/jgp.200409061

Unlike for some ion channels, the mechanism by which membrane voltage is transduced into conformational changes for cation-coupled cotransporters is not well understood. The two mutants investigated here offer an opportunity to study this mechanism in a Na^+-coupled cotransport system because they exhibit easily distinguishable characteristics that can be altered in situ by chemical mutagenesis. We interpreted both steady-state and presteady-state analyses to show that the cys substitution and cys modification induce major conformational changes associated with preferred state occupancy of the empty carrier, in agreement with the concept of an alternating access model for cation-coupled electrogenic cotransporters. We further suggest that for NaPi-IIa, these conformational changes lead to an altered access by protons that can interact with voltage-sensitive elements of the NaPi-IIa protein and that the two extracellular linker regions studied here may be involved in major structural rearrangements of the protein during transport.

MATERIALS AND METHODS

The experimental methods and materials used in this study were essentially the same as described in the previous article (Ehnes et al., 2004) with the following additions.

Reagents and Solutions

The solution compositions (in mM) were as follows. (a) Control superfusate (ND100): NaCl (100), KCl (2), $CaCl_2$ (1.8), $MgCl_2$ (1), HEPES-TRIS (10) (for pH 8.0–6.2) or HEPES-MES (10) (for pH 5.6–5.0). For presteady-state protocols, $CaCl_2$ was replaced with equimolar $BaCl_2$ to reduce contamination from endogenous Ca^{2+}-activated Cl^- channels. (b) Control superfusate (ND0): as for ND100 with choline chloride used to replace Na^+. Solutions with intermediate Na^+ concentrations for determining the Na^+ activation kinetics were prepared by mixing ND0 and ND100 in the appropriate proportions or adding the molar equivalent of NaCl for concentrations >100 mM.

Functional Assays and Data Analysis

Steady-state Assays. The P_i activation kinetics were determined at 100 mM Na^+, with six P_i concentrations (total P_i, pH 7.4) in the range 0.01–3 mM P_i; the Na^+ activation kinetics were determined at 1 mM P_i (total P_i, pH 7.4) with six Na^+ concentrations in the range 10–125 mM. The proton dependency was determined using ND100 with pH ranging from 5.0 to 8.0 in 0.6 pH unit increments and total P_i = 1 mM. Voltage dependency of the kinetic parameters was determined using the voltage staircase protocol as previously described (Ehnes et al., 2004), and endogenous oocyte currents were eliminated by subtracting the holding current recorded when the oocyte was superfused in a P_i-free control solution with the same ionic composition as the test solution.

The P_i activation data were fit with a form of the Michaelis-Menten equation:

$$I_{P_i} = I_{P_i}^{max}([P_i]/([P_i] + K_m^{P_i})) + K, \quad (1)$$

where $[P_i]$ is the P_i concentration, $K_m^{P_i}$ is the apparent affinity for P_i, and $I_{P_i}^{max}$ is the maximum cotransport rate. K is a variable offset to take account of the reversal of I_{P_i} that arises from the above subtraction procedure when the net electrogenic activity, contributed by the cotransport and leak modes, is less than the maximum leak activity. The Na^+ activation data were fit with the modified Hill equation:

$$I_{P_i} = I_{P_i}^{max}([Na]^{n_H}/([Na]^{n_H} + (K_m^{Na})^{n_H})) + K, \quad (2)$$

where [Na] is the concentration of Na^+, n_H is the Hill coefficient, K_m^{Na} is the apparent affinity for Na^+, and K is a variable offset, as above. For characterizing proton interactions, Eq. 2 was used with proton concentration substituted for [Na] and $n_H < 0$, to predict the apparent inhibition constant K_i^H for protons.

Presteady-state Relaxations. These were acquired using voltage steps from $V_h = -60$ mV to test potentials in the range −180 mV to +60 mV. Signals were averaged fourfold, sampled at 50 μs/point, and low-pass filtered at 400 Hz. To improve the signal-to-noise ratio, capacitive current subtraction was used to effect partial suppression of the capacitive transient and thereby allow recordings to be made at high gain without distorting the acquired signal due to amplifier clipping. Relaxations were quantified by fitting a decaying double exponential function using a fitting algorithm based on the Chebychev transform supplied with pClamp v. 8 (Axon instruments, Inc.). To resolve the charge movement associated with the exogenous protein, the subtraction method of Hazama et al. (1997) was employed; the fast component, assumed to represent the capacitive oocyte charging, was extrapolated to the step onset and subtracted from the total transient current. For some batches of oocytes it was necessary to apply a linear baseline correction to eliminate contamination from endogenous Cl^- currents activated at depolarizing or hyperpolarizing potentials.

To quantify charge movements, we numerically integrated the component of intramembranous charge movement (Q) attributed to the exogenous protein, commencing ~2.5 ms after the step onset, at which time the membrane was assumed 100% charged. Q–V data were fitted with the Boltzmann relation:

$$Q = Q_{hyp} + Q_{max}/(1 + \exp(-ze(V - V_{0.5})/kT)), \quad (3)$$

where Q_{max} is the maximum charge translocated, Q_{hyp} is the steady-state charge at the hyperpolarizing limit and depends on V_h, $V_{0.5}$ is the voltage at which the charge is distributed equally between each state, z is the apparent valency per cotransporter, e is the elementary charge, k is Boltzmann's constant, and T is the absolute temperature. This model lumps all mobile charges associated with a particular transition into one effective charged particle (valency z) that moves across the whole transmembrane field in one kinetic step (and assuming sharp energy barriers). The voltage dependence of the relaxation time constant ($\tau - V$) obtained from the exponential fitting was further quantified by fitting an equation that incorporates the apparent inward and outward rates for this particle, given by:

$$\tau = 1/(\alpha\exp(-zeV/2kT) + \beta\exp(zeV/2kT)), \quad (4)$$

where α and β are the inward and outward rates, respectively, at $V = 0$ and we assume the barrier is symmetrical within the transmembrane field. Eqs. 3 and 4 were fit to the data by nonlinear regression analysis with Q_{hyp}, Q_{max}, z, $V_{0.5}$, α, and β as free parameters, at T = 293 K. All curve fitting using Eqs. 1–4 was performed using the nonlinear regression analysis available with GraphPad Prism version 3.02/4.02 for Windows (GraphPad Software).

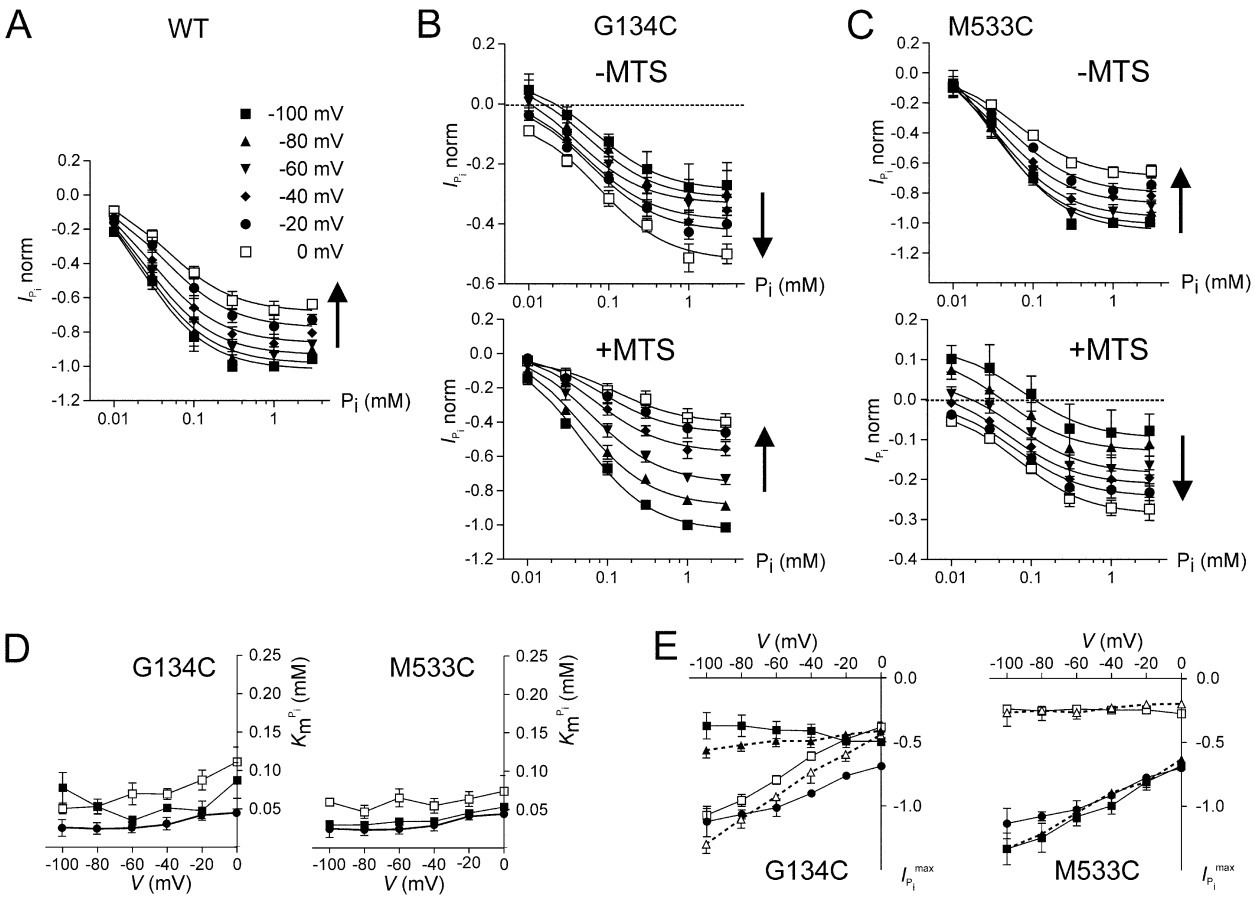

FIGURE 1. Voltage dependency of P_i activation in 100 mM Na^+. (A) P_i activation characteristics for WT-expressing oocytes determined at six membrane potentials from −100 mV to 0 mV as indicated by different symbols. Each data point is the difference between current recorded in ND100 + P_i and ND100 shown as mean ± SEM (n = 3). Currents were normalized to the magnitude of I_{P_i} at 1 mM P_i, V = −100 mV for each cell. Currents for these cells ranged from −76 to −88 nA at 1 mM, V = −100 mV. Arrow indicates direction of depolarization. Continuous lines are fits to the data points using Eq. 1. (B) P_i activation characteristics for G134C-expressing oocytes (n = 4) determined at six membrane potentials as in A, before (top) and after (bottom) incubation in 1 mM MTSEA for 3–5 min. Note the different ordinate scales for the −MTS and +MTS cases. Currents were normalized to the magnitude of I_{P_i} for G134C + MTS at 1 mM P_i, V = −100 mV. Currents for these cells ranged from −22 to −69 nA at 1 mM, V = −100 mV. (C) P_i activation characteristics for M533C-expressing oocytes (n = 4) determined at six membrane potentials as in A before (top) and after (bottom) incubation in 1 mM MTSEA for 3–5 min. Note the different ordinate scales for the −MTS and +MTS cases. Currents were normalized to the magnitude of I_{P_i} for M533C − MTS at 1 mM P_i, V = −100 mV. Currents for these cells ranged from −61 to −123 nA at 1 mM, V = −100 mV. (D) Voltage dependency of apparent P_i affinity ($K_m^{P_i}$) for G134C (left) and M533C (right). Data points indicate mean ± SEM of $K_m^{P_i}$ reported from fits to P_i activation data for the individual oocytes pooled in A–C. WT, filled circles; mutant − MTS, filled squares; mutant + MTS, empty squares. (E) Voltage dependency of predicted maximum P_i-dependent current ($I_{max}^{P_i}$) for G134C (left) and M533C (right) with WT data superimposed. $I_{max}^{P_i}$ is shown as mean ± SEM predicted from fits to data for the individual oocytes pooled in A–C, with WT data superimposed. WT, filled circles; mutant − MTS, filled squares; mutant + MTS, empty squares. Maximum cotransport activity determined using the leak correction procedure (see text) is also shown. Mutant − MTS, filled triangles; mutant + MTS, empty triangles, with points joined by dashed lines.

RESULTS

Voltage Dependency of Apparent Substrate Affinities

In the accompanying cysteine scanning study on mutants in ECL-1 and ECL-4 (Ehnes et al., 2004), we used a simple two-point screening assay to assess if the mutants deviated significantly from the wild type (WT) with respect to substrate activation. This assay was performed at only one membrane potential (−50 mV), and our findings suggested that the cys engineering did not lead to large changes in the apparent substrate affinities. However, it is known that such phenomenological kinetic parameters of NaPi-IIa are functions of membrane potential (Forster et al., 1998). Therefore, to investigate if this could contribute to the novel voltage-dependent behavior of G134C and M533C, we determined the voltage dependency of substrate activation for each mutant before and after 2-aminoethyl MTS hydrobromide (MTSEA) incubation under conditions previously shown to result in

complete modification of the novel cysteines (Ehnes et al., 2004).

Fig. 1 shows the P_i activation data in 100 mM Na^+ for oocytes from the same donor frog that expressed WT (A), G134C (B), and M533C (C). Each panel depicts the normalized P_i-dependent current (I_{P_i}) at different membrane potentials in the range $-100 \leq V \leq 0$ mV. For G134C (Fig. 1 B) and M533C (Fig. 1 C), the same assay was made before (top) and after (bottom) incubation in 1 mM of the MTS reagent MTSEA for 3–5 min. Currents were normalized to the magnitude of I_{P_i} at −100 mV, 1 mM P_i for WT and G134C + MTS and M533C − MTS before pooling. In each case, I_{P_i} displayed saturation for $P_i \geq 1$ mM. Under this condition, the inverse relationship between I_{P_i} and membrane potential for G134C − MTS and M533C + MTS contrasted with the "WT-like" response for G134C + MTS and M533C − MTS, in which increasing hyperpolarization led to increased electrogenic activity. We also observed that for G134C − MTS and M533C + MTS at low P_i, I_{P_i} reversed direction. This is a consequence of subtracting the maximum leak (in ND100) from the current recorded in ND100 + P_i (Forster et al., 1998; Ehnes et al., 2004) (see DISCUSSION). As shown in each panel, the pooled data could be well described by fitting a Michaelis-Menten function with variable offset parameter to account for the sign reversal (Eq. 1). The larger error bars associated with G134C − MTS and M533C + MTS at −100 mV, in particular, most likely arise from the uncertainties in resolving these currents as they were typically <20 nA in magnitude and would be more prone to contamination from endogenous conductances.

To compare the effect of MTS treatment and take account of any systematic errors between individual oocytes, we refit the data of each cell individually (WT, $n = 3$; G134C and M533C, $n = 4$) and pooled the reported estimates of the apparent affinity for P_i interaction with the transporter ($K_m^{P_i}$). These are shown plotted as a function of voltage for G134C (Fig. 1 D, left) and M533C (Fig. 1 D, right) with WT values superimposed for comparison**.** Both mutants showed a relatively weak voltage dependency for $K_m^{P_i}$, as we have previously reported for the WT (Forster et al., 1998). Over the voltage range -100 mV $\leq V \leq 0$ mV, $K_m^{P_i}$ was close to the WT for M533C − MTS. Although the reported mean $K_m^{P_i}$ for M533C + MTS was systematically larger (∼30%) compared with M533C − MTS, a paired t test indicated no significant difference in $K_m^{P_i}$ between M533C − MTS and M533C + MTS ($P < 0.05$). For G134C − MTS, there was more scatter in the $K_m^{P_i}$ estimates because of the smaller currents with no statistical difference from the WT until V approached 0 mV. On the other hand, the mean $K_m^{P_i}$ for G134C + MTS was generally larger than either WT or G134C − MTS, and a paired t test revealed a significant difference ($P < 0.05$) between the respective $K_m^{P_i}$ s of G134C − MTS and G134C + MTS for $V \geq -40$ mV.

Fig. 1 E shows the predicted maximum currents ($I_{P_i}^{max}$) obtained from the fits of the normalized data for G134C (left, squares) and M533C (right, squares), compared with typical WT values (circles). These data showed that with saturating P_i (a) the voltage dependency for G134C − MTS and M533C + MTS was reduced compared with the WT, G134C + MTS, or M533C − MTS, as we previously documented (Ehnes et al., 2004); (b) the voltage dependency $I_{P_i}^{max}$ for M533C was close to the WT; (c) G134C + MTS showed an increased voltage dependency compared with the WT; and (d) at $V = 0$, the predicted $I_{P_i}^{max}$ for G134C − MTS and G134 + MTS were very close, whereas that of M533C + MTS was reduced by ∼70%. Also shown in Fig. 1 E (triangles) is the maximum cotransport mode activity determined by applying the leak correction procedure to I_{P_i} at 3 mM P_i, using the leak estimated from the PFA response as previously described (Ehnes et al., 2004). This agreed reasonably well with the $I_{P_i}^{max}$ predicted from the fits with Eq. 1, particularly for M533C.

Fig. 2 shows the Na^+ activation data at 1 mM P_i for oocytes that expressed WT (A), G134C (B), and M533C (C). Each panel depicts the P_i-dependent current (I_{P_i}) at different membrane potentials in the range $-100 \leq V \leq 0$ mV. As for the P_i activation (Fig. 1), the normalized and pooled data for G134C and M533C are shown before (top) and after (bottom) incubation in 1 mM MTSEA for 3–5 min. The data for G134C + MTS, M533C − MTS, and the WT displayed a similar pattern with a strong voltage dependency at the maximum Na^+ (125 mM) used in these assays. For G134C − MTS and M533C + MTS, the relative P_i currents were suppressed compared with G134C + MTS and M533C − MTS, respectively, and in all cases I_{P_i} showed evidence of saturation with increasing Na^+ concentration. Like the P_i activation data, there was an inverse relationship with voltage for the maximum dependent current, and, moreover, a reversal of I_{P_i} was observed for G134C − MTS and M533C + MTS at low Na^+ concentrations. The data were fit with a form of the modified Hill equation with a variable offset (Eq. 2) to estimate the apparent Na^+ affinity for cotransport (K_m^{Na}) (Fig. 2 D). Reliable fits of Eq. 2 to the WT, G134C + MTS, and M533C − MTS data were obtained with n_H as a free parameter. We found that n_H was reasonably constant when averaged over the estimates at each test potential (WT, 2.0 ± 0.1; G134C + MTS, 1.8 ± 0.1; M533C − MTS, 2.2 ± 0.2). These data confirmed a cooperative Na^+ interaction with the engineered transporters and suggested that for G134C + MTS, the cooperativity was possibly reduced compared with the WT. For the G134C − MTS and M53C + MTS data, where the currents were typi-

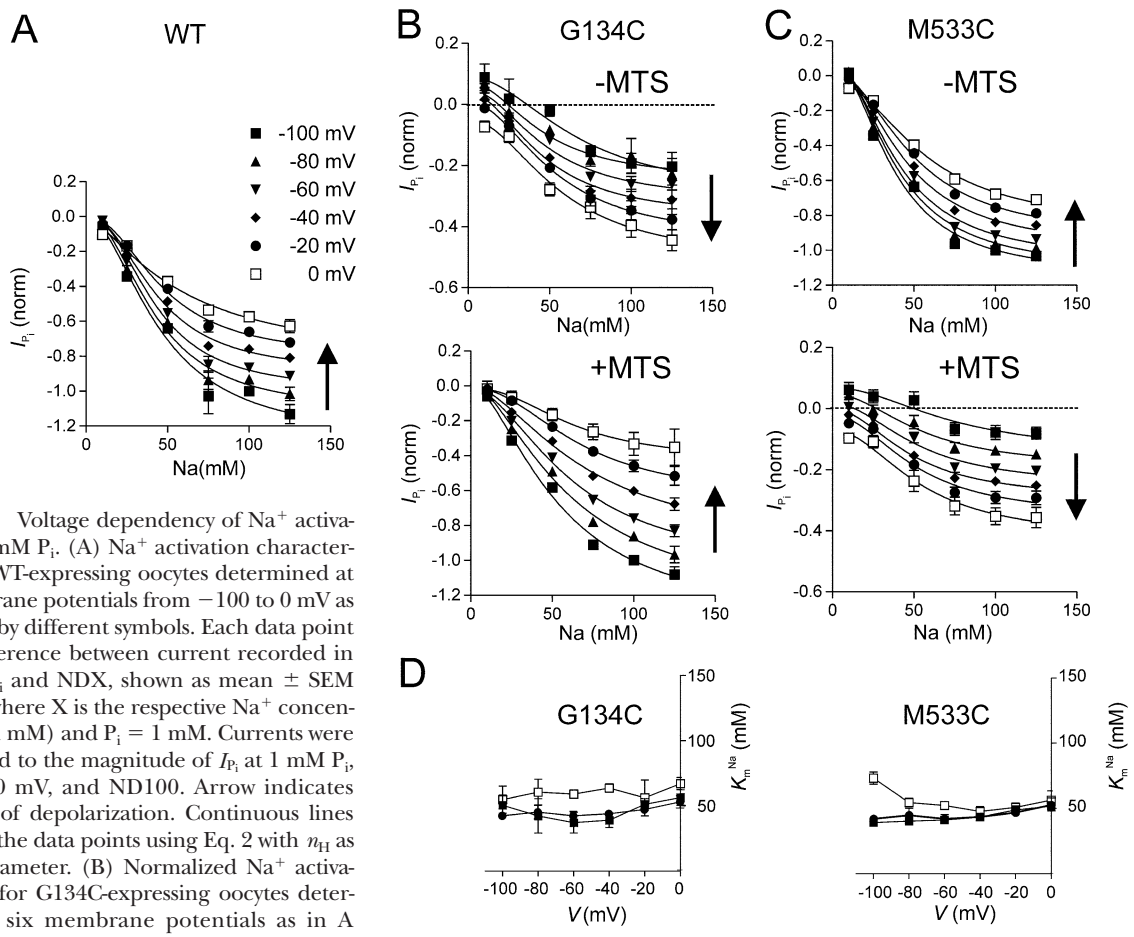

FIGURE 2. Voltage dependency of Na^+ activation in 1 mM P_i. (A) Na^+ activation characteristics for WT-expressing oocytes determined at six membrane potentials from −100 to 0 mV as indicated by different symbols. Each data point is the difference between current recorded in NDX + P_i and NDX, shown as mean ± SEM (n = 4), where X is the respective Na^+ concentration (in mM) and P_i = 1 mM. Currents were normalized to the magnitude of I_{P_i} at 1 mM P_i, V = −100 mV, and ND100. Arrow indicates direction of depolarization. Continuous lines are fits to the data points using Eq. 2 with n_H as a free parameter. (B) Normalized Na^+ activation data for G134C-expressing oocytes determined at six membrane potentials as in A before (top) and after (bottom) incubation in 1 mM MTSEA for 3–5 min. Continuous lines are fits to the data points using Eq. 2 with n_H as a free parameter for G134C + MTS, and n_H = 2 for G134C − MTS. Note the different ordinate scales for the −MTS and +MTS cases. Currents were normalized to the magnitude of I_{P_i} for G134C + MTS, ND100, V = −100 mV. (C) Normalized Na^+ activation data for M533C-expressing oocytes (n = 4) determined at six membrane potentials as in A before (top) and after (bottom) incubation in 1 mM MTSEA for 3–5 min. Continuous lines are fits to the data points using Eq. 2 with n_H as a free parameter for M533C − MTS, and n_H = 2 for M533C + MTS. Note the different ordinate scales for the −MTS and +MTS cases. Currents were normalized to the magnitude of I_{P_i} for M533C − MTS, ND100, V = −100 mV. (D) Voltage dependency of apparent Na^+ affinity (K_m^{Na}) for G134C (left) and M533C (right). Data points indicate mean ± SEM of $K_m^{P_i}$ reported from fits to Na^+ activation data for the individual oocytes pooled in A–C. WT, filled circles; mutant − MTS, filled squares; mutant + MTS, empty squares.

cally <−30 nA, reliable fits of Eq. 2 over the same voltage range were only obtained by constraining n_H = 2.

To compare the effect of MTS treatment on the apparent affinity for Na^+ activation and take account of any systematic errors between individual oocytes, we refit the data of each cell (n = 4) individually and pooled the reported estimates of K_m^{Na}. These are shown as a function of voltage for G134C (Fig. 2 D, left) and M533C (Fig. 2 D, right). For M533C − MTS, K_m^{Na} was indistinguishable from the WT value, although the M533C + MTS data deviated significantly for $V \leq -80$ mV (paired t test, $P < 0.05$). For G134C − MTS, there was no statistically significant deviation from WT. The larger mean K_m^{Na} for G134C + MTS suggested that there was a systematic increase in K_m^{Na}, but this amounted to ∼35% over the entire voltage range and would lie within the normal variation observed among different batches of oocytes.

Proton Interactions with G134C and M533C

The reduced slope and cotransport activity of the *I–V* data for G134C − MTS and M533C + MTS under conditions of maximum turnover rate (Fig. 1 E) were reminiscent of the effect of external acidification on the WT NaPi-IIa P_i-dependent current, whereby protons were shown to reduce its steady-state voltage dependency (Forster et al., 2000). To investigate if an increased sensitivity to external protons could influence the steady-state kinetic changes documented at pH 7.4, we determined the P_i-dependent activity as a function of V and external pH with 1 mM (total) P_i in the pH range 5–8 (Fig. 3).

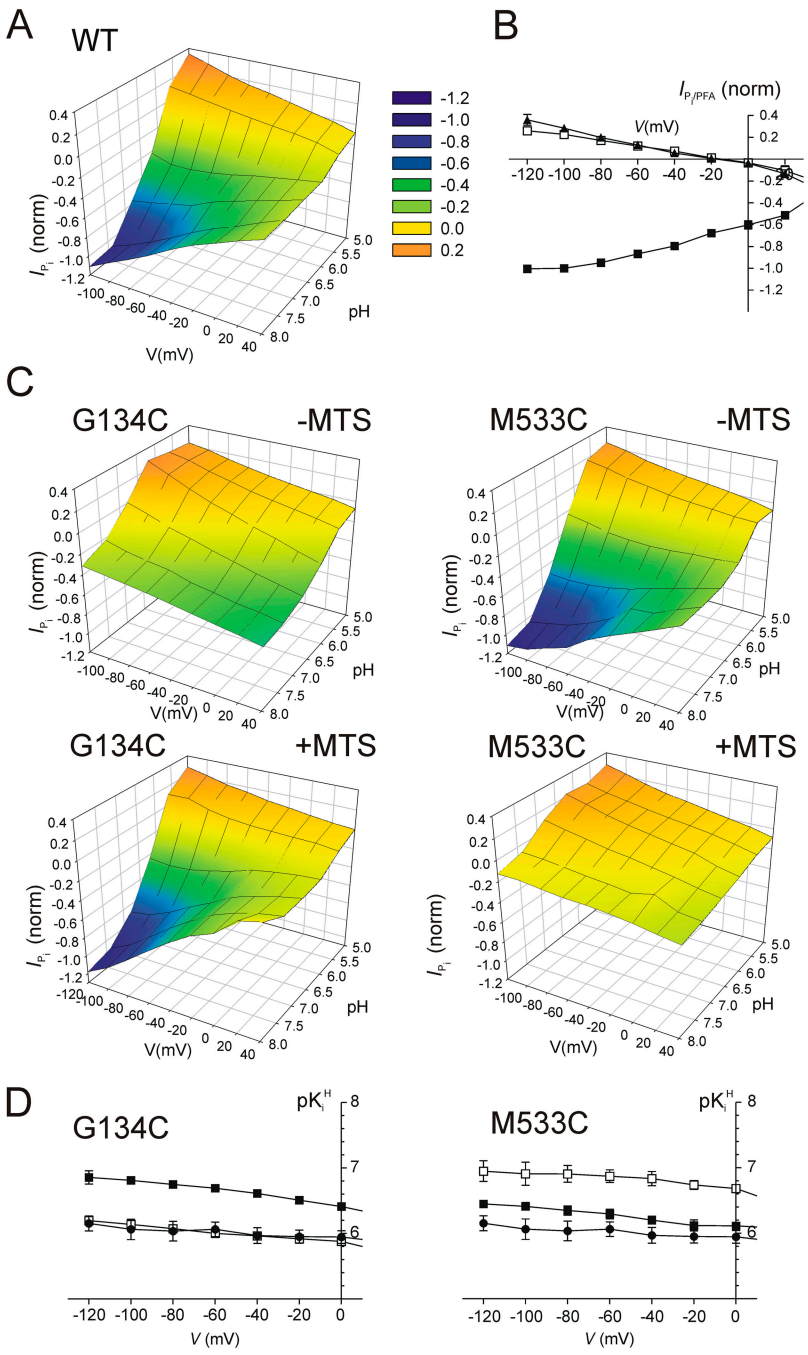

FIGURE 3. Effect of MTS exposure on pH and voltage dependency. (A) Steady-state pH–*V* profile of WT showing I_{P_i} (1 mM total P_i) as a function of external pH and *V*. Currents were normalized to the magnitude of I_{P_i} at −100 mV, pH 7.4, and pooled (n = 4). Error bars omitted for clarity. Legend indicates color and corresponding I_{P_i} (norm). (B) Normalized, pooled (n = 5) *I–V* data for WT that compares I_{P_i} at pH 5.0 (open squares) with PFA-dependent current at pH 7.4 (filled triangles), normalized to the magnitude of I_{P_i} at −100 mV, pH 7.4 (filled squares). (C) Steady-state pH–*V* profiles of mutant G134C (left) and mutant M533C (right) showing I_{P_i} (1 mM total P_i) as a function of external pH and *V* before (−MTS) and after (+MTS) exposure to 1 mM MTSEA. Currents were normalized to the magnitude of I_{P_i} at −100 mV, pH 7.4, for G134C + MTS and M533C − MTS. Each data point is the mean of four cells from the same donor frog. Error bars omitted for clarity. The assay was repeated after exposure for 5 min to 1 mM MTSEA. Colored contour planes are as in A. (D) Voltage dependency of apparent inhibition constant for protons, K_i^H, (expressed in pH units) for G134C (left) and M533C (right) before (filled) and after (open) exposure to MTSEA. pK_i^H for WT is shown superimposed in both cases (filled circles). Data points were fitted with the modified Hill equation (Eq. 2) with n_H as a free parameter and external proton concentration expressed logarithmically. Error bars indicate SEM of fit estimate for pK_i^H.

For WT NaPi-IIa, over a 3-decade change in external proton concentration, application of P_i evoked an electrogenic response such that with increasing external acidification, the slope of the normalized *I–V* curve changed sign and at pH 5.0, I_{P_i} reversed its dependency on membrane potential (Fig. 3 A). The voltage dependency of I_{P_i} at pH 5.0 appeared similar to the PFA-dependent current measured at pH 7.4, and there was excellent agreement between these currents when measured on the same oocytes and normalized to their respective I_{P_i} at pH 7.4 (1 mM P_i) (Fig. 3 B). These data provided strong evidence that the P_i-dependent current at pH 5.0 was equivalent to the blockage of the leak current that we have previously reported to be pH insensitive (Forster et al., 2000). As expected, we also documented that at pH 5.0, $^{32}P_i$ uptake by WT NaPi-IIa was negligible when compared with the background (unpublished data). Taken together, these results established that at pH 5.0, P_i interacted with the transporter, but the cotransport mode was fully suppressed.

As shown in Fig. 3 C, G134C and M533C displayed complementary pH–*V* profiles under the same experi-

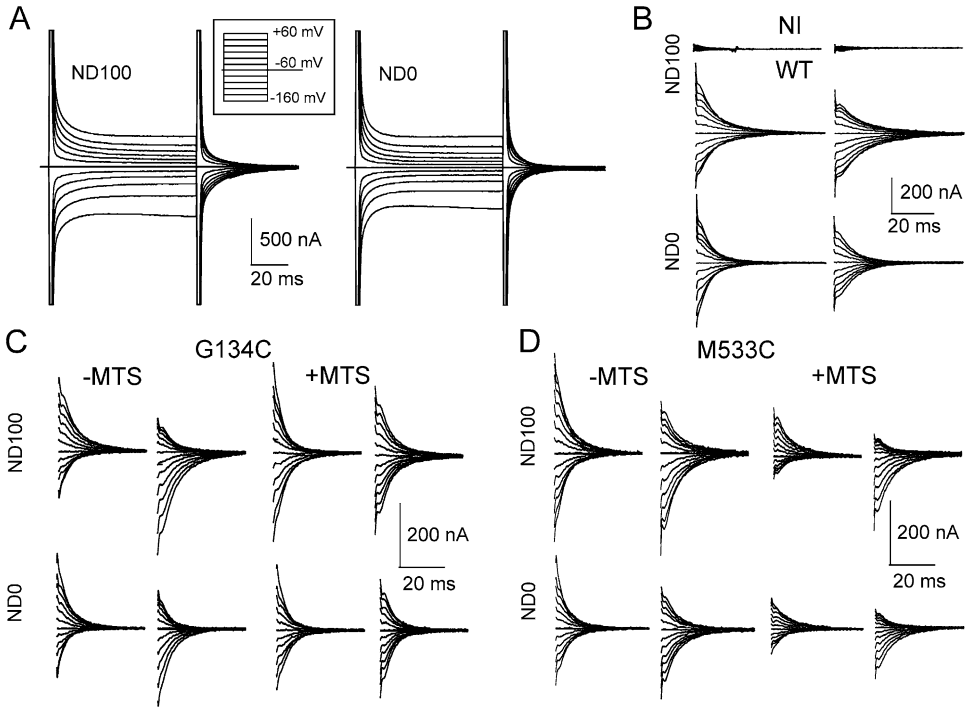

FIGURE 4. Effect of MTS exposure on presteady-state relaxations of mutants. (A) Representative presteady-state relaxations recorded from an oocyte expressing the WT NaPi-IIa protein superfused in 100 mM Na^+ (ND100) and 0 mM Na^+ (ND0) for the voltage step protocol shown in the inset. (B) Main component of presteady-state relaxation for a noninjected oocyte (NI) and the same WT-expressing cell in *A*, resolved by applying a two-exponential fitting procedure (see MATERIALS AND METHODS). The ON (step from −60 mV to test potential) and OFF (step from test potential to −60 mV) relaxations are shown for superfusion in ND100 (top and middle traces) and ND0 (bottom traces). (C) Main ON and OFF relaxations for a representative G134C-expressing oocyte before (−MTS) and after (+MTS) exposure to 1 mM MTSEA (1 mM) for 3 min, superfused in ND100 and ND0. (D) Main ON and OFF relaxations for a representative M533C-expressing oocyte before (−MTS) and after (+MTS) exposure to 1 mM MTSEA (1 mM) for 3 min, superfused in ND100 and ND0.

mental conditions. Over a 3-decade range in external proton concentration, the pH–*V* profiles of G134C + MTS and M533C − MTS were similar to WT, whereas for G134C − MTS and M533C + MTS, the inverse voltage dependency and reduced activity, already documented at pH 7.4, were preserved. Like the WT, a consistent feature of the pH–*V* profiles was a close agreement between I_{P_i} at pH 5.0 and I_{PFA} (unpublished data). To quantify the proton interactions before or after MTS modification, we fit the *I–V* data with the modified Hill equation (Eq. 2) with protons as the variable substrate, to obtain an apparent inhibition constant (K_i^H) for each test voltage (Fig. 3 D), with K_i^H expressed in pH units (pK_i^H). pK_i^H was a weak function of *V* and increased slightly at hyperpolarizing potentials, with the largest change (0.4 pH units) for G134C − MTS and smallest for the WT (∼0.1 pH units). Over the voltage range examined, pK_i^H for G134C + MTS was indistinguishable from the WT, whereas pK_i^H for G134C − MTS increased by ∼0.7 pH units. We documented reciprocal behavior for M533C, although pK_i^H for M533C − MTS itself was ∼0.3 pH units higher than the WT. The predicted n_H from these fits for WT, G134C + MTS, and M533C − MTS decreased from ∼−1 at $V = -100$ mV to ∼−2 at $V = 0$. For G134C − MTS and M533C + MTS, n_H increased in a complementary manner. These findings suggested that cys substitution at Gly-134 and modification of Cys-533 had altered the cooperativity of proton interactions compared with the WT. Moreover, they provided evidence of an increased sensitivity to external protons for G134C − MTS and M533C + MTS. Nevertheless, for G134C − MTS or M533C+MTS, removal of external protons did not restore the level of P_i-dependent electrogenic activity to that of the WT. This can be seen from their pH–*V* profiles and from the predicted extrapolated current, as pH → ∞, obtained from the fits (unpublished data). This indicated that the cys engineering had induced changes in the transporter kinetics that were independent of the proton interactions.

Presteady-state Charge Distributions of G134C and M533C

To gain further insight into underlying molecular mechanisms associated with the altered steady-state *I–V* data of the G134C/M533C pair, we investigated if changes also occurred to the kinetics of the presteady-state charge movements that accompany rapid changes in membrane potential. These experiments were all performed at pH 7.4 in the absence of P_i. Fig. 4 A depicts presteady-state relaxations in ND100 and ND0 for a representative WT-expressing oocyte in response to the voltage step protocol shown (Fig. 4 A, inset). These relaxations were superimposed on the oocyte capacitive charging transients and were not observed for noninjected oocytes under the same conditions (unpublished data). Fig. 4 B shows the presteady-state relax-

TABLE I

Boltzmann Fit Parameters

	−MTSEA		+MTSEA	
	ND0	ND100	ND0	ND100
G134C				
α (s^{-1})[a]	31 ± 3	37 ± 3	22 ± 2	19 ± 1
β (s^{-1})[a]	60 ± 4	52 ± 3	123 ± 5	109 ± 5
z[a]	0.5 ± 0.04	0.4 ± 0.04	0.5 ± 0.03	0.5 ± 0.03
$V_{0.5}$ (mV)[b]	−2 ± 3	+6 ± 3	−69 ± 6	−86 ± 5
z[b]	0.5 ± 0.02	0.5 ± 0.01	0.4 ± 0.04	0.4 ± 0.02
M533C				
α (s^{-1})[a]	28 ± 1	24 ± 1	37 ± 3	36 ± 3
β (s^{-1})[a]	74 ± 3	56 ± 2	43 ± 3	42 ± 3
z[a]	0.4 ± 0.02	0.4 ± 0.02	0.5 ± 0.04	0.4 ± 0.05
$V_{0.5}$ (mV)[b]	−42 ± 11	−28 ± 8	+16 ± 13	+22 ± 4
z[b]	0.5 ± 0.03	0.5 ± 0.02	0.5 ± 0.06	0.6 ± 0.02

[a]Mean ± SEM of fit pooled τ–*V* data ($n = 4$) using Eq. 4.

[b]Mean ± SEM of pooled data from fits to individual *Q*–*V* data ($n = 4$) using Eq. 3.

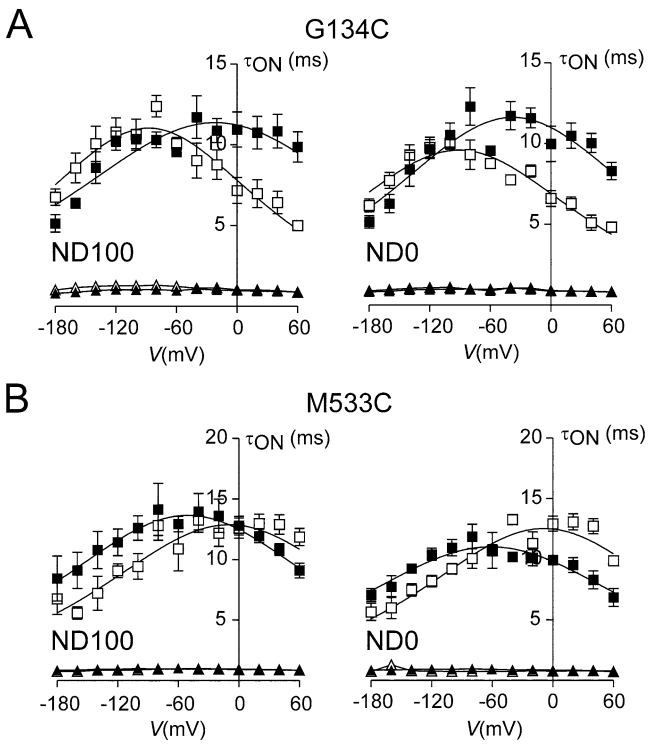

FIGURE 5. Analysis of presteady-state relaxations; ON time constants (τ_{ON}) for mutant G134C (A) and M533C (B). Voltage dependencies of time constants (τ_{ON}) were obtained by fitting presteady-state relaxations in response to voltage steps from −60 mV to the indicated voltage with a double exponential (see MATERIALS AND METHODS). Each point represents mean ± SEM of four cells. Fast τ_{ON} (triangles), slow τ_{ON} (squares); before MTSEA (filled symbols); after MTSEA (empty symbols) incubation (1 mM, 3 min). Continuous lines were obtained by fitting Eq. 4 to the data (Table I). Data for two superfusion conditions: ND100 (left) and ND0 (right). Data points at the holding potential (−60 mV) were determined from fits to the OFF relaxations.

ations for the ON (step from −60 mV to test potential) and OFF (step from test potential to −60 mV) on an expanded scale, after removing the capacitive charging transient and holding current (see MATERIALS AND METHODS) for the same cell as in A. For comparison, the same data manipulation procedure applied to a noninjected oocyte (NI) from the same donor frog showed no detectable charge movement within the same time window (top traces, ND100 superfusion only). The relaxations appear almost symmetrically distributed around the baseline trace at $V_h = -60$ mV because for the WT rat NaPi-IIa, the midpoint potential ($V_{0.5}$) of the charge distribution typically lies in the range −70 to −50 mV (e.g., Forster et al., 1998, 2000), i.e., $V_h \cong V_{0.5}$.

Representative voltage step–induced currents recorded before (−MTS) and after (+MTS) exposure to MTSEA (1 mM, 3 min) for G134C and M533C are shown in Fig. 4 (C and D), respectively. For ND100 superfusion, G134C-expressing oocytes showed an altered charge distribution around $V_h = -60$ mV, from an asymmetrical form before MTS exposure to a more WT-like symmetrical distribution (Fig. 4 B) after treatment. This behavior was also documented in 0 mM external Na^+ (ND0). In contrast, M533C showed the opposite behavior, whereby a WT-like symmetrical charge distribution became more asymmetrical after MTS treatment, also for ND0 superfusion. We also observed qualitatively similar results for MTSET- and MTSES-treated oocytes (unpublished data). These findings indicated that the intrinsic charge of the MTS reagent was not critical for inducing changes in the kinetics.

The faster component for both ON and OFF transitions had a time constant (τ) ~1 ms and showed little voltage dependency, and we therefore assumed that it arose primarily from the capacitive charging of the oocyte membrane. The slower ON component showed a strong voltage dependency that changed after MTS treatment, as evidenced by the shift in the peak τ from ~0 to −60 mV. We quantified these changes by fitting the τ–*V* data with an equation for relaxations derived from a two-state Boltzmann model (Eq. 4) (Table I). The two mutants showed complementary behavior, as suggested by the presteady-state records in Fig. 4 (C and D). For G134C + MTS (Fig. 5 A) with superfusion in either ND100 or ND0, there was a shift of the peak in the hyperpolarizing direction, whereas for M533C + MTS (Fig. 5 B), shifts in the depolarizing direction were found for both ND100 and ND0. In each case, exponential curve fitting of the OFF transition resolved a slow component that was only weakly voltage dependent (unpublished data). We would expect this for a system in which the reaction rate is dependent on the target potential. The parameters derived from the fits to Eq. 4 (Table I) indicated that for a given superfusion

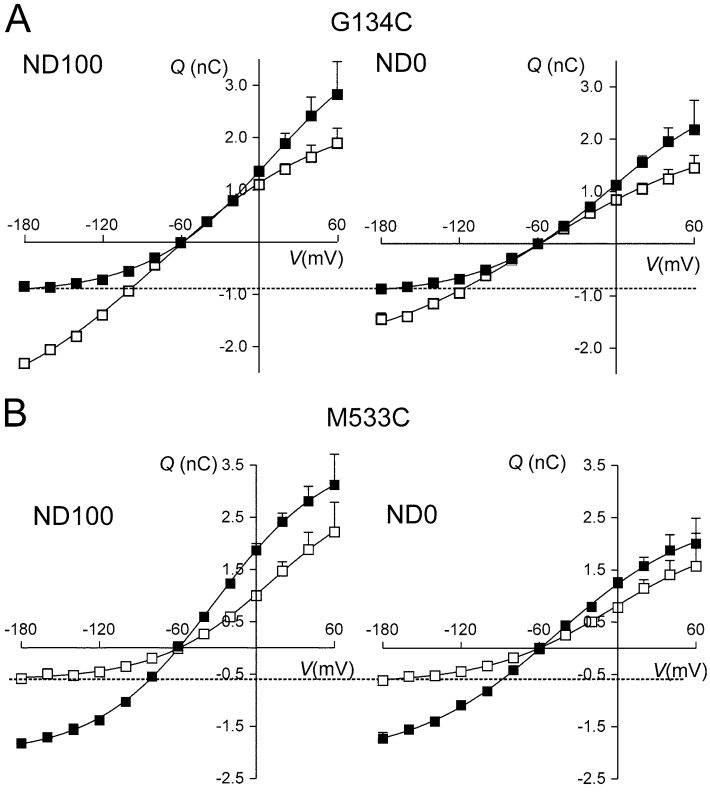

FIGURE 6. Analysis of presteady-state relaxations: charge–voltage (Q–V) data for a representative oocyte expressing G134C (A) and M533C (B). Each point is given by $(Q_{ON}–Q_{OFF})/2$, where Q_{ON} and Q_{OFF} are the charges moved for the ON and OFF voltage steps from and to −60 mV, respectively. Errors smaller than symbol size are not shown. Left, superfusion in ND100; right, superfusion in ND0 for the same oocyte. Filled symbols, before MTSEA exposure; empty symbols, after MTSEA exposure. Dashed lines have been drawn to indicate the apparent equality of charge movement at hyperpolarizing potentials for ND100 and ND0 superfusion for G134C − MTS and M533C + MTS. Continuous lines were obtained by fitting Eq. 3 to the data. For G134C, the fit parameters were as follows: in ND100 (±MTS), Q_{max} = 5.1/5.9 nC, Q_{hyp} = −0.9/−3.4 nC; $V_{0.5}$ = −7/−77 mV; z = 0.5/0.4; and in ND0 (±MTS), Q_{max} = 4.0/4.3 nC, Q_{hyp} = −1.0/−2.1 nC; $V_{0.5}$ = −5/−59 mV; z = 0.5/0.4. For M533C, the fit parameters were as follows: in ND100 (±MTS), Q_{max} = 5.8/3.7 nC, Q_{hyp} = −2.0/−0.7 nC; $V_{0.5}$ = −32/+11 mV; z = 0.6/0.6; and in ND0 (±MTS), Q_{max} = 4.8/2.9 nC, Q_{hyp} = −2.1/−0.6 nC; $V_{0.5}$ = −48/−5 mV; z = 0.5/0.5.

condition, the apparent rate constants at 0 mV showed the greatest sensitivity with respect to MTS treatment, whereas the estimated apparent valency remained reasonably constant.

Fig. 6 A shows the charge–voltage (Q–V) relationship for a representative G134C-expressing oocyte for superfusion in ND100 and ND0 before and after MTS exposure. Each point represents the mean of the absolute charge moved after the ON and OFF transitions.[1] Before MTS exposure, saturation was clearly observed at hyperpolarizing potentials for both ND100 and ND0, and, moreover, the charge moved for steps to potentials $< V_h$ was the same for both ND100 and ND0. After MTSEA exposure, the charge distribution showed a clear difference between superfusion in ND100 and ND0 for hyperpolarizing potentials as well as less saturation in this voltage range. The Q–V data for a representative M533C-expressing oocyte showed the opposite behavior (Fig. 6 B). Before MTS exposure there was a small difference in charge movement between ND100 and ND0, and evidence of saturation was observed at both hyperpolarizing and depolarizing extremes. After MTS exposure, there was much stronger saturation for hyperpolarizing steps with equality of charge movement for the two superfusion conditions, as for G134C − MTS. To quantify these changes, the Q–V data were fit with a Boltzmann function (Eq. 3), and the fitting results pooled (n = 4) for each mutant are summarized in Table I. The fitted data showed reasonable agreement between the predicted apparent valency (z) derived from the Q–V (Eq. 3) or τ–V (Eq. 4) fits. This parameter also remained reasonably constant before and after MTS treatment and suggested that the treatment had not altered the intrinsic voltage sensitivity of the protein, but only its voltage dependency. For G134C − MTS and M533C + MTS, the ratio of the predicted hyperpolarizing charge derived from the Boltzmann fit in ND100 to that in ND0 ($Q_{hyp}^{100}/Q_{hyp}^{0}$) was unity as suggested from the Q–V data. For the G134C +

[1]Charge balance (equality between ON (QON) and OFF (QOFF) charge movements, as demanded by charge conservation) was excellent in the voltage range ($-180 \le V \ge 0$ mV) with a deviation ≤10% (Fig. 6). This confirmed that in this voltage window, all of the charge moved that was associated with the slow relaxation could be recovered. For $V > +20$ mV, the difference increased. An underestimate in QON could result from our inability to detect all charge movement for depolarizing ON transitions because of the limited time window, i.e., uncertainties in the first 2.5 ms after the step onset during the capacitive charging led us to ignore charge movement during this initial interval. Alternatively, very slow charge movements that require a longer time window to resolve might remain undetected or masked by contamination from endogenous Cl^- currents. Although we cannot fully exclude contamination from endogenous membrane proteins in injected oocytes, we were unable to detect charge imbalance in noninjected oocytes (Fig. 4 B). Moreover, in our hands, contributions to charge movement from the endogenous Na^+/K^+-ATPase (e.g., Rakowski, 1993) were considered insignificant as we were unable to detect any change in the presteady-state relaxations after incubating selected cells in 100 mM ouabain, a potent blocker of this pump.

MTS, the ratio >1 confirmed that additional mobile charge was available in the presence of external Na^+. For M533C, $Q_{hyp}^{100}/Q_{hyp}^{0}$ remained close to unity before and after MTS exposure.

DISCUSSION

We have focused on the electrogenic behavior of two mutant NaPi-IIa cotransporters (G134C and M533C) that contain a novel Cys at site Gly-134 in the first predicted extracellular linker (ECL-1) and one at site Met-533 in the fourth predicted extracellular linker (ECL-4), respectively. In an accompanying study (Ehnes et al., 2004), we established that (a) these and other substituted cysteines in ECL-1 and ECL-4 were accessible from the external hydrophilic environment and (b) the voltage-dependent kinetics of G134C and M533C, in particular, were profoundly altered compared with the WT fingerprint. This depended on whether or not the novel Cys was modified by external MTS reagents; G134C + MTS and M533C − MTS showed "WT-like" characteristics, whereas G134C − MTS and M533C + MTS showed weaker voltage dependency that suggested rate-limiting behavior at hyperpolarizing potentials. Moreover, the effect of cys modification on the voltage dependency was independent of the charge of the MTS reagent. The aim of this study was to identify the kinetic transitions that were affected by the cysteine engineering and develop structure–function relationships for these linkers.

We used the eight-state kinetic scheme for NaPi-IIa depicted in Fig. 7 A to relate the functional effects of the cys engineering to specific partial reactions in the overall transport cycle. This model, derived from studies on the WT (Forster et al., 1998, 2000), accounts for voltage-dependent cotransport through two processes: (1) the movement of intrinsic mobile charges in response to changes in the transmembrane electric field, which exposes a Na^+ binding site, and (2) the movement of one Na^+ ion within the transmembrane field to this site (Fig. 7 A, transitions 1–8 and 1–2, respectively). Presteady-state charge movements measured in the absence of external Na^+ result from empty carrier conformational changes, whereas in the presence of external Na^+, additional charge movement is contributed by Na^+ binding/debinding (Forster et al., 1997, 1998). The model includes the minimum possible number of states to account for NaPi-IIa kinetics.

Substrate and Proton Interactions in the Steady State

The steady-state assays revealed a unique characteristic of the P_i-dependent currents, namely the reversal of I_{P_i} documented at hyperpolarizing potentials for G134C − MTS and M533C + MTS in the P_i and Na^+ activation assays at low P_i and Na^+, respectively (Figs. 1 and 2), and for the WT and both mutants at low pH (Fig. 3). This results from the subtraction procedure used to obtain I_{P_i} and the presence of a leak mode that also contributes to the electrogenic response, in addition to the cotransport mode. We have previously proposed that these modes are reciprocally related, so that in 0 mM P_i, maximum leak activity occurs, whereas at saturating P_i, the leak is fully suppressed and only the cotransport mode contributes to electrogenic activity (Kohler et al., 2002b). At intermediate P_i, the P_i-dependent electrogenic activity will comprise components from both modes; however, the relative contributions to the measured P_i-dependent currents remain to be determined. Moreover, Na^+ acting as a common cation complicates the experimental separation of the two transport modes at intermediate P_i. In the case of WT NaPi-IIa, where the leak accounts for ~10% of total electrogenic activity (Forster et al., 1998) at pH 7.4, its effect is usually ignored. Under these conditions, I_{P_i}, obtained from the subtraction procedure, is typically inward for $V < 0$ mV, and the activation kinetics can be well described by fitting data using the Michaelis-Menten equation. However, in general, we would not expect the P_i dependency of the net electrogenic activity to follow a strict Michaelis-Menten characteristic, unless the activation of cotransport and deactivation of leak by P_i are strictly reciprocal. For example, if P_i suppressed the leak with a higher affinity than it activated the cotransport mode, so that at low P_i the magnitude of the combined cotransport and leak activity is less than the maximum leak activity, the subtraction procedure would yield apparent outward currents, as we have documented. This dual interaction of P_i with NaPi-IIa suggests the existence of two binding sites for P_i, but at present, we have no supporting structure–function evidence.

Given the uncertainties concerning the leak dependency on P_i and Na^+, we found that the most straightforward approach to account for the current reversal of the P_i and Na^+ activation kinetics was to fit the data using the standard Michaelis-Menten (Eq. 1) or modified Hill equations (Eq. 2) with a variable offset. The $I_{P_i}^{max}$ predicted from the fits to the P_i activation data agreed reasonably well with the maximum cotransport activity determined using the leak-correction procedure. This suggested that any errors introduced by the P_i-dependent leak component were not significant under our experimental conditions for characterizing the cotransport kinetics.

From the steady-state P_i and Na^+ activation assays, we documented relatively small deviations from the WT behavior for the apparent substrate affinities (K_m^{Na} and K_m^{Pi}) in the voltage range $-100 \leq V \leq 0$ mV, independent of the state of modification of the novel Cys. Deviations reported by the fitting procedure would not be

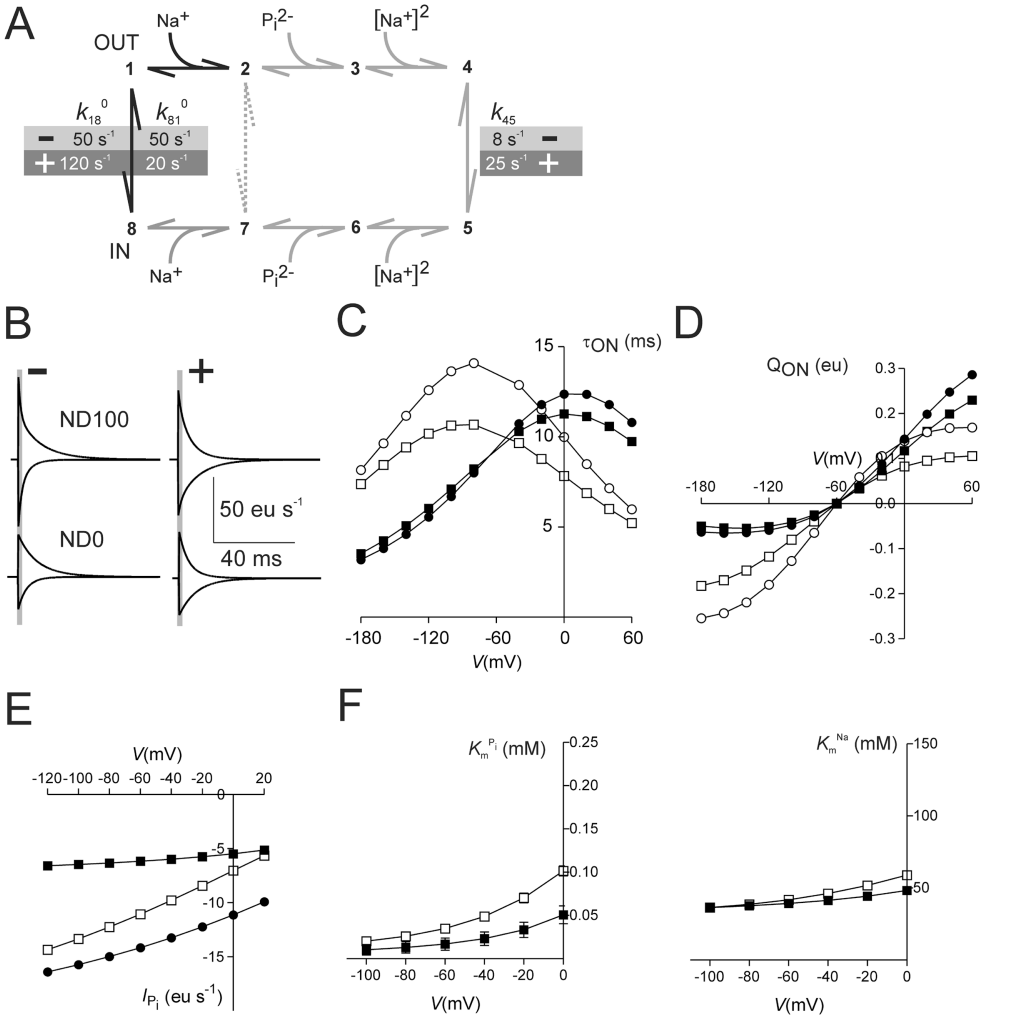

FIGURE 7. Modeling voltage-dependent presteady-state and steady-state kinetics for G134C − MTS and G134C + MTS. (A) Eight-state kinetic scheme for NaPi-IIa. Voltage-dependent transitions are shown bold. All other transitions are electroneutral. Critical transitions for simulating G134C − MTS (−) and G134C + MTS (+) are 1–8, 8–1, and 4–5. The corresponding voltage-independent rates used in the simulations are indicated. Dashed transition indicates a proposed leak pathway. (B) Simulations of presteady-state relaxations before (−) and after (+) MTS modification of Cys-134 using the model scheme of A for steps to potentials in the range −180 to +80 mV from V_h = −60 mV and two superfusion conditions. The vertical gray bars indicate the initial 2.5-ms interval after which presteady-state currents were resolved experimentally. Differential equations describing the transitions were solved for the state occupancies as a function of time. The presteady-state current per cotransporter molecule can be expressed as $-e(\alpha'(k_{12}X_1 - k_{21}X_2) - \delta^*(k_{18}X_1 - k_{81}X_8) + \alpha''(k_{78}X_7 - k_{87}X_8))$ (e.g., Parent et al., 1992), where X_n is the occupancy of state n and k_{ij} is the transition rate from state i to state j. The empty carrier (1–8) carries an equivalent charge of −1 that moves an equivalent electrical distance δ through the membrane. The Na^+ binding transitions (1–2 and 8–7) also involve movement of +1 charge through equivalent electrical distances α' and α'', respectively. To simplify the simulations, $\alpha'' = 0.3$, $\alpha' = 0.3$, and $\delta = 0.4$ and the corresponding energy barriers were symmetrical. The rate constants for voltage-dependent transitions are given by $k_{18} = k_{18}^o \exp(\delta eV/2kT)$, $k_{81} = k_{81}^o \exp(-\delta eV/2kT)$, $k_{12} = \text{Na}\ k_{12}^o \exp(-\alpha' eV/2kT)$, $k_{21} = k_{21}^o \exp(\alpha' eV/2kT)$, where k_{ij}^o is the rate constant for transition ij at $V = 0$, and Na is the concentration of Na^+ (mM). Other fixed rate constants for the simulations were $k_{12}^o = 2000\ s^{-1}M^{-1}$, $k_{21}^o = 600\ s^{-1}$, $k_{23} = 7.5 \times 10^6\ s^{-1}M^{-1}$, $k_{32} = 1000\ s^{-1}$, $k_{34} = 10^6\ s^{-1}M^{-2}$, $k_{43} = 1000\ s^{-1}$, $k_{54} = 25\ s^{-1}$, $k_{78} = 100$, $k_{87} = 10^6\ s^{-1}M^{-1}$, $k_{67} = 1000\ s^{-1}$, $k_{76} = 10^6\ M^{-1}s^{-1}$, $k_{65} = 10^5\ s^{-1}M^{-2}$, $k_{56} = 1000$, $k_{23} = 0.005\ s^{-1}$. To satisfy microscopic reversibility, k_{32} and k_{76} were defined in terms of the other rate constants. (C) Predicted τ–V data was obtained by applying a single exponential fit to the ON presteady-state currents for voltages in the range −180 to +60 mV, commencing 2.5 ms after the step onset. Filled symbols, −MTS; open symbols, +MTS; circles, ND100; squares, ND0. Model parameters are as given in A and B above for the −MTS and +MTS conditions with $P_i = 0$. (D) Predicted Q–V data obtained by numerical integration of the presteady-state currents, commencing 2.5 ms after the step onset. Filled symbols, −MTS; open symbols, +MTS; circles, ND100; squares, ND0. Model parameters are as given in A and B above for the −MTS and +MTS conditions with $P_i = 0$. (E) Predicted steady-state I–V data for the −MTS (filled squares) and +MTS (*open squares*) conditions, using rate constants given in A and assuming $P_i = 1$ mM and external $Na^+ = 100$ mM. The steady-state current is proportional to $k_{14}X_1 - k_{41}X_4$, i.e., the net flux for the only transition that involves transmembrane charge movement. Filled circles represent the simulated I–V data without changing k_{45} (see text). (F) Apparent substrate affinities for P_i activation ($K_m^{P_i}$) (left) and Na^+ activation (K_m^{Na}) (right) as a function of membrane potential. $K_m^{P_i}$ was obtained from a fit using the Michaelis-Menten equation (Eq. 1) to the steady-state activation data simulated with P_i in the range 0–3 mM and $Na^+ = 100$ mM. K_m^{Na} was obtained from a fit using the modified Hill equation (Eq. 2) with Na^+ in the range 0–125 mM and $P_i = 1$ mM. Filled symbols, −MTS; open symbols, +MTS. Error bars indicate ±SEM reported by fitting algorithm.

able to account for the dramatic change in both voltage dependency and maximum transport activity caused by the cys engineering. We therefore excluded transitions 2–3 and 3–4 (Fig. 7 A), previously found to be critical determinants of these parameters (Forster et al., 1998, 2000), from further consideration. On the other hand, we found that the sensitivity of the transporter to protons changed depending on the state of modification

of the substituted Cys (Fig. 3 D). The apparent proton inhibition constants for G134C − MTS and M533C + MTS were smaller than for the WT, which suggested that cys substitution at Gly-134 or cys modification at Met-533 had induced a conformation in which protons could more easily modify the kinetics. For the WT, we have previously identified the empty carrier and final Na^+ binding transitions to be proton sensitive (Forster et al., 2000). The latter interaction, in which protons compete with Na^+ ions (Fig. 7 A, transition 3–4), manifests itself as an approximately twofold increase in K_m^{Na} (e.g., Hartmann et al., 1995) with external acidification. That we did not observe a large change in K_m^{Na} for either mutant suggests that the interaction of protons with the last Na^+ binding transition had not been affected by the cys engineering. Moreover, as reducing the external proton concentration did not in itself restore the WT-like activity for G134C − MTS or M533C + MTS, this suggested that the cys engineering at these sites had affected transitions in the transport cycle that were proton insensitive. Moreover, the depolarizing shift in the presteady-state Q–V and τ–V data, documented for G134C − MTS and M533C + MTS in ND0, was remarkably similar to the effect of external acidification on the WT presteady-state relaxations also in ND0 (Forster et al., 2000), which were shown to result in a weaker steady-state voltage dependency. We therefore focused our attention on the empty carrier to explain the changes in voltage-dependent kinetics.

Simulations Confirm Influence of Empty Carrier Kinetics on Voltage Dependency

To demonstrate how the empty carrier kinetics can influence cotransport function, we used the eight-state model to simulate the observed behavior for the G134C mutant. Minor changes to the model parameters would also allow prediction of the M533C behavior. The starting point for our simulations was based on the estimates of the apparent valency and rate constants for G134C + MTS in ND0 (Table I) of the main detectable presteady-state relaxation. In the model, these rates correspond to the empty carrier transition rates at $V = 0$ (k_{18}^0 and k_{81}^0). Other rate constants were chosen to give the observed steady-state activation behavior in terms of the apparent affinity for P_i (~0.05 mM) and for Na^+ (~40–50 mM) and the chord slope of the steady-state P_i activation I–V data in the range −100 to 0 mV. We assumed that all transitions were operating under nonrapid equilibrium conditions and only the empty carrier (1–8) and first Na^+ binding (1–2) transitions were voltage dependent and each could be described by one kinetic step (and assuming sharp energy barriers) (e.g., Parent et al., 1992, Loo et al., 2002).

As illustrated in Fig. 7 B, we could simulate the effect of MTS on the main presteady-state relaxations for G134C, observed in ND0 and ND100, by changing only the rate constants of the empty carrier transition at $V = 0$. The rate constants for G134C − MTS differed slightly from those in Table I, which most likely reflects uncertainties in the exponential fitting due to noise or artifacts at extreme test potentials and the simplification of the empty carrier kinetics to a single transition. The simulated data show that for a ±120-mV voltage step from −60 mV, there is less charge movement in the hyperpolarizing direction in the G134C − MTS condition compared with the depolarizing step, whereas the charge movement becomes more symmetrically distributed in the G134C + MTS condition (Fig. 4 C). The simulations also predict that in ND100, a fast component is introduced by the Na^+ binding/debinding transition (1–2) that is most easily seen for the −MTS simulation. As indicated by the vertical bars superimposed on the traces of Fig. 7 B, the time window used for the presteady-state analysis in this study precluded characterization of this component from the experimental data. Quantification of fast relaxing components ($\tau \sim$ 1–2 ms) using the two-electrode voltage clamp is also dependent on the speed and homogeneity of the oocyte membrane voltage control, as well as the recording signal-to-noise ratio and expression level. The simulated presteady-state relaxations were quantitated in terms of the time constant of the main relaxation (τ_{ON}) (Fig. 7 C) and the charge moved by voltage steps (Q_{ON}) (Fig. 7 D). The τ_{ON}–V data reflect the same behavior observed for G134C (Fig. 5 A), whereby a hyperpolarizing shift in the maximum occurs for the +MTS case. The simulated Q_{ON}–V data also recapitulate the behavior of the measured data (Fig. 6 A), whereby for G134C − MTS, the charge movement saturates in the hyperpolarizing direction and there is only a marginal increase in charge movement due to the presence of 100 mM Na^+.

The simulated steady-state I–V data for I_{P_i} (Fig. 7 E), assuming 1 mM P_i and 100 mM Na^+, indicated that changes to k_{18}^0 and k_{81}^0 could account for an altered voltage dependency of I_{P_i} for G134C − MTS (or M533C + MTS), but not the reduced maximum turnover rate (Fig. 1 E). We took account of this in our model by reducing the fully loaded carrier transition k_{45}. To simulate the behavior of M533C + MTS, k_{45} would have to be further reduced to account for smaller steady-state activity (Fig. 1 E). Lastly, we determined the voltage dependency of the apparent substrate affinities (K_m^{Pi} and K_m^{Na}) (Fig. 7 F) by simulating steady-state I–V data with the same substrate concentrations used experimentally and fitting the simulated data with a Michaelis-Menten function (Eq. 1) for the $K_m^{P_i}$ determination and the modified Hill equation (Eq. 2) for the K_m^{Na} determination. From the fit to the Na^+ activation data, the Hill coefficient for the −MTS case

increased from 2.0 (−100 mV) to 2.5 (0 mV), and for the +MTS case, it increased from 2.1 (−100 mV) to 2.4 (0 mV). As shown in Fig. 7 F, both $K_m^{P_i}$ and K_m^{Na} decreased with hyperpolarization; however, for $K_m^{P_i,i}$ for the +MTS case, it was approximately twofold larger at all potentials. Interestingly, we also observed a similar trend in the estimates of $K_m^{P_i}$ and K_m^{Na} reported by the fitting algorithm, which, despite the uncertainties in the estimates of these parameters from the experimental data, confirms the robustness of the model to describe the transport activity.

Overall, the simulations suggest that the empty carrier rates (k_{18} and k_{81}) are crucial determinants of the NaPi-IIa kinetics. At any *V*, they define the probability of occupying a given state, in particular, the occupancy of state 2, which precedes P_i binding and subsequent cotransport. Fig. 8 shows the voltage dependency of occupancies of the predominantly occupied states for three superfusion conditions: ND0, ND100, and ND100 + 1 mM P_i. In ND0, the simulation predicts that for G134C − MTS (or M533C + MTS), the empty carrier remains mostly in state 1 for hyperpolarizing potentials. This would correspond to an outward-facing conformation of the protein. For G134C + MTS (or M533C − MTS), the empty carrier is distributed between states 1 and 8 and this distribution is shifted to predominantly state 1 only for extreme hyperpolarizing potentials. In ND100 for the −MTS condition, the probability of occupying state 8 is low, and the carrier occupancy moves from state 1 to state 2 as the probability of Na^+ binding increases with hyperpolarization. The charge movement contributed by the empty carrier would be small for hyperpolarizing steps for this condition, with the rapid Na^+ binding transition (1–2) contributing most of the charge movement. In contrast, for the +MTS condition, the transporter must first leave state 8 (inward facing, empty carrier) to reach state 2 via the intermediate state 1. Compared with the −MTS condition, we would expect this to involve a much larger structural reorientation for a given change in *V* and concomitant charge movement for hyperpolarizing steps. Finally, in the presence of saturating P_i, the main states occupied are 4 (fully loaded carrier, outward facing) and 8 (empty carrier, inward facing). The voltage dependency of the state 4 occupancy now reflects the steady-state *I–V* data for each condition; for −MTS, state 4 is preferred at hyperpolarizing potentials, whereas for +MTS, the transporter is distributed between states 4 and 8 depending on *V*. The voltage-dependent shift in the occupancies of states 4 and 8 for +MTS is also reflected in the stronger voltage dependency of $K_m^{P_i}$ for this condition (Fig. 7 F). A qualitatively similar trend is also predicted for K_m^{Na}; however, this parameter is also a strong function of the final Na^+ binding transition that is assumed to involve a

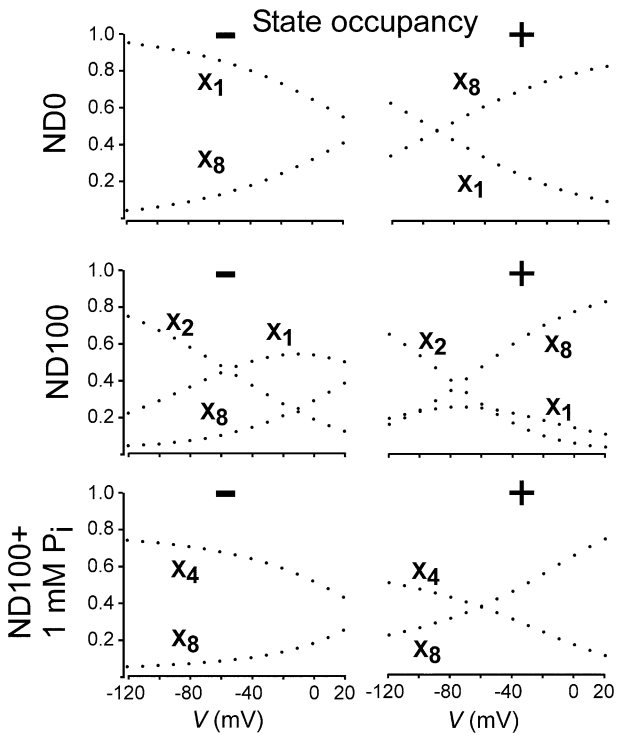

FIGURE 8. Simulations of occupancy of states 1, 2, 4, and 8 of the model scheme depicted in Fig. 7 A, as a function of membrane potential in zero external Na^+ (ND0), 100 mM external Na^+ (ND100), and 100 mM external Na^+ with 1 mM P_i (ND100 + 1 mM P_i), before (−) and after (+) modification of Cys-134.

highly cooperative binding of two Na^+ ions (Forster et al., 1998, 2000).

The behavior of WT NaPi-IIa corresponds closely to that of G134C + MTS (or M533C − MTS) in which the preferred orientation of the empty carrier in the absence of external Na^+ and $V = 0$ is inward facing and this can be altered by membrane hyperpolarization to the outward-facing conformation. A similar situation has been described by Loo et al. (2002) for the sodium glucose cotransporter SGLT-1, whereby the empty carrier is predicted to undergo a voltage-dependent reorientation from inward to outward conformation for hyperpolarizing *V*. This behavior suggests a common voltage-dependent mechanism for these Na^+-coupled cotransport systems. Moreover, it is consistent with alternating access schemes for membrane transport proteins in which large conformational changes occur to the empty carrier that would alternately offer accessibility of the substrate binding sites to the cytosol or external medium (Loo et al., 1998, 2002). For NaPi-IIa, the state occupancy is also a strong function of external protons (Forster et al., 2000); the action of which on the empty carrier kinetics can be emulated by the molecular manipulations performed at sites Gly-134 and Met-533. The altered preferred orientation of the carrier for G134C − MTS and M533C + MTS can also ex-

plain their increased sensitivity of cotransport activity to external protons, as this would presumably increase proton accessibility to the Na^+ binding sites.

Structure–Function Implications

In summary, the effect of introducing a Cys at Gly-134 or MTS modification of Cys-533 is to stabilize the empty carrier conformation so that it is increasingly likely to occupy the outward-facing conformation for $V < 0$. Thus, we have been able to alter the preferred orientation of the empty carrier through cys substitution or cys modification or both, depending on the linker region. The proposed interactions of the modified sites with the voltage-dependent parts of NaPi-IIa reveal a novel structure–function relationship; functionally, they result in modified steady-state cotransport kinetics that correlate with changes to the presteady-state kinetics. When incorporated into an alternating access model for NaPi-IIa, the altered rate constants of the presteady-state charge movements indicate that these interactions induce major voltage-dependent reorientations of the protein structure.

In the absence of 3-D structural data for NaPi-IIa, we can only speculate how the Cys engineering at sites 134 and 533 could lead to the functional behavior documented in this study. Based on previous cys mutagenesis studies (Lambert et al., 2001, Kohler et al., 2002a,b), we have proposed that sites in ECL-3 and ICL-1 contribute to a cotransport pathway through NaPi-IIa, possibly by forming two reentrant loops in a common hydrophilic vestibule. This is also consistent with NaPi-IIa being a functional monomer (Kohler et al., 2000) and the requirement that the COOH-terminal and NH_2-terminal halves of the protein together form a functional transporter (Ehnes et al., 2002). These halves are most likely stabilized by two disulfide bridges (Kohler et al., 2003), which thereby place constraints on the spatial relationship of the predicted transmembrane domains. Major conformational changes are assumed to occur during the transport cycle according to the alternating access model, as proposed for the recently crystallized GlpT and LacY transporters (Abramson et al., 2003; Huang et al., 2003). For NaPi-IIa, we speculate that these involve movement of TMD-2/TMD-3 associated with ICL-1 in the NH_2-terminal half and TMD-5/TMD-6 associated with ECL-3 in the COOH-terminal half. Gly-134 would confer the necessary flexibility to ECL-1 for TMD-2 to adopt inward and outward-facing conformations according to the alternating access scheme, depending on the membrane potential. Cys substitution at 134 might constrain these movements and stabilize the outward-facing conformation, as predicted from the simulations. This preferred orientation would also hinder the substrate translocation transition in agreement with the slower rate for partial reaction 4–5 (Fig. 7 A). Addition of a bulky MTS reagent to this Cys would destabilize the protein to restore a WT-like inward-facing conformation. In the COOH-terminal half of the protein, the Met-533-Cys substitution is well tolerated, but when Cys-533 is modified, the additional bulk of the MTS reagent could now sterically hinder movements of TMD-6, for example, so that the protein adopts an outward-facing conformation similar to that induced by Cys-134.

We thank Dr. Don Loo (University of California at Los Angeles, Los Angeles, CA) for valuable discussions on the interpretation of the voltage dependency mechanism and Dr. Leila Virkki (University of Zurich) for helpful comments on the manuscript.

This work was supported by grants to H. Murer from the Swiss National Science Foundation (31-46523), the Hartmann Müller-Stiftung (Zurich), the Olga Mayenfisch-Stiftung (Zurich), and the Union Bank of Switzerland (Zurich) (Bu 704/7-1).

Lawrence G. Palmer served as editor.

Submitted: 12 March 2004
Accepted: 14 September 2004

REFERENCES

Abramson, J., I. Smirnova, V. Kasho, G. Verner, H.R. Kaback, and S. Iwata. 2003. Structure and mechanism of the lactose permease of *Escherichia coli*. *Science*. 301:610–615.

Ehnes, C., I.C. Forster, K. Kohler, J. Biber, and H. Murer. 2002. Functional studies on a split type II Na/P(i)-cotransporter. *J. Membr. Biol.* 188:227–236.

Ehnes, C., I.C. Forster, K. Kohler, A. Bacconi, G. Stange, J. Biber, and H. Murer. 2004. Structure–function relations of the first and fourth predicted extracellular linkers of the type IIa Na^+/Pi cotransporter. I. cysteine scanning mutagenesis. *J. Gen. Physiol.* 124:475–488.

Forster, I., J. Biber, and H. Murer. 2000. Proton-sensitive transitions of renal rat type II Na^+-coupled phosphate cotransporter kinetics. *Biophys. J.* 79:215–230.

Forster, I., N. Hernando, J. Biber, and H. Murer. 1998. The voltage dependence of a cloned mammalian renal type II Na^+/P_i cotransporter (NaPi-2). *J. Gen. Physiol.* 112:1–18.

Forster, I.C., C.A. Wagner, A.E. Busch, F. Lang, J. Biber, N. Hernando, H. Murer, and A. Werner. 1997. Electrophysiological characterization of the flounder type II Na^+/Pi cotransporter (NaPi-5) expressed in *Xenopus laevis* oocytes. *J. Membr. Biol.* 160:9–25.

Hartmann, C.M., C.A. Wagner, A.E. Busch, D. Markovich, J. Biber, F. Lang, and H. Murer. 1995. Transport characteristics of a murine renal Na/Pi-cotransporter. *Pflugers Arch.* 430:830–836.

Hazama, A., D.D. Loo, and E.M. Wright. 1997. Presteady-state currents of the rabbit Na^+/glucose cotransporter (SGLT1). *J. Membr. Biol.* 155:175–186.

Huang, Y., M.J. Lemieux, J. Song, M. Auer, and D.N. Wang. 2003. Structure and mechanism of the glycerol-3-phosphate transporter from *Escherichia coli*. *Science*. 301:616–620.

Kohler, K., I.C. Forster, G. Lambert, J. Biber, and H. Murer. 2000. The functional unit of the renal type IIa Na^+/P_i cotransporter is a monomer. *J. Biol. Chem.* 275:26113–26120.

Kohler, K., I.C. Forster, G. Stange, J. Biber, and H. Murer. 2002a. Identification of functionally important sites in the first intracellular loop of the NaPi-IIa cotransporter. *Am. J. Physiol. Renal Physiol.* 282:F687–F696.

Kohler, K., I.C. Forster, G. Stange, J. Biber, and H. Murer. 2002b.

Transport function of the renal type IIa Na^+/P_i cotransporter is codetermined by residues in two opposing linker regions. *J. Gen. Physiol.* 120:693–705.

Kohler, K., I.C. Forster, G. Stange, J. Biber, and H. Murer. 2003. Essential cysteine residues of the type IIa Na^+/Pi cotransporter. *Pflugers Arch.* 446:203–210.

Lambert, G., I.C. Forster, G. Stange, J. Biber, and H. Murer. 1999. Properties of the mutant Ser-460-Cys implicate this site in a functionally important region of the type IIa Na^+/P_i cotransporter protein. *J. Gen. Physiol.* 114:637–652.

Lambert, G., I.C. Forster, G. Stange, K. Kohler, J. Biber, and H. Murer. 2001. Cysteine mutagenesis reveals novel structure–function features within the predicted third extracellular loop of the type IIa Na^+/P_i cotransporter. *J. Gen. Physiol.* 117:533–546.

Loo, D.D., B.A. Hirayama, E.M. Gallardo, J.T. Lam, E. Turk, and E.M. Wright. 1998. Conformational changes couple Na^+ and glucose transport. *Proc. Natl. Acad. Sci. USA.* 95:7789–7794.

Loo, D.D.F., S. Eskandari, B.A. Hirayama, and E.M. Wright. 2002. A kinetic model for secondary active transport. *In* IMA Volumes in Mathematics and Its Applications. Volume 129: Membrane Transport and Renal Physiology. H.E. Layton and A.M. Weinstein, editors. Springer Verlag, New York. 1–19.

Parent, L., S. Supplisson, D.D. Loo, and E.M. Wright. 1992. Electrogenic properties of the cloned Na^+/glucose cotransporter. II. A transport model under nonrapid equilibrium conditions. *J. Membr. Biol.* 125:63–79.

Rakowski, R.F. 1993. Charge movement by the Na/K pump in *Xenopus* oocytes. *J. Gen. Physiol.* 101:117–144.

3.4 Summary of publication:

Functionally important residues in the predicted 3rd transmembrane domain of the type IIa sodium-phosphate cotransporter (NaPi-IIa).

Funktionell wichtige Aminosäurereste in der vorhergesagten dritten Transmembrandomäne von NaPi Typ IIa, dem Natrium-Phosphat-Cotransporter

Der Na/P_i Cotransporter Typ IIa (NaPi-IIa) vermittelt den elektrogenen Transport von drei Na^+-Ionen und einem divalenten Pi-Ion (und einer positiven Nettoladung) über die Zellmembran. Der Vergleich der Sequenzen der elektrogenen NaPi-IIa- und NaPi-IIb- Isoformen mit der des elektroneutralen NaPi-IIc zeigte auf, dass die dritte Transmembrandomaene (TMD) eine mögliche massgebliche Determinante für die Substratbindung darstellt. Um die Rolle der TMD-3 im Hinblick auf die Topologie und dem zugrunde liegenden Mechanismus der Funktion von NaPi-IIa aufzuklären, unterzogen wir es einer „Cystein-Scanning Mutagenese".
Die Konstrukte wurden in Xenopus Oocyten exprimiert und die Pi-Transportkinetik durch elektrophysiologische Messungen und Aufnahme radioaktiv markierter Indikatoren untersucht. In den Mutanten, die einen ausreichenden Strom für eine Analyse lieferten, hatte die Cystein Substitution nur eine geringfügige Veränderung der Pi-Transportkinetik zur Folge. Nur ein Mutationsort am extrazellulären Ende der TMD-3 schien erreichbar für Methanethiosulfonat-Reagenzien zu sein. Dennoch führten zusätzliche Mutationen an den Stellen D224 (ersetzt durch E,G oder N) und N227 (ersetzt durch D oder Q) zu merklichen Veränderungen der Spannungs- und Substratabhängigkeit des Pi-abhängigen Stroms. Durch den Austausch von Asp-224 ergab sich eine Mutante, die elektroneutral und Na+-abhängig Pi transportierte. Da der elektrogene Cotransporter NaPi-II pro Zyklus 3 Na+-Ionen transportiert, der elektroneutrale NaPi-IIc jedoch nur 2, vermuteten wir, dass dieser Verlust der Elektrogenizität von dem Verlust einer der 3 Na+ -Bindungsstellen im NaPi-IIa herrührt.

Functionally important residues in the predicted 3rd transmembrane domain of the type IIa sodium-phosphate cotransporter (NaPi-IIa)

Leila V. Virkki, Ian C. Forster, Andrea Bacconi, Jürg Biber, Heini Murer

Author address: University of Zürich, Institute of Physiology and Center for Integrative Human Physiology, Winterthurerstrasse 190, CH-8057 Zürich, Switzerland.

tel +41 44 6355053

fax +41 44 6356814

Author email address: leilav@physiol.unizh.ch

Running head: Mutagenesis in TMD-3 of NaPi-IIa

ABSTRACT. The type IIa Na^+/P_i cotransporter (NaPi-IIa) mediates electrogenic transport of three Na^+ and one divalent P_i ion (and one net positive charge) across the cell membrane. Sequence comparison of electrogenic NaPi-IIa and IIb isoforms with the electroneutral NaPi-IIc isoform pointed to the third transmembrane domain (TMD) as a possibly significant determinant of substrate binding. To elucidate the role of TMD-3 in the topology and mechanism underlying NaPi-IIa function we subjected it to cysteine scanning mutagenesis. The constructs were expressed in *Xenopus* oocytes and P_i transport kinetics were assayed by electrophysiology and radiotracer uptake. Cys substitution resulted in only marginally altered kinetics of P_i transport in those mutants providing sufficient current for analysis. Only one site, at the extracellular end of TMD-3, appeared to be accessible to methanethiosulfonate reagents. However, additional mutations carried out at D224 (replaced by E, G or N) and N227 (replaced by D or Q) resulted in markedly altered voltage and substrate dependencies of the P_i-dependent currents. Replacing Asp-224 (highly conserved in electrogenic a and b isoforms) with Gly (the residue found in the electroneutral c isoform) resulted in a mutant that mediated electro*neutral* Na^+-dependent P_i transport. Since electrogenic NaPi-II transports 3 Na^+/transport cycle, whereas electroneutral NaPi-IIc only transports 2, we speculate that this loss of electrogenicity might result from the loss of one of the three Na^+ binding sites in NaPi-IIa.

KEYWORDS Structure-function, cysteine scanning, stoichiometry, electrophysiology, voltage clamp

INTRODUCTION.

The physiological role of type II sodium-phosphate cotransporters is to facilitate cellular uptake of inorganic phosphate (P_i) by coupling it to the transmembrane Na^+ gradient. Three different Na/P_i cotransporter isoforms are known to date. The type IIa cotransporter (NaPi-IIa) is predominantly expressed in brush border membranes of the kidney proximal tubule and is a major contributor to regulated P_i reabsorption [17, 18, 23]. The type IIb cotransporter is expressed in (among other tissues) the intestine, where it mediates P_i absorption from the gut lumen [4, 9]. Similar to the IIa isoform, the recently cloned type IIc cotransporter is expressed in the kidney proximal tubule and is strongly upregulated in response to a low-P_i diet [21, 22]. The main functional difference between the isoforms is that whereas type IIa and IIb cotransporters are electrogenic, type IIc is electroneutral.

Topology analyses based on hydropathy plots and hidden-Markov modeling predict at least eight transmembrane domains (TMDs) for type II Na/P_i cotransporters (see Figure 1). Intracellular orientation of the N and C termini have been verified using epitope tagging, as has the extracellular location of a large glycosylated loop between TMDs 3 and 4 [8, 16]. Substituted cysteine accessiblity mutagenesis (SCAM) studies suggested that the long linking regions between TMDs 2-3 and 5-6 enter the membrane to form part of the transport corridor [6, 10, 11, 15]. Also the short external loops connecting TMDs 2-3 and 7-8 contain functionally sensitive sites important with respect to defining the voltage sensitivity of NaPi-IIa [2, 3].

Sequence comparison between the different isoforms show that amino acids in the putative TMDs and in the two re-entrant loops are highly conserved. Moreover, a comparison of all currently available sequence data reveals that there are very few non-conservative substitutions between the electrogenic and electroneutral isoforms [1]. One prominent substitution appears in TMD-3, where Asp-224 (numbering based on human NaPi-IIa) in the electrogenic IIa and IIb isoforms is substituted with a glycine in the electroneutral IIc. Since

TMD-3 is also amphipathic and could therefore form part of an aqueous transport pathway, we hypothesized that this TMD might be important in substrate recognition and transport function in Na/P_i cotransporters. In this study we therefore focussed on TMD-3 by first performing cysteine scanning mutagenesis of 19 consecutive amino acids predicted to constitute TMD-3 and second, investigating the effects of mutagenesis at sites highlighted from bioinformatic considerations.

EXPERIMENTAL PROCEDURES

Molecular biology and oocyte expression. The cDNA encoding human NaPi-IIa (*NPT2a*, SLC34A1) was previously subcloned into a KSM expression vector to improve its expression in *Xenopus laevis* oocytes [26]. Mutant transporters were generated using the Quickchange Site-directed Mutagenesis kit (Stratagene) according to manufacturer's directions. Mutants were verified by sequencing (Microsynth). Before introducing novel Cys residues in TMD-3, we first replaced the native Cys-225 with Ser (C225S). All mutants in which we introduced a novel Cys were constructed on this C225S backbone, all other mutants were constructed on the wild-type (WT) backbone. The plasmids were linearized using Xba1 (Promega) and used as a template for the synthesis of capped cRNA using the Message Machine T3 kit (Ambion).

Stage V-VI defolliculated oocytes from *Xenopus laevis* were isolated and maintained as described previously [27]. Oocytes were injected with 50 nl of cRNA (0.2 µg/µl) encoding WT or mutant NaPi-IIa. Control oocytes were injected with 50 nl of water. Oocytes were incubated at +18 °C in modified Barth's solution, containing (in mM) 88 NaCl, 1 KCl, 0.41 $CaCl_2$, 0.82 $MgSO_4$, 2.5 $NaHCO_3$, 2 $Ca(NO_3)_2$, 7.5 HEPES, pH 7.5 adjusted with TRIS. The solution was supplemented with 5 mg/l doxycyclin. Electrophysiology and radiotracer flux experiments were performed 2-5 days after injection. Each data set is obtained from at least two batches of oocytes from two different donor frogs.

Two-electrode voltage clamp. We used a custom-built voltage clamp optimized for fast clamping speed [5] to make recordings from control oocytes and oocytes expressing WT

NaPi-IIa or mutants. The voltage clamp was controlled and data aquired using a computer running pClamp 8 software (Axon Instruments), which also controlled valves for solution switching. Solutions were cooled to 20-22 °C before introduction to the oocyte recording chamber at a rate of 5 ml min^{-1}. The oocyte was initially superfused with ND100 solution, containing (in mM) 100 NaCl, 2 KCl, 1.8 $CaCl_2$, 1 $MgCl_2$, 10 HEPES, titrated to pH 7.4 using TRIS. We obtained different concentrations of P_i by adding K_2HPO_4/KH_2PO_4 in proportions giving the desired pH. In some experiments it was necessary to substitute $CaCl_2$ with $BaCl_2$ to suppress the activation of endogenous Cl^- channels at hyperpolarizing voltages. In solutions where the Na^+ concentration was varied (ND0-ND100), NaCl was substitued equimolarly with choline Cl. In some experiments, we replaced NaCl with Na glucuronate to reduce the external Cl^- concentration.

Measurement of apparent P_i and Na^+ affinities. The oocyte was clamped to a membrane potential of -50 mV and the holding current was continuously recorded. To measure P_i-induced currents (I_{Pi}), the superfusate was switched to one containing P_i and deflection in the holding current was monitored. When the current had reached its maximum, the perfusate was switched back and washout of P_i was monitored by observing the return of holding current to baseline. When I_{Pi} were to be recorded for another Na^+ concentration or pH, the holding current was first allowed to stabilize in the new baseline solution before switching to one including P_i. For determining the apparent K_m for P_i, P_i–induced current deflections were measured using different P_i concentrations while keeping the Na^+ concentration constant. For determining the apparent K_m for Na^+, the oocyte was first perfused with a specific concentration of Na^+ before switching to a solution containing P_i in the same solution (the P_i concentration was kept constant throughout the experiment)

The apparent K_m for P_i and Na^+ was determined by fitting data with the modified Hill equation:

$$I_{Pi} = I_{Pi,\,max}\,[S]^H / ([S]^H + (K_m)^H) \qquad \text{Equation 1}$$

where I_{Pi} is the P_i-induced current, $I_{Pi,\ max}$ is the extrapolated maximal P_i-induced current, [S] is the concentration of substrate (Na^+ or P_i), K_m is the concentration of substrate that gives half-maximum response, and *H* is the Hill coefficient. For determining K_mP_i, *H* was constrained to 1.

Incubation with methanethiosulfonate (MTS) reagents. Sodium (2-sulfonatoethyl)methane thiosulfonate (MTSEA), [2-(trimethylammonium) ethyl]methanethiosulfonate bromide (MTSET) and sodium (2-sulfonatoethyl)methane thiosulfonate (MTSES) were dissolved in DMSO at a concentration of 1M and stored at -20°C. Immediately before use, the MTS reagents were diluted to a final concentration of 1 mM in ice-cold ND100 solution and applied using gravity feed through a stainless-steel cannula placed close to the oocyte. During application, the oocyte was held at -50 mV and the current tracing monitored continuously. Before MTS application, I_{Pi} was measured using 1 mM P_i in ND100 solution.

Measuring the voltage-dependency of P_i-induced currents. The voltage-dependency of P_i – induced currents were measured by applying holding potentials from -160 or -140 mV to +40 mV and recording currents in the presence and absence of P_i, as described previously [5]. For determining the P_i -dependency of the current, we varied the P_i concentration while keeping the Na^+ concentration constant. For determining the Na^+-dependency of the current, the oocyte was first perfused with a specific concentration of Na^+ and subsequent recordings were obtained in the presence and absence of P_i. In both cases, current records obtained in the absence of P_i were subtracted from those recorded in the presence of P_i to obtain the P_i-dependent current. To compensate for the differences in expression levels between individual oocytes, the data obtained from each oocyte were normalized to the P_i-dependent current recorded at -100 mV with 100 mM Na^+ and 1 mM P_i in the bath at pH 7.4 before fitting the data with Eq 1 plus a variable offset. The offset is included to account for the leak current,

which is present in NaPi-IIa –expressing oocytes in the absence of P_i, but blocked by P_i with an unknown affinity [2, 25].

Radiotracer uptake. A group of oocytes (5-9 oocytes/group) was first allowed to equilibrate in uptake solution without tracer. After aspiration of as much of this solution as possible, we added 100 µl uptake solution containing radiotracer ($^{32}P_i$, ^{22}Na or both). The uptake was allowed to proceed for 15-30 min before it was stopped by washing the oocytes three times with 4 ml ice-cold ND0 solution containing 2 mM cold P_i. If no P_i was present in the uptake solution, washing was performed with ice-cold ND0 solution.

Uptake of $^{32}P_i$ alone was carried out using ND100 solution and 1 mM cold P_i, to which $^{32}P_i$ (^{32}P-orthophosphate, specific activity 10 mCi/mmol P_i) was added. For dual uptake of both $^{32}P_i$ and ^{22}Na, it was necessary to lower the Na^+ concentration to achieve a high enough specific activity for Na^+. Therefore these experiments were carried out using ND40 solution with 2-3 mM cold P_i, and containing the isotopes ^{32}P-orthophosphate (specific activity 3 mCi/mmol P_i) and ^{22}Na (specific activity 350 µCi/mmol Na; Amersham).

After washing oocytes were placed individually in a scintillation vial and lysed in 250 µl 10% SDS. ^{32}P and ^{22}Na activities of individual oocytes were counted using a Packard Tri-Carb 2900TR scintillation counter. For the dual uptake experiments the counts of the two isotopes were separated using a Dual DPM assay with quench curves.

Western blotting. Pools of three oocytes were lysed in 60 µl homogenization buffer (100 mM NaCl, 200 mM Tris-HCl, 3% pentaethyleneglycol mono-*n*-dodecyl ether (Calbiochem), pH 7.6). Yolk proteins were removed by centrifugation (3 min 16 000g). 10 µl supernatant was mixed with 10 µl loading buffer (380 mM Tris-HCl, 8% SDS, 4 mM EDTA, 40% glycerol, 4 mg/ml bromophenol blue, pH 6.8) and separated on a 9% SDS-PAGE gel. Separated proteins were transferred onto a nitrocellulose membrane (Schleicher & Schuell). The membrane was preincubated in blotting solution (5% nonfat milk in 100 mM NaCl, 50 mM Tris-HCl, pH 7.4) and then probed for NaPi-IIa protein using a rabbit polyclonal

antibody raised against a synthetic C-terminal peptide (dilution 1:2000 in blotting solution). Signal was detected by incubating the blot with a horseradish peroxidase-conjugated $F(ab')_2$ fragment (Amersham) and then exposing it to a solution containing 0.0165% H_2O_2, 1.25 mM luminol and 0.2 mM p-coumaric acid in 100 mM Tris-HCl, pH 8.5. Chemiluminescence was detected using autoradiography.

Reagents. All standard chemicals and reagents were obtained from either Sigma or Fluka Chemie AG. ^{32}P-orthophosphate was purchased from New England Nuclear and ^{22}Na was from Amersham. The Cys-reactive reagents MTSEA, MTSET and MTSES were from Toronto Research Chemicals.

Data presentation and statistical analysis All data is shown as means ±SEM, where n denotes the number of experiments. Error bars are not shown when they are smaller than the symbols. Statistical analysis of the data was carried out using two-tailed t-test or one-tailed ANOVA with Tukey's post-test, with $p<0.05$ considered significant. Both statistical analysis and curve fitting were done using GraphPad Prism 3.0 software (GraphPad Software).

RESULTS

Cysteine scanning mutagenesis in TMD-3

Our first strategy to determine structure-function relationships in TMD-3 was to perform cysteine scanning mutagenesis (SCAM). TMD-3 contains one native Cys (C225), which was removed to avoid possible interaction between this Cys and newly introduced residues, or that the possibility that the mutagenesis would change the reactivity of C225S by making it more exposed. To establish the feasibility of using this substitution as a backbone for the subsequent cysteine scanning mutagenesis (SCAM), we first compared the P_i-and Na^+-activation kinetics of WT and C225S-expressing oocytes at a holding potential of -50 mV. The P_i-induced currents (I_{Pi}) at 100 mM Na^+ were obtained by subtracting the steady-state current in 0 mM P_i from that at the given P_i. The data were easily fit with a Michaelis-Menten function (Eq. 1, $H = 1$) (Figure 2A). The fitting algorithm reported that the apparent affinity

constant for P_i (K_mP_i) was significantly reduced for the C225S mutant (47 ±16 μM), compared to the WT (94 ±22 μM, n= 10 each). Furthermore, the maximum P_i-dependent current was approximately halved for C225S, compared to WT.

The corresponding Na^+-activation at 1 mM P_i is shown in Figure 2B. As we have previously reported for the human WT NaPi-IIa [25], C225S also displayed a clear sigmoidicity for I_{Pi} with increasing [Na^+]. Fitting these data with Eqn 1 (*H*, unconstrained) indicated a small but statistically significant decrease in K_mNa in the C225S mutant (30 ±7 mM), compared to the WT (34 ±5 mM), n=5. For WT and C225S, *H* was 2.8 ±0.9 and 2.2 ±1, respectively, consistent with cooperative Na^+ interaction with the protein. Moreover, we observed that the maximum P_i-dependent current mediated by the C225S mutant was half that of the WT, consistent with the P_i-activation data.

To determine if the voltage-dependency of P_i transport was affected by the C225S mutation, we measured I_{Pi} at different voltages. Figure 2C shows the current-voltage (I-V) relationship for oocytes expressing WT or C225S NaPi-IIa. The current at each voltage was reduced for the C225S mutant, as compared to WT, but the shapes of the I-V –relationships were similar, which indicated that the voltage-dependency was not affected by the mutation. Taken together, these data indicated that the Cys-Ser substitution at 225 was well tolerated, but with an approximately 50% decrease in maximum transport rate.

Using the C225S background, we next substituted one by one 19 residues in TMD-3 with Cys (from Val-222 to Thr-241). To identify which mutants were capable of mediating P_i transport we measured $^{32}P_i$ uptake using 1 mM cold P_i and 100 mM Na^+. Figure 3A shows P_i uptake in oocytes expressing the various Cys mutants used in this study. The results show that removing the native Cys in TMD-3 (C225S) resulted in a ~50 % decrease in P_i uptake, which was consistent with the ~50% decrease in P_i-induced currents shown in Figure 2. Of the 19 novel Cys mutants engineered on the C225S background four mutants (D224C-C225S, N227C-C225S, P236C-C225S and E238C-C225S) did not mediate significant P_i transport.

Only one mutant (F226C-C225S) showed the same level of P_i transport as C225S. Of the remaining mutants, six mediated ~50% of the C225S transport activity with the last eight mutants mediating even less.

Next, we measured P_i-induced currents in the Cys mutants at a membrane voltage of -50 mV, to determine if the basic electrogenicity of P_i transport had been affected by the mutagenesis. All mutants that mediated significant $^{32}P_i$ transport in Figure 3A also showed P_i-induced currents. Moreover, to determine if the voltage dependency of P_i transport was altered in any of the novel Cys mutants, we measured P_i-dependent currents at different voltages in oocytes expressing WT or mutant NaPi-IIa. All the functional mutants tested (residues 226, 228-232, 234, 235, 237 and 239-241) had I-V –relationships similar to those of C225S shown in Figure 2C (data not shown).

To assess if the reduction in P_i transport seen in some mutants was due to reduced protein expression, we performed Western blotting on whole-oocyte lysates. Figure 3B shows a Western blot of cell lysates of control oocytes and oocytes expressing WT and mutant NaPi-IIa protein. The low-molecular weight band corresponds to the predicted molecular weight of unglycosylated monomeric NaPi-IIa protein (68.9 kD), whereas the weaker band around 80-100 kD corresponds to the glycosylated form. No signal was detectable in the control lane, indicating that the signal in the other lanes is specific for NaPi-IIa.

A comparison of the $^{32}P_i$ uptake data in Figure 3A with the Western blots shown in Figure 3B, indicates that only a few mutants expressed at the same level as the WT. Of these, D224C-C225S did not show significant P_i uptake, indicating that although protein was synthesized, it either did not function correctly or was not targeted to the membrane. The only mutants that showed C225S-like expression and at least 50% of its P_i uptake were F226C-C225S, W228C-C225S, S230C-C225S, A239C-C225S and A240C-C225S.

For mutants that showed sufficient P_i-induced currents, we measured K_mP_i to determine if a change in this kinetic parameter could account for the reduced transport activity (Figure 3C).

Most mutants with large enough P_i-induced currents to yield a reliable measurement over the range of P_i concentrations used (0.01 to 1 mM) had similar K_mP_i, compared to C225S. S230C-C225S was the only mutant with a marked increase in K_mP_i (110 ±10 μM, compared to 47 ±16 μM for C225S), however this value is still well below the concentration of P_i used in the uptake study (1 mM). Since S230C-C225S showed an increase in K_mP_i, we decided to also determine K_mNa for this mutant. Its K_mNa was significantly increased at 55 ±2 mM, compared to 30 ±7 mM for C225S. Taken together, these results indicated that, the reduced P_i transport activity seen in Figure 3A could not be explained by a reduction in P_i affinity.

To perform a cysteine scanning of the novel TMD-3 mutants, we compared I_{Pi} under voltage clamp conditions (100 mM Na^+, -50 mV) before and after exposure to the methanethiosulfonate (MTS) MTSEA at a concentration of 1 mM, which we have previously used as a benchmark condition to detect Cys residues at functionally important sites, e.g. [3, 15]. Only one mutant, A240C-C225S, showed a change in I_{Pi} after MTSEA treatment for 5 min. For this mutant, I_{Pi} was reduced by ~50%, and no further change in I_{Pi} was obtained even with increasing the treatment period to 15 min (Figure 3D). Similar results were obtained with MTSET (1 mM), which confirmed that the site was accessed from the extracellular compartment. In contrast, applying MTSES for up to 15 min had no effect on P_i-induced currents. Furthermore, A240C-C225S-expressing oocytes previously exposed to MTSES retained their MTSEA sensitivity, indicating that MTSES was unable to react with this novel Cys under these conditions.

Site-directed mutagenesis at three sites in TMD-3

Our second strategy to determine the structure-function relationships in TMD-3 made use of a sequence comparison of this region between electrogenic and electroneutral type II Na/P_i cotransporters (Figure 1B) and the position of three oxygen-containing polar/charged residues on one face of TMD-3 (Figure 1C), which might be involved in Na^+ ion coordination..

(i)Asp-224. The charged residue Asp-224 is conserved among the electrogenic type IIa and IIb Na/P_i cotransporters, but is substituted by Gly in the electroneutral NaPi-IIc. To determine if Asp-224 is important for electrogenicity of transport, we made mutations where Asp-224 was substituted with Gly, Glu, or Asn. All mutants mediated P_i transport, as shown by the $^{32}P_i$ uptake assay in Figure 4A, albeit at much reduced rates compared to WT, especially for D224N. Western blotting of total oocyte lysates showed that abundant protein was produced for all mutants (Figure 4B). However, P_i-induced currents were observed for D224E, but not for D224G or D224N (Figure 4C). K_mP_i (measured at -50 mV) for D224E was significantly decreased (0.031 ±0.007 mM, n=6), compared to WT (0.089 ±0.007 mM). Furthermore, the shape of the I-V –curve was altered for D224E, so that D224E-mediated P_i-induced currents were clearly voltage dependent only at potentials more negative than -40 mV, whereas currents mediated by WT are voltage-dependent throughout the measurable range (Figure 4C). Removing Cl^- from the bath did not change the shape of the I-V –curves, which indicates that Cl ions did not affect the voltage dependency of P_i transport in this mutant (not shown).

We measured P_i-induced currents at different voltages in WT and D224E-expressing oocytes at different concentrations of P_i (at constant 100 mM Na^+) or Na^+ (at constant 1 mM P_i), and calculated the voltage-dependency of K_mP_i and K_mNa from this data. A comparison of the I-V-curves in Figure 5A (WT) and B (D224E) shows that at low P_i (0.01 mM) they are similar. The upward deflection with increasing hyperpolarization results from a block of P_i-sensitive leak current in oocytes expressing NaPi-IIa [2, 25]. When the P_i-concentration was increased D224E-mediated currents acquired a more prominent curvature than the WT. A similar pattern was seen when P_i was kept constant and Na^+ was varied (Figure 5D and E). Extracting K_mP_i from the data of Figure 5A and B using Eq. 1 and plotting it against V_m in Figure 5C shows that K_mP_i for D224E was strongly voltage-dependent. K_mP_i was also significantly reduced, compared to WT, throughout the measurable range. Extracting the K_mNa values from the data in Figure 5D and E using Eq 1 (H constrained to 2.0) and plotting

it against V_m in Figure 5F revealed that for D224E, K_mNa was strongly voltage dependent, increasing over four-fold between -40 mV and -140 mV. For the WT, K_mNa was largely voltage-independent.

To see if P_i transport mediated by the D224G mutant was Na^+ dependent, we measured $^{32}P_i$ uptake in the presence and absence of external Na^+. As shown in Figure 6A, P_i uptake in oocytes expressing WT and D224G was abolished in the absence of Na^+. To ascertain if Na^+ is also transported by D224G and to establish the Na:Pi stoichiometry, we performed simultaneous uptake of ^{22}Na and $^{32}P_i$ (Figure 6B). Na^+ uptake measured in the absence of P_i shows that Na^+ uptake was low compared to the P_i-induced Na^+ uptake (Figure 6B inset). For the WT, a linear regression line was fitted to the data with a slope of 2.7 ±0.04, in agreement with a Na:P_i stoichiometry of 3:1 as previously reported [7, 25]. For D224G, the slope of the regression line was 10 ±0.8, implying that 10 Na^+ ions were transported with each P_i. In the absence of detectable P_i-induced currents, the results indicated that D224G mediated significant P_i-dependent non-stoichiometric Na^+ transport, possibly Na^+-Na^+ exchange.

(ii) Asn-227. Given that oxygen-containing residues may play a role in coordinating Na^+ ions, as has been proposed for the Na-K-ATPase [20], we decided to carry out additional mutagensis at Asn-227, a residue located one turn away from Asp-224 in the putative α-helical TMD-3. Replacing Asn with the negatively charged Asp (N227D) led to a poorly expressed construct that was unable to mediate significant P_i uptake (Figure 7A and B). However, when Asn was replaced with Gln (N227Q), the construct expressed well and mediated significant P_i uptake (Figure 7A and B) and P_i-induced currents (Figure 7C). The apparent P_i and Na^+ affinities determined at -50 mV were markedly decreased compared to WT. Figure 7D shows a plot of the P_i-induced current as a function of the P_i concentration, normalized to $I_{Pi,\,max}$. The data were fitted with Eq. 1 (H = 1) K_mP_i for N227Q was 4.2 ±1.7 mM, compared to 0.096 ±0.011 mM for WT. We then attempted to estimate K_mNa for N227Q

with 3 mM P_i, however lack of saturation precluded a reliable estimate. The fit shown in Figure 7E suggests for N227Q a K_mNa > 100 mM.

The P_i-induced current response in N227Q differed from that of the WT with a current reversal potential observed at around +40 mV (Figure 7C). Removal of external Cl^- (replaced by glucuronate) had no effect on the outward current, indicating that it is not carried by inward movement of Cl^- ions (data not shown).

(iii) Glu-238. In the helical wheel TMD-3 representation (Figure 1C), Glu-238 lies on the same face of a putative α-helix as Asp-224 and Asn-227. It is the only other charged residue in TMD-3 besides Asp-224 and highly conserved, and replacing it with a Cys resulted in a very poorly expressed construct for which we could measure neither $^{32}P_i$ transport nor P_i-induced currents (Figure 3A). We therefore decided to explore this site further by mutating it to an Asp or a Gln. Both E238D and E238Q mediated P_i-induced currents that were ~50% of WT (data not shown). However, the substrate affinities were reduced. For E238D, K_mP_i was 0.24 ±0.06 and K_mNa was 69 ±4 mM, whereas for E238Q K_mP_i was 0.15 ±0.03 and K_mNa 75 ±5 (n=4). This compares to a K_mP_i of 0.091 ±0.022 and K_mNa of 34 ±5 mM for the WT.

DISCUSSION

In this study we have employed two approaches (SCAM and site-directed mutagenesis) to elucidate novel structure-function relationships of the predicted 3rd trasnsmembrane domain (TMD-3) of the human NaPi-IIa transporter. Previous studies in which we have applied SCAM to the rat NaPi-IIa, have focussed on the predicted linker regions (see Figure 1 A) ECL-1, ECL-4 [2, 3], ECL-3 [15] and ICL-1 [10]. The choice of TMD-3, as the first TMD to be investigated, was based on its proximity to ICL-1, which we propose has re-entrant properties and may form part of the substrate translocation pathway [10] and the presence of sites of potential importance in coordinating Na^+ ions [19, 20].

SCAM suggests that TMD-3 is not readily accessible from the extracellular aqueous milieu

Ideally, when carrying out cysteine accessibility studies it would be advantageous to remove all (13) native Cys which otherwise might react with SH-reactive reagents. However, work on the rat NaPi-IIa isoform has shown that removing a number of the native Cys markedly reduces functional P_i cotransport expressed in *Xenopus* oocytes [12], making these constructs problematic to work with. Fortunately, none of the native Cys in WT NaPi-IIa are accessible to membrane-impermeant MTS reagents [12, 13]. We therefore decided to remove only Cys-225, the one native cysteine in putative TMD-3, before proceeding with SCAM. both as a precaution against possible disulfide bridge formation within the TMD-3 stretch or that mutagenesis in TMD-3 might cause Cys-225 to become MTS-reactive. The C225S mutant showed a ~50% decrease in P_i transport activity compared to WT, a reduction similar to that previously observed for the rat isoform [13]. Otherwise this mutant exhibited transport characteristics similar to WT NaPi-IIa, which confirmed its suitability as a SCAM backbone.

Introducing novel Cys residues on a C225S background resulted in reduced or completely abolished P_i transport activity for all mutants except F226C-C225S. The Western blots shown in Figure 3B indicate that in most cases this correlated with reduced protein expression in the oocyte. The notable exception is D224C-C225S, where the signal on the Western blot was as strong as for the WT but neither P_i-induced currents nor P_i transport were detected. Also Cys substitution at polar/charged Asn-227 and Glu-238, lying on the same face of the putative α-helix (Figure 1C), resulted in lack of P_i transport activity in spite of detectable protein expression. Interestingly, the only mutant with an increased K_mP_i, namely S230C-C225S, is found on the same side of a putative α-helix as D224, Asn-227 and E-238. The implications of these findings are discussed further below.

Unlike our previous SCAM studies on linker regions, where accessibility was readily determined experimentally in terms of altered transport function, only one double mutant in the present study (A240C-C225S) was functionally modified by MTS reagents. For this mutant MTSEA or MTSET treatment reduced P_i-induced currents by ~50%. It is not clear

why MTS reagents only partially blocked I_{Pi} in this mutant. Unfortunately the currents were too low after MTS modification to allow us to determine whether the P_i or Na^+ affinities or the turnover rate of the transporter had been altered by the modification. Nevertheless, its modified behaviour indicated that the top of TMD-3 is accessible from the extracellular milieu, which confirmed the topological predictions for this motif. The negative findings for the other mutants suggest that the remainder of TMD-3 is buried within the protein, at least under the labelling conditions we employed (100 mM Na^+, -50 mV holding potential). Alternatively, the residues were indeed labelled without detectable change of function, however this seems unlikely, given that mutagenesis at several of these sites (see below) resulted in dramatic changes in their electrogenic characteristics. Unfortunately, the low expression levels of most Cys mutants precluded a biochemical confirmation of labelling by using MTS-biotin, as we have previously reported for Cys mutants engineered in the loop regions of the rat NaPi-IIa isoform [3, 14].

Sites on the hydrophilic face of TMD-3 are critical determinants of electrogenicity and substrate interaction

Oxygen atoms are important in coordinating metal ions in proteins [19, 20, 24], which suggests that they could also be important in forming a binding site for Na^+ ions in NaPi-IIa . Moreover, it is significant that TMD-3 contains three oxygen-containing residues all located on the same hydrophilic face of the helical wheel representation of TMD-3 Mutagenesis at Asp-224 had profound effects on the P_i transport function of NaPi-IIa. The most notable mutation was D224G where we replaced Asp, a residue conserved in all electrogenic type IIa and IIb transporters, with Gly that appears at the equivalent position in electroneutral NaPi-IIc. D224G mediated low, but significant Na^+-dependent P_i uptake. The amount of Na^+-dependent P_i uptake in Figure 6A corresponded to ~10 nA of current (assuming that one charge is transported per P_i), which is well above the detection limit of our system. Since we were unable to detect any P_i-induced currents in D224G-expressing oocytes, the result

showed that this single point mutation was able to convert an electrogenic transporter into an electroneutral one. This suggests that the carboxylic acid side chain of Asp-224 may participate in forming a binding site for one of the three Na^+ ions transported by NaPi-IIa per transport cycle, and its removal compromised this binding site. This hypothesis is strengthened by the observation that a triple-mutation of electroneutral NaPi-IIc (S187A-S191A-G195D), in which the Gly of NaPi-IIc at the position equivalent to Asp-224 in NaPi-IIa was changed to Asp, is electrogenic and operates with a 3:1 $Na:P_i$ stoichiometry, in contrast to the 2:1 stoichiometry of the WT NaPi-IIc [1]. However, the D224G mutation alone was not sufficient to recreate the full kinetic profile of the NaPi-IIc WT, as shown by the large P_i-induced Na^+ leak (Figure 6B).

The importance of the length of the carboxylic side chain of Asp-224 for NaPi-IIa electrogenicity was further underscored by the altered voltage dependency of P_i-induced currents by D224E, and the dramatically altered voltage dependency of K_mNa (Figure 5F). For D224E the apparent Na^+ affinity was larger than that of the WT at V_m more positive than -60 mV, but decreased and became lower than that of the WT at potentials more negative than -80 mV. Additionally the apparent P_i affinity was strongly decreased at hyperpolarizing potentials, but as K_mNa was measured at saturating P_i (1 mM) throughout the voltage range, whereas K_mP_i was not (100 mM Na^+; oocytes did not tolerate prolonged exposure to hyperosmotic solutions), the effect of voltage on K_mP_i could, at least partially, be secondary to its effect on K_mNa.

Asn-227, which is located one turn further along the α-helical TMD-3 may also play a significant role in the transport function of NaPi-IIa. Substitution with Cys (N227C-C225S) resulted in a construct unable to mediate functional P_i uptake in oocytes. However, protein expression was also low, so the absence of P_i transport may have been due to impaired expression. This was also most likely the case for N227D, where the polar amine group of Asn was substituted with the charged carboxyl of Asp. However, when we replaced Asn with

the polar, but slightly longer Gln, the resulting construct expressed well and mediated electrogenic P_i transport, albeit with considerably reduced Na^+ and P_i affinities. Interestingly, a similar phenotype was reported for mutagenesis at Asn-199 in the predicted ICL-1 (marked with a grey circle in Figure 1A). At this site substitution with Cys as well as shorter polar (Thr) or non-polar (Ala) side chains resulted in reduced apparent substrate affinities, whereas substitution of larger or charged residues (Asp, His, Gln, Arg) resulted in fully suppressed cotransport function [10]. Taken together, our present findings suggest that Asn-227 also contributes to the substrate binding site and may be in close proximity to Asn-199 in ICL-1.

Ser-230 lies a further turn along TMD-3. Interestingly, S230C-C225S expressed well but this was the only mutant to show a significantly reduced apparent P_i and. Na^+ affinity compared to the C225S alone. One explanation for this behaviour is that substitution of polar Ser with less polar Cys may impede the movement of Na^+ towards its putative binding site further down this amphipathic helix. Finally, Glu-238, lying a further two turns along the α-helix, is the only other charged residue of TMD-3. Cys substitution at this site was not tolerated, but substitution with the charged Asp or polar Gln resulted in functional mutants that mediated electrogenic P_i transport with reduced substrate affinities.

Taken together, the results of the Cys scanning mutagenesis and the additional mutagenesis of Asp-224, Asn-227, Ser-230 and Glu-238 are consistent with TMD-3 forming an amphipathic helix that contains important elements for substrate binding.

CONCLUSIONS

This is the first study describing cysteine scanning mutagenesis in a NaPi-IIa protein TMD. An introduced Cys located at the predicted top (extracellular) end of TMD-3 could be functionally modified using MTS reagents, confirming the predicted topology and suggesting that the remainder of TMD-3 is largely buried in the membrane. Additional mutagenesis at Asp-224 identified this residue to be critical for electrogenic P_i transport in NaPi-IIa, and this has been recently confirmed by mutagenesis at the equivalent site in the electroneutral mouse

NaPi-IIc [1]. The amphipathic nature of the α-helical segment of TMD-3 and the effect of mutagenesis on polar or charged amino acids clustering on one side of the helix indicate that this region participates in forming a binding site for a sodium ion and is critical for establishing the 3:1 Na^+:P_i stoichiometry required for electrogenic Na^+-coupled P_i cotransport.

ACKNOWLEDGEMENTS

This work was supported by grants from the Swiss National Science Foundation, the Gebert Rüf Stiftung, the Hartmann-Müller Stiftung (Zürich), the Fridericus Stiftung (Vaduz), the Olga Mayenfish-Stiftung (Zürich) and the Union Bank of Switzerland.

REFERENCES

1. Bacconi, A., Virkki, L.V., Biber, J., Murer, H., Forster, I.C. 2005. Renouncing electrogenicity is not free of charge: switching on electrogenicity in a Na^+-coupled phosphate cotransporter. *Proc. Natl. Acad. Sci. U. S. A.* **submitted**

2. Ehnes, C., Forster, I.C., Bacconi, A., Kohler, K., Biber, J., Murer, H. 2004. Structure-function relations of the first and fourth extracellular linkers of the type IIa Na^+/P_i cotransporter: II. Substrate interaction and voltage dependency of two functionally important sites. *J. Gen. Physiol.* **124:**489-503

3. Ehnes, C., Forster, I.C., Kohler, K., Bacconi, A., Stange, G., Biber, J., Murer, H. 2004. Structure-function relations of the first and fourth predicted extracellular linkers of the type IIa Na^+/Pi cotransporter: I. Cysteine scanning mutagenesis. *J. Gen. Physiol.* **124:**475-88

4. Feild, J.A., Zhang, L., Brun, K.A., Brooks, D.P., Edwards, R.M. 1999. Cloning and functional characterization of a sodium-dependent phosphate transporter expressed in human lung and small intestine. *Biochem. Biophys. Res. Commun.* **258:**578-82

5. Forster, I., Hernando, N., Biber, J., Murer, H. 1998. The voltage dependence of a cloned mammalian renal type II Na^+/P_i cotransporter (NaPi-2). *J. Gen. Physiol.* **112:**1-18

6. Forster, I.C., Kohler, K., Biber, J., Murer, H. 2002. Forging the link between structure and function of electrogenic cotransporters: the renal type IIa Na^+/P_i cotransporter as a case study. *Prog. Biophys. Mol. Biol.* **80:**69-108

7. Forster, I.C., Loo, D.D., Eskandari, S. 1999. Stoichiometry and Na^+ binding cooperativity of rat and flounder renal type II Na^+-P_i cotransporters. *Am. J. Physiol.* **276:**F644-9

8. Hayes, G., Busch, A., Lotscher, M., Waldegger, S., Lang, F., Verrey, F., Biber, J., Murer, H. 1994. Role of N-linked glycosylation in rat renal Na/Pi-cotransport. *J. Biol. Chem.* **269:**24143-9

9. Hilfiker, H., Hattenhauer, O., Traebert, M., Forster, I., Murer, H., Biber, J. 1998. Characterization of a murine type II sodium-phosphate cotransporter expressed in mammalian small intestine. *Proc. Natl. Acad. Sci. U. S. A.* **95:**14564-9

10. Kohler, K., Forster, I.C., Stange, G., Biber, J., Murer, H. 2002. Identification of functionally important sites in the first intracellular loop of the NaPi-IIa cotransporter. *Am. J. Physiol.* **282:**F687-96

11. Kohler, K., Forster, I.C., Stange, G., Biber, J., Murer, H. 2002. Transport function of the renal type IIa Na^+/P_i cotransporter is codetermined by residues in two opposing linker regions. *J. Gen. Physiol.* **120:**693-703

12. Kohler, K., Forster, I.C., Stange, G., Biber, J., Murer, H. 2003. Essential cysteine residues of the type IIa Na^+/P_i cotransporter. *Pflugers Arch.* **446:**203-10

13. Lambert, G., Forster, I.C., Biber, J., Murer, H. 2000. Cysteine residues and the structure of the rat renal proximal tubular type II sodium phosphate cotransporter (rat NaPi IIa). *J. Membr. Biol.* **176:**133-41

14. Lambert, G., Forster, I.C., Stange, G., Biber, J., Murer, H. 1999. Properties of the mutant Ser-460-Cys implicate this site in a functionally important region of the type IIa Na^+/P_i cotransporter protein. *J. Gen. Physiol.* **114:**637-52

15. Lambert, G., Forster, I.C., Stange, G., Kohler, K., Biber, J., Murer, H. 2001. Cysteine mutagenesis reveals novel structure-function features within the predicted third extracellular loop of the type IIa Na^+/P_i cotransporter. *J. Gen. Physiol.* **117:**533-46

16. Lambert, G., Traebert, M., Hernando, N., Biber, J., Murer, H. 1999. Studies on the topology of the renal type II NaPi-cotransporter. *Pflugers Arch.* **437:**972-8

17. Murer, H., Forster, I., Biber, J. 2004. The sodium phosphate cotransporter family SLC34. *Pflugers Arch.* **447:**763-7

18. Murer, H., Hernando, N., Forster, I., Biber, J. 2000. Proximal tubular phosphate reabsorption: molecular mechanisms. *Physiol. Rev.* **80:**1373-409

19. Nayal, M., Di Cera, E. 1994. Predicting Ca^{2+}-binding sites in proteins. *Proc. Natl. Acad. Sci. U. S. A.* **91:**817-21

20. Ogawa, H., Toyoshima, C. 2002. Homology modeling of the cation binding sites of $Na^{+}K^{+}$-ATPase. *Proc. Natl. Acad. Sci. U. S. A.* **99:**15977-15982

21. Ohkido, I., Segawa, H., Yanagida, R., Nakamura, M., Miyamoto, K. 2003. Cloning, gene structure and dietary regulation of the type-IIc Na/Pi cotransporter in the mouse kidney. *Pflugers Arch.* **446:**106-15

22. Segawa, H., Kaneko, I., Takahashi, A., Kuwahata, M., Ito, M., Ohkido, I., Tatsumi, S., Miyamoto, K. 2002. Growth-related renal type II Na/Pi cotransporter. *J. Biol. Chem.* **277:**19665-72

23. Tenenhouse, H.S., Murer, H. 2003. Disorders of renal tubular phosphate transport. *J. Am. Soc. Nephrol.* **14:**240-8

24. Toyoshima, C., Nakasako, M., Nomura, H., Ogawa, H. 2000. Crystal structure of the calcium pump of sarcoplasmic reticulum at 2.6 A resolution. *Nature* **405:**647-55

25. Virkki, L.V., Forster, I.C., Biber, J., Murer, H. 2005. Substrate interactions in the human type IIa sodium-phosphate cotransporter (NaPi-IIa). *Am. J. Physiol.* **in press**

26. Virkki, L.V., Forster, I.C., Hernando, N., Biber, J., Murer, H. 2003. Functional characterization of two naturally occurring mutations in the human sodium-phosphate cotransporter type IIa. *J. Bone Miner. Res.* **18:**2135-41

27. Werner, A., Biber, J., Forgo, J., Palacin, M., Murer, H. 1990. Expression of renal transport systems for inorganic phosphate and sulfate in *Xenopus laevis* oocytes. *J. Biol. Chem.* **265:**12331-6

FIGURE LEGENDS

Figure 1. Topology and sequence alignment. A. Topology model of human NaPi-IIa contains eight putative transmembrane segments and intracellular N and C termini. Open squares indicate residues in the extracellular and intracellular linker regions (ECL and ICL, respectively) that were mutated in previous cysteine scanning accessibility studies [2, 3, 10, 15]. Of these, Asn-199, which is postulated to interact with sites in TMD-3, is indicated with a grey sqare. Residues mutated to cysteines in TMD-3 (this study) are indicated by a letter corresponding to the amino acid in a white circle. The native Cys-225 (denoted by a diamond) was changed to Ser. B. Alignment of the amino acid sequence in TMD-3 of human NaPi-IIa, IIb and IIc. Non-conserved residues are indicated by black lettering on white background. C. Helical wheel analysis of TMD-3 in NaPi-IIa. Charged residues are indicated by white lettering in a black oval and polar residues by black lettering inside a white oval.

Figure 2. Characterization of the C225S mutant. A. P_i dose-response. The P_i-induced current was plotted as a function of P_i concentration. Closed circles WT, open circles C225S. The data were fitted with Eq. 1, yielding the following fit parameters: for WT K_mP_i = 0.094 ±0.02 mM, $I_{Pi,\ max}$ = 95 ±6 nA, for C225S K_mP_i = 0.047 ±0.02, $I_{Pi,\ max}$ 44±4 nA, n=10. B. Na^+ dose-response. The P_i-induced current was plotted as a function of the Na^+ concentration. Closed squares WT, open squares C225S. The data was fitted with Eq. 1, yielding for the WT K_mNa = 34 ±5 mM, *H* = 2.8 ±0.9, $I_{Pi,\ max}$ = 94 ±11 nA, for C225S K_mNa = 30 ±7 mM, *H* = 2.3 ±1, $I_{Pi,\ max}$ = 44 ±7 nA, n=5. C. Current-voltage relationship. Current recordings were acquired in ND100 solution in the presence or absence of 1 mM P_i, and subtracted to obtain the P_i-dependent current, which was plotted as a function of voltage. Closed diamonds WT, open diamonds C225S, closed triangles control oocytes. n=5-7.

Figure 3. P_i transport and Western analysis. A. P_i uptake in oocytes expressing WT and mutant NaPi-IIa. P_i uptake was measured using $^{32}P_i$ as a tracer. For clarity, WT is denoted

with a white bar, C225S with a black bar, and other mutants with grey bars. The dashed line denotes P_i transport mediated by C225S, and dotted line 50% of this. Asterisk * denotes statistically significant difference from control ($p<0.05$). B. Western blot. Whole-cell lysates from oocytes expressing WT or mutant NaPi-IIa were probed with a NaPi-IIa-specific C-terminal antibody. The sizes of the molecular weight markers are indicated in the figure. The figure is a composition of four separate blots. C. Apparent K_mP_i of WT and mutant NaPi-IIa. WT open square, C225S open circle, other mutants black circles. Grey bar indicates 95% confidence interval for K_mP_i of C225S. n=3-10. D. Effect of MTSEA. Continuous current tracings are shown for oocytes expressing C225S (top) or A240C-C225S (bottom) before (left) or after (right) MTSEA treatment (1 mM for 5 min). The recordings were started in ND100 soution, followed by application of 1 mM P_i (indicated by a black line). The Pi-dependet current was determined before and after MTSEA application for each oocyte. MTSEA treatment reduced the Pi-induced current by ~50% in A240C-C225S-expressing oocytes, but not in any other mutants tested.

Figure 4. Mutants at Asp-224. A. P_i uptake. P_i uptake, using $^{32}P_i$ as a tracer, was measured in control oocytes and oocytes expressing mutant engineered at D224 in NaPi-IIa. Asterisk * denotes statistically significant difference from control ($p<0.05$). B. Western blot. Whole-cell lysates from oocytes expressing WT or mutant NaPi-IIa was probed with a NaPi-IIa-specific antibody. The sizes of the molecular weight markers are indicated in the figure. C. Current-voltage relationships. P_i-induced currents were plotted against membrane potential in control oocytes and oocytes expressing WT or mutant NaPi-IIa. Closed circles WT, open circles D224E, open squares D224N, open triangles D224G, closed triangles control.

Figure 5. Voltage-dependency of P_i-induced currents in D224E. A. P_i dose-response in oocytes expressing WT NaPi-IIa. Currents were acquired before and after application of P_i and the P_i-dependent current was plotted as a function of the membrane potential. Circles 1

mM P_i, diamonds 0.3 mM P_i, inverted triangles 0.1 mM P_i, triangles 0.03 mM, squares 0.01 mM P_i. B. P_i dose-response in oocytes expressing D224E. Symbols are as in A. C. Voltage-dependency of K_mP_i. Data in panels A and B were fitted with Eq. 1 and the resulting K_m-values were plotted as a function of voltage. Filled circles WT, open circles D224E. D. Na^+ dose-response in oocytes expressing WT NaPi-IIa. Currents were acquired before and after application of 1 mM P_i at each Na^+ concentration and the P_i-dependent current was plotted as a function of the membrane potential. Open squares 100 mM Na^+, circles 75 mM Na^+, diamonds 50 mM Na^+, inverted triangles 25 mM Na^+, triangles 10 mM Na^+, squares 0 mM Na^+. E. Na^+ dose-response in oocytes expressing D224E. Symbols are as in D. F. Voltage-dependency of K_mNa. Data in panels D and E were fitted with Eq. 1 and the resulting K_m-values were plotted as a function of voltage. Filled squares WT, open squares D224E.

Figure 6. Transport characteristics by D224G. A. Na^+-dependency of P_i uptake. P_i uptake was measured using $^{32}P_i$ as a tracer, in the presence or absence of Na^+ in control oocytes and oocytes expressing WT or the D224G mutant. Asterisk * denotes statistically significant difference from control ($p<0.05$). B. Dual uptake of Na^+ and P_i. Simultaneous uptake of Na^+ and P_i (measured using ^{22}Na and $^{32}P_i$ as tracers) in control oocytes (closed circles), and in oocytes expressing WT (closed triangles) or D224G (open circles) NaPi-IIa. Inset shows Na^+ uptake data for oocytes in the same batch in the absence of P_i. The data were fitted with a regression line (straight lines in graph) with a slope of 2.7 ±0.04 for WT and 10 ±0.8 for D224G. The lines were forced to go through the mean values obtained for control oocytes.

Figure 7. Mutants at Asn-227. A. P_i uptake. P_i uptake, using $^{32}P_i$ as a tracer, was measured in control oocytes and oocytes expressing mutant engineered at N227 in NaPi-IIa. Asterisk * denotes statistically significant difference from control ($p<0.05$). B. Western blot. Whole-cell lysates from oocytes expressing WT or mutant NaPi-IIa were probed with a NaPi-IIa-specific antibody. The size of the molecular weight markers is indicated in the figure. C. Current-

voltage relationships. P_i-induced currents were plotted against membrane potential in control oocytes and oocytes expressing WT or mutant NaPi-IIa. Closed circles WT, open circles N227Q, open triangles N227D, closed triangles control. D. K_mP_i of N227Q. Currents were acquired continuously at a holding potential of -50 mV. The current deflections induced by P_i application were plotted as a function of the P_i concentration as fitted with Eq 1. The data were normalized to $I_{Pi,\,max}$. K_mP_i for WT was 0.096 ±0.011 mM, for N227Q 4.2 ±1.7 mM. n=6. E. K_mNa of N227Q. The current deflections induced by 3 mM P_i at different Na^+ concentrations was plotted as a function of the Na^+ concentration as fitted with Eq 1. For the WT, K_mNa = 37 ±14, $I_{Pi,\,max}$ 100 ±20, H = 1.6 ±0.6. For N227Q, a reliable fit of Eq 1 to the data was prevented by the lack of saturation, but indicates a K_mNa of >100 mM. n=4-5.

Figure 1

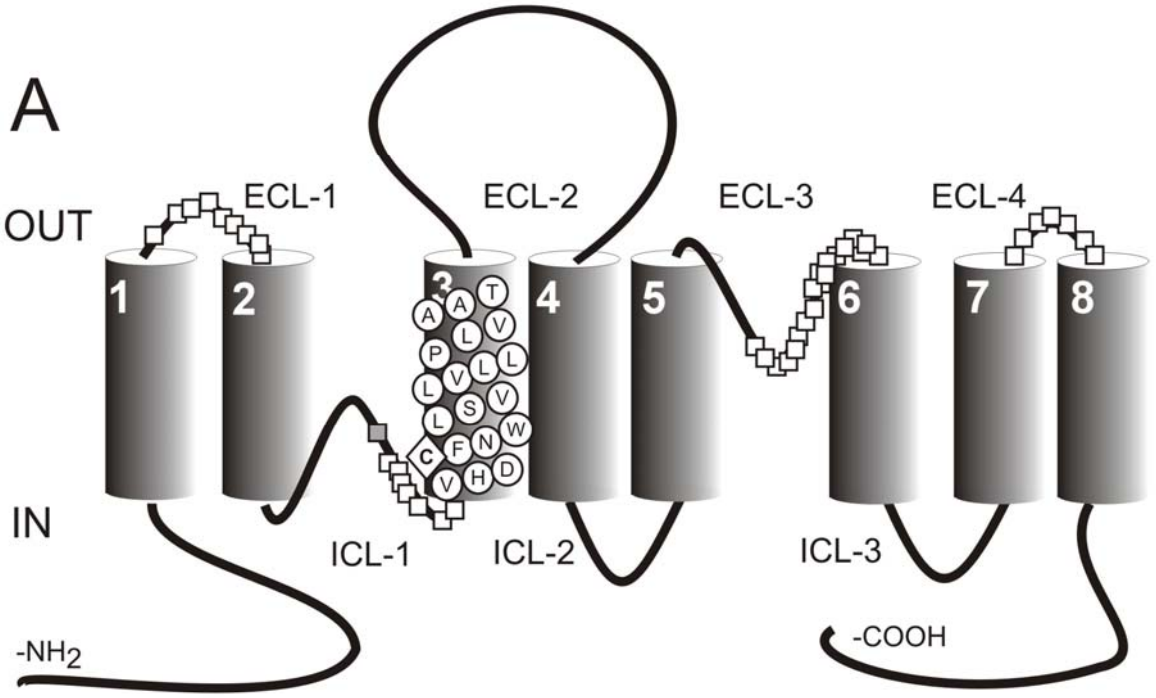
A
OUT
IN
ECL-1
ECL-2
ECL-3
ECL-4
1
2
3
4
5
6
7
8
ICL-1
ICL-2
ICL-3
-NH2
-COOH


B
222
241
VHDCFNWLSVLVLLPLEAAT NaPi-IIa
VHDFFNWLSVLVLLPLEAAT NaPi-IIb
VHGIFNWLTVLVLLPLESAT NaPi-IIc

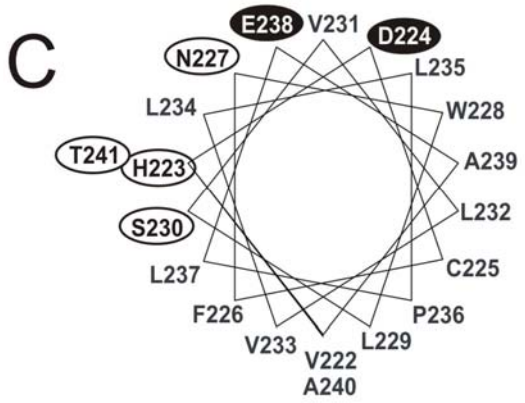
C
E238
V231
D224
N227
L235
L234
W228
T241
H223
A239
S230
L232
L237
C225
F226
P236
V233
L229
V222
A240

Figure 2

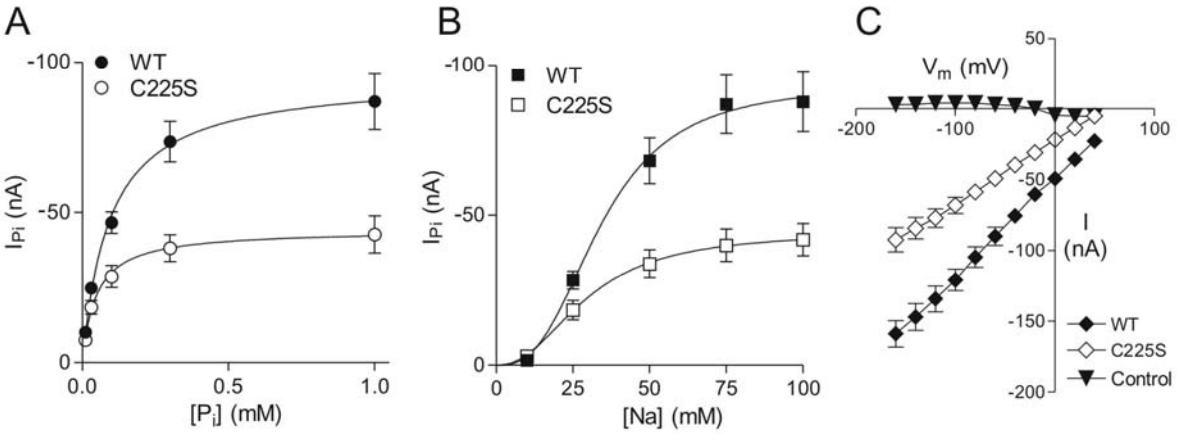
A
WT
C225S
-100
-50
0
I_{Pi} (nA)
0.0
0.5
1.0
[P_i] (mM)
B
WT
C225S
-100
-50
0
I_{Pi} (nA)
0
25
50
75
100
[Na] (mM)
C
V_m (mV)
50
-200
-100
100
-50
-100
-150
-200
I
(nA)
WT
C225S
Control

Figure 3

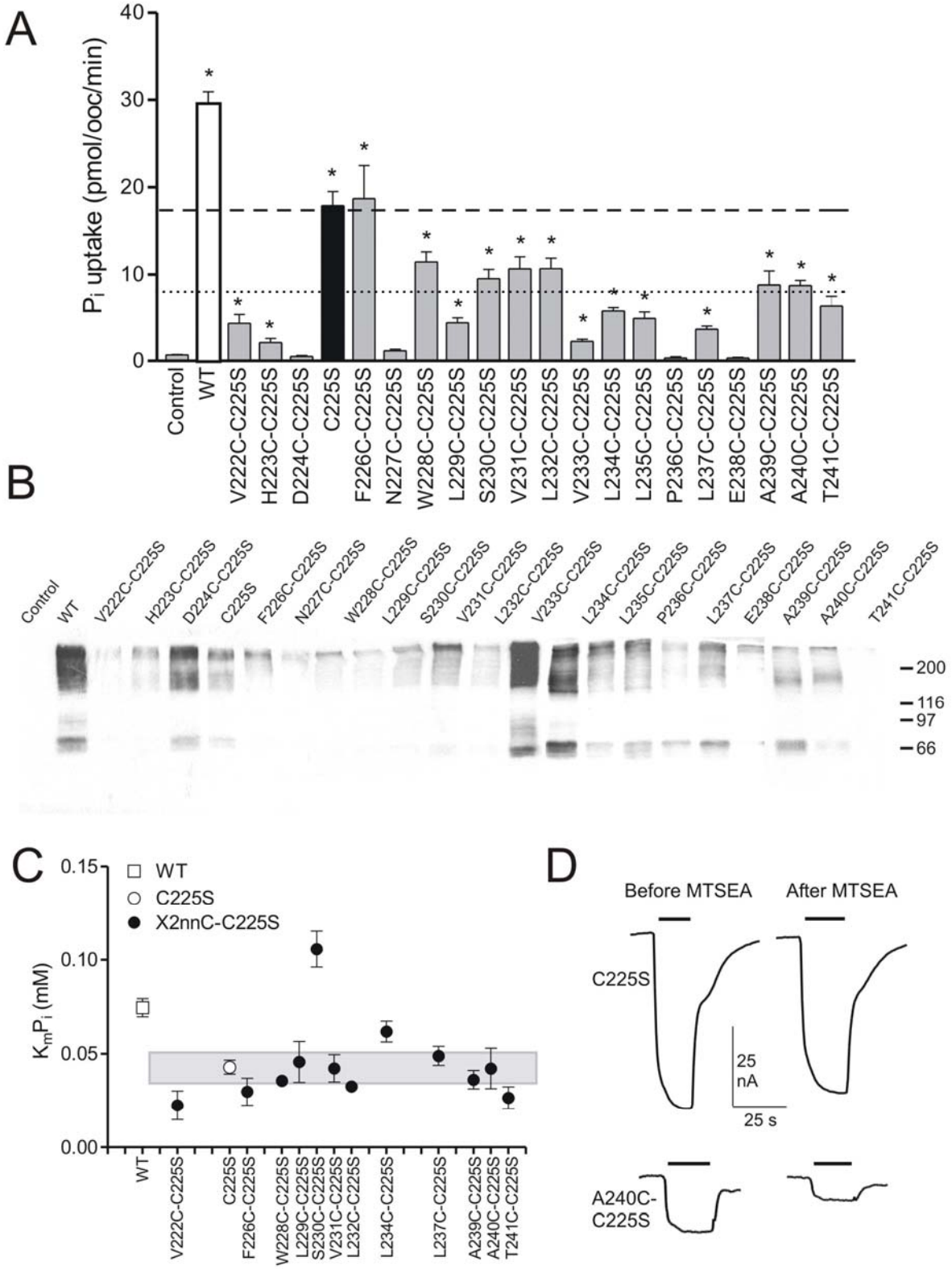
A
P_i uptake (pmol/ooc/min)
40
30
20
10
0
Control
WT
V222C-C225S
H223C-C225S
D224C-C225S
C225S
F226C-C225S
N227C-C225S
W228C-C225S
L229C-C225S
S230C-C225S
V231C-C225S
L232C-C225S
V233C-C225S
L234C-C225S
L235C-C225S
P236C-C225S
L237C-C225S
E238C-C225S
A239C-C225S
A240C-C225S
T241C-C225S
B
Control
WT
V222C-C225S
H223C-C225S
D224C-C225S
C225S
F226C-C225S
N227C-C225S
W228C-C225S
L229C-C225S
S230C-C225S
V231C-C225S
L232C-C225S
V233C-C225S
L234C-C225S
L235C-C225S
P236C-C225S
L237C-C225S
E238C-C225S
A239C-C225S
A240C-C225S
T241C-C225S
200
116
97
66
C
WT
C225S
X2nnC-C225S
K_mP_i (mM)
0.15
0.10
0.05
0.00
WT
V222C-C225S
C225S
F226C-C225S
W228C-C225S
L229C-C225S
S230C-C225S
V231C-C225S
L232C-C225S
L234C-C225S
L237C-C225S
A239C-C225S
A240C-C225S
T241C-C225S
D
Before MTSEA
After MTSEA
C225S
25 nA
25 s
A240C-C225S

Figure 4

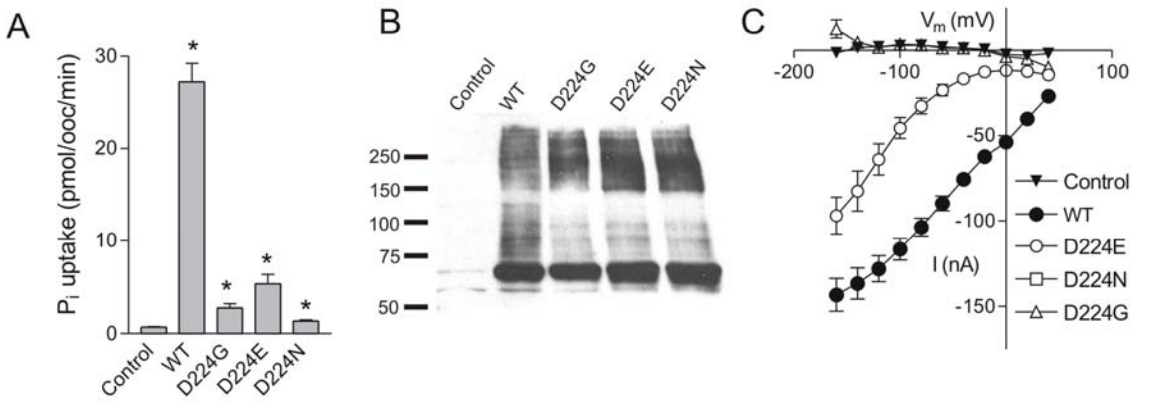
A
P_i uptake (pmol/ooc/min)
30
20
10
0
*
*
*
*
Control
WT
D224G
D224E
D224N
B
Control
WT
D224G
D224E
D224N
250
150
100
75
50
C
V_m (mV)
-200
-100
100
-50
-100
-150
I (nA)
Control
WT
D224E
D224N
D224G

Figure 5

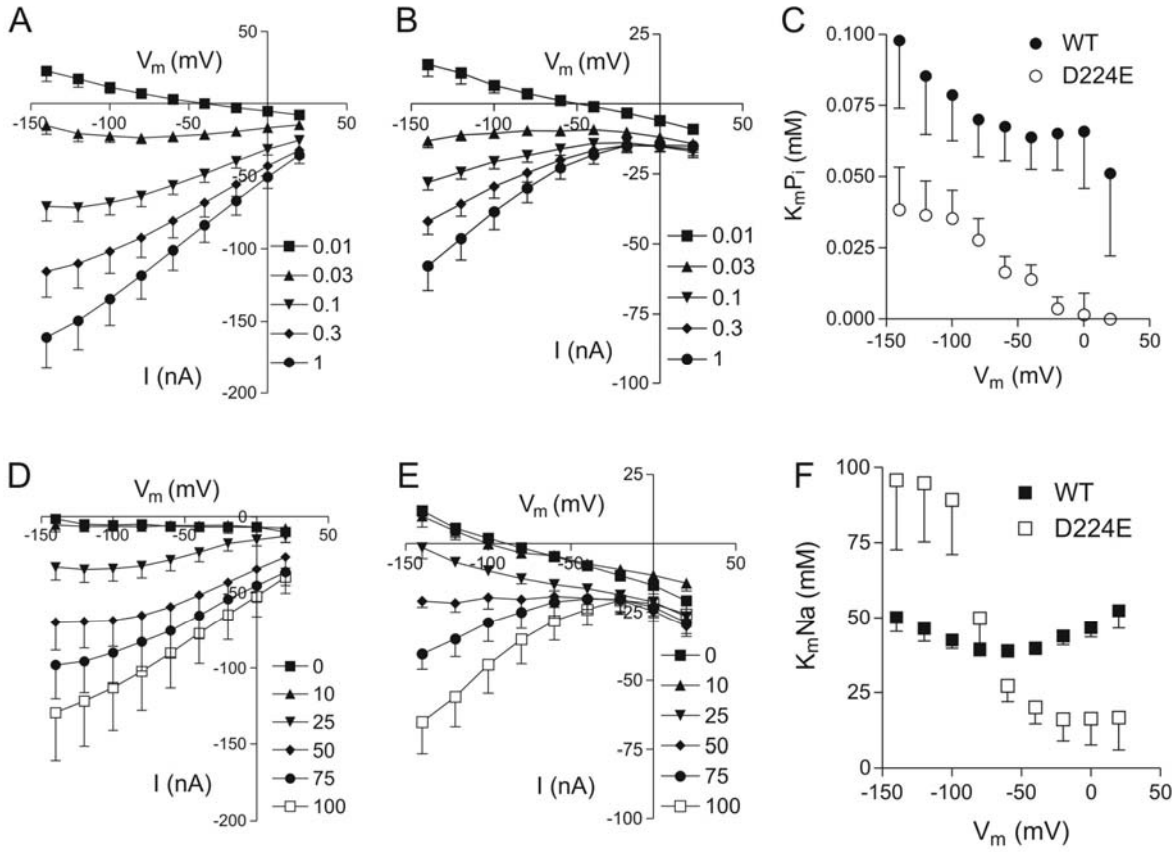
A
Vm (mV)
I (nA)
0.01
0.03
0.1
0.3
1
B
Vm (mV)
I (nA)
0.01
0.03
0.1
0.3
1
C
WT
D224E
KmPi (mM)
Vm (mV)
D
Vm (mV)
I (nA)
0
10
25
50
75
100
E
Vm (mV)
I (nA)
0
10
25
50
75
100
F
WT
D224E
KmNa (mM)
Vm (mV)

Figure 6

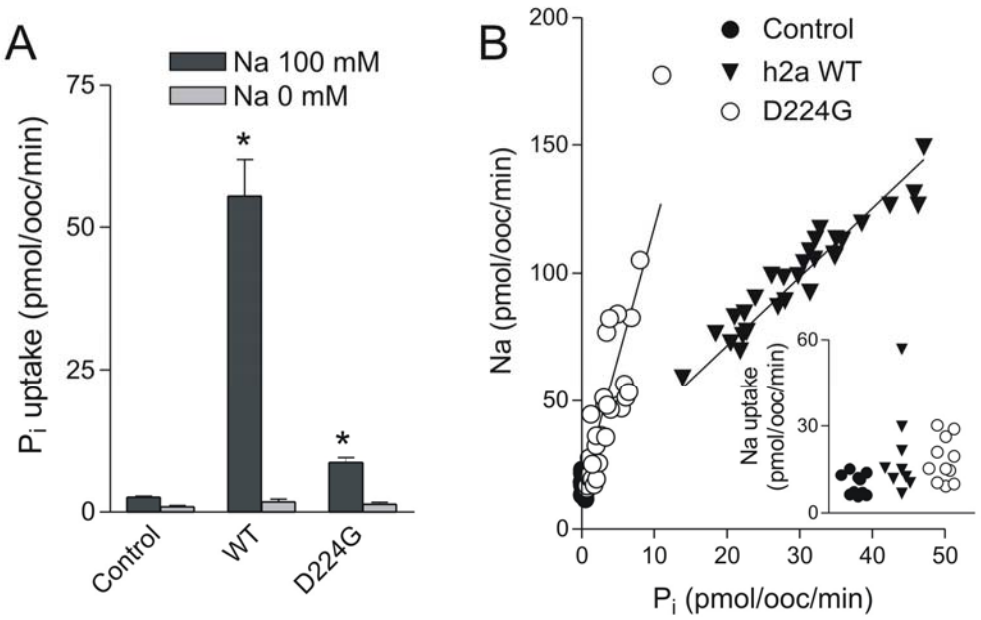
A
Na 100 mM
Na 0 mM
P_i uptake (pmol/ooc/min)
75
50
25
0
*
*
Control
WT
D224G
B
Control
h2a WT
D224G
Na (pmol/ooc/min)
200
150
100
50
0
Na uptake (pmol/ooc/min)
60
30
0
0
10
20
30
40
50
P_i (pmol/ooc/min)

Figure 7

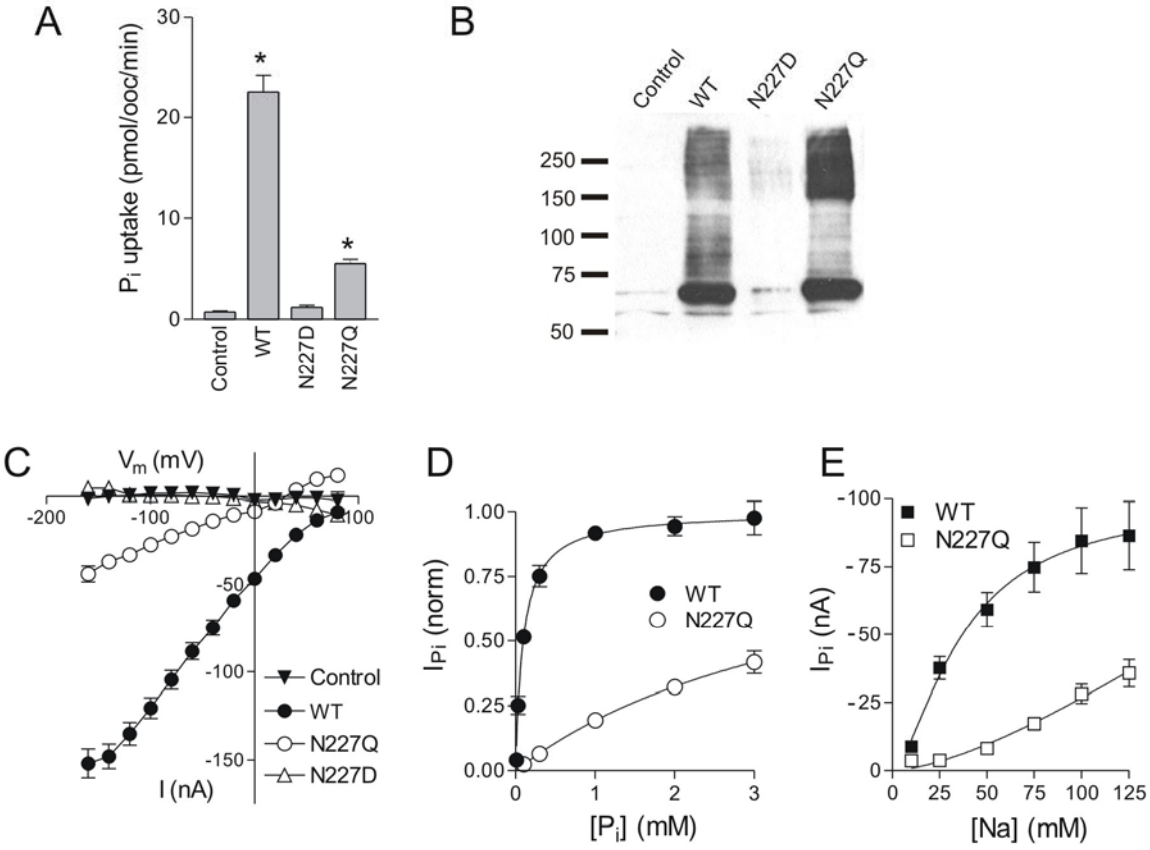
A
P_i uptake (pmol/ooc/min)
30
20
10
0
*
*
Control
WT
N227D
N227Q
B
Control
WT
N227D
N227Q
250
150
100
75
50
C
V_m (mV)
-200
-100
100
-50
-100
-150
I (nA)
Control
WT
N227Q
N227D
D
I_{Pi} (norm)
1.00
0.75
0.50
0.25
0.00
0
1
2
3
$[P_i]$ (mM)
WT
N227Q
E
I_{Pi} (nA)
-100
-75
-50
-25
0
0
25
50
75
100
125
[Na] (mM)
WT
N227Q

3.5 Summary of publication:

Temperature-dependent kinetics of the cotransport and leak modes of the flounder type IIb Na^+/P_i cotransporter.

Temperatur-abhängige Kinetik des Cotransporter- und Leck-Moduses des Typ IIb Na^+/P_i Cotransporters der Flunder

Die temperatur-abhängige Cotransporter-Kinetik und der Leckstrom-Modus des Na^+-gekoppelten P_i Cotransporters (NaPi-IIb) der Flunder wurde im ‚steady-state' bestimmt. Der Cotransporter-Modus wurde mithilfe von Pi-induzierten Änderungen im Haltestrom bei gesättigter P_i-Konzentration (1mM) untersucht. Um den Leckstrom-Modus zu untersuchen, wurde der Haltestrom mit 1 mM Phosphonoameisensäure (PFA) bei Abwesenheit von P_i unterdrückt. Die Transportuntersuchungen wurden mit Hilfe der Elektrophysiologie, genauer mit der ‚two-electrode voltage clamp'-Methode für Temperaturen im Bereich von 5-20°C durchgeführt. Die Abnahme der Temperatur führte zu einer signifikanten Reduktion des P_i- und PFA-induzierten Stroms. Die Arrhenius Darstellung lieferte Schätzungen von ~ 17 kcal M^{-1} für die Aktivierungsenergie bei -100mV für den Cotransporter-Modus verglichen mit 11 kcal M^{-1} für den Leckstrom-Modus. Um die kinetischen Übergänge, die diese Temperaturabhängigkeit vermitteln, zu bestimmen, wurden ‚presteady state' Ströme bei unterschiedlichen Temperaturen bei An- und Abwesenheit von externem Na^+ in 0mM P_i gemessen. Das Einfuegen dieser Daten zu einer einzelnen Bolzmann Funktion laesst vermuten, dass die beobachteten Effekte der Cotransporter-Kinetik durch die Temperatur-abhängige Veränderung der Kinetik des leeren Carriers und die Interaktion des ersten Na^+-Ions mit dem Protein erklärt werden könnten. Diese Resultate bestätigen, dass die Temperaturabhängigkeit des Cotransporter-Moduses mit dem von anderen Carrier Proteinen übereinstimmt. Ausserdem scheint es, dass der Leckstrom-Modus des elektrogenen Typ II Na^+/P_i Cotransporters durch die Reorientierung des leeren Carriers und die Interaktion des ersten Na^+-Ions aktiviert wird, was eher mit einem Uniport- als mit einem Kanal-Mechanismus übereinstimmt.

Temperature-dependent kinetics of the cotransport and leak modes of the flounder type IIb Na^+/P_i cotransporter.

Andrea Bacconi, Heini Murer and Ian C. Forster*,

Institute of Physiology and Center for Integrative Human Physiology (CIHP), University of Zurich, Winterthurerstrasse 190,CH-8057, Zurich, Switzerland

Running title: Temperature dependency of NaPi-IIb kinetics

* Corresponding author: Ian C. Forster, PhD
Institute of Physiology, University of Zurich,
Winterthurerstrasse 190, CH-8057, Zurich, Switzerland
Tel: +41 44 635 5059
Fax: +41 44 635 5025
Email: IForster@access.unizh.ch

Abstract

The temperature dependent kinetics of cotransport and leak modes of the flounder Na^+-coupled P_i cotransporter (NaPi-IIb) were determined in the steady-state. The cotransport mode was assayed from P_i-induced change in holding current for saturating P_i (1 mM). The leak mode was assayed as the current suppressed by 1 mM phosphonoformic acid (PFA) in the absence of P_i. Transport assays were performed by electrophysiology using the two-electrode voltage clamp for temperatures in the range 5-20 ^oC. Decreasing the temperature resulted in a significant reduction in the P_i and PFA-induced currents. Arrhenius plots gave estimates of the activation energy at -100 mV for the cotransport mode as ~ 17 kcal M^{-1} compared with 11 kcal M^{-1} for the leak mode. To identify kinetic transitions involved in conferring the temperature dependency, presteady state currents were recorded at different temperatures in the presence and absence of external Na^+ in 0 mM P_i. Fitting these data to a single Boltzmann function suggested that a temperature dependent alteration in the empty carrier kinetics and interaction of the first Na^+ ion with the protein could account for the observed effects on cotransport kinetics. These findings confirm that the temperature dependency of the cotransport mode is consistent with other carrier proteins. Moreover, the leak mode in electrogenic type II Na^+/P_i cotransporters appears to be activated by the reorientation of the empty carrier and first Na^+ ion interaction, consistent with a uniport rather than channel mechanism.

Keywords: P_i cotransport, uncoupled leak, temperature, presteady-state

Introduction

Secondary active transporters are membrane proteins that mediate the uphill movement of a specific solute by coupling to the downhill movement of a specific ion, (e.g. H^+, K^+ or Na^+) according to the free energy associated with the driving ion's own electrochemical gradient. The coupling confers a strict stoichiometric ratio between the driven and driving species. Moreover, the maximum transport rate is determined by rate limiting transitions in the cotransport cycle that, in general, are determined by either extrinsic (e.g. substrate concentration, membrane potential) or intrinsic factors (e.g. rates of reorientation of fully loaded or empty carrier). This contrasts with the behaviour of ion channels which, when in the conducting or open state, exhibit rates of movement of the transported ions that are up to 3 orders of magnitude faster than for carriers that can be attributed to electrodiffusive movement of the solute through the pore region. The kinetic and molecular models proposed to account for the functional data also reflect these differences between carriers and channels. Furthermore, the activation energy for movement of an ion through a channel is much less than that associated with the transport cycle of a carrier (van Winkle, 1999). This observation reflects the thermodynamic distinction between channels and transporters, which relates to the greater apparent complexity in the conformational changes involved in the translocation process in the latter case, where ordered substrate binding/debinding and alternating accessibility of substrates to their respective binding sites are common features of their transport kinetics. Recently, the distinction between carriers and channels has become less clear following a number of studies on cotransporters that have identified leak modes in the absence of substrate, and which exhibit channel-like properties (e.g. (Defelice, 2004; Kavanaugh, 1998; Sonders and Amara, 1996)). Moreover evidence has emerged from functional studies on a bacterial homolog of the ClC channel that a mutation can switch the mode of operation from that of an antiporter with strict stoichiometric coupling to the characteristic ClC channel mode (Accardi and Miller, 2004).

The distinction between carrier and leak modes can be experimentally demonstrated by determining their temperature dependency, based on the assumption that the activation energy of translocating solutes according to a carrier mechanism is significantly greater than that associated with

electrodiffusion for a channel (e.g. (van Winkle, 1999)). For example studies on a serotonin transporter (5HT) (Beckman and Quick, 2001) and the GABA transporter GAT4 (Karakossian et al., 2005) reported significantly different temperature coefficients for the cotransport and leak modes.

Electrogenic type II Na^+-coupled P_i cotransporters that belong to the SLC34 family **(**e.g: http://www.bioparadigms.org**)** also exhibit both a strict stoichiometrically coupled cotransport mode behaviour (Forster et al., 1999; Virkki et al., 2005) as well as leak-mode behaviour (reviewed in (Forster et al., 2002)). A Na^+-dependent leak mode for the rat NaPi-IIa cotransporter was proposed from the finding that the P_i transport inhibitor phosphonoformic acid (foscarnet or PFA) applied in the absence of P_i to NaPi-IIa-expressing *Xenopus* oocytes under voltage clamp conditions led to decrease in the holding current (Forster et al., 1998). The magnitude of the PFA-dependent suppression was proportional to the cotransport mode activity, which suggested a direct association of this pathway with functional expression of the cotransporter. Moreover, its reversal potential was shifted in a Nernstian manner according to the external Na^+ concentration. Subsequently, the NaPi-IIa Na^+-leak mode was incorporated into a kinetic scheme (Forster et al., 1998) as a "uniporter" pathway, similar to that proposed for other Na^+-driven cotransporters (e.g. the sodium glucose cotransporter (SGLT-1), (Chen et al., 1997; Parent et al., 1992); the thyroid Na^+/I^- cotransporter (NIS) (Eskandari et al., 1997) and the Na^+-dependent dicarboxylate cotransporter (Yao and Pajor, 2000)**.** This scheme (Figure 5) predicts that the leak and cotransport modes are mutually exclusive, but share the same empty carrier and Na^+ binding transitions. Studies involving both wild-type (WT) and mutant NaPi-IIa constructs (Kohler et al., 2002a; Kohler et al., 2002b; Virkki et al., 2005) also provided experimental evidence in supported of this idea. Nevertheless, the reversal potential of the PFA-sensitive current lies far to the left of what would be predicted if Na^+ were the only ion involved (typically -20 mV with external 100 mM Na^+) and this observation therefore suggests that the PFA-sensitive current is more complex than originally proposed. Moreover, recent observations (Bacconi, Virkii and Forster, unpublished results) indicate that Cl^- ions may also be involved, adding weight to the concept proposed for excitatory amino acid cotransporters (e.g (Wadiche

and Kavanaugh, 1998) that an independent, substrate gated, channel-like pathway could also be involved.

To gain further insight into the mecahanism of the NaPi-II cotransport and leak modes, we have taken a thermodynamic approach to determine the temperature dependencies of the respective transport rates. We used the type IIb Na^+/P_i cotransporter cloned from flounder (fl-NaPi-IIb) because of the 5-10-fold higher electrogenic activity when expressed in *Xenopus* oocytes (Werner et al., 1994) compared with its mammalian cousin. NaPi-IIb from flounder has been shown previously to exhibit leak and cotransport modes (Forster et al., 2000) and displays similar kinetic features associated with the mammalian NaPi-IIa ((Forster et al., 1999; Forster et al., 2000; Forster et al., 1997) and therefore the findings should be applicable to mammalian members of the SLC34 family.

Materials and methods

Reagents and solutions

All reagents were obtained from Sigma or Fluka (Switzerland).

Solutions:

i. Oocyte incubation (modified Barth's solution) (in mM): NaCl (88); KCl (1); $CaCl_2$(0.41); $MgSO_4$(0.82); $NaHCO_3$ (2.5); $Ca(NO_3)_2$(0.33); HEPES (7.5); adjusted to pH 7.6 with TRIS and supplemented with antibiotics (10 mg/l gentomycin, streptomycin).
ii. Control superfusate (ND100) (in mM): NaCl (100); KCl (2); $CaCl_2$(1.8); $MgCl_2$(1); HEPES (5) and adjusted to pH 7.4 with TRIS.
iii. Control superfusate (ND0): as for ND100, but with N-methyl*d*-glucamine or choline chloride used to replace Na^+. Solutions were adjusted to pH 7.4 with HCl or KOH as required.
iv. Substrate test solutions: inorganic phosphate (P_i) was added to ND100 from 1 M K_2HPO_4 and KH_2PO_4stocks that were mixed to give the required pH (7.4).

Molecular biology and expression in Xenopus laevis oocytes

The procedures for oocyte preparation and cRNA injection have been described in details elsewhere (Werner et al., 1990). Oocytes were 50 nl of water containing 10 ng cRNA. Oocytes were incubated in modified Barth's solution and the experiments performed 3–4 days after injection. All pooled data were generated with oocytes from at least two different donor frogs.

Electrophysiology

The standard two-electrode voltage-clamp technique was used as previously described (Forster et al., 1998). The voltage clamp was a laboratory-built system with membrane current measured using a virtual ground bath electrode and with active series resistance compensation to reduce clamp errors. Oocytes were mounted in a small recording chamber (100 μl volume) and continuously superfused (5 ml/min) with test solutions precooled to 5°C. Data were acquired online using Digidata 1200 hardware and compatible pClamp8 software (Axon instruments, Union City, Calif., USA). Currents were prefiltered at a bandwidth

less than twice the sampling rate (typical sampling rate=50 μs/point; 8-pole low-pass filtering at 500 Hz, 3 dB bandwidth).

Temperature control

Test solutions were precoled at ~5°C and continuously superfused (5 ml/min) in the recording chamber (100 μl volume) that was made from thermally conductive epoxy (Electrolube ER2074) attached to a heating cooling block. The block temperature was controlled by an external temperature regulated water bath. Oocyte temperature was monitored by an electronic thermometer immersed in the control superfusate solution of the test chamber

Presteady-state relaxations

Presteady-state relaxations were acquired using voltage steps from a holding potential V_h = –60 mV to test potentials in the range –180 mV to +80 mV. Typically, 4-fold signal averaging was used. Relaxations were quantified by fitting a decaying double exponential function using a fitting algorithm. To resolve the charge movement associated with the exogenous protein, the subtraction method of (Hazama et al., 1997) was employed; the fast component, assumed to represent the capacitive oocyte charging, was extrapolated to the step onset and subtracted from the total transient current. The slower component was numerically integrated the to give the charge (Q) attributable to the exogenous protein. The Q–V data were fitted with the Boltzmann relation:

$$Q = Q_{\mathrm{hyp}} + Q_{\mathrm{max}}/(1 + \exp(-ze(V - V_{0.5})/\mathrm{kT})), \quad (1)$$

where Q_{max} is the maximum charge translocated, Q_{hyp} is the steady-state charge at the hyperpolarizing limit and depends V_h, $V_{0.5}$ is the voltage at which the charge is distributed equally between each state, z is the apparent valency per cotransporter, e is the elementary charge, k is Boltzmann's constant, and T is the absolute temperature. This model lumps all mobile charges associated with a particular transition into one effective charged particle (of valency z) that moves across the whole transmembrane field in transition (and assuming sharp energy barriers).

The voltage dependence of the relaxation time constant (τ–V) obtained from the exponential fitting was further quantified by fitting an equation that incorporates the apparent inward and outward rates for this particle, given by:

$$\tau = 1/(\alpha \exp(-zeV/2kT) + \beta \exp(zeV/2kT)), \quad (2)$$

where α and ß are the inward and outward rates, respectively, at V = 0 and we assume the barrier is symmetrical within the transmembrane field. Eqs.1 and 2 were fit to the data by nonlinear regression analysis with Q_{hyp}, Q_{max}, z, $V_{0.5}$, α, and ß as free parameters, for T = 278, 283, 288, 293 K. All curve fitting using Eqs. 1–2 was performed using the nonlinear regression analysis algorithms in GraphPad Prism version 3.02/4.02 for Windows (GraphPad Software).

Results

Temperature dependency of steady-state currents induced by P_i and PFA

The steady-state P_i-dependent current was determined by subtracting the currents recorded in response to a series of voltage steps in the range -180 mV to +80 mV for superfusion in ND100 from the corresponding records for superfusion in ND100 + 1 mM P_i. Figure 1 shows representative current traces for an oocyte at 20 ^oC and at 15 ^oC. In the absence of P_i (ND100) presteady-state relaxations, superimposed on the oocyte capacitive charging transient were observed as previously reported for the flounder NaPi-IIb (Forster et al., 2000; Forster et al., 1997). These were suppressed in the presence of 1 mM P_i and the magnitude of the steady-state holding current at each potential was increased. At 15 ^oC, the relaxations became slower and the pulse length was increased as a precaution to ensure that a steady-state current was reached. As for 20 ^oC, the relaxations were suppressed with 1 mM P_i. Moreover, the steady-state P_i-dependent current (I_{P_i}) was significantly reduced at the lower temperature. Figure 1 B shows I-V data pooled from n = 4 oocytes, normalized to I_{P_i} at -100 mV at 20 ^oC, for a larger range of temperatures. Figure 1 C shows the corresponding data for the PFA-blockable current (I_{PFA}) for the same oocytes, normalized for each cell to I_{P_i} at -100 mV. These currents showed a reversal between -30 mV and -20 mV that appeared to be temperature independent. Determination of exact reversal potential was not possible because of the relatively small magnitude of I_{PFA} (currents in the range 10-15 nA at -100 mV).

The temperature dependency of the two currents was compared by replotting the I-V data in the form of an Arrhenius plot as illustrated in Figure 2. For I_{P_i}, the data were well fit by a linear regression line over a range of potentials from -180 mV to 0 mV (Figure 2 A). For I_{PFA}, the data were less reliable, particularly near the reversal potential. From the slopes of the Arrhenius plots, the activation energy for the P_i-and PFA-dependent currents was evaluated as shown in Figure 2 C. The activation energy (E_a) for I_{P_i} showed some variation with membrane potential but was larger than E_a for I_{PFA} for all potentials. The mean value of E_a for I_{P_i} of ~18 kcal M^{-1} would correspond to a 10 ^oC temperature coefficient (Q_{10}) of 3, which is typical for values reported in other

studies on cotransporter membrane proteins (e.g. (Beckman and Quick, 2001; Binda et al., 2002; Wadiche and Kavanaugh, 1998). For $-I_{PFA,}$, the activation energy would correspond to a Q_{10} ~2.

Temperature dependency of presteady-state relaxations

We next investigated the effect of temperature on the presteady-state relaxations that occur following a change in membrane voltage to identify which transitions might be involved in conferring the temperature dependency to the cotransport function. These assays were performed in the absence of P_i to restrict the number of distinct conformational state the transporter can occupy. Figure 3A shows representative presteady-state currents recorded from an oocyte superfused with ND100 at 4 temperatures. As the temperature was reduced, the NaPi-IIb related relaxations superimposed on the capacitive charging transient became slower and the initial amplitude also decreased. We quantified these data by fitting the total relaxation to a double exponential function to yield two time constants. The faster time constant remained in the range 0.7-0.8 ms over the whole temperature range and showed little voltage dependency. This represents the capacitive charging of the oocyte. The slower time constant showed both temperature and voltage dependency as illustrated in Figure 3 B (left panel). The voltage at which the time constant peaked remained relatively constant. In the absence of external Na^+ (ND0) presteady-state relaxations were also recorded and a qualitatively similar dependency on temperature was also documented as shown in Figure 3 B (right panel). For ND0 superfusion, the voltage at which the time constant peaked shifted in the hyperpolarizing direction as the temperature decreased.

Integration of the slower relaxations yielded an estimate of the charge moved for each voltage step from the holding potential to the corresponding target potiential. For superfusion in ND100 (Figure 3 C, left panel), there was a marked reduction in the amount of charge moved as the temperature decreased for depolarizing potentials, whereas in the hyperpolarizing region, the change was less noticeable. In contrast, for superfusion in ND0, the charge distribution changed in both the hyperpolarizing and depolarizing regions. To quantitate these changes, the Q-V data were fit with a single Boltzmann function (Eqn 1).

The temperature dependency of the Boltzmann fit parameters is shown

in Figure 4. The voltage at which 50% of the charge is moved ($V_{0.5}$) showed relatively little dependency on temperature for ND100 superfusion, whereas in ND0, there was ~100 mV shift in the charge distribution towards hyperpolarizing potentials (more negative $V_{0.5}$) as the temperature decreased. This also corresponded to the shift observed for the time constant (Figure 3 B). The shift is also clearly seen when the Q-V data of Figure 4 C are normalized to the predicted maximum charge (Q_{max}) and aligned so that all Q-V curves coincide at the depolarizing limit (Figure 4 B). The dependency of Q_{max} on temperature (Figure 4 C) showed relatively little variation in ND0, and in agreement with the Q-V data of Figure 4 C, there was an approximately 50% reduction in available charge in ND100. At 5 ^{o}C, the predicted Q_{max} in ND100 was similar to that in ND0. Finally, the apparent valency of the charge movements (z) was larger in ND100 compared to ND0 and in each case showed the opposite variation with temperature.

Finally, we expressed the temperature dependency of the presteady-state relaxation time constant in the form of an Arrhenius plot (Figure 4 D). The linear regression of these data for -100 mV gave an activation energy of 9.5 $\pm$ 1.2 kcal M^{-1} for ND100 and 8.6 $\pm$ 0.2 kcal M^{-1} for ND0. These values were not significantly different.

Discussion

This study represents the first report on the temperature dependency of the type II Na^+/P_i cotransport system expressed in *Xenopus* oocytes. In the steady state, the apparent activation energy for the cotransport mode was found to be significantly higher than that for the leak mode, as assayed using the Na^+/P_i contransport inhibitor, PFA. This might suggest the possibility of two distinct mechanisms responsible for these two modes. However, unlike other cotransport systems that have been similarly characterized, the temperature dependency of the NaPi-IIb leak mode is too large for it to be considered a simple ion channel conductance. This contrasts with the findings of other studies, for example, the serotonin transporter (Beckman and Quick, 2001) or the GABA transport GAT4 (Karakossian et al., 2005), where Q_{10} values close to unity were reported, consistent with an electrodiffusive process. From the steady-state data alone we are unable to exclude the possibility that there is a "channel" component of the leak pathway. The activation energy as determined from the Arrhenius plot represents an apparent estimate as if the two transport processes (leak or cotransport mode) were lumped into a single reaction obeying 1st order kinetics. In the case of NaPi-II, where a number of kinetic steps are involved, Ea estimates are average values. Nevertheless, the excellent fits obtained from the linear regression analysis, suggest that over the temperature range explored in this study, there are no reactions with significantly different temperature dependencies.

From the analysis of the presteady-state data we found that the relaxations in the presence and absence of external Na^+ showed significant temperature dependency. Of particular importance was the finding that the empty carrier (ND0 superfusion) showed little variation in the predicted Q_{max} from the Boltzmann fit with temperature, which contrasted with the finding of significant shift in the $V_{0.5}$ towards hyperpolarizing potentials as temperature was lowered. These findings indicate that temperature does not alter the total amount of mobile charge available, as would be expected, but more negative potentials are required to effect a reorientation of the empty carrier. According to the currently proposed mechanism for type II Na^+/P_i cotransporters (e.g. (Ehnes et al., 2004a; Ehnes et al., 2004b; Forster et al., 2000) for hyperpolarizing potentials, the empty carrier is distributed between outward and

inward facing conformations (corresponding to states 1 and 8, respectively in Figure 5), with hyperpolarization favoring state 1. Thus, according to our findings in the present study, the effect of lowering temperature is to increase the proportion of transporters that occupy an inward facing conformation in the absence of external Na^+. Thus, lowering temperature has a twofold effect on the empty carrier kinetics: it decreases the 0 voltage rate constants, thereby slowing the turnover rate of the transporter and alters the occupancy of the empty carrier by increasing the backward rate constant to favour an inward facing conformation (state 8, Figure 5). These predictions are supported by the fit parameters obtained by the τ –V data fitting for ND0 superfusion with Equation 2, the results of which are given in Table 1. Here it can be seen that both α and β (corresponding to the rate constants associated with the forward and backward transitions, respectively, of the empty carrier (Figure 5, transition 1-8) both decrease with decreasing temperature. Furthermore, with the exception of the values at 20 ^oC, where the fit of the model showed more uncertainty, the ratio α/β decreases with decreasing temperature, corresponding to the shift in the peak of the τ-V curve and the $V_{0.5}$ shift of the Q-V data.

The analysis of the temperature dependency of the fitted time constants in terms of an Arrhenius plot gave an activation energy for superfusion in ND0 or ND100 of approximately 8 kcal M^{-1}. Interestingly, this is slightly below the activation energy found for the PFA suppressed leak current (~11 kcal M^{-1}). This would suggest that the steady-state PFA-sensitive leak current and the presteady-state charge movements associated with the empty carrier and first Na^+ binding transition are related to the same mechanism, in accordance with our current kinetic scheme for electrogenic type IIa and IIb Na^+/P_i cotransporters (Figure 5). The difference of 3 kcal M^{-1} may reflect the interaction of PFA itself with the protein. The increase in activation energy associated with the cotransport mode of approximately 7 kcal M^{-1}, would then be a measure of the energetic cost incurred by the additional substrate interactions (P_i and Na^+ binding) required to fully load the carrier and translocate to the intracellular side. Our findings, however, cannot exclude the possibility that the leak current arises from a substrate gated channel, as has been proposed for excitatory amino acid transporters (e.g. (Wadiche and Kavanaugh, 1998)) and the high activation

energy we determined for the NaPi-IIb leak mode reflects the activation energy of the gating mechanism itself, i.e. the reorientation of the empty carrier (transition 8-1) and the subsequent binding of a Na^+ ion (transition 1-2).

In conclusion, this study has confirmed that the cotransport mode of the flounder type IIb Na^+/P_i cotransporter shows an apparent activation energy consistent with other carrier type membrane transporters. The study has enabled us to dissect the leak mode from the cotransport mode kinetics and our findings suggest that the activation of the leak mode follows the reorientation of the empty carrier and first Na^+-interaction transitions.

References

Accardi, A. and Miller, C. (2004) Secondary active transport mediated by a prokaryotic homologue of ClC Cl- channels. *Nature*, **427**, 803-807.

Beckman, M.L. and Quick, M.W. (2001) Substrates and temperature differentiate ion flux from serotonin flux in a serotonin transporter. *Neuropharmacology*, **40**, 526-535.

Binda, F., Bossi, E., Giovannardi, S., Forlani, G. and Peres, A. (2002) Temperature effects on the presteady-state and transport-associated currents of GABA cotransporter rGAT1. *FEBS Lett*, **512**, 303-307.

Chen, X.Z., Coady, M.J., Jalal, F., Wallendorff, B. and Lapointe, J.Y. (1997) Sodium leak pathway and substrate binding order in the Na+-glucose cotransporter. *Biophys J*, **73**, 2503-2510.

Defelice, L.J. (2004) Going against the flow. *Nature*, **432**, 279.

Ehnes, C., Forster, I.C., Bacconi, A., Kohler, K., Biber, J. and Murer, H. (2004a) Structure-function relations of the first and fourth extracellular linkers of the type IIa Na+/Pi cotransporter: II. Substrate interaction and voltage dependency of two functionally important sites. *J Gen Physiol*, **124**, 489-503.

Ehnes, C., Forster, I.C., Kohler, K., Bacconi, A., Stange, G., Biber, J. and Murer, H. (2004b) Structure-function relations of the first and fourth predicted extracellular linkers of the type IIa Na+/Pi cotransporter: I. Cysteine scanning mutagenesis. *J Gen Physiol*, **124**, 475-488.

Eskandari, S., Loo, D.D., Dai, G., Levy, O., Wright, E.M. and Carrasco, N. (1997) Thyroid Na+/I- symporter. Mechanism, stoichiometry, and specificity. *J Biol Chem*, **272**, 27230-27238.

Forster, I., Biber, J. and Murer, H. (1999) Electrophysiological analysis of renal Na(+)-coupled divalent anion transporters. *Pharm Biotechnol*, **12**, 251-267.

Forster, I., Hernando, N., Biber, J. and Murer, H. (1998) The voltage dependence of a cloned mammalian renal type II Na+/Pi cotransporter (NaPi-2). *J Gen Physiol*, **112**, 1-18.

Forster, I.C., Biber, J. and Murer, H. (2000) Proton-sensitive transitions of renal type II Na(+)-coupled phosphate cotransporter kinetics. *Biophys J*, **79**, 215-230.

Forster, I.C., Kohler, K., Biber, J. and Murer, H. (2002) Forging the link between structure and function of electrogenic cotransporters: the renal type IIa Na+/Pi cotransporter as a case study. *Prog Biophys Mol Biol*, **80**, 69-108.

Forster, I.C., Wagner, C.A., Busch, A.E., Lang, F., Biber, J., Hernando, N., Murer, H. and Werner, A. (1997) Electrophysiological characterization of the flounder type II Na+/Pi cotransporter (NaPi-5) expressed in Xenopus laevis oocytes. *J Membr Biol*, **160**, 9-25.

Hazama, A., Loo, D.D. and Wright, E.M. (1997) Presteady-state currents of the rabbit Na+/glucose cotransporter (SGLT1). *J Membr Biol*, **155**, 175-186.

Karakossian, M.H., Spencer, S.R., Gomez, A.Q., Padilla, O.R., Sacher, A., Loo, D.D., Nelson, N. and Eskandari, S. (2005) Novel properties of a mouse gamma-aminobutyric acid transporter (GAT4). *J Membr Biol*, **203**, 65-82.

Kavanaugh, M.P. (1998) Neurotransmitter transport: models in flux. *Proc Natl Acad Sci U S A*, **95**, 12737-12738.

Kohler, K., Forster, I.C., Stange, G., Biber, J. and Murer, H. (2002a) Identification of functionally important sites in the first intracellular loop of the NaPi-IIa cotransporter. *Am J Physiol Renal Physiol*, **282**, F687-696.

Kohler, K., Forster, I.C., Stange, G., Biber, J. and Murer, H. (2002b) Transport function of the renal type IIa Na+/P(i) cotransporter is codetermined by residues in two opposing linker regions. *J Gen Physiol*, **120**, 693-705.

Parent, L., Supplisson, S., Loo, D.D. and Wright, E.M. (1992) Electrogenic properties of the cloned Na+/glucose cotransporter: II. A transport model under nonrapid equilibrium conditions. *J Membr Biol*, **125**, 63-79.

Sonders, M.S. and Amara, S.G. (1996) Channels in transporters. *Curr Opin Neurobiol*, **6**, 294-302.

van Winkle, L. (1999) *Biomembrane Transport*. Academic Press.

Virkki, L.V., Forster, I.C., Biber, J. and Murer, H. (2005) Substrate interactions in the human type IIa sodium-phosphate cotransporter (NaPi-IIa). *Am J Physiol Renal Physiol*, **288**, F969-981.

Wadiche, J.I. and Kavanaugh, M.P. (1998) Macroscopic and microscopic properties of a cloned glutamate transporter/chloride channel. *J Neurosci*, **18**, 7650-7661.

Werner, A., Biber, J., Forgo, J., Palacin, M. and Murer, H. (1990) Expression of renal transport systems for inorganic phosphate and sulfate in Xenopus laevis oocytes. *J Biol Chem*, **265**, 12331-12336.

Werner, A., Murer, H. and Kinne, R.K. (1994) Cloning and expression of a renal Na-Pi cotransport system from flounder. *Am J Physiol*, **267**, F311-317.

Yao, X. and Pajor, A.M. (2000) The transport properties of the human renal Na(+)-dicarboxylate cotransporter under voltage-clamp conditions. *Am J Physiol Renal Physiol*, **279**, F54-64.

Acknowledgements.

This work was supported by grants to H. Murer from the Swiss National Science Foundation.

Figure legends

Figure 1. Steady-state temperature dependency of currents recorded from a representative NaPi-IIb expressing oocyte.

A: Recordings made at 20 ^{o}C (left panels) and 15 ^{o}C (right panels). Currents were recorded in response to a voltage jump protocol from a holding potential of −60 mV to potentials in the range −180 to 80 mV at 40 mV intervals as indicated, in the absence (ND100) and presence of 1 mM P_i,. The dashed lines indicate the steady-state response at −60 mV for the two superfusion conditions. The lower panel shows the P_i-dependent current (I_{P_i}) as the difference between corresponding traces in ND100 and ND100+ 1mM P_i. Note that a longer pulse was used at 15 ^{o}C to ensure that a steady-state was reached.

B: *I-V* plots of the I_{P_i} at the indicated temperatures. Data are mean ± SEM for 4 oocytes, normalized to I_{P_i} at 20 ^{o}C and -100 mV.

D: *I-V* plots of the PFA-dependent current (I_{PFA}). Data were obtained using the same protocols as in A except that 1 mM PFA was substituted for 1 mM P_i and the data plotted as $-I_{PFA}$, which was taken as a measure of the leak. For each cell, the —I_{PFA} data were first normalized to I_{P_i} at -100 mV before pooling.

Figure 2. Temperature dependency for I_{P_i} and -I_{PFA}.

A: Arrhenius plots of the normalized I_{P_i} replotted from the data in Fig.1 B for the membrane potentials indicated. Straight lines represent lineare regression fits to the data points to yield the apparent activation energy (see text).

B: Arrhenius plots for normalized $-I_{PFA}$ replotted from the data in Fig 1 C for the membrane potentials indicated. Straight lines represent linear regression fits to the data points to yield the apparent activation energy (see text).

C: Activation energy (Ea) as a function of membrane potential for I_{P_i} (filled squares) and -I_{PFA} (open squares). Note that for -I_{PFA} we were unable to determine E_a for pontentials close to the -I_{PFA} reversal potential because of data unreliability.

Figure 3. Temperature effects on the kinetics of presteady state currents.
A: Presteady-state relaxations recorded from the same oocyte in response to voltage steps from a holding potential of −60 mV to voltages in the range -180 mV to +80 mV for the same oocyte at the 4 temperatures indicated. The steady-state holding currents have been subtracted for each set.
B: Voltage dependency of the main relaxation time constant (τ-V) reported by a two exponential fit to the data in A for the 4 temperatures indicated. Continuous lines are fits with Equation 2 to the data points. Left panel: superfusion in ND100; right panel superfusion in ND0.
C: Voltage dependency of the charge (Q-V) associated with the main relaxation component for the 4 temperatures indicated. Continuous lies are fits with Equation 1 to the data points. Left panel: superfusion in ND100; right panel superfusion in ND0.

Figure 4. Temperature dependency of fit parameters from Q-V and τ-V data.
A: Midpoint voltage ($V_{0.5}$) reported from fit of Equation 1 to Q-V data as a function of temperature for ND100 (filled squares) and ND0 (open squares).
B: Normalized Q-V data of Fig. 3 C replotted after normalization and adjustment to the depolarizing limit predicted from the fits, to illustrate the relative insensitivity of $V_{0.5}$ for superfusion in ND100 (filled symbols) compared with the ND0 data (open symbols). Each set of Q-V data was normalized to the predicted Q_{max}, offset by the normalized Q_{hyp} (Equation 1) and then refit using Equation 1.
C: Predicted Q_{max} reported from the Q-V fit as a function of temperature. Same symbols as in A.
D: Predicted effective valency (z) reported from the Q-V fit as a function of temperature. Same symbols as in A
E: Arrhenius plot of main relaxation time constant for ND100 (filled symbols) and ND0 (closed symbols) at –100 mV. Lines are linear regression fits to data points.

Figure 5. Kinetic scheme of electrogenic type II Na^+/P_i cotransport. The PFA-blockable leak mode involves states 1-2-7-8. In the presence of saturating P_i, the transport cycle proceeds through states 3 and 4 to the fully loaded carrier.

Table 1. Fit parameters reported by fit of Equation 2 to the τ-V data for ND0 superfusion.

Temp ^{o}C	α (ms^{-1})	β (ms^{-1})	*z*
20	0.049±0.004	0.170±0.010	0.20±0.04
15	0.041±0.003	0.069±0.003	0.37±0.03
10	0.022±0.001	0.051±0.001	0.38±0.02
5	0.012±0.001	0.034±0.001	0.28±0.03

.

Figure 1

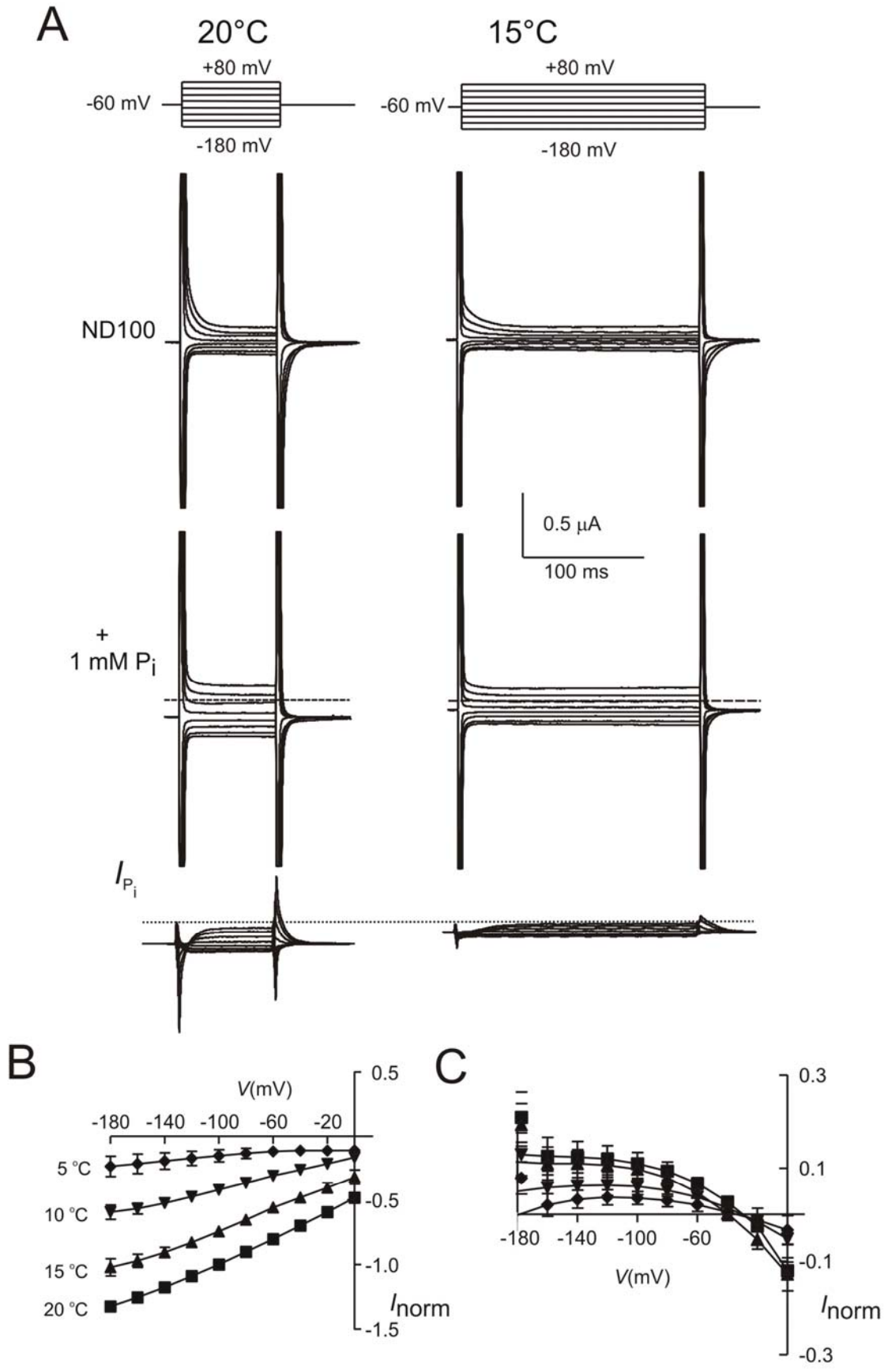
A
20°C
15°C
+80 mV
-60 mV
-180 mV
ND100
0.5 µA
100 ms
+
1 mM Pi
IPi
B
V(mV)
-180 -140 -100 -60 -20
5 °C
10 °C
15 °C
20 °C
0.5
-0.5
-1.0
-1.5
Inorm
C
0.3
0.1
-0.1
-0.3
-180 -140 -100 -60
V(mV)
Inorm

Figure 2

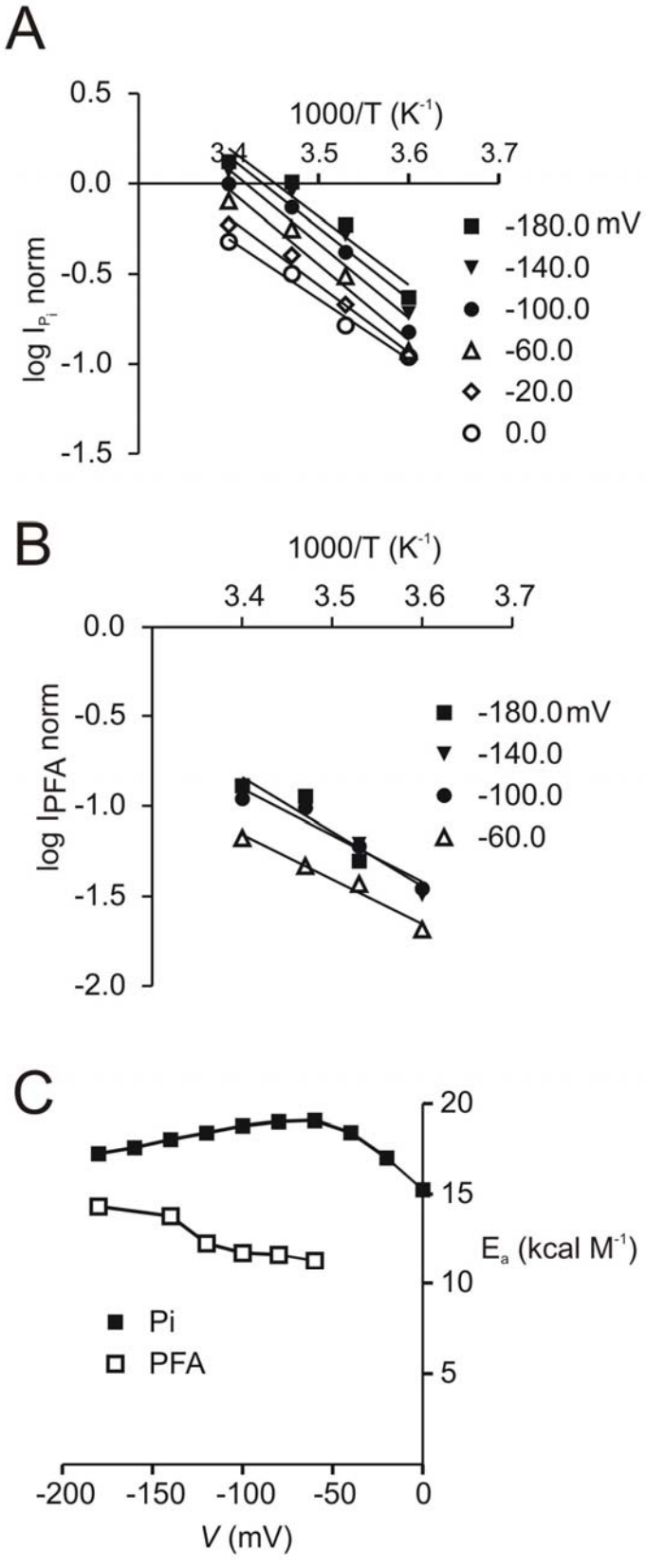
A
1000/T (K-1)
3.4
3.5
3.6
3.7
0.5
0.0
-0.5
-1.0
-1.5
log IPi norm
-180.0 mV
-140.0
-100.0
-60.0
-20.0
0.0
B
1000/T (K-1)
3.4
3.5
3.6
3.7
0.0
-0.5
-1.0
-1.5
-2.0
log IPFA norm
-180.0 mV
-140.0
-100.0
-60.0
C
20
15
10
5
Ea (kcal M-1)
Pi
PFA
-200
-150
-100
-50
0
V (mV)

Figure 3

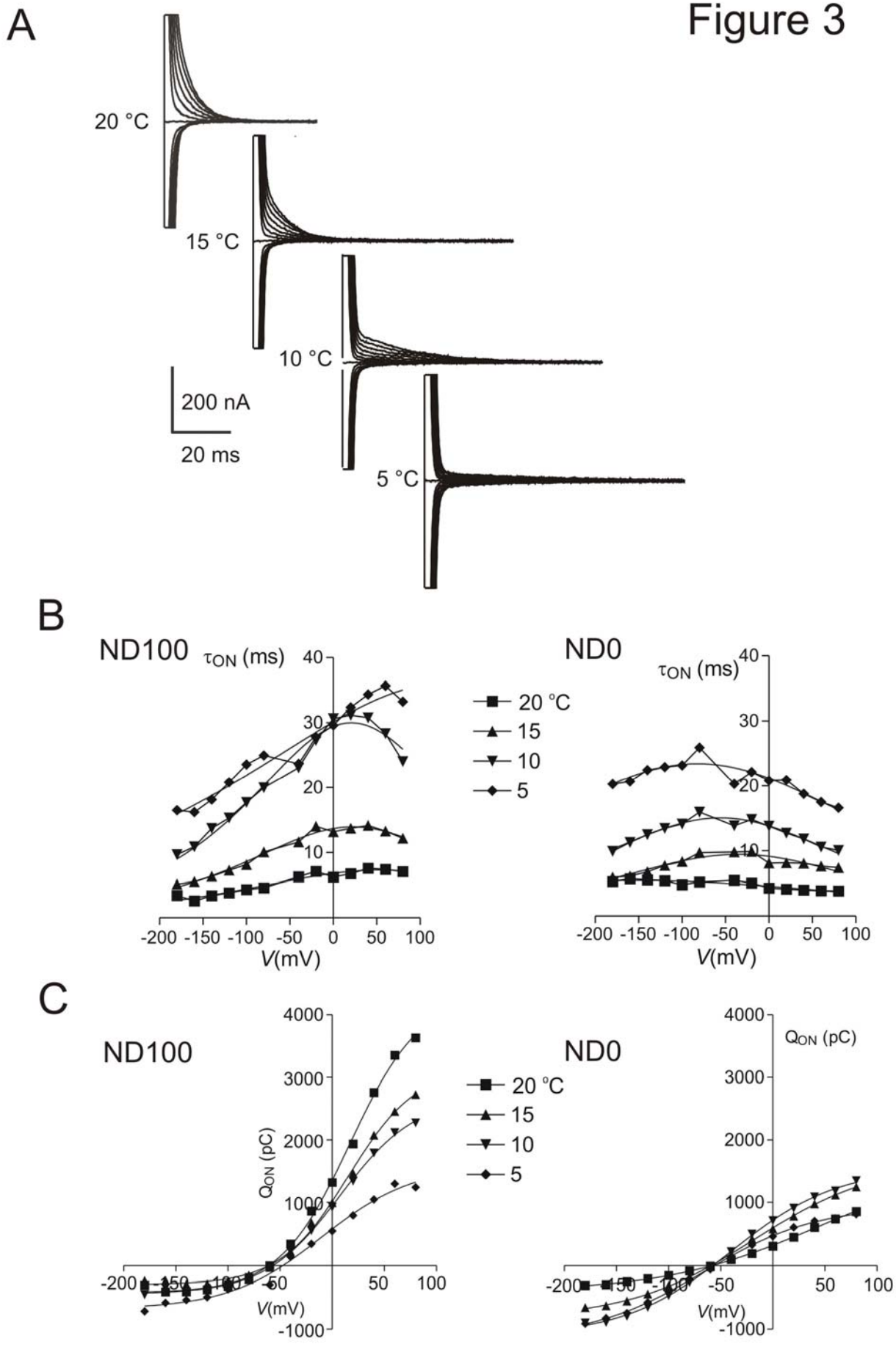
A
20 °C
15 °C
10 °C
5 °C
200 nA
20 ms
B
ND100
τON (ms)
40
30
20
10
-200 -150 -100 -50 0 50 100
V(mV)
20 °C
15
10
5
ND0
τON (ms)
C
ND100
QON (pC)
4000
3000
2000
1000
-1000
V(mV)
ND0
QON (pC)

Figure 4

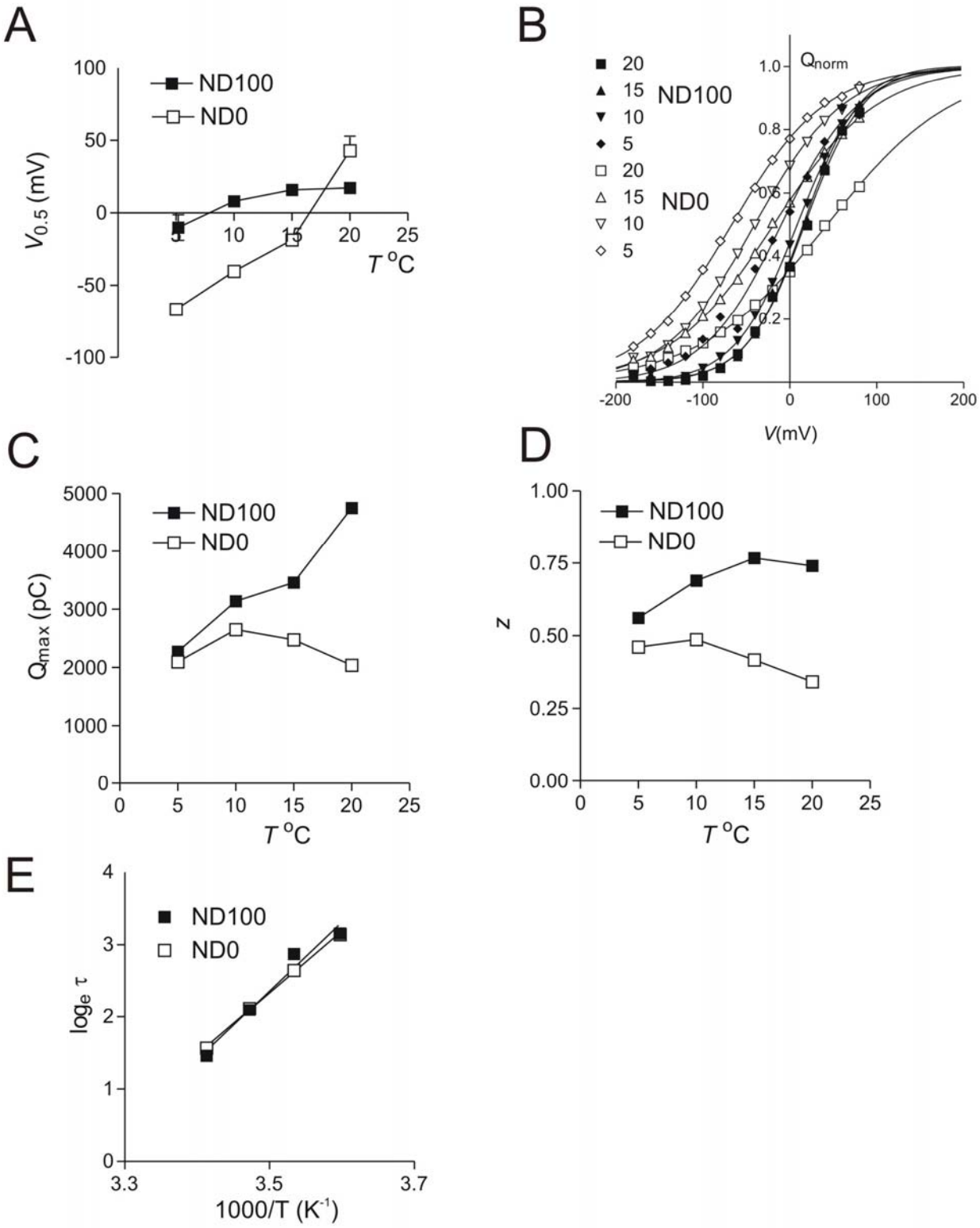
A
100
50
0
-50
-100
ND100
ND0
$V_{0.5}$ (mV)
5
10
15
20
25
T °C
B
20
15
10
5
20
15
10
5
ND100
ND0
Q_{norm}
1.0
0.8
0.6
0.4
0.2
-200
-100
0
100
200
V(mV)
C
5000
4000
3000
2000
1000
0
ND100
ND0
Q_{max} (pC)
0
5
10
15
20
25
T °C
D
1.00
0.75
0.50
0.25
0.00
ND100
ND0
z
0
5
10
15
20
25
T °C
E
4
3
2
1
0
ND100
ND0
$\log_e \tau$
3.3
3.5
3.7
1000/T (K^{-1})

Figure 5

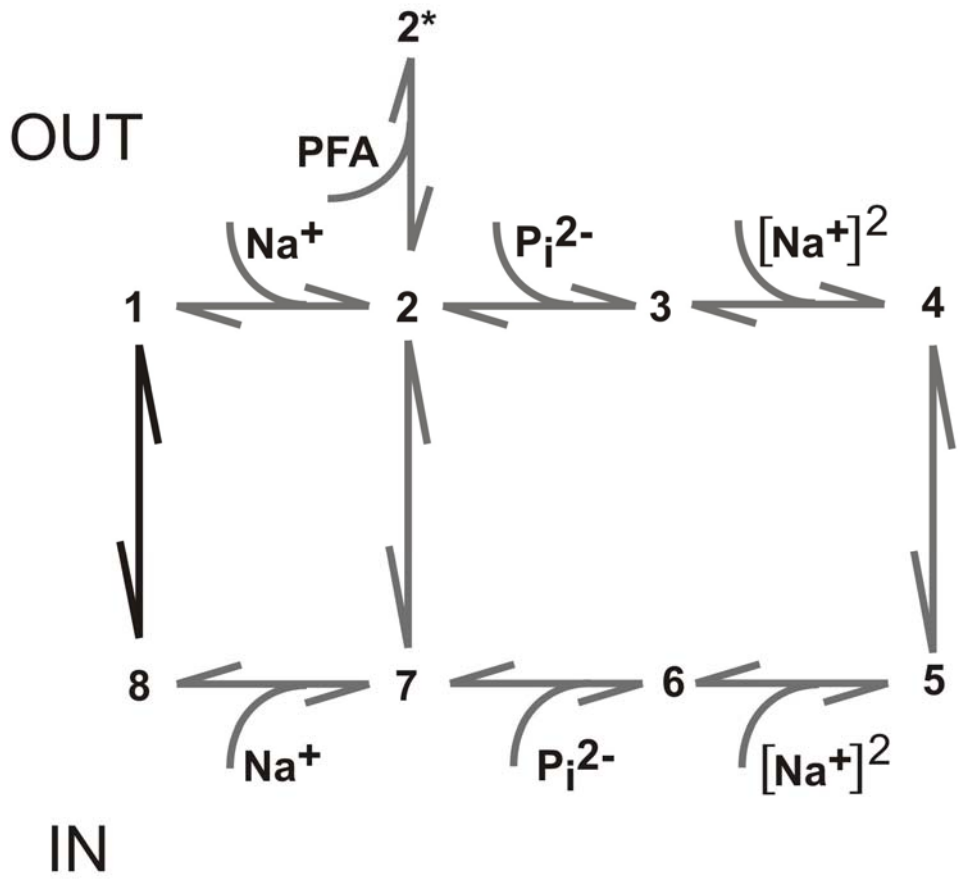

4. DISCUSSION

Until 2002, all type II Na^+-coupled P_i cotransporters were assumed electrogenic, based on experimental studies on both renal NaPi-IIa and intestinal NaPi-IIb isoforms and the high molecular identity between isoforms from different species (for review (Forster et al., 2002; Murer et al., 2000)). However, the situation changed dramatically with the cloning and functional expression in *Xenopus* oocytes of the type IIc that was found mediate electroneutral Na^+-dependent P_i transport (Segawa et al., 2002). Its high degree of similarity at the molecular level with other members of the SLC34 family, particularly in the concensus transmembrane domain regions suggested that relatively small changes in the amino acid sequence might be responsible for conferring electrogenicity/electroneutrality to a transporter. Moreover, NaPi-IIc was found to be more strongly expressed in weaning animals, which suggested a different physiological role for this transporter. These characteristics therefore raised questions that concerned both the biophysics and physiology of Na^+-driven P_i cotransport: i) what are the molecular determinants of electrogenic vs. electroneutral Na^+-coupled P_i cotransport?; ii) what is the physiological relevance of an electroneutral type II isoform?

4.1 Biophysics of transporter coupling stoichiometry

The coupling stoichiometry of membrane transport proteins has considerable physiological significance because it defines the concentrating ability of the transporter and the associated energetic cost to a cell and therefore underscores one of the fundamental differences between active carriers and channels. The importance of stoichiometry characterization is well established in recent studies on the norepinephrine transporter (Defelice, 2004), the mannitol transporter (Veldhuis et al., 2005), the human sodium sulphate cotransporter (Busch et al., 1994b), the EmrE (Rotem and Schuldiner, 2004) and the sodium bicarbonate transporter (Gross and Kurtz, 2002; Muller-Berger et al., 2001). In the case of type II Na^+/P_i transporters, functional studies based on electrophysiological and radiolabelled P_i uptake assays, using *Xenopus laevis* oocytes, established a Na^+:P_i stoichiometry of 3: 1 for the electrogenic type II Na^+/P_i cotransporter (NaPi-IIa) and its cousin NaPi-IIb, cloned from flounder (Forster et al., 1999). It therefore followed that the first step to identify the molecular elements involved in the unique transport characteristic of NaPi-IIc was to determine its stoichiometry. The electroneutrality of NaPi-IIc suggested that the number of Na^+ ions transported for each divalent P_i was reduced, however other possibilities could also account for the

electroneutrality, for example, the involvement of counter ions. To determine the stoichiometry unambiguously, we performed simultaneous uptake experiments with radiolabelled Na and P_i and established that the Na:P_i coupling stoichiometry was 2:1 for NaPi-IIc (Figure 12). In addition, uptake studies with different substrate concentrations strongly suggested that ordered substrate binding was involved in which Na^+ was the last to bind.

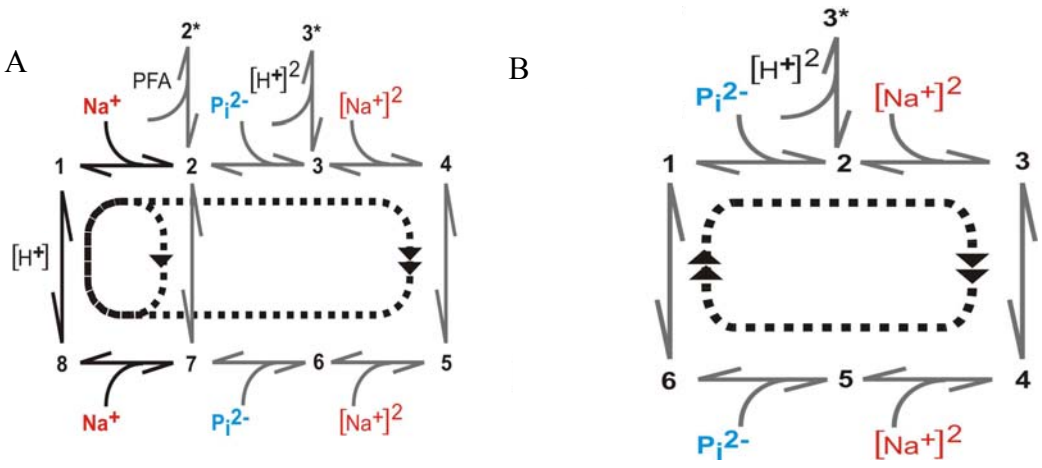

Figure 12: Proposed kinetic schemes for NaPi-IIa (A) and NaPi-IIc (B). Numbers represent the main conformational states. For the electrogenic NaPi-IIa,the two transport modes for the Na^+ leak and the cotransport are indicated by dotted lines (see figure 11 for more details). For NaPi-IIc the Na^+ leak mode is lost and only the cotransport mode is active leading to an overall electroneutral transport cycle. Additional transitions for PFA and H^+ interactions as determined experimentally are also shown.

The relevance of this finding to Na^+-coupled cotransport can best be understood by considering the energetics of a symporter carrier protein. NaPi-IIc. Given $\Delta\mu_{xi}$ the chemical potential difference (CPD) for a generic solute X_i across the membrane, for a transporter with a fix stoichiometry n_1 (X_1) : n_2 (X_2), where X_1 and X_2 are the two transporter substrates, at equilibrium the CPD for X_1 in one direction is balanced by the CPD for X_2 in the opposite direction:

$$n_1\Delta\mu_{X1} = -n_2\Delta\mu_{X2} \quad (1)$$

which leads to the following expression (at 29.5 °C):

$$\left(\frac{[X_1]_i}{[X_1]_o}\right)^{n_1} = \left(\frac{[X_2]_o}{[X_2]_i}\right)^{n_2} 10^{-\frac{V_m(n_1z_1+n_2z_2)}{60}} \quad (2)$$

where z_1, z_2 are the valences for X_1 and X_2 , V_m is the membrane potential difference and $[X_i]_o$ and $[X_i]_i$ are the extracellular and intracellular concentrations of X_i .

Setting now $X_1 = P_i = HPO_4^{2-}$ and $X_2 = Na^+$, z_1=-2, z_2=1, then at V_m = -60 mV and $[Na]_o/[Na]_i$ = 10, values observed in an epithelial cell, then equation (2) gives:

$$\frac{[Pi]_o}{[Pi]_i} = 10^2 \quad \text{for Na:Pi ratio of 2: 1} \qquad (3)$$

$$\frac{[Pi]_o}{[Pi]_i} = 10^4 \quad \text{for Na:Pi ratio of 3: 1} \qquad (4)$$

Expressions (3) and (4) show that in the same epithelial cell with a 10-fold Na^+ concentration gradient and a V_m of -60 mV, the sodium electrochemical gradient can generate a P_i concentration gradient 100 times higher for transporters with a coupling stoichiometry of 3:1 compared to 2:1 (Figure 1, (Bacconi et al., 2005). This implies a higher P_i concentrating efficiency in electrogenic type II Na^+/P_i cotransporters.

We next investigated the NaPi-IIc electroneutral phenotype by engineering a series of chimeras between the electrogenic and electroneutral homologs. After expression in *Xenopus* oocytes, we studied the functional properties of the chimeras by electrophysology and radiolabelled P_i uptake (Figure 2, (Bacconi et al., 2005). The conclusion of this study was that the first six transmembrane domains (out of a predicted eight) and connecting loops in the electrogenic/electroneutral phenotype were necessary for electrogenicity of NaPi-IIa. On the one hand, this finding emphasized the importance of the two reentrant loops ICL-1 and ECL-3 involved in the transport pathway (Kohler et al., 2002a; Kohler et al., 2002b; Kohler et al., 2003) of the electrogenic NaPi-II transporters, as the only electrogenic chimera also contained both loops. On the other hand, it was obvious that elements that conferred electrogenic behavior were distributed throughout the primary sequence.

In a second approach, we performed a multiple sequence alignment of 4 currently available mammalian NaPi-IIc sequences and 17 sequences of NaPi-IIa as well as NaPi-IIb homologs. The analysis showed the highest homology within the predicted transmembrane domains (TMDs) and three main clusters of sites preserved among the type IIa and IIb but different in the type IIc (Figure 3, (Bacconi et al., 2005)). Two of these clusters included ICL-1 and ECL-3, which was consistent with the conclusion made from the chimera study. Among the sites identified, TMD-3 contained a unique feature that comprised a charged amino acid (aspartic acid (D)) preceded by a cluster of non-polar amino acids (two alanines (A)) in NaPi-IIa and NaPi-IIb. The corresponding residues wereubstituted by a glycine (G) and a group of two polar amino acids (serines (S)) in NaPi-IIc. Three point mutations (S189A, S191A, G195D) made in the mouse NaPi-IIc backbone resulted in a functional triple mutantAAD-IIc) that was electrogenic. (Figure 4, (Bacconi et al., 2005)). Moreover, additional mutant constructs in which only one or two of the IIa - IIc substitutions were made, did not result in electrogenic contransport activity, thus these changes appeared to be the minimum required for electrogenicity.

The analysis of the AAD-IIc mutant suggested that the substitutions created, directly or indirectly, a Na^+ interaction site, the occupancy of which leds to the stoichiometric translocation of an additional Na^+ ion per transport cycle (Figure 4, (Bacconi et al., 2005)). The documentation of presteady-state charge movements in the absence of external Na^+ (Figure 6, (Bacconi et al., 2005)) further supports the idea that voltage sensing elements were introduced into AAD-IIc; this seems to be a necessary condition for electrogenicity in type II Na+/P_i cotransporters. A detailed kinetic analysis of AAD-IIc and comparison with the typical fingerprint of electrogenic NaPi-IIa/b homologs revealed significant functional differences (Figure 5, (Bacconi et al., 2005)): a weak steady-state voltage dependency, which, according to the alternating access model, suggests that the empty carrier favors an outward-facing conformation for depolarizing voltages (V<0), a low apparent affinity for P_i and a transient charge imbalance, which may indicate that the mutagenesis had created a channel-like leakage pathway. These differences underline the complexity of the interactions among the structural elements involved in the transporter activity.

Uptake and electrophysiological assays on the reciprocal of the AAD-IIc mutant (SSG-IIa) did not allow a determination of its stoichiometry-predicted to be 2:1. The uptake levels were too close to non-injected or water-injected oocytes to distinguish between the mutated transporter uptake and the oocyte background. The absence of a detectable band at the expected molecular weight by Western blot for SSG-IIa meant that we could not exclude a lack of surface expression as the reason for its low functional activity. In any case, the reduced uptake for the SSG-IIa mutant, either due to a loss of function or poor surface expression, highlights the critical role of the three point mutations in defining the transport pathway and/or structural stability and membrane targetting. This conclusion is strengthened by the behavior of the human NaPi-IIa mutant D224G, which displays a $^{32}P_i$ uptake significantly higher than water injected oocytes, but clearly lower than the NaPi-IIc wild type (Virkki et al., 2005). Its behavior suggests that the carboxylic acid side chain of Asp-224 may participate in forming a binding site for one of the three Na^+ ions transported by NaPi-IIa per transport cycle, and its removal compromised this binding site.

4.2 Physiological consequences of electroneutrality in type IIc NaPi cotransporters

The physiological significance of an electroneutral Na^+/P_i cotransporter during growth is unknown. An electroneutral transporter would transport less P_i across the apical membrane of the proximal tubule, because the driving force for Na^+ would be smaller, as shown above. Two factors oppose the entry of P_i from the tubular lumen into the cell, the inside negative cell potential and the high intracellular P_i concentration. The intracellular P_i concentration measured in isolated perfused

kidneys using nuclear magnetic resonance (NMR) was reported to be significantly lower in growing animals than in adult (Barac-Nieto et al., 1991), which would provide a greater driving force for an electroneutral Na^+/P_i cotransporter in growing animals. It is possible that the induction of type IIc protein in superficial nephrons of weaning rats may be related not only to the developmental stage but also may be affected by different amounts of P_i in the available food (Traebert et al., 1999). In a recent publication, different segments of the superficially and juxtamedullary nephrons in adult mice were laser-microdissected to determine mRNA and protein expression of NaPi-IIa and NaPI-IIc (Madjdpour et al., 2004). This study reported that NaPi-IIc was upregulated at the mRNA and protein levels in all nephron generations analyzed when the mice were subjected to a low P_i diet. It suggests that NaPi-IIc can still play a physiological role in adults, although its protein levels are reduced compared with weaning animals. The reduced stoichiometry of type IIc could have important consequences for reducing energy consumption during development. Compared to the electrogenic NaPi-IIa, NaPi-IIc would result in less Na^+ loading of the cell so that the energetic requirements of the Na-K-ATPase would also be concomitantly reduced.

Conferring electrogenic behavior to the electroneutral NaPi-IIc and the accompanying increase in stoichiometry raises an important question that may be relevant to of Na^+-driven cotransporters: what is more important: the voltage dependency of the membrane transport or the 3:1 stoichiometry of NaPi-IIa? In other words, we may ask: is the voltage dependency in the AAD-IIc, or more generally in the electrogenic type II Na^+/P_i cotransporters, simply a consequence of the 3:1 stoichiometry or is it *per se* advantageous to have voltage as a driving force in membrane transporters? If we have a transporter in developing cells where substrate translocation takes place in a non voltage-dependent manner, like NaPi-IIc, it would allow the cell to constantly uptake substrate without adding to the energetic cost of maintaining a specific membrane potential. On the other hand, for the electrogenic NaPi-IIa, we would expect its concentrating ability to vary significantly, depending on the membrane potential because membrane potential not only alters the driving force of Na^+ ions, but also modulates the rate constants that define the transitions between empty carrier states and first Na^+ binding transition (Figure 12).

4.3 Cysteine scanning in NaPi-IIa.

During the period of this dissertation work, the author was a co-investigator on two projects that involved cysteine scanning, the results of which directly impacted on the understanding of the electrogenicity of Na^+-coupled P_i cotransport. The main findings of these studies are summarized below, as they relate to understanding the electrogenicity of type II Na^+/P_i cotransport.

4.3.1 SCAM in ECL-1 and ECL-4: insights into voltage-dependent conformational changes

The importance of putative reentrant loops for the transport function of NaPi-IIa had been established with previous investigations from our laboratory that dealt with the 3rd extracellular loop (ECL-3, Figure 13) and the first intracellular loop (ICL-1, Figure 13) (Kohler et al., 2002a; Kohler et al., 2002b; Lambert et al., 2001). In a continuation of this work, we investigated the 1st and 4th extracellular loops using SCAM combined with a detailed kinetic analysis of the most interesting cysteine mutants (Ehnes et al., 2004a; Ehnes et al., 2004b). Nine and 7 residues in the predicted ECL-1 and ECL-4 respectively, were mutated one by one into cysteines. All mutants except Q537C were functional with a molecular weight corresponding to the WT. The labelling assay performed with these mutants, using impermeable MTSEA-biotin, provided evidence for their accessibility from the external milieu. Further support for the extracellular localization of the two loops came from the changes in cotransport kinetics of the mutated cotransporters after exposure to the externally applied MTS reagent MTSET, which is positively charged and membrane impermeable. Interestingly, the mutants showed very different alterations in their respective electrogenic kinetics after MTS labeling; for some mutants MTS exposure left the transport activity unchanged, whereas for others it was only partially inhibited after completion of the MTS labeling reaction. Interestingly, the G134C mutant showed increased electrogenic cotransport activity, but a reduced $^{32}P_i$ uptake. This apparent discrepancy was resolved when account was taken of the absence of membrane voltage control in the ^{32}Pi uptake experiments. This would allow the oocyte membrane to depolarize in the presence of P_i due to the net inward movement of positive charge and hence reduce the transport driving force. To investigate this altered voltage dependency in more detail, we studied the effect of mutations G134C and M533C in ECL-1 and ECL-4 respectively (Fig. 14, below).

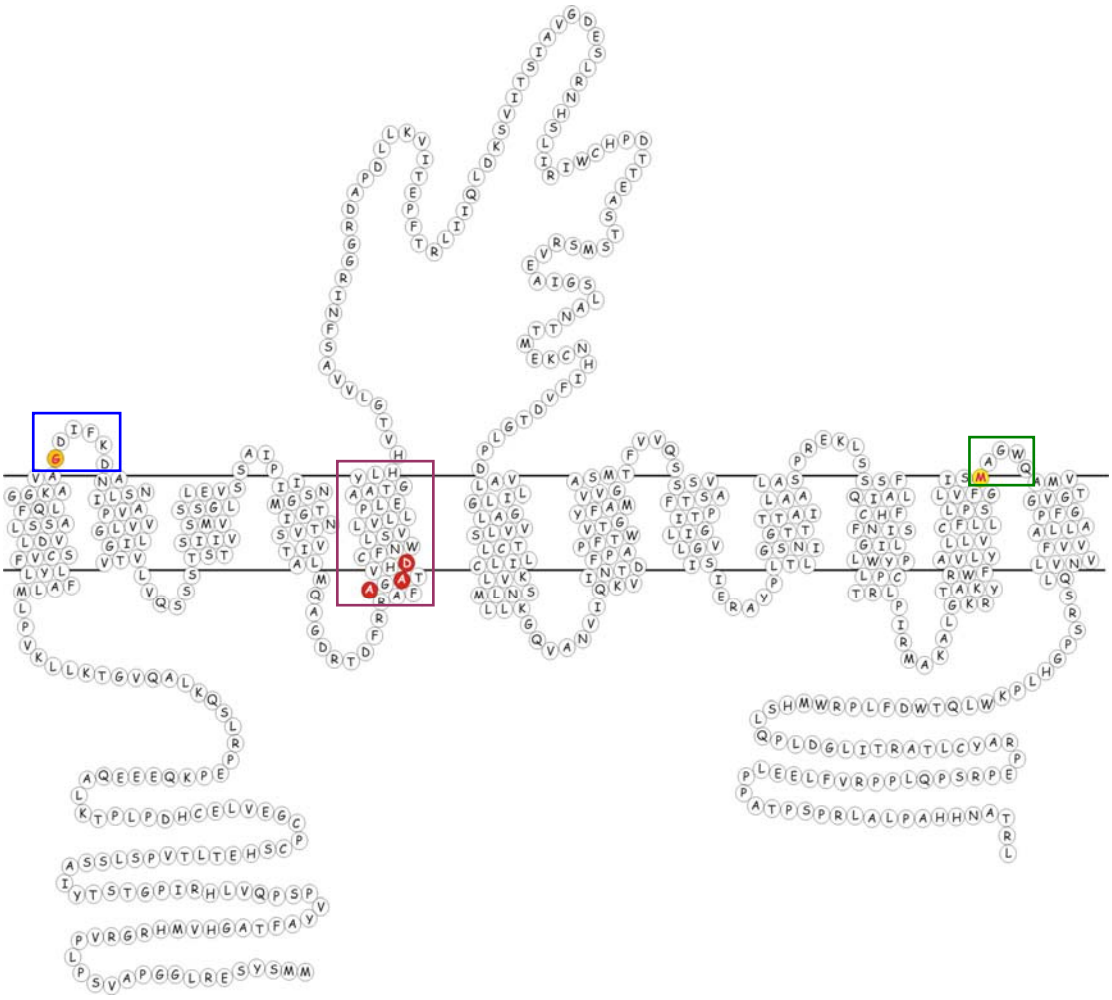

Figure 13: Secondary topology model of mouse NaPi-IIa, derived from HMMTOP (http://www.enzim.hu/hmmtop/) showing areas that affect its voltage dependency and confer electrogenicity. Red balls represent the G134C and M533C mutants in ECL-1 (blue square) and ECL-4 (green square) respectively. Orange balls indicate the position of the AAD-motif in the predicted 3rd transmembrane domain (purple square).

The detailed steady-state dose-response analysis for the two mutants suggested that changes in the apparent P_i and Na^+ affinities due to cysteine substitutions or subsequent MTS modification were not responsible for the changes of cotransport activities. However, the voltage dependency of cotransport, analyzed by measuring P_i induced currents at different membrane potentials, was significantly altered compared to the WT. Reciprocal electrogenic behaviour was observed for these two mutants depending on the state of cys-modification. G134C-MTS and M533C+MTS exhibited a weak voltage dependency, whereas the voltage dependency of G134C+MTS exceeded that of the WT and M533C-MTS was indistinguishable from the WT (see Figure 14)(Ehnes et al., 2004a; Ehnes et al., 2004b). The unique, complementary behaviour of G134C and M533C was further investigated by a detailed kinetic analysis of presteady-state charge movements. This study suggested that changes in steady-state voltage dependency could be attributed to changes in the rate

constants associated with the empty carrier transitions without changing the intrinsic valency of the carrier.

One possible interpretation of these findings might be that TMD-1 and TMD-8 are relatively static and the respective linkers allow flexibility for movement of the remaining TMDs during the transport cycle. Thus, in ECL-1, Gly-134 might allow TMD-3 to move in response to changes in voltage. This flexibility is lost when the Gly-Cys substitution is made. Modification of Cys-134 would appear to restore the original flexibility, perhaps through a steric interaction of the bulky MTS reagent with neighboring structures, to restore a WT-like voltage dependency. Conversely, at the "reciprocal" site (Met-533) in ECL-4, cys-substitution was tolerated, but when modified, the voltage dependent kinetics resembled those of the mutant G134C before cys-modification, as if the bulky MTS reagent at this site restricted movement of the preceding TMD-7.

4.3.2 SCAM and mutagenesis in TMD-3

The functional role of the predicted transmembrane domain 3 (TMD-3) was investigated by SCAM applied to the human NaPI-IIa isoform, independently from the study of NaPi-IIc electroneutrality (Virkki et al. 2005, submitted). This was the first detailed study of a putative transmembrane domain region of NaPi-IIa. The choice of TMD-3 was based on its proximity to ICL-1, which had been proposed as re-entrant to form part of the substrate translocation pathway (Kohler et al., 2002a; Kohler et al., 2002b)) and the presence of sites of potential importance in coordinating Na^+ ions (Nayal and Di Cera, 1994; Ogawa and Toyoshima, 2002). Unlike other SCAM studies on intra- and extracellular linker regions, in which accessibility to novel cysteines was routinely observed (Ehnes et al., 2004a; Ehnes et al., 2004b; Kohler et al., 2002a; Kohler et al., 2002b; Kohler et al., 2003; Lambert et al., 2001), only one site was found to result in a change of function after MTS incubation of the respective mutant. MTSEA or MTSET treatment reduced P_i-induced currents by ~50%, which indicated that the top (extracellular end) of TMD-3 was accessible from the extracellular milieu and confirmed the topological predictions for this motif. To possibilities could account for the lack of modified behavior for the other mutants. First, the remaining of TMD-3 may be buried within the protein, at least under the labelling conditions we employed (100 mM Na^+, -50 mV holding potential) and may not be exposed to the aqueous environment accessible from the external side. Second, the residues were indeed labelled without detectable change of function, however this seems unlikely, given that mutagenesis at several of these sites resulted in dramatic changes in their electrogenic characteristics.

In this study, the kinetic characteristics of mutants at three sites in TMD-3 were investigated in more detail. The Asn-Cys substitution at site 227 resulted in a construct unable to mediate functional P_i uptake in oocytes but no electrogenic activity. Although protein expression was also low for this construct, the lack of electrogenic activity strongly suggested that electroneutral transport occurred; a result consistent with the findings at the equivalent site in the mouse NaPi-IIc (see above) where a charge was introduced at this site in the AAD-IIc mutant. Mutant S230C-C225S mutant was well expressed, and this was the only mutant to show a change in the apparent P_i and Na^+ affinities, without MTS application. Finally, Glu-238, lying a further two turns along the α-helix, is the only other charged residue of TMD-3. Cys substitution at this site was not tolerated, but substitution with a charged Asp or polar Gln resulted in functional mutants that mediated electrogenic P_i transport with reduced substrate affinities.

Taken together, the results of the Cys scanning mutagenesis and the additional mutagenesis of Asp-224, Asn-227, Ser-230 and Glu-238 are consistent with TMD-3 forming an amphipathic helix that contains important elements for substrate binding. These results underscored the functionally critical role played by TMD-3 using a different approach. The lack of functional mutants due to a reduced expression of mutant proteins could suggest an additional role of TMD-3 in protein stabilization during the folding process.

4.3.3 Voltage dependency in NaPi-IIa

The identification of ECL-1 and ECL-4 by SCAM highlights an important distinction between channels and carriers with regard to the nature of the voltage dependent transitions in these membrane transporter proteins. Voltage dependent channels have a voltage sensor responsible for the open or closed state that is not directly involved in forming the ionic pathway (Chanda et al., 2005). In contrast, for electrogenic NaPi-II, the results of the SCAM analysis of ECL-1 and ECL-4 (Ehnes et al., 2004a; Ehnes et al., 2004b) suggested the existence of a more complex mechanism in the voltage dependent transitions The SCAM data suggested that they do not form part of the cotransport pathway, but they are involved in defining the voltage dependent kinetics of NaPi-IIa. Previous structure-function studies on the ICL-1 and ECL-3 (Kohler et al., 2002b) demonstrated their contribution to the cotransport pathway suggesting the binding of the first sodium as the main voltage dependent kinetic step. The investigation of type IIc stoichiometry and the TMD-3 SCAM strengthen this idea. Combined electrophysiological and ^{32}Pi uptake assays experiments on mouse NaPi-IIc showed a voltage independent kinetic cycle in this transporter. In addition, we performed mutagenesis studies of residues in the TMD-3 on human NaPi-IIa, observing an altered voltage

dependency for most of the functional mutants. These findings together with the chimera and bioinformatics studies on NaPi-IIc suggest a possible synergic effect of voltage dependent elements in type II transporters to modulate the binding probability of the first Na^+, strengthening the idea that more than one part of the protein is involved in conferring electrogenicity.

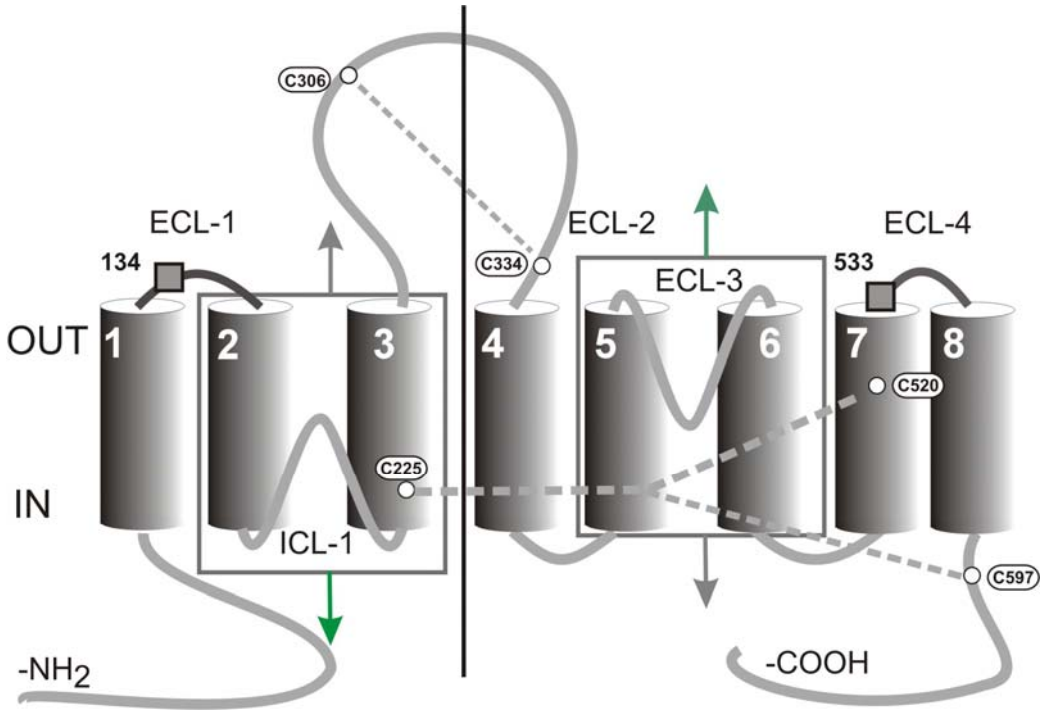

Figure 14: Hypothetical model for the complementary movements of the two halves of type II Na^+/P_i cotransporters. The matching colored arrows indicate the respective direction of the movement that would depend on the transmembrane electrical field. The dashed lines indicate disulfide bridges that stabilize the tertiary structure.

The voltage dependent transition might be similar to the rocker model proposed for the glycerol-3P (Huang et al., 2003; Lemieux et al., 2005): ECL-1 and ECL-4 could be among the elements that respond to membrane voltage changes. Their complementary movement could affect the relative position of TMD-3 and thus modulate the depth of the energy well for the first Na^+ ion.

4.4 The mechanism of the uncoupled leak

This study addressed the nature of the uncoupled leak current of type II Na^+/P_i cotransporters. It was concerned directly with the issues raised previously (see Section 2.8) that relate to the blurring of the divisions between channels and carriers. All electrogenic NaPi-II cotransporters display a PFA dependent change in the holding current in the absence of P_i. This current was originally accounted for by assuming it represent a uniport mode of the transporter, whereby Na^+ ions can "leak" through the protein at a rate governed by the translocation of an electroneutral complex, comprising a single Na^+ ion and the effective charge of the empty carrier

(Forster et al., 1998; Forster et al., 2002), see Figure 10). That the PFA-dependent leak current shows a reversal potential (E_r^{PFA}) that does not correspond to the predicted Nernst potential for Na^+ ions could be accounted for by assuming a finite intracellular P_i concentration (Forster et al., 2000). However, the validity of this assumption has not been demonstrated experimentally. Interestingly, preliminary experiments (Bacconi, Virrki and Forster, unpublished results) in which external Cl^- ions were substituted by gluconate showed a shift in E_r^{PFA}, which indicates that the identity of the leak current is more complex than previously thought and, moreover, suggests the notion of a channel-like behaviour, analogous to that reported for some neurotransmitter transporters (e.g. (Otis and Jahr, 1998)).

Using a two-electrode voltage clamp assay at different temperatures, we determined the activation energy (E_a) for the steady-state currents at different voltages for the P_i induced current and the uncoupled leak current. The E_a's for P_i and the PFA-dependent currents were significantly different. For the cotransport mode we obtained a E_a> 17 kcal/mol (-180mV < V < 0), which agreed with the expected values reported for transporters, whereas for the leak current $E_a \sim 12$ kcal/mol (-120mV < V < -60 mV range). This is larger than the value expected for electrodiffusion through an ion channel (van Winkle, 1999). We expect the P_i induced current to be highly dependent on conformational changes within the protein, similar to the behaviour reported for the Na^+/glucose cotransporter (SGLT1) (Petersen and DeFelice, 1999), the GABA transporter (Binda et al., 2002), the Drosophila 5HT transporter dSERT (Beckman and Quick, 2001), and the human glutamate transporter EAAT1 (Wadiche and Kavanaugh, 1998). In addition to the steady-state data, we also recorded presteady-state currents at different temperatures. These data indicated that lowering the temperature shifted the equilibrium potential of a Boltzmann fit to the Q/V data as temperature was lowered, together with an increase in the main relaxation time constant. Detailed analysis of the presteady-state kinetics in the presence and absence of external Na^+ indicated that the activation energy for the relaxation time constants was 8 kcal/mol (V = -100 mV). This might reflect temperature-dependent changes in the kinetics of Na^+ binding, the empty carrier or both. The former has been also observed in the GABA transporter (Binda et al., 2002) and in SGLT1 (Petersen and DeFelice, 1999) and they could be interpreted with a differential effect of temperature on the unidirectional rate constants**.** Taken together, these findings suggest that the empty carrier reorientation and interaction of the first Na^+ ion with the protein are in part responsible for the apparent activation energy of the leak mode.

The recent publication of the crystal structure for a bacterial homolog (Yamashita et al., 2005) of the human glutamate transporter EAAT1 (Wadiche and Kavanaugh, 1998) suggested a possible explanation of the different temperature coefficents of the cotransport and leak modes of

NaPi-II. The structure showed a trimeric organization for the transporter with a central part that could represent a pathway for ion movement through the protein. In the case of type II Na^+/P_i cotransporters, a protein oligomerization could create the "channel" or pore for ion movement in the transporter leak mode that would then close in response to the substrate application as a consequence of a conformational change by each of the functional monomers. This would also result in a higher activation energy than expected for a simple channel because of the requirement of substrate interaction with the protein. This hypothesis was previously suggested by Eskandari and colleagues for the EAAT1 transporter, where it was shown by freeze fracture techniques on oocytes expressing the glutamate transporter that it could be organized as a pentamer (Eskandari et al., 2000).

5. Future perspectives

5.1 *Vibrio cholerae*

The cloned *Vibrio cholerae* prokaryotic Na^+/P_i cotransporter homologue (Lebens et al., 2002) (vNaPi) represents an interesting tool for structural studies on type II cotransporters. It shows high sequence similarity with the type II Na^+/P_i cotransporter family and secondary topology prediction algorithm suggests the existence of 8-12 predicted transmembrane domains, although the sequence length of this prokaryotic homologue is approximately 30% shorter than a mammalian one. Bacterial expression systems with their robust membrane targeting mechanism, which directly integrates proteins into the plasma membrane, and the advantage of simplified functional assays will facilitate the characterization and/or structural determination of membrane proteins. To date we have been unable to express this protein in *Xenopus* oocytes, however recent overexpression experiments for vNaPi open the possibility for a future crystallization attempt.

In the meantime, this protein can be used for computational protein prediction studies like homology modelling. vNaPi is a good candidate for these studies because its sequence is short and many crystal structures from bacterial proteins are available. This can be useful when performing the alignment and the calculations. Figure 5.1 shows a pilot homology modelling study on vNaPi using the glycerol-3P as template. The predicted structure has 12 transmembrane domains and the TMD equivalent to the previously discussed TMD-3 is located at the junction between the two halves of vNaPi, suggesting its possible structural role. These studies are a useful tool to investigate possible structural features for transporters, but a full set of experimental data is necessary to verify the validity of the proposed model.

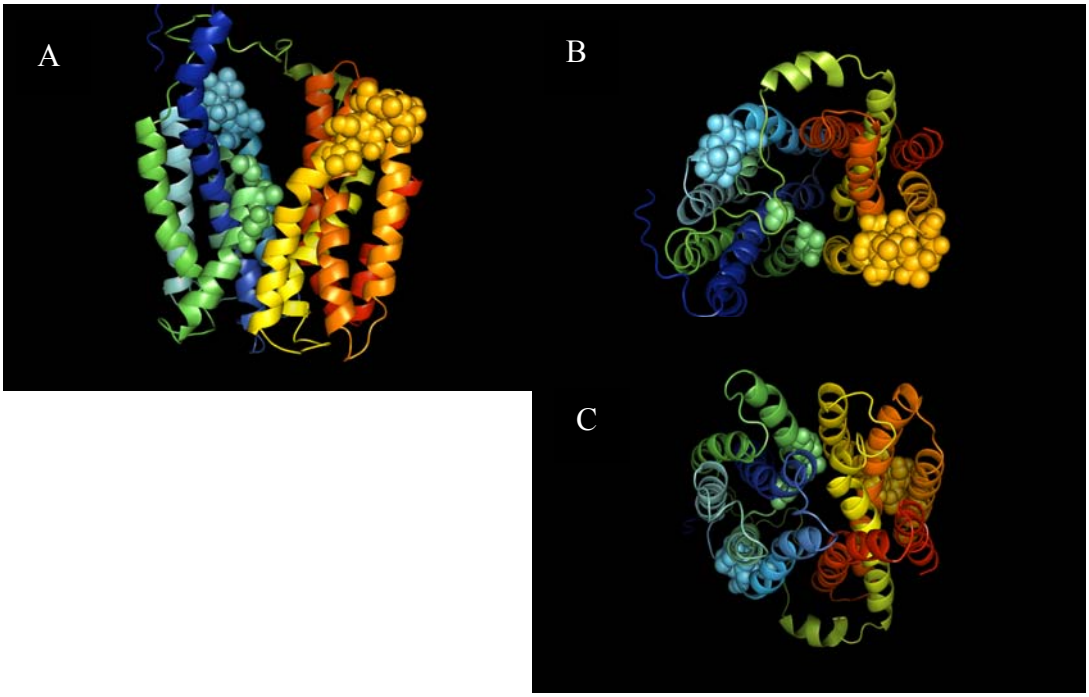

Figure 15: Hypothetical 3-D structure of vNaPi. The structure was generated by homology with the crystal structure of GlpT from *E. Coli* (PDB No. 1PW4, see (Huang et al., 2003)). The alignments were done with ClustalW (Thompson et al., 1994) and BLOSUM62 (Henikoff and Henikoff, 1992), with gap penalties of 10 for insertion and 0.1 for extension. The homology modeling used *Nest*, a program within the JACKAL suite (Xiang and Honig, 2001) and refinement was done with MODELLER (Sali and Blundell, 1993). For validation we used PROCHECK (Laskowski et al., 1993) and WHATCHECK (van Aalten et al., 1996). (A) Side view showing relative positions of the helices. Yellow and blue balls represent the vNaPi equivalent of the mammalian ECL-1 and ECL-4. Green balls represent the vNaPi equivalent of the mammalian TMD-3; (B) View from the extracellular side showing the 12 transmembrane helicies.; (C) Cytoplasmic view, marks as above. Figure drawn using PYMOL (http://pymol.sourceforge.net/).

5.2 Cut open voltage clamp and voltage clamp fluorometry

The recent introduction of the cut open (COVC) and voltage clamp fluorimetry (VCF) techniques constitute powerful tools to investigate further the kinetics of type II Na^+/P_i cotransporters as well as reveal new structure-function relationships. The COVC will allow access the intracellular compartment in oocytes expressing type II Na^+/P_i cotransporters; this technique will allow SCAM experiments to be performed on residues accessible only from the intracellular compartment. Moreover, fundamental questions can be addressed concerning the steady-state electrogenic NaPi-II kinetics such as whether or not reverse mode cotransport can take place. The COVC also offers an order of magnitude improvement of the resolution of presteady-state charge

movements because of the smaller area of voltage clamped membrane, which allows a more uniform and faster voltage clamping of the oocyte to be achieved.

Voltage clamp fluorometry (VCF) is a powerful technique that combines electrophysiology with fluorescence microscopy to investigate localized protein conformational changes under voltage clamp conditions (Cha et al., 1998) it will be possible to link single residues movement with the transport activity, thereby defining a map of the mobile residues during the different transitions of the type II NaPi transport cycle.

5.3 Further NaPi-IIc/NaPi-IIa investigations

The present study used NaPi-IIc as a tool to investigate the biophysical aspects of type II transport kinetics but there are still many open questions about the physiology and biophysics of type II Na^+/P_i cotransporters. The generation of a knock-out mouse for NaPi-IIc would possibly help to understand the importance of this protein during development clarifying its possible physiological roles on a mouse model. Moreover, for NaPi-IIc the substrate binding order has not been yet clarified and this could be addressed by performing a detailed kinetic study at different Na^+ and P_i concentrations. A further and more general aspect of Na^+/P_i cotransporter kinetics is the identification of other elements that confer its voltage dependency. The discovery of AAD-IIc (see above) suggested the critical role played by the three amino acids in the voltage dependent pattern of type II Na^+/P_i cotransporters. Its kinetic features are somewhat different from the wild type and the IIa-IIc chimeras suggesting that additional site must be involved in the fine tuning type II electrogenicity and voltage dependency. Another aspect which must be clarified is the biophysical nature of the proposed leak pathway. The presented temperature dependency studies suggested it has a channel-like behavior and further investigations will be required to clarify this prediction.

6. References

Abramson, J., Smirnova, I., Kasho, V., Verner, G., Kaback, H.R. and Iwata, S. (2003) Structure and mechanism of the lactose permease of Escherichia coli. *Science*, **301**, 610-615.

Accardi, A. and Miller, C. (2004) Secondary active transport mediated by a prokaryotic homologue of ClC Cl- channels. *Nature*, **427**, 803-807.

al-Mahrouq, H.A. and Kempson, S.A. (1991) Photoaffinity labeling of brush-border membrane proteins which bind phosphonoformic acid. *J Biol Chem*, **266**, 1422-1427.

Bacconi, A., Virkki, L.V., Biber, J., Murer, H. and Forster, I.C. (2005) Renouncing electroneutrality is not free of charge: Switching on electrogenicity in a Na+-coupled phosphate cotransporter. *Proc Natl Acad Sci U S A*, **102**, 12606-12611.

Barac-Nieto, M., Dowd, T.L., Gupta, R.K. and Spitzer, A. (1991) Changes in NMR-visible kidney cell phosphate with age and diet: relationship to phosphate transport. *Am J Physiol*, **261**, F153-162.

Baumann, K., de Rouffignac, C., Roinel, N., Rumrich, G. and Ullrich, K.J. (1975) Renal phosphate transport: inhomogeneity of local proximal transport rates and sodium dependence. *Pflugers Arch*, **356**, 287-298.

Beckman, M.L. and Quick, M.W. (2001) Substrates and temperature differentiate ion flux from serotonin flux in a serotonin transporter. *Neuropharmacology*, **40**, 526-535.

Biber, J., Custer, M., Werner, A., Kaissling, B. and Murer, H. (1993) Localization of NaPi-1, a Na/Pi cotransporter, in rabbit kidney proximal tubules. II. Localization by immunohistochemistry. *Pflugers Arch*, **424**, 210-215.

Binda, F., Bossi, E., Giovannardi, S., Forlani, G. and Peres, A. (2002) Temperature effects on the presteady-state and transport-associated currents of GABA cotransporter rGAT1. *FEBS Lett*, **512**, 303-307.

Boron, W. and Boulpaep, E.L. (2003) *Textbook of Medical Physiology*. W.B. Saunders Company.

Braun, W. and Go, N. (1985) Calculation of protein conformations by proton-proton distance constraints. A new efficient algorithm. *J Mol Biol*, **186**, 611-626.

Broer, S., Schuster, A., Wagner, C.A., Broer, A., Forster, I., Biber, J., Murer, H., Werner, A., Lang, F. and Busch, A.E. (1998) Chloride conductance and Pi transport are separate functions induced by the expression of NaPi-1 in Xenopus oocytes. *J Membr Biol*, **164**, 71-77.

Burckhardt, G., Stern, H. and Murer, H. (1981) The influence of pH on phosphate transport into rat renal brush border membrane vesicles. *Pflugers Arch*, **390**, 191-197.

Busch, A., Waldegger, S., Herzer, T., Biber, J., Markovich, D., Hayes, G., Murer, H. and Lang, F. (1994a) Electrophysiological analysis of Na+/Pi cotransport mediated by a transporter cloned from rat kidney and expressed in Xenopus oocytes. *Proc Natl Acad Sci U S A*, **91**, 8205-8208.

Busch, A.E., Biber, J., Murer, H. and Lang, F. (1996a) Electrophysiological insights of type I and II Na/Pi transporters. *Kidney Int*, **49**, 986-987.

Busch, A.E., Schuster, A., Waldegger, S., Wagner, C.A., Zempel, G., Broer, S., Biber, J., Murer, H. and Lang, F. (1996b) Expression of a renal type I sodium/phosphate transporter (NaPi-1) induces a conductance in Xenopus oocytes permeable for organic and inorganic anions. *Proc Natl Acad Sci U S A*, **93**, 5347-5351.

Busch, A.E., Wagner, C.A., Schuster, A., Waldegger, S., Biber, J., Murer, H. and Lang, F. (1995) Properties of electrogenic Pi transport by a human renal brush border Na+/Pi transporter. *J Am Soc Nephrol*, **6**, 1547-1551.

Busch, A.E., Waldegger, S., Herzer, T., Biber, J., Markovich, D., Murer, H. and Lang, F. (1994b) Electrogenic cotransport of Na+ and sulfate in Xenopus oocytes expressing the cloned Na+SO4(2-) transport protein NaSi-1. *J Biol Chem*, **269**, 12407-12409.

Carvelli, L., McDonald, P.W., Blakely, R.D. and Defelice, L.J. (2004) Dopamine transporters depolarize neurons by a channel mechanism. *Proc Natl Acad Sci U S A*, **101**, 16046-16051.
Cha, A., Zerangue, N., Kavanaugh, M. and Bezanilla, F. (1998) Fluorescence techniques for studying cloned channels and transporters expressed in Xenopus oocytes. *Methods Enzymol*, **296**, 566-578.
Chanda, B., Asamoah, O.K., Blunck, R., Roux, B. and Bezanilla, F. (2005) Gating charge displacement in voltage-gated ion channels involves limited transmembrane movement. *Nature*, **436**, 852-856.
Clementi, M.E., De Rosa, M.C., Bertonati, C., Capo, C., Cataldi, E., Petruzzelli, R. and Giardina, B. (2001) The hemoglobins of the "fossil fish" Acipenser naccarii: functional properties and their structural basis. *Hemoglobin*, **25**, 447-451.
Custer, M., Lotscher, M., Biber, J., Murer, H. and Kaissling, B. (1994) Expression of Na-P(i) cotransport in rat kidney: localization by RT-PCR and immunohistochemistry. *Am J Physiol*, **266**, F767-774.
Custer, M., Meier, F., Schlatter, E., Greger, R., Garcia-Perez, A., Biber, J. and Murer, H. (1993) Localization of NaPi-1, a Na-Pi cotransporter, in rabbit kidney proximal tubules. I. mRNA localization by reverse transcription/polymerase chain reaction. *Pflugers Arch*, **424**, 203-209.
de la Horra, C., Hernando, N., Lambert, G., Forster, I., Biber, J. and Murer, H. (2000) Molecular determinants of pH sensitivity of the type IIa Na/P(i) cotransporter. *J Biol Chem*, **275**, 6284-6287.
Defelice, L.J. (2004) Going against the flow. *Nature*, **432**, 279.
DeFelice, L.J., Adams, S.V. and Ypey, D.L. (2001) Single-file diffusion and neurotransmitter transporters: Hodgkin and Keynes model revisited. *Biosystems*, **62**, 57-66.
Doyle, D.A., Morais Cabral, J., Pfuetzner, R.A., Kuo, A., Gulbis, J.M., Cohen, S.L., Chait, B.T. and MacKinnon, R. (1998) The structure of the potassium channel: molecular basis of K+ conduction and selectivity. *Science*, **280**, 69-77.
Dutzler, R., Campbell, E.B., Cadene, M., Chait, B.T. and MacKinnon, R. (2002) X-ray structure of a ClC chloride channel at 3.0 A reveals the molecular basis of anion selectivity. *Nature*, **415**, 287-294.
Dutzler, R., Campbell, E.B. and MacKinnon, R. (2003) Gating the selectivity filter in ClC chloride channels. *Science*, **300**, 108-112.
Ehnes, C., Forster, I.C., Bacconi, A., Kohler, K., Biber, J. and Murer, H. (2004a) Structure-function relations of the first and fourth extracellular linkers of the type IIa Na+/Pi cotransporter: II. Substrate interaction and voltage dependency of two functionally important sites. *J Gen Physiol*, **124**, 489-503.
Ehnes, C., Forster, I.C., Kohler, K., Bacconi, A., Stange, G., Biber, J. and Murer, H. (2004b) Structure-function relations of the first and fourth predicted extracellular linkers of the type IIa Na+/Pi cotransporter: I. Cysteine scanning mutagenesis. *J Gen Physiol*, **124**, 475-488.
Ehnes, C., Forster, I.C., Kohler, K., Biber, J. and Murer, H. (2002) Functional studies on a split type II Na/P(i)-cotransporter. *J Membr Biol*, **188**, 227-236.
Eskandari, S., Kreman, M., Kavanaugh, M.P., Wright, E.M. and Zampighi, G.A. (2000) Pentameric assembly of a neuronal glutamate transporter. *Proc Natl Acad Sci U S A*, **97**, 8641-8646.
Forster, I., Biber, J. and Murer, H. (1999) Electrophysiological analysis of renal Na(+)-coupled divalent anion transporters. *Pharm Biotechnol*, **12**, 251-267.
Forster, I., Hernando, N., Biber, J. and Murer, H. (1998) The voltage dependence of a cloned mammalian renal type II Na+/Pi cotransporter (NaPi-2). *J Gen Physiol*, **112**, 1-18.
Forster, I.C., Biber, J. and Murer, H. (2000) Proton-sensitive transitions of renal type II Na(+)-coupled phosphate cotransporter kinetics. *Biophys J*, **79**, 215-230.

Forster, I.C., Kohler, K., Biber, J. and Murer, H. (2002) Forging the link between structure and function of electrogenic cotransporters: the renal type IIa Na+/Pi cotransporter as a case study. *Prog Biophys Mol Biol*, **80**, 69-108.

Galli, A., Blakely, R.D. and DeFelice, L.J. (1998) Patch-clamp and amperometric recordings from norepinephrine transporters: channel activity and voltage-dependent uptake. *Proc Natl Acad Sci U S A*, **95**, 13260-13265.

Galli, A., Petersen, C.I., deBlaquiere, M., Blakely, R.D. and DeFelice, L.J. (1997) Drosophila serotonin transporters have voltage-dependent uptake coupled to a serotonin-gated ion channel. *J Neurosci*, **17**, 3401-3411.

Gross, E. and Kurtz, I. (2002) Structural determinants and significance of regulation of electrogenic Na(+)-HCO(3)(-) cotransporter stoichiometry. *Am J Physiol Renal Physiol*, **283**, F876-887.

Hartmann, C.M., Wagner, C.A., Busch, A.E., Markovich, D., Biber, J., Lang, F. and Murer, H. (1995) Transport characteristics of a murine renal Na/Pi-cotransporter. *Pflugers Arch*, **430**, 830-836.

Hayes, G., Busch, A., Lotscher, M., Waldegger, S., Lang, F., Verrey, F., Biber, J. and Murer, H. (1994) Role of N-linked glycosylation in rat renal Na/Pi-cotransport. *J Biol Chem*, **269**, 24143-24149.

Henikoff, S. and Henikoff, J.G. (1992) Amino acid substitution matrices from protein blocks. *Proc Natl Acad Sci U S A*, **89**, 10915-10919.

Hilfiker, H., Hattenhauer, O., Traebert, M., Forster, I., Murer, H. and Biber, J. (1998) Characterization of a murine type II sodium-phosphate cotransporter expressed in mammalian small intestine. *Proc Natl Acad Sci U S A*, **95**, 14564-14569.

Hilgemann, D.W. and Lu, C.C. (1999) GAT1 (GABA:Na+:Cl-) cotransport function. Database reconstruction with an alternating access model. *J Gen Physiol*, **114**, 459-475.

Hille, B. (2001) *Ion Channels of Excitable Membranes*. Sinauer Associates.

Hoffmann, N., Thees, M. and Kinne, R. (1976) Phosphate transport by isolated renal brush border vesicles. *Pflugers Arch*, **362**, 147-156.

Huang, Y., Lemieux, M.J., Song, J., Auer, M. and Wang, D.N. (2003) Structure and mechanism of the glycerol-3-phosphate transporter from Escherichia coli. *Science*, **301**, 616-620.

Hunte, C., Screpanti, E., Venturi, M., Rimon, A., Padan, E. and Michel, H. (2005) Structure of a Na+/H+ antiporter and insights into mechanism of action and regulation by pH. *Nature*, **435**, 1197-1202.

Javitch, J.A. (1998) Probing structure of neurotransmitter transporters by substituted-cysteine accessibility method. *Methods Enzymol*, **296**, 331-346.

Jiang, Q.X., Wang, D.N. and MacKinnon, R. (2004) Electron microscopic analysis of KvAP voltage-dependent K+ channels in an open conformation. *Nature*, **430**, 806-810.

Jiang, Y., Lee, A., Chen, J., Ruta, V., Cadene, M., Chait, B.T. and MacKinnon, R. (2003a) X-ray structure of a voltage-dependent K+ channel. *Nature*, **423**, 33-41.

Jiang, Y., Ruta, V., Chen, J., Lee, A. and MacKinnon, R. (2003b) The principle of gating charge movement in a voltage-dependent K+ channel. *Nature*, **423**, 42-48.

Kaback, H.R., Sahin-Toth, M. and Weinglass, A.B. (2001) The kamikaze approach to membrane transport. *Nat Rev Mol Cell Biol*, **2**, 610-620.

Kamdar, G., Penado, K.M., Rudnick, G. and Stephan, M.M. (2001) Functional role of critical stripe residues in transmembrane span 7 of the serotonin transporter. Effects of Na+, Li+, and methanethiosulfonate reagents. *J Biol Chem*, **276**, 4038-4045.

Karlin, A. and Akabas, M.H. (1998) Substituted-cysteine accessibility method. *Methods Enzymol*, **293**, 123-145.

Kavanaugh, M.P. and Kabat, D. (1996) Identification and characterization of a widely expressed phosphate transporter/retrovirus receptor family. *Kidney Int*, **49**, 959-963.

Kavanaugh, M.P., Miller, D.G., Zhang, W., Law, W., Kozak, S.L., Kabat, D. and Miller, A.D. (1994) Cell-surface receptors for gibbon ape leukemia virus and amphotropic murine

retrovirus are inducible sodium-dependent phosphate symporters. *Proc Natl Acad Sci U S A*, **91**, 7071-7075.
Khademi, S., O'Connell, J., 3rd, Remis, J., Robles-Colmenares, Y., Miercke, L.J. and Stroud, R.M. (2004) Mechanism of ammonia transport by Amt/MEP/Rh: structure of AmtB at 1.35 A. *Science*, **305**, 1587-1594.
Kohl, B., Herter, P., Hulseweh, B., Elger, M., Hentschel, H., Kinne, R.K. and Werner, A. (1996) Na-Pi cotransport in flounder: same transport system in kidney and intestine. *Am J Physiol*, **270**, F937-944.
Kohler, K., Forster, I.C., Lambert, G., Biber, J. and Murer, H. (2000) The functional unit of the renal type IIa Na+/Pi cotransporter is a monomer. *J Biol Chem*, **275**, 26113-26120.
Kohler, K., Forster, I.C., Stange, G., Biber, J. and Murer, H. (2002a) Identification of functionally important sites in the first intracellular loop of the NaPi-IIa cotransporter. *Am J Physiol Renal Physiol*, **282**, F687-696.
Kohler, K., Forster, I.C., Stange, G., Biber, J. and Murer, H. (2002b) Transport function of the renal type IIa Na+/P(i) cotransporter is codetermined by residues in two opposing linker regions. *J Gen Physiol*, **120**, 693-705.
Kohler, K., Forster, I.C., Stange, G., Biber, J. and Murer, H. (2003) Essential cysteine residues of the type IIa Na+/Pi cotransporter. *Pflugers Arch*, **446**, 203-210.
Lambert, G., Forster, I.C., Biber, J. and Murer, H. (2000) Cysteine residues and the structure of the rat renal proximal tubular type II sodium phosphate cotransporter (rat NaPi IIa). *J Membr Biol*, **176**, 133-141.
Lambert, G., Forster, I.C., Stange, G., Biber, J. and Murer, H. (1999) Properties of the mutant Ser-460-Cys implicate this site in a functionally important region of the type IIa Na(+)/P(i) cotransporter protein. *J Gen Physiol*, **114**, 637-652.
Lambert, G., Forster, I.C., Stange, G., Kohler, K., Biber, J. and Murer, H. (2001) Cysteine mutagenesis reveals novel structure-function features within the predicted third extracellular loop of the type IIa Na(+)/P(i) cotransporter. *J Gen Physiol*, **117**, 533-546.
Laskowski, R., MacArthur, M., Moss, D. and Thornton, J. (1993) PROCHECK: a program to check the stereochemical quality of protein structures. *J. Appl. Cryst.*, **26**, 283-291.
Lebens, M., Lundquist, P., Soderlund, L., Todorovic, M. and Carlin, N.I. (2002) The nptA gene of Vibrio cholerae encodes a functional sodium-dependent phosphate cotransporter homologous to the type II cotransporters of eukaryotes. *J Bacteriol*, **184**, 4466-4474.
Lemieux, M.J., Huang, Y. and Wang da, N. (2005) Crystal structure and mechanism of GlpT, the glycerol-3-phosphate transporter from E. coli. *J Electron Microsc (Tokyo)*, **54 Suppl 1**, i43-i46.
Lester, H.A., Cao, Y. and Mager, S. (1996) Listening to neurotransmitter transporters. *Neuron*, **17**, 807-810.
Levinthal, C. (1968) Are there pathways for protein folding? *Extrait du Journal de Chimie Physique*, **65 no 1**, 44-45.
Locher, K.P. (2004) Structure and mechanism of ABC transporters. *Curr Opin Struct Biol*, **14**, 426-431.
Locher, K.P. and Borths, E. (2004) ABC transporter architecture and mechanism: implications from the crystal structures of BtuCD and BtuF. *FEBS Lett*, **564**, 264-268.
Locher, K.P., Lee, A.T. and Rees, D.C. (2002) The E. coli BtuCD structure: a framework for ABC transporter architecture and mechanism. *Science*, **296**, 1091-1098.
Long, S.B., Campbell, E.B. and Mackinnon, R. (2005) Crystal structure of a mammalian voltage-dependent Shaker family K+ channel. *Science*, **309**, 897-903.
Lu, C.C. and Hilgemann, D.W. (1999a) GAT1 (GABA:Na+:Cl-) cotransport function. Kinetic studies in giant Xenopus oocyte membrane patches. *J Gen Physiol*, **114**, 445-457.
Lu, C.C. and Hilgemann, D.W. (1999b) GAT1 (GABA:Na+:Cl-) cotransport function. Steady state studies in giant Xenopus oocyte membrane patches. *J Gen Physiol*, **114**, 429-444.

Ma, C. and Chang, G. (2004) Structure of the multidrug resistance efflux transporter EmrE from Escherichia coli. *Proc Natl Acad Sci U S A*, **101**, 2852-2857.

MacKerell, J.A.D., Bashford, D., Bellott, M., Dunbrack Jr., R.L., Evanseck, J.D., Field, M.J., Fischer, S., Gao, J., Guo, H., Ha, S., Joseph-McCarthy, D., Kuchnir, L., Kuczera, K., Lau, F.T.K., Mattos, C., Michnick, S., Ngo, T., Nguyen, D.T., Prodhom, B., Reiher, I., W.E., Roux, B., Schlenkrich, M., Smith, J.C., Stote, R., Straub, J., Watanabe, M., Wiorkiewicz-Kuczera, J., Yin, D. and Karplus, M. (1998) All-atom empirical potential for molecular modeling and dynamics Studies of proteins. *Journal of Physical Chemistry B*, **102**, 3586-3616.

Madjdpour, C., Bacic, D., Kaissling, B., Murer, H. and Biber, J. (2004) Segment-specific expression of sodium-phosphate cotransporters NaPi-IIa and -IIc and interacting proteins in mouse renal proximal tubules. *Pflugers Arch*, **448**, 402-410.

Maduke, M., Pheasant, D.J. and Miller, C. (1999) High-level expression, functional reconstitution, and quaternary structure of a prokaryotic ClC-type chloride channel. *J Gen Physiol*, **114**, 713-722.

Magagnin, S., Werner, A., Markovich, D., Sorribas, V., Stange, G., Biber, J. and Murer, H. (1993) Expression cloning of human and rat renal cortex Na/Pi cotransport. *Proc Natl Acad Sci U S A*, **90**, 5979-5983.

Muller-Berger, S., Ducoudret, O., Diakov, A. and Fromter, E. (2001) The renal Na-HCO3-cotransporter expressed in Xenopus laevis oocytes: change in stoichiometry in response to elevation of cytosolic Ca2+ concentration. *Pflugers Arch*, **442**, 718-728.

Murata, K., Mitsuoka, K., Hirai, T., Walz, T., Agre, P., Heymann, J.B., Engel, A. and Fujiyoshi, Y. (2000) Structural determinants of water permeation through aquaporin-1. *Nature*, **407**, 599-605.

Murer, H. and Biber, J. (1996) Molecular mechanisms of renal apical Na/phosphate cotransport. *Annu Rev Physiol*, **58**, 607-618.

Murer, H. and Biber, J. (1997) A molecular view of proximal tubular inorganic phosphate (Pi) reabsorption and of its regulation. *Pflugers Arch*, **433**, 379-389.

Murer, H. and Biber, J. (1998) Membrane permeability. Epithelial transport proteins: physiology and pathophysiology. *Curr Opin Cell Biol*, **10**, 429-434.

Murer, H., Forster, I. and Biber, J. (2004) The sodium phosphate cotransporter family SLC34. *Pflugers Arch*, **447**, 763-767.

Murer, H., Forster, I., Hilfiker, H., Pfister, M., Kaissling, B., Lotscher, M. and Biber, J. (1998) Cellular/molecular control of renal Na/Pi-cotransport. *Kidney Int Suppl*, **65**, S2-10.

Murer, H., Hernando, N., Forster, I. and Biber, J. (2000) Proximal tubular phosphate reabsorption: molecular mechanisms. *Physiol Rev*, **80**, 1373-1409.

Nayal, M. and Di Cera, E. (1994) Predicting Ca^{2+}-binding sites in proteins. *Proceedings of the National Academy of Sciences of the United States of America*, **91**, 817-821.

Ogawa, H. and Toyoshima, C. (2002) Homology modeling of the cation binding sites of $Na^{+}K^{+}$-ATPase. *Proceedings of the National Academy of Sciences of the United States of America*, **99**, 15977-15982.

Olah, Z., Lehel, C., Anderson, W.B., Eiden, M.V. and Wilson, C.A. (1994) The cellular receptor for gibbon ape leukemia virus is a novel high affinity sodium-dependent phosphate transporter. *J Biol Chem*, **269**, 25426-25431.

Otis, T.S. and Jahr, C.E. (1998) Anion currents and predicted glutamate flux through a neuronal glutamate transporter. *J Neurosci*, **18**, 7099-7110.

Petersen, C.I. and DeFelice, L.J. (1999) Ionic interactions in the Drosophila serotonin transporter identify it as a serotonin channel. *Nat Neurosci*, **2**, 605-610.

Rao, F., Settanni, G., Guarnera, E. and Caflisch, A. (2005) Estimation of protein folding probability from equilibrium simulations. *J Chem Phys*, **122**, 184901.

Rotem, D. and Schuldiner, S. (2004) EmrE, a multidrug transporter from Escherichia coli, transports monovalent and divalent substrates with the same stoichiometry. *J Biol Chem*, **279**, 48787-48793.

Salas-Burgos, A., Iserovich, P., Zuniga, F., Vera, J.C. and Fischbarg, J. (2004) Predicting the three-dimensional structure of the human facilitative glucose transporter glut1 by a novel evolutionary homology strategy: insights on the molecular mechanism of substrate migration, and binding sites for glucose and inhibitory molecules. *Biophys J*, **87**, 2990-2999.

Sali, A. and Blundell, T.L. (1993) Comparative protein modelling by satisfaction of spatial restraints. *J Mol Biol*, **234**, 779-815.

Samarzija, I., Molnar, V. and Fromter, E. (1983) pH--dependence of phosphate absorption in rat renal proximal tubule. *Proc Eur Dial Transplant Assoc*, **19**, 779-783.

Segawa, H., Kaneko, I., Takahashi, A., Kuwahata, M., Ito, M., Ohkido, I., Tatsumi, S. and Miyamoto, K. (2002) Growth-related renal type II Na/Pi cotransporter. *J Biol Chem*, **277**, 19665-19672.

Settanni, G., Rao, F. and Caflisch, A. (2005) Phi-value analysis by molecular dynamics simulations of reversible folding. *Proc Natl Acad Sci U S A*, **102**, 628-633.

Su, A., Mager, S., Mayo, S.L. and Lester, H.A. (1996) A multi-substrate single-file model for ion-coupled transporters. *Biophys J*, **70**, 762-777.

Sui, H., Han, B.G., Lee, J.K., Walian, P. and Jap, B.K. (2001) Structural basis of water-specific transport through the AQP1 water channel. *Nature*, **414**, 872-878.

Szczepanska-Konkel, M., Yusufi, A.N. and Dousa, T.P. (1987) Interactions of [14C]phosphonoformic acid with renal cortical brush-border membranes. Relationship to the Na+-phosphate co-transporter. *J Biol Chem*, **262**, 8000-8010.

Szczepanska-Konkel, M., Yusufi, A.N., VanScoy, M., Webster, S.K. and Dousa, T.P. (1986) Phosphonocarboxylic acids as specific inhibitors of Na+-dependent transport of phosphate across renal brush border membrane. *J Biol Chem*, **261**, 6375-6383.

Tate, C.G., Ubarretxena-Belandia, I. and Baldwin, J.M. (2003) Conformational changes in the multidrug transporter EmrE associated with substrate binding. *J Mol Biol*, **332**, 229-242.

Tatsumi, S., Segawa, H., Morita, K., Haga, H., Kouda, T., Yamamoto, H., Inoue, Y., Nii, T., Katai, K., Taketani, Y., Miyamoto, K.I. and Takeda, E. (1998) Molecular cloning and hormonal regulation of PiT-1, a sodium-dependent phosphate cotransporter from rat parathyroid glands. *Endocrinology*, **139**, 1692-1699.

Tenenhouse, H.S., Gauthier, C., Martel, J., Gesek, F.A., Coutermarsh, B.A. and Friedman, P.A. (1998a) Na+ -phosphate cotransport in mouse distal convoluted tubule cells: evidence for Glvr-1 and Ram-1 gene expression. *J Bone Miner Res*, **13**, 590-597.

Tenenhouse, H.S., Roy, S., Martel, J. and Gauthier, C. (1998b) Differential expression, abundance, and regulation of Na+-phosphate cotransporter genes in murine kidney. *Am J Physiol*, **275**, F527-534.

Thompson, J.D., Higgins, D.G. and Gibson, T.J. (1994) CLUSTAL W: improving the sensitivity of progressive multiple sequence alignment through sequence weighting, position-specific gap penalties and weight matrix choice. *Nucleic Acids Res*, **22**, 4673-4680.

Traebert, M., Hattenhauer, O., Murer, H., Kaissling, B. and Biber, J. (1999) Expression of type II Na-P(i) cotransporter in alveolar type II cells. *Am J Physiol*, **277**, L868-873.

van Aalten, D.M., Bywater, R., Findlay, J.B., Hendlich, M., Hooft, R.W. and Vriend, G. (1996) PRODRG, a program for generating molecular topologies and unique molecular descriptors from coordinates of small molecules. *J Comput Aided Mol Des*, **10**, 255-262.

van Winkle, L. (1999) *Biomembrane Transport*. Academic Press.

Veldhuis, G., Broos, J., Poolman, B. and Scheek, R.M. (2005) Stoichiometry and substrate affinity of the mannitol transporter, EnzymeIImtl, from Escherichia coli. *Biophys J*, **89**, 201-210.

Virkki, L.V., Forster, I.C., Biber, J. and Murer, H. (2005) Substrate interactions in the human type IIa sodium-phosphate cotransporter (NaPi-IIa). *Am J Physiol Renal Physiol*, **288**, F969-981.

Wadiche, J.I. and Kavanaugh, M.P. (1998) Macroscopic and microscopic properties of a cloned glutamate transporter/chloride channel. *J Neurosci*, **18**, 7650-7661.
Walters, D.E. and Kaplan, R.S. (2004) Homology-modeled structure of the yeast mitochondrial citrate transport protein. *Biophys J*, **87**, 907-911.
Werner, A. and Kinne, R.K. (2001) Evolution of the Na-P(i) cotransport systems. *Am J Physiol Regul Integr Comp Physiol*, **280**, R301-312.
Werner, A., Moore, M.L., Mantei, N., Biber, J., Semenza, G. and Murer, H. (1991) Cloning and expression of cDNA for a Na/Pi cotransport system of kidney cortex. *Proc Natl Acad Sci U S A*, **88**, 9608-9612.
Widdas, W.F. (1952) Inability of diffusion to account for placental glucose transfer in the sheep and consideration of the kinetics of a possible carrier transfer. *J Physiol*, **118**, 23-39.
Wright M. W., El-Mehidi N. S., Bruford E. A., Khodiyar V. K., Lovering R. C., Lush M. J., C. C. Talbot Jr., Wain H. M. and Povey S. (2003) Family matters - naming genes within families. *European Journal of Biochemistry*, **Supplement 1**.
Xiang, Z. and Honig, B. (2001) Extending the accuracy limits of prediction for side-chain conformations. *J Mol Biol*, **311**, 421-430.
Yamashita, A., Singh, S.K., Kawate, T., Jin, Y. and Gouaux, E. (2005) Crystal structure of a bacterial homologue of Na+/Cl--dependent neurotransmitter transporters. *Nature*, **437**, 215-223.
Yernool, D., Boudker, O., Jin, Y. and Gouaux, E. (2004) Structure of a glutamate transporter homologue from Pyrococcus horikoshii. *Nature*, **431**, 811-818.

7. ACKNOWLEDGEMENTS

I would like to thank Heini Murer for the possibility he gave me to work in this lab. Thank you for the support and interest in my work and in my future carrier.

I am grateful for the support I got from Ian Forster. The countless hours spent discussing were a useful light in the dark hours of my PhD work. Many thanks for the big effort he spent in the correction of this manuscript.

Thank you to Jürg Biber and Nati Hernando for the technical help and all the useful suggestions.

Thanks to all the people on J-floor who contributed to create a nice working enviroment.

Thank you to the present and future readers of this PhD thesis.

8. CURRICULUM VITAE

Name: ANDREA

Second Name: BACCONI

Place and date of birth: Varese (VA), 21st April 1976, Italy

Nationality: Italian

Previous studies:

September 1982-June 1990:	Elementary School, Casale Litta (VA) and Middle school, Varese (VA), Italy.
September 1990-July 1995:	High school Liceo Scientifico "Galileo Ferraris", Varese (VA), Italy.
July 1995:	Maturità (60 out of 60)
September 1997- July 2002:	Biological Sciences at University of Insubria, Varese (VA), Italy.
February 2001-July 2002:	Thesis project: "Relationship between charge movement and transport associated current in the GABA neuronal co-transporter rGat1" At DBSF University of Insubria, Varese (VA), Italy. Subject: cellular and molecular physiology.
July 2002:	Master Degree (Laurea) (110 out of 110 *cum laude*) at University of Insubria, Varese (VA), Italy.

Since September 2002:	PhD Student at UNIVERSITY OF ZURICH, INSTITUTE OF PHYSIOLOGY, Winterthurerstrasse 190, 8057 Zürich Group of “Renal transport physiology” Title:” The price of electrogenicity : studies on the carrier and channel like properties of a type II NaPi cotransporter system” PhD Supervisors: Prof. Dr. Heini Murer Prof. Dr Jürg Biber Dr. Ian C. Forster